# Characterisation of wear particles genarated during accelerated testing of total hip replacement

Hussain, Azad

# Implant Lifetime Prediction : Accelerated testing and characterisation of total hip replacements

CHARACTERISATION OF WEAR PARTICLES GENERATED DURING ACCELERATED TESTING OF TOTAL HIP REPLACEMENTS


## Azad Hussain


A thesis submitted for the degree of Doctor of Philosophy
at the University of London

Supervised by: Dr. J. Shelton

September 2004


Interdisciplinary Research Centre in Biomedical Materials (IRC),
Queen Mary, University of London,
Mile End Road, London, E1 4NS, UK.

# Abstract

Total hip replacements have been in use for over 30 years, and have shown great improvement from design to surgery since the first generation of implants were introduced. The greater need for hip replacements has led to the development of test methods that can be applied in the lab, which can predict the lifetime of a particular implant. To achieve this aim this study has sought to investigate key parameters, which may affect wear and its subsequent effect upon the production of particles for various material combinations and bearing geometries, under high (jogging) and low (walking) loads, with concurrent assessment of wear reduction, particle size and morphology.

The clinical use of cross-linked polyethylene (XLPE) has been shown to reduce wear and thereby the onset of osteolysis in total hip arthroplasty. Hip simulator studies have suggested that while XLPE generates low wear under smooth counterface bearing surfaces, there appears to be an increased sensitivity to scratched femoral head conditions which can occur in the patient. However, these simulator studies have not combined damaged articular surfaces with a severe gait model, representing the worst-case scenario for high-risk, active patients. This hip simulator study has shown that the size distribution of wear particles generated in tests on 5 MRads crosslinked polyethylene can be influenced by the degree of patient activity. Fast jogging showed a greater influence on the number of sub-micron-sized wear particles (5-fold increase compared to walking) than on volumetric wear rate (26 $mm^3/10^6$ cycles compared to 29 $mm^3/10^6$ cycles). Fast jogging also did not generate the largest wear particles (>10 μm) produced by normal walking. Roughening of the Co-Cr-Mo femoral heads created a 1700-fold increase in the numbers of sub-micron PE particles under fast jogging. The clinical significance of this result suggests that highly active patients will generate high numbers of bioactive PE wear particles within the accepted bioactive range, 0.2–10μm.

Metal-on-metal (MOM) hip arthroplasty has also seen rapid growth worldwide. However, there remains concern over their long-term biocompatibility due to systemic ion release. Therefore, the aim of this current investigation was to test the hypothesis that larger diameter MOM bearings (greater than 40 mm) will generate smaller Co-Cr-Mo wear particles compared to a 28 mm size bearing, and reduce the total wear particle surface area, and to test the hypothesis that 'severe' gait conditions will greatly increase the size of Co-Cr-Mo wear particles, thereby causing a sizable increase in wear particle surface area. Walking with a 28 mm bearing produced the largest wear rate of at 0.92 $mm^3/10^6$ cycles, whereas the 40 mm and 56 mm bearings, generated lower wear rates of 0.39 $mm^3/10^6$ cycles and 0.32 $mm^3/10^6$ cycles respectively. Simulated fast jogging created a 3-fold increase in the number of elongated (needle) wear particles compared to normal walking, and generated a 20-fold increase in total wear particle surface area per year of use compared to normal walking. The clinical significance of this result suggests that highly active patients with MoM implants will exhibit greater ion release, although this may be minimised by using larger diameter bearings for active or younger patients.

# Acknowledgements

First I would like to thank Dr Julia Shelton, my supervisor, for her enduring patience, thank you for all your help and Dr John Bowsher for all the help along the way and late night chats.

Thank you to all my fellow compadres, Miss. I. Meththananda (we had some good arguments), Miss. S. Williams, Mr. K. Scott, Miss K.E. Baria, Mr. R. Twycross-Lewis, Mr. J Campbell, Mr. A. Hon, Miss. S. Hoque, Mr and Mrs Spary, Mr J. Drabble, Mr S. Brunton and everyone that I have met along the journey.

For all the technical help and support that I've received I would like to say a sincere thank you, without whom I would not have any results to present, Dr. J. Mitchell, Mr. D Porter, Dr. Z. Luklinska, Mr. M. Willis (TEM analysis), and Mr R. Whitenstall (SEM analysis). Finsbury Instruments Limited, Mr Philip Miles for help with surface topography measurements. Dr. S. Williams for your help in scratch tests. Mrs C. Jones, Mr V. Ford for all your advice

Special thank you to Miss M. Phillips, for keeping me sane and grounded.

Many thanks to my family, sometimes you drive me mad but you are never boring

Finally, I would like to gratefully acknowledge the financial support of the EPSRC.

ازادي

# Contents

# Abbreviations

| | |
|---|---|
| THRs | Total hip replacements |
| TJRs | Total joint replacements |
| TKRs | Total knee replacements |
| SEM | Scanning electron microscopy |
| n | Number of observations |
| NaOH | Sodium hydroxide |
| KOH | Potassium hydroxide |
| IQR | Interquartile range |
| UHMWPE | Ultra-high molecular weight polyethylene |
| XLPE | Crosslinked polyethylene |
| HDPE | High density polyethylene |
| PTFE | Polytetrafluoroethylene |
| CoCr | Cobalt-chromium |
| CoCrMo | Cobalt-chromium Molybdenum |
| PE | Polyethylene |
| PMMA | Polymethylmethacrylate |
| SS | Stainless steel |
| Ti6A14V | Titanium-aluminium-vanadium alloy |
| $ZrO_2$ | Zirconia |
| BW | Body Weight |
| ECD | Equivalent circle diameter |

# Nomenclature

| | | |
|---|---|---|
| X | Sliding Distance | m |
| V | Wear Volume | $mm^3$ |
| *k* | Wear Factor | $mm^3/N\ m$ |
| $J_R$ | Hip Joint Resultant Force | N |
| $R_A$ | Heel Strike Force | N |
| $R_B$ | Minimum Stance Phase Force | N |
| $R_C$ | Maximum Stance Phase Force | N |
| *F* | Gait Frequency | Hz |
| *T* | Time | Seconds |
| C | Radial Clearance | m |
| $R_l$ | Femoral Head Radius | m |
| D | Femoral Head Diameter | m |
| $R_a$ | Surface Roughness Average | μm |
| $R_p$ | Peak Profile Height | μm |
| $R_v$ | Maximum Valley Depth | μm |
| $R_t$ | Maximum Profile Height | μm |
| *E'* | Equivalent young's modulus | Pa |
| $M_{t1}$ | Initial mass of test specimen | g |
| $M_{t2}$ | Final mass of test specimen | g |
| $M_{s1}$ | Aver. initial mass of sock controls | g |
| $M_{t2}$ | Aver. final mass of sock controls | g |
| $\delta M_t$ | Loss of mass | g |
| A | Area of Contact | $mm^2$ |
| W | Load | N |

# List of Figures

# List of Tables

# Chapter 1 Introduction

Total hip replacement is the process of completely removing the existing hip and replacing it with an artificial hip. Today, over 60,000 THRs are implanted within the UK. The main goal of total hip replacement is to improve the quality of life of the patient by reducing the amount of pain in the hip and restoring near normal function to the hip.

THR has a huge impact on its patients. If successful, it can benefit the patient tremendously, and restore function in the hip allowing the patient to perform every day tasks such as walking and climbing stairs without difficulty and reducing pain and discomfort in the hip. However, implant failure can lead to complications that can be extremely detrimental to the patient. The patient can be subjected to more discomfort, pain and loss of function. In order to reduce the instances of failure, it is important to understand the causes and effects of failure. Given that a total hip replacement has such a large impact on its patients, all avenues from design to implantation must be explored through *in vitro* and *in vivo* studies.

THR system have been used with excellent clinical success for the past four decades. A recent study of 320 Charnley low-friction arthroplasties following 20-30 years of implantation, showed a 93 % success rate. However, there are still issues that still remain unresolved. Aseptic loosening of THR implant is the most severe problem encountered and is recognised as a major cause of failure, which requires revision surgery. Many studies have shown that wear debris of THR materials is a major factor, which in turn leads to local bone loss (osteolysis) and aseptic loosening. The majority of the wear debris is generated at the bearing surface between the artificial femoral head and acetabular cup. Therefore, materials used in modern implants require superior wear resistance properties, as well as good biocompatibility.

The clinical use of crosslinked Ultra-High Molecular Weight Polyethylene (UHMWPE) has become the material of choice, in terms of reducing wear in turn reducing the amount of

debris generated at the articulating surface. *In vitro* studies have confirmed that the wear resistance of ultra-high molecular weight polyethylene can be significantly increased when applying high dose irradiation, such as gamma radiation in an inert atmosphere such as nitrogen (Wroblewski *et al*, 1996), with many studies reporting extremely low quantities of wear, typically as low as 2.0 $mm^3$ per million cycles for highly crosslinked polyethylene (Oonishi *et al*, 1997). However there are concerns over the range of wear rates produced and the nature of the debris that is generated. Although crosslinked PE has shown improved resistance to wear, and much is understood about the nature and process of osteolysis, bioactive particles are still produced by crosslinked PE and remains an unresolved issue.

The influence of femoral roughness on polyethylene wear has been widely investigated on various devices. Linear pin-on-disc wear machines reported a significant increase in polyethylene wear with increased counterface roughness, however, recent studies using multi-directional simulator studies using bovine serum as the lubricating medium, have shown a less marked effect of increased femoral head roughening (Wang *et al*, 1998a, Barbour *et al*, 2000). Such tests have concluded that the influence of increased roughness up to an $R_a$ of 0.05 μm has very little effect on the wear of crosslinked polyethylene. However these studies only considered normal walking, with a maximum load of 2700 N and therefore the generation of wear particles may in this situation be considered to have a minimal effect upon implant lifetime or that the onset of osteolysis is at best delayed.

Many studies have looked at the generation of wear debris following normal walking tests, however normal walking is only one of a multitude of activities that is undertaken by a patient. With younger and more active patients requiring hip implants, the need to test implants under severe conditions representing worst case scenarios situation such as rough femoral heads, rough femoral heads combined with increased activity such as jogging and the potential bioactive particles that may be generated as a result of these activities, need to be studied in detail.

# Chapter 2 Literature Review

## 2.1 Hip Anatomy & Biomechanics

### 2.1.1 The Natural Hip Joint

The hip joint in the human body is composed of bone, articular cartilage, a synovial membrane and a fibrous capsule. All the components mentioned combined with synovial fluid can articulate at very low range of coefficient of friction , under various physiological loads generated through walking and running. A cross-section of a human synovial joint is shown in Figure 2.1.

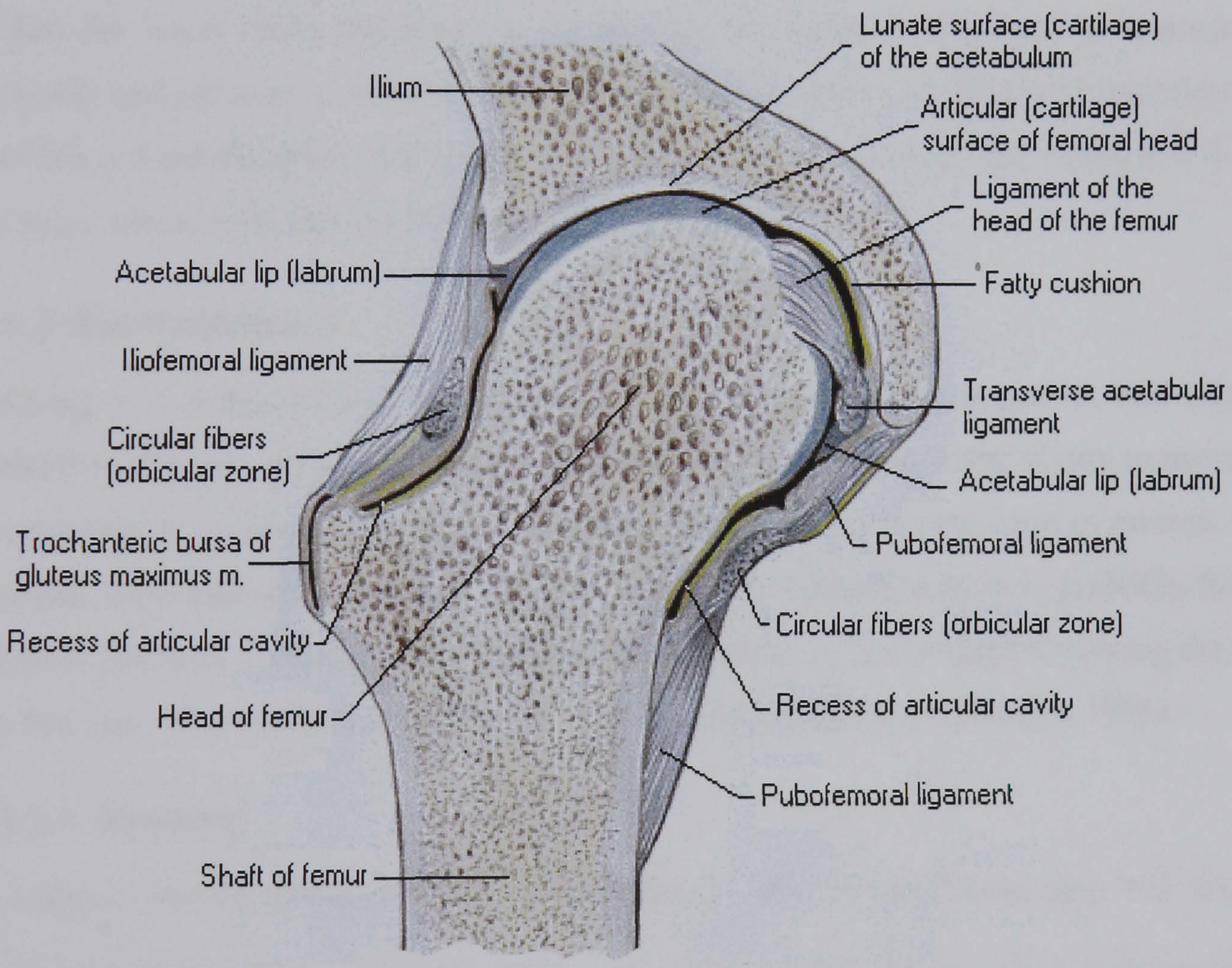


Figure 2.1: A cross-section of the human hip joint (Adapted from Tortora & Grabowski, 2000)

### 2.1.2 The Femur

Within the human body there are two types of bone, compact and cancellous. Compact (or cortical) bone makes up approximately 80% of the human skeleton, major load bearing bones are composed of compact bone. Cancellous bone is a porous form, and is typically found at the ends or in the core of most bones. Together, these two bone types form a lightweight composite material, which is highly efficient in bending and distributing force. The mechanical properties of bone are also highly variable. Biological composites such as bone are highly complex and the mechanical properties depend on microstructure, orientation, rate and type of loading (tension or compression), environment (wet or dry) and the type of bone being examined. (Grabowski & Tortora, 2001).

Within the lower limbs the femur is the longest, strongest and heaviest bone present. Its proximal end articulates with the acetabulum of the hip joint, its distal end articulates with the tibia and patella (knee joint). The neck of the femur is a constricted region and is below the head; structurally this is the weakest point on the bone.

### 2.1.3 Biomechanics

Walking is a fundamental aspect of human movement and development, and taken for granted by the age of 2-3 years of age. It provides the human with the ability to move from one position to another with great efficiency. It is also a very unique form of motion, as it is bipedal, some animals do exhibit this, but the human walking pattern is probably the most efficient (Rose & Gamble, 1994), walking is "a method of locomotion involving the use of the two legs, alternately, to provide both support and propulsion" (Whittle, 1996).

#### 2.1.3.1 Walking

In normal walking there are five main instances that occur during gait and these are summarised here. At Heel contact (HS): Leg and knee are straight, this is followed by foot flat (TO), where there is no flexion at the knee. Midstance (MS) occurs with the hip moving into extension with the knee also moving into extension in the trailing the leg. The fourth

stage (HS) involves the extension of the hip (abduction), with the knee in flexion moving to extension. The final stage is known as toe off (TO) where there is forward movement of the hip with the knee going into flexion from near full extension. This followed by mid-swing and heel contact of the opposite leg, thus completing a single gait cycle, Figure 2.2.

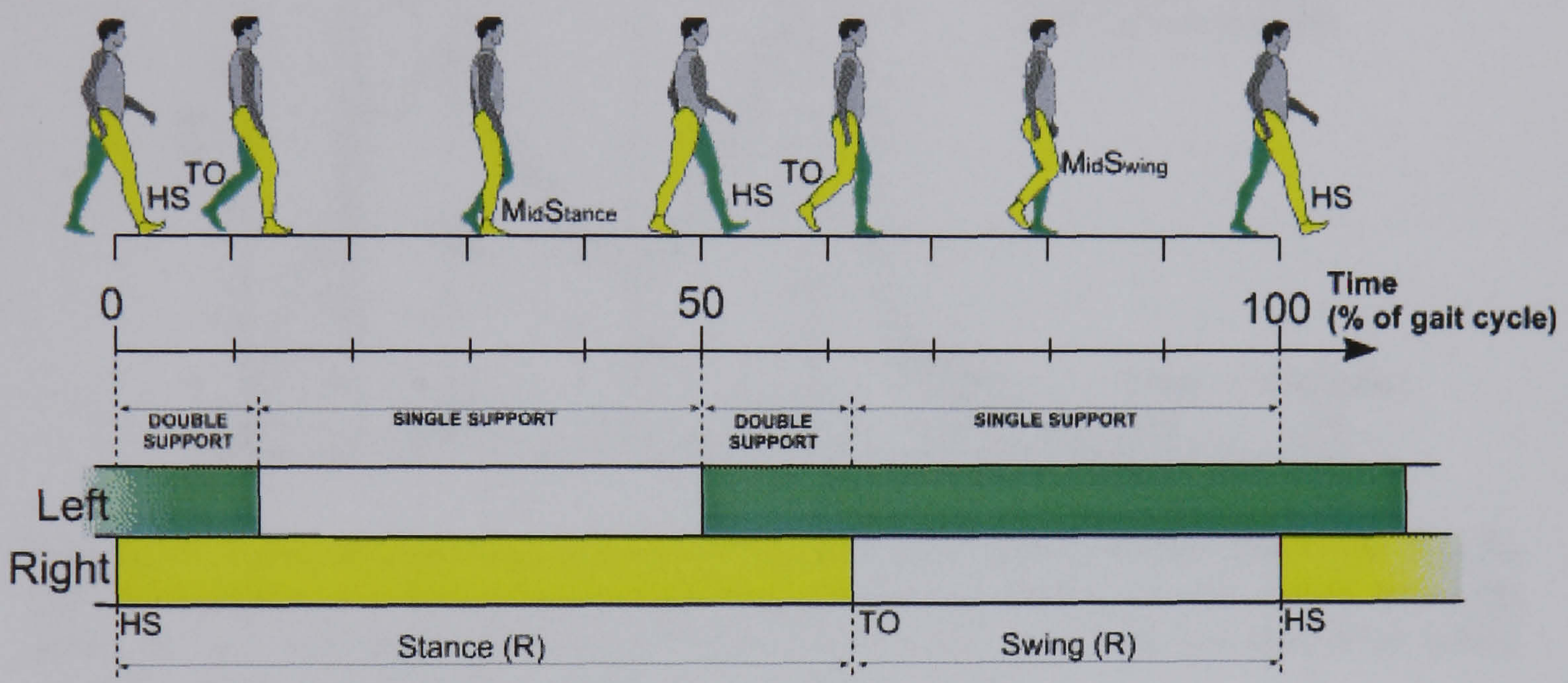


Figure 2.2: Schematic representation of one complete gait cycle (Rose & Gamble, 1994)

Paul (1966) was one of the first to carry out studies into hip joint forces during walking. The data was obtained by means of a floor mounted force plate, from which data was then analysed using equilibrium equations and plotted graphically to produce the classic m-curve force profile, shown in Figure 2.3, which identifies one walking cycle. respectively.

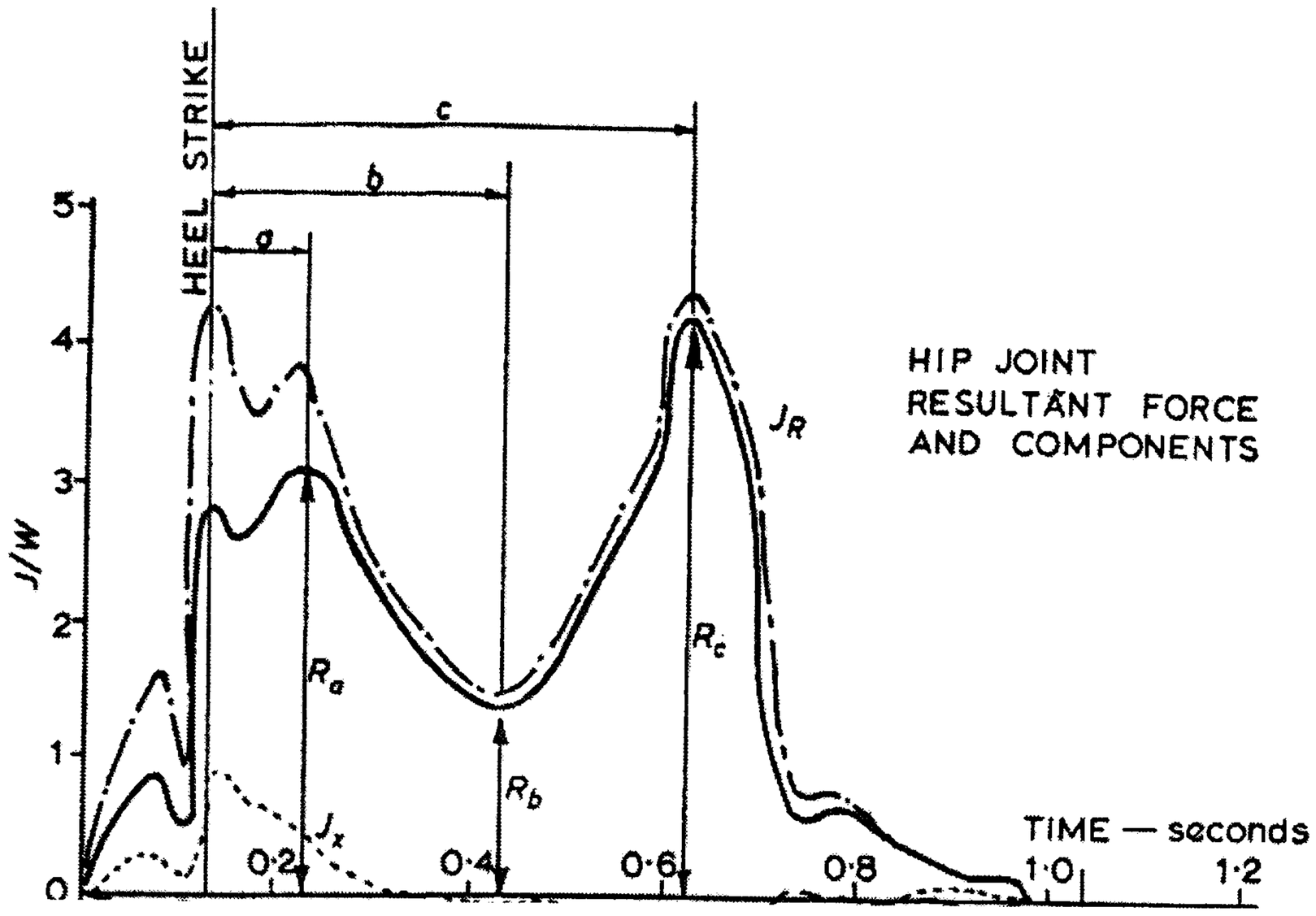


Figure 2.3: Forces transmitted through the hip at various points on the gait cycle. $R_A$, $R_B$ and $R_C$ represent the forces transmitted through the hip during toe-off, stance, and heel strike, at 3.29, 1.24 and 3.88 times the body weight (BW). $J_R$, is the resultant force acting on the hip joint, represented by curves $J_x$, $J_y$, $J_z$ (Paul, 1966).

### 2.1.3.2 Jogging

Jogging is one of the few sports activities which has been studied following hip replacement surgery. Studies by Bergmann *et al.* (1993) using an instrumented prosthesis provided important information into the forces transmitted through the hip joint. Investigations carried out by Bergmann *et al.* (1993) reported the presence of a double peak (m-curve) during walking, showing agreement with many other studies, although Bergmann *et al.* reported a reduction in the toe-off force. Bergmann *et al.* also investigated the forces transmitted through the hip during very fast walking and jogging in two patients. During jogging at 6 km/hr the BW increased to 500%, as shown in Figure 2.4.

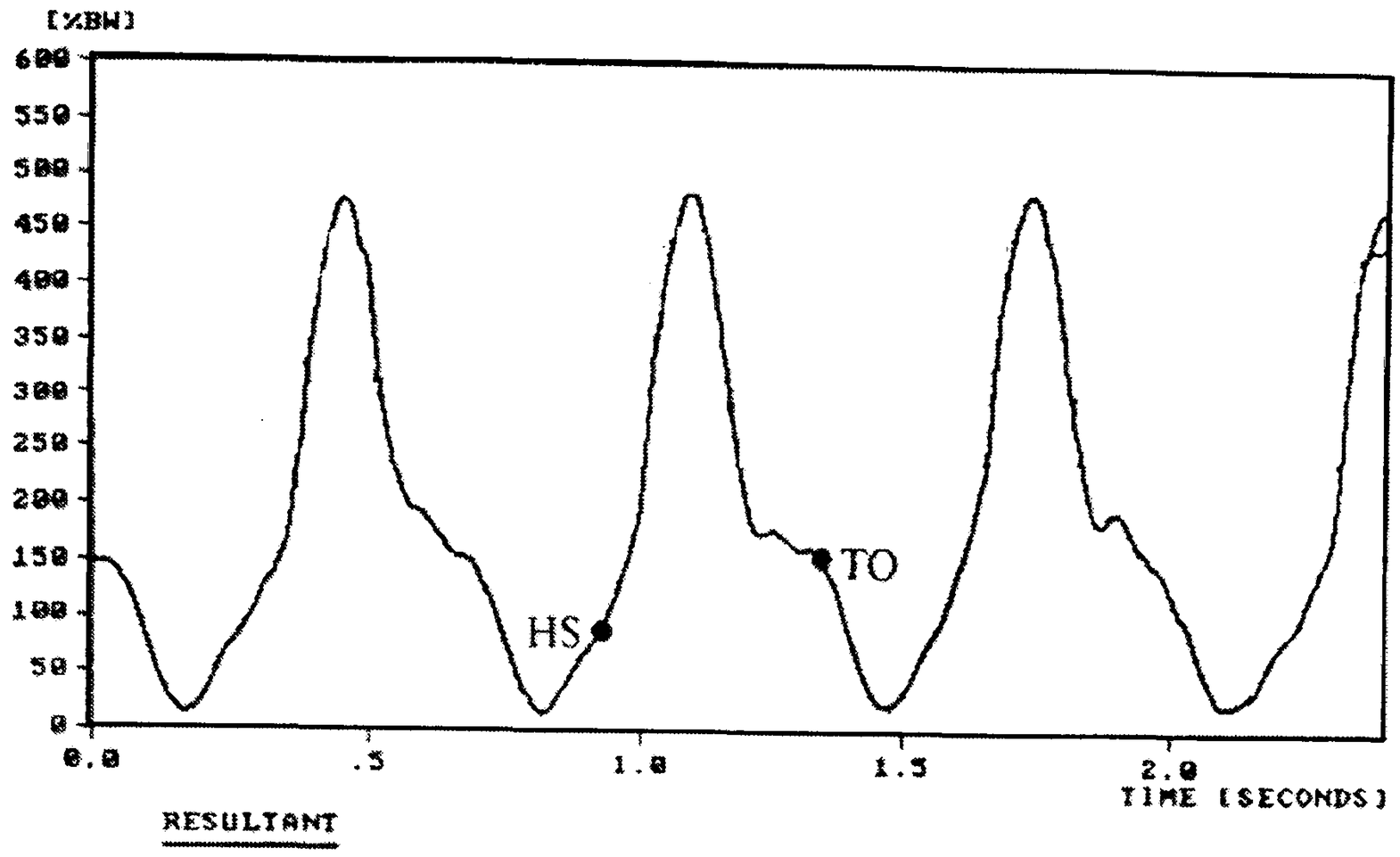


Figure 2.4: Forces in the hip joint during jogging at 6km/hr where $R_{max}$ is the peak force during one step, showing heel strike and toe off (Bergmann *et al.*, 1993)

Further studies were also carried for patients walking up and down stairs, walking up stairs caused an increase of 10% BW and walking downstairs caused an increase of 20% BW (Bergmann *et al.*, 1995). Although the forces generated during these everyday activities are low when compared to either walking or jogging, investigations into wear under these conditions are few and far between, considering now that activity is now recognised as one of the major factors that affects wear, (Schmalzried *et al.*. 2000). Studies into wear under these activities would provide a greater understanding of what is occurring *in vivo* with regards to the performance of a THR under various different types of activities and its long term performance.

### 2.1.4 Increased Activity

Literature regarding patient activity after THR is limited with differing views expressed from one study to another. Recent studies have documented patients who have returned to low impact sports such as sailing, swimming, scuba diving, cycling, golfing and bowling to name but a few. Moderate-impact sports such as cross-country skiing, speed walking, backpacking, ice-skating, tennis, aerobics, volleyball, softball, and alpine skiing have also been reported as being cautiously recommended. High impact sports such as baseball,

basketball, climbing, football, martial arts, parachuting, racquetball, running, soccer, sprinting, and volleyball are not recommended as impact loading increases the wear on an implant. However some studies have shown that moderate exercise can be beneficial for the longevity of joint replacements (Kloen *et al.*, 2000, Healy *et al.*, 2001).

The relationship between patient activity and the rate of revision is still unclear, Dubs *et al.* (1983), reported higher rates of revision for patients who did not participate in sports. This is in contrast to revision rates observed by Kilgus *et al.* (1991) who reported higher revision rates for active patients, although this did not become clear until 10 years after a primary THR. With this in mind, the need for hip replacements that function well under high activity and generate low wear rates is an issue that must be considered. Since the emergence of the principle of low friction arthroplasty pioneered by Charnley, wear has been seen as a function of time rather than as a function of use. However this view is now changing with more emphasis on the types of activities undertaken by a patient after a THR and what affects this may have on the performance of a prosthesis (Schmalzried *et al.* 2000).

Several recent studies have attempted to observe and quantify patient activity in relation to wear in THRs. "Wear is a function of use, not time" the title and conclusion of a recent study by Schmalzried *et al.* (2000) who studied both male and female subjects in order to correlate wear with activity. The study showed that gender and weight significantly affected wear, with male patients being more active than female patients. However the study was limited in that data was obtained from radiographs thus wear mechanisms could not be established. Therefore damage to femoral heads resulting from abrasive wear mechanisms, which are commonly observed in retrieved femoral heads which can also influence the wear and morphology of polyethylene debris cannot be observed through radiographs (Hall *et al.*, 1996, Elfick *et al.*, 2001), which would provide additional information into the wear mechanisms.

## 2.2 Introduction to Total Hip Replacements (THR)

Total hip arthroplasty is a major surgical operation where diseased cartilage and bone is removed surgically and replaced with a prosthesis comprised of artificial biomaterials, which will allow the joint to resume its near normal functions and freeing the patient of pain. This form of surgery has now become widely accepted for the treatment of diseased and damaged joints, and there is a plethora of designs and types of materials that are available to hip prosthesis manufacturers. Figure 2.5 is an example of a total hip replacement *in situ*.

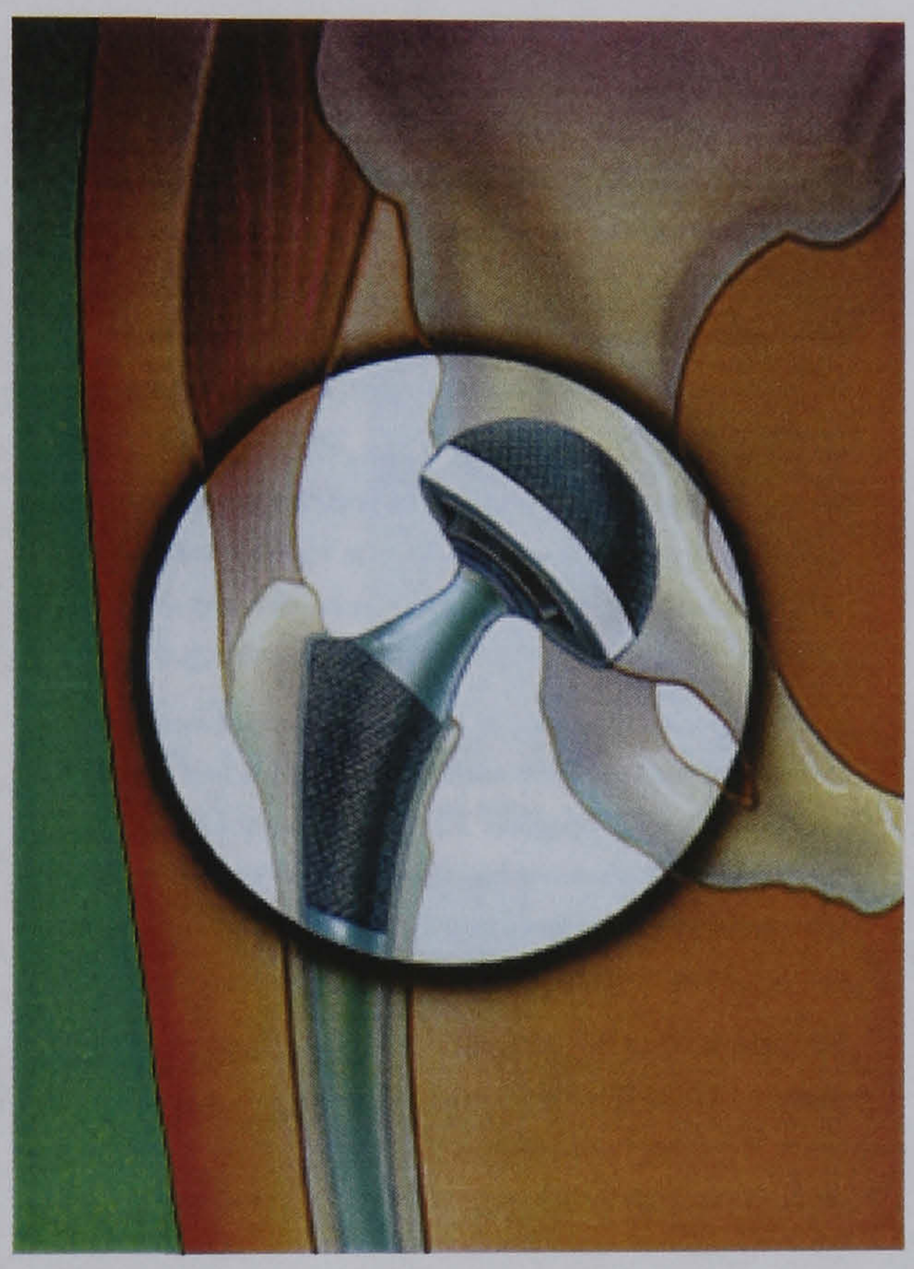

Figure 2.5: Illustrated example of a Total Hip Replacement *in situ* (http://orthoinfo.aaos.org/booklet/images/master_1.jpg)

The first hip replacement operation in England was carried out by G. K. McKee in 1951, using a ball and cup type joint. The first operation used a stainless steel femoral stem and acetabular component, which failed within the year due to aseptic loosening. The second operation used cobalt-chrome screws for fixation and lasted for 3 years. These first generation implants had 42 mm diameter heads, this was later modified to 31.75 mm and was manufactured from Vitallium™, which was the commercial name for CoCrMo alloy.

Unfortunately short term failures lead to the abandonment of metal-on-metal THR by the mid 70's (Zahiri *et al*.., 1999)

In 1962 Charnley introduced the use of High Density Polyethylene (HDPE), which was thought to have high resistance to wear and produced considerably less wear debris than PTFE. The coefficient of friction HDPE was also five times higher than that of PTFE, with the wear resistance also higher by 500-1000 times in laboratory tests (Charnley, 1979). Figure 2.6 is an illustration of the type of THR Charnley developed under the principle of low friction arthroplasty.

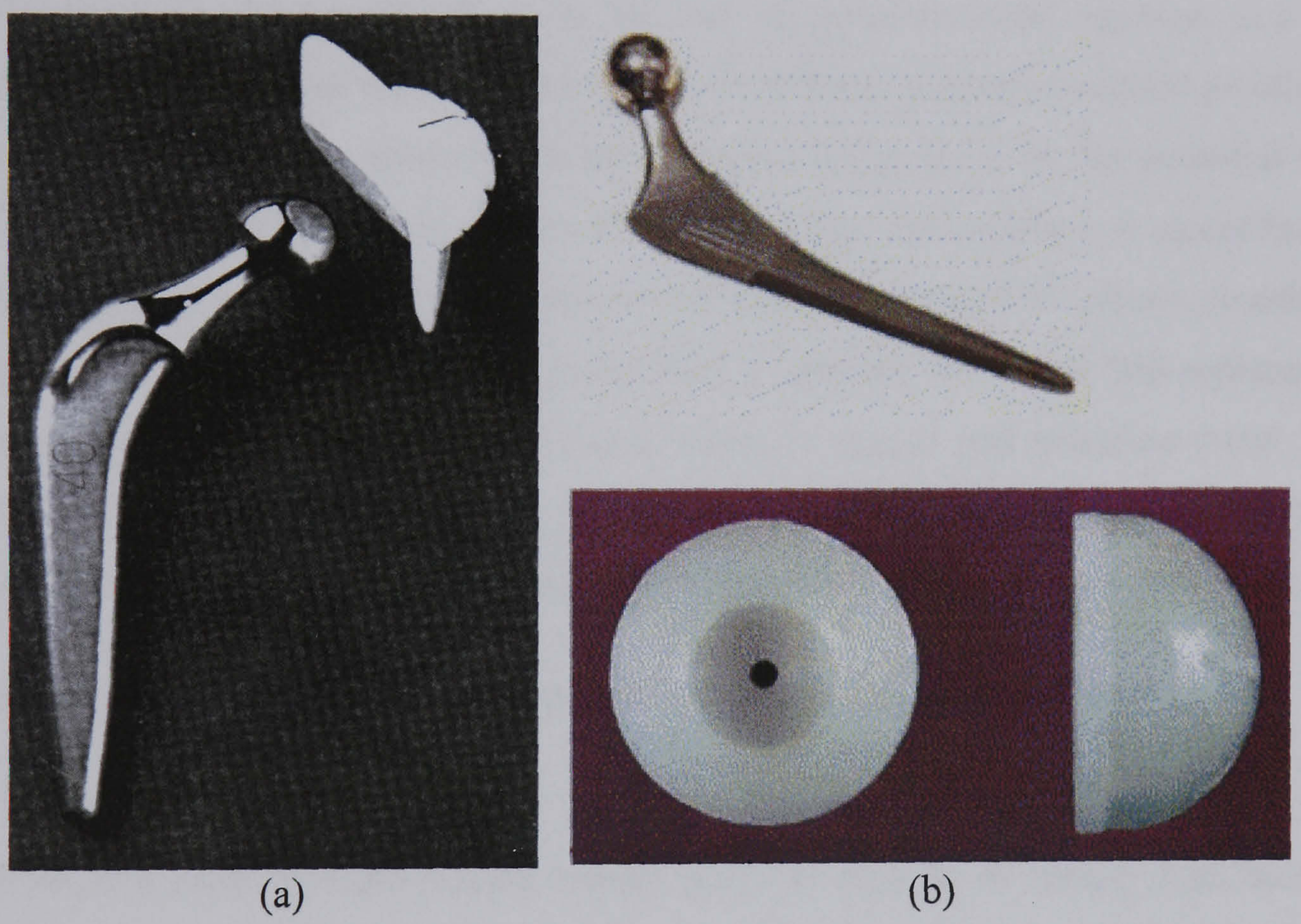

(a) (b)

Figure 2.6: (a) Cobra prosthesis developed by Charnley (1979), and (b) a modern THR using UHMWPE acetabular cup (Katti, 2004)

Today it is more common to use UHMWPE as the bearing surface with a metal head; these have proved to be very successful in the short term and also in the long term with survivorship results of up to 20-30 years (Lewis, 2001). In the UK approximately 60,645 total hip replacements are performed annually of which 95%, use a UHMWPE acetabular cup (Tennent & Goddard, 2000). Although the low friction arthroplasty principle is still

favoured over metal-on-metal implants, it is causing increasing concern due to its high rates of wear and the osteolysis caused by wear in younger and more active patients. This has spurred new research into metal-on-metal implants and its potential benefits for younger or active patients. Metal-on-metal is coming back into fashion as a result of the long-term survivorship of the first generation of metal-on-metal implants. There are now 10 year survivorship results from the Metasul™ hip prostheses, with wear rates reported to be up to 60 times less than conventional metal-on-polyethylene bearings with no failures due to osteolysis (Wagner & Wagner, 2000). Osteolysis does still occur in metal-on-metal hip replacements, but it may be a secondary reaction to other processes that are occurring *in vivo* (Beaule *et al.*, 2001). Osteolysis in the case of metal-on-metal implants is a multi-factorial process and as yet the nature of osteolysis relating to metal-on-metal prostheses is not yet fully understood. A greater concern to surgeons appears to be the potential release of ions and metallosis in patients with metal-on-metal hip replacements. A recent literature review by Campbell *et al.* (2004) has shown that the incidence of metallosis constitutes a very small percentage of the overall population of people with total hip replacements. Furthermore, no link as yet has been found between cancer and metal-on-metal THRs, however to fully understand the process of ion release, its relation to toxicity and metallosis to metal-on-metal THRs, will require long term studies that may take several decades.

## 2.3 Ultra High Molecular Weight Polyethylene (UHMWPE)

### 2.3.1 What is it?

UHMWPE is a semi-crystalline polyethylene polymer with an extremely high molecular weight. Polyethylenes are formed by addition polymerisation of the monomer ethylene. During the polymerisation reaction, chains may grow in length and form side chains. High density polyethylenes are long chain polymers with little or no side branching, the nominal molecular weight is 3 million or higher with a density of 0.958 g/cm$^3$ (Petty, 1991). It contains a simple backbone arrangement (-[$CH_2$-$CH_2$]$_n$, where n is above a million) which is flexible, therefore it is able to fold up to provide compact crystalline regions. UHMWPE molecular chains are extremely long and entangled, which provides improved resistance to wear.

molecular chains are extremely long and entangled, which provides improved resistance to wear.

### 2.3.2 Material Properties

Within the matrix of UHMWPE there are well-ordered (crystalline) and disordered (amorphous) regions. Crystalline regions contain molecular chains perpendicular to the chain folds, in the amorphous region the chains are randomly folded along with random connections, a diagram of the internal structure is shown in Figure 2.7.

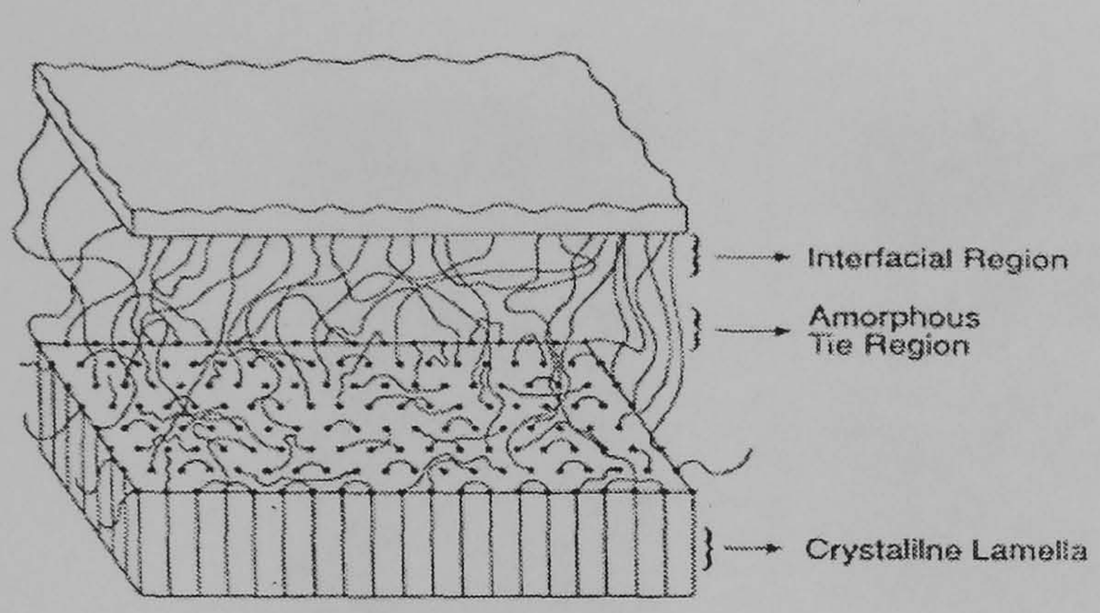


(a) (b)

Figure 2.7: A schematic illustrating the internal structure of UHMWPE (a), showing crystalline and amorphous regions (Naidu *et al.*, 1997) and (b) a TEM micrograph of the lamellae (Muratoglu *et al.*, 2001)

The mechanical properties of UHMWPE can be defined by four parameters, crystallinity, the number of tie molecules, degree of crosslinking and orientation of crystal (Wang *et al.*, 1997). Table 2.1 shows a comparison of the properties of both HDPE and UHMWPE. The high density of HDPE is due to its crystallinity, with an increased fracture toughness and a reduction in its brittleness, however it is less resistance to wear due to its low molecular weight. Figure 2.8 is a diagram illustrating the varying levels of crosslinking in both HDPE and non-irradiated and irradiated UHMWPE.

Table 2.1: Comparison of the physical properties of HDPE and UHMWPE (Li & Burstein, 1994)

| Property | UHMWPE | HDPE |
|---|---|---|
| Molecular weight (millions g/mole) | 2-6 | 0.05-0.2 |
| Density ($g/m^3$) | 930-945 | 952-965 |
| Tensile yield (MPa) | 19.3-23 | 26.2-33.1 |
| Melting point ($^0C$) | 125-135 | 130-137 |
| Elongation at break (%) | 200-350 | 10-1200 |

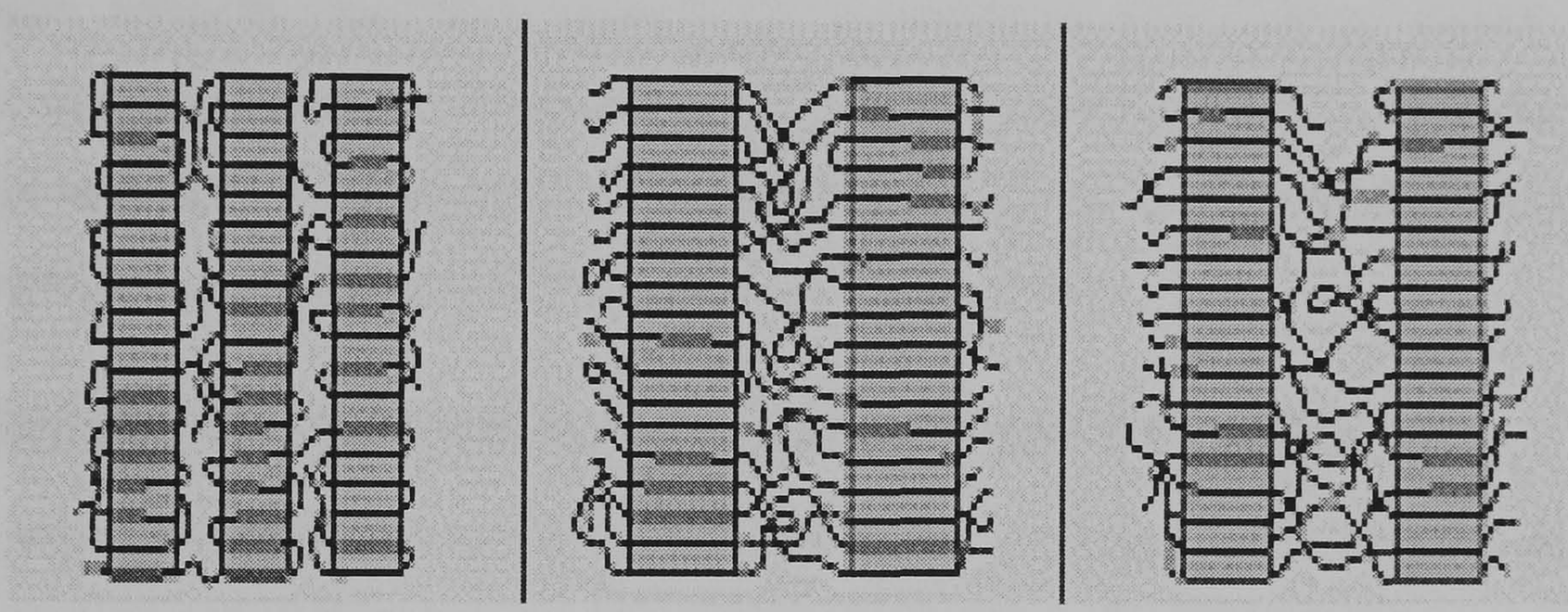

Figure 2.8: Comparison of crosslinking in HDPE, UHMWPE and Gamma irradiated UHMWPE, showing increasing levels of crosslinking due to irradiation resulting in improved wear resistance properties.

(http://www.orthoteers.co.uk/Nrujp~ij33lm/Orthuhmwpe.htm)

UHMWPE has excellent corrosion resistance, environmental stress cracking, cyclic failure with a very low coefficient of friction (Coughlan & Hug, 1986, Yamac, 1999), with the molecular weight in the range of 2-6 millions g/mole, which gives its extremely high wear resistance properties and enhanced mechanical properties. These properties do not necessarily reduce the amount of wear that may occur *in vivo* with an UHMWPE acetabular component (Yamamoto *et al.*, 2001). Irradiation and ageing of UHMWPE can increase resistance to abrasive wear, under both smooth and rough femoral heads compared to non irradiated PE (McKellop *et al.*, 1999).

### 2.3.3 Principles of Crosslinking

Cross-linking is defined as linking between molecules in the amorphous region, which restricts the molecular mobility, and thus reduces molecular orientation, subsequently increases wear resistance under multi-direction motion (Wang *et al.*, 1996, Wroblewski *et al.*, 1996, Goldman *et al.*, 1998, McKellop *et al.*, 1999). Although crosslinking also reduces the mechanical and physical properties of the polyethylene, such as toughness, tensile modulus, tensile elongation, ultimate tensile strength, yield strength, hardness, crystallinity and melting temperature compared to HDPE.

Three main methods have been used in the crosslinking of polymers, namely ionising radiation (radiation-induced crosslinking), Free Radical Generating Chemical (FRGC) (chemical- induced crosslinking) and the third method involves grafting a silane compound onto the polymer (silane-induced crosslinking) (Lewis, 2001).

### 2.3.4 Gamma Sterilisation & Radiation-induced Crosslinking

Gamma radiation sterilisation is by far the most cost effective and effective sterilisation method that is employed and is the preferred method for the majority of prostheses manufacturers.

Gamma irradiation has been used since the 1970s as one of the methods of sterilisation for UHMWPE cups. Studies have shown that gamma irradiation can reduce the wear volume (Yamamoto *et al.*, 2001). Irradiation of UHMWPE leads to a combination of chain scission and the production of free radicals (unpaired molecules) and the introduction of oxygen containing groups into the polymer molecule chain and also crosslinking. The degree of reaction is dependant upon many factors, such as the environment in which irradiation is carried out, irradiation dose, molecular weight and the crystallinity of the original material before irradiation. At 2-4 MRads, which is the radiation dose for sterilisation, chain scission dominates and there is very little crosslinking. These radicals are long-lived and are able to diffuse into or dissolve in the material during shelf storage, this can reduce the properties of the UHMWPE over time, this process also occurs *in vivo*. At higher doses, 5-

100 MRads, the free radicals that were formed can recombine to form crosslinks. Post-irradiation-induced crosslinking can eliminate free radicals that may be present.

A very high dose (greater than 5 MRads) will lead to an increase in the crosslinks within the material. McKellop *et al.*. (1998) reported that the mean wear rate of UHMWPE could be reduced by up to 87% with an irradiation dose of 9.5 MRads, however the high dose can also lead to oxidative degradation. Gamma irradiation in an inert atmosphere helps to reduce the wear rate compared to irradiation in air (Costa *et al.*., 1998). A more recent study by Muratoglu *et al.* (2001) proposed a new method for crosslinking at a high temperature of 125 °C with a radiation dose of 9.5 MRads, showing improved wear resistance and high oxidation resistance along with improved mechanical properties compared to non crosslinked polyethylene. At high temperatures, the speed of crosslinking increases leading to link up of free radicals, it also leads to an increased mobility of free radicals trapped within the crystalline region again leading to more crosslinking. However more independent studies are required to fully understand the improvements in mechanical properties using the protocol for crosslinking outlined by Muratoglu *et al.*.

### 2.3.5 Chemical-induced Crosslinking

This involves mixing a FRGC with the resin powder during the processing stage of UHMWPE. The FRGC degrades at high temperatures, which results in the production of free radicals that remove hydrogen atoms in the polymer molecules. Reactive sites are left within the chains, reactive sites from other neighbouring chains link to form the structure, so crosslinking occurs in the molten state. The drawbacks are the agglomeration of crosslinks, imperfections within the crystals will arise, and there are by products, which if not eliminated can affect the long-term stability of the material (Lewis, 2001)

### 2.3.6 Ethylene Oxide Sterilisation (EtO)

Ethylene oxide gas (EtO) has been used as a sterilisation method for over a decade (Bruck & Mueller, 1988). It is extremely toxic, and is used to neutralise bacteria, spores, and viruses. EtO can be used for the sterilisation of UHMWPE, as it contains no constituents that will react with or bind to the toxic gas. Studies have shown that using ethylene oxide gas

sterilisation does not influence the physical, chemical, and mechanical properties of UHMWPE (Wang *et al.*, 1997).

Recent studies have shown that acetabular cups that were sterilized using EtO showed notably less surface damage and delamination than gamma radiation sterilized components. The radiation sterilized components, on the other hand, had decreased elongation to failure, decreased toughness, and increased crystallinity (White *et al.*, 1996). EtO sterilization does not seem to induce surface damage, which may be exacerbated by oxidative embrittlement of UHMWPE following gamma radiation sterilization in air (Costa *et al.*, 1998). Current trends appear to indicate that gamma irradiation in an inert atmosphere is the most popular choice of crosslinking due to the relative ease of process and the degree of crosslinking that occurs.

## 2.4 Metal-on-Metal (MoM) Total Hip Replacement

### 2.4.1 Why Metal?

Metal has remerged as a material of choice for the manufacture of total hip replacements along with UHMWPE THRs. Reintroduced recently with improved alloys, design, and manufacturing. Currently metal-on-metal bearings are used for surface hip replacement and for total hip replacement. They have clinically proven wear resistance higher than that of metal-on-polyethylene bearings. The other advantages are that the metal on metal bearing couple will polish away scratches on the surfaces, the so-called self-polishing capability (Heisel H. et al, 2003). Second, total hip joints with very large femoral ball components and thin-walled large cups may be manufactured practically only from this material. Total hips with very large femoral balls may also be less prone to dislocation.

There is, as yet, one disadvantage. Metal on metal couplings produce high blood levels of metal ions, as yet, the significance of this fact is not clear.

### 2.4.2 Characteristics and properties of cobalt chrome alloys used for THRs

There are two types of cobalt chromium alloys. One is the cobalt CoCrMo alloy, which is used to cast a product and the other is the CoCrMo alloy, which is usually wrought by (hot) forging. The castable CoCrMo alloy has been used for many decades in dentistry and recently, in making artificial joints. Cobalt-based alloys are highly resistant to corrosion and especially to attack by chloride within the crevice. As in all highly alloyed metals in the body environment, galvanic corrosion can occur, but to a lesser extent than in the iron-based alloys.

Cobalt-based alloys are quite resistant to fatigue and to cracking caused by corrosion, and they are not brittle, since they have a minimum of 8% elongation. However, as is true of other alloys, cobalt based alloys may fail because of fatigue fracture (but less often than stainless steel stems). The abrasive wear properties of the wrought CoCrMo alloy are similar to the cast CoCrMo alloy. The superior fatigue and ultimate tensile strength of the wrought CoCrMo alloy make it suitable for the applications which require long service without fracture or stress fatigue. Such is the case for the stems of the hip joint prosthesis. Both the cast and wrought alloys have excellent corrosion resistance. The modulus of elasticity for the CrCo alloys does not change with the changes in their ultimate tensile strength. The values are higher than other materials such as stainless steels. The properties of various forms of cobalt based alloys are shown in table 2.3.

Table 2.2: Cobalt-Chromium Alloy Properties (Minimum properties from ASTM standards)

| Type | Condition | Tensile Strength [MPa] | Yield Strength [MPa] | Elongation [%] |
|---|---|---|---|---|
| Cast CoCrMo (F76) | | 655 | 450 | 8 |
| Wrought CoNiCrMo (F562) | Solution Annealed | 795-1000 | 240-655 | 50 |
| | Cold-worked | 1790 | 1585 | 8 |
| | Fully Annealed | 600 | 276 | 50 |

## 2.5 Wear Debris

### 2.5.1 UHMWPE Wear

Wear *in vivo* has been a major concern in the use of THRs, as particulates that are produced as a result of wear usually elicit a local host response, observed cellular response is dependent up on the size and nature of the wear material produced. The problems caused by wear debris was first identified by Charnley (1979) after the failure of the PTFE hip replacement, but believed that the erosion was linked with infection with the problem compounded by wear debris rather than wear debris being a cause.

One of the earliest studies into the cause of osteolysis was conducted by Harris *et al.* (1976) who observed the presence of osteolysis in the femur. Subsequent analysis of retrieved tissues contained macrophages and voids which were believed to have been caused by the presence of PMMA particles. More recent studies have, through the analysis of retrieved tissues, shown a granulomatous tissue reaction together with macrophages, giant cells containing particles of polyethylene, metal and PMMA. However it was still assumed that PMMA was the main cause of the inflammatory response (Petty, 1991). This led to the term 'cement disease', as the common link was the failure of fixation and the subsequent disintegration of the cement surface. Yet with the advent of cementless fixation techniques the problem was still present, which led to further problems described as metallosis in some

titanium stems, but no metallic debris were found in retrieved tissues (Schmalzried, 1992). This led to the conclusion that UHMWPE wear debris was the cause of the inflammatory response, the evidence for this has been growing since the 1980s through the analysis of retrieved tissues. Lombardi *et al.* (1989) reported the presence of osteolysis in two patients who had implants where no cement had been used, and believed it was caused by the metallic wear debris originating from the femoral head, both patients had a dense, fibrous, blackened membrane, which contained metallic debris both in the membrane and hystiocytes, however this is still an unresolved issue (Heisel *et al.*. 2003)

The biological response combined with other factors plays an important role in the success or failure of the hip implant. The current belief is that wear debris, in particular UHMWPE wear debris, produced at the articulating surface is transported into the perioprosthetic tissue, where it elicits an inflammatory response leading to phagocytosis by macrophages (Ingham *et al.*, 2000). This leads to the release of pro-inflammatory cytokines and mediators, such as IL-1, IL-6 and TNF-α which stimulate osteoclastic bone resorption which then leads to osteolysis and eventual failure of the prosthesis, this process is recognised as aseptic loosening.

### 2.5.2 UHMWPE wear debris in vivo

The size and morphology of the particles plays a very important role when considering the distribution of the wear debris around the implant. Histological studies of retrieved tissue have shown that particles less than 5 μm in size tend to be found in macrophages, where as particles larger than 5 μm are associated with giant cells, found around the femoral and acetabular components of THRs (Petty, 1991, Schmalzried, 1992).

Using tissue digestion techniques and SEM image analysis it now possible to determine the size, morphology and distribution of UHMWPE particles (Campbell *et al.*, 1994, Maloney *et al.*, 1994, Campbell *et al.*, 1995). The studies by Campbell *et al.* and Maloney *et al.* have shown particles to be present *in vivo* down to a size range of 0.3-0.5 μm, but it has now

been surmised that particles can be even smaller than this, typically in the range of 0.1 μm and smaller (Scott *et al.*, 2001).

Five major particle morphological types have been identified through retrieval studies, from sub-micron to micron sized particles. Rounded (0.05-1 μm), granular or elongated (1-5 μm), thin fibrils, which have a diameter (0.2-0.3 μm) and length (5-25 μm), platelet type particles (10-400 μm), flakes or shreds (20 μm to 7 mm). Agglomerations of particles as a result of the isolation process are also commonly observed (Campbell *et al.*, 1995, McKellop *et al.*, 1995, Hailey *et al.*, 1995, Campbell *et al.*, 1996, Wang *et al.*, 1996 Tipper *et al.*, 2000, Affatato *et al.*, 2001). Individual particles can be analysed further by way of shape descriptors, Equivalent Circle Diameter (ECD, a measure of size having units of length), Aspect Ratio (AR), Elongation (E), Roundness (R) (Mabrey *et al.*, 2001). Particles are likely to differ in shape, but may not necessarily differ in size, when comparing wear debris generated from a THR to wear debris generated from a TKR; Kobayashi *et al.* (1997) found no significant difference when comparing ECD of THR particles to the ECD of TKR particles. Figures 2.9 – 2.11 show typical particle morphologies observed during SEM analysis Figure 2.9 (a) shows agglomeration of both granular type and fibril like particles, from 0.1 to several μm in size. Figure 2.9 (b) shows elongated particles greater than 5 μm in length surrounded by many submicron sized particles which are within the bioactive range (Fisher *et al.*, 2000). Particles can be categorised according to shape, but as mentioned before they have many different morphologies.

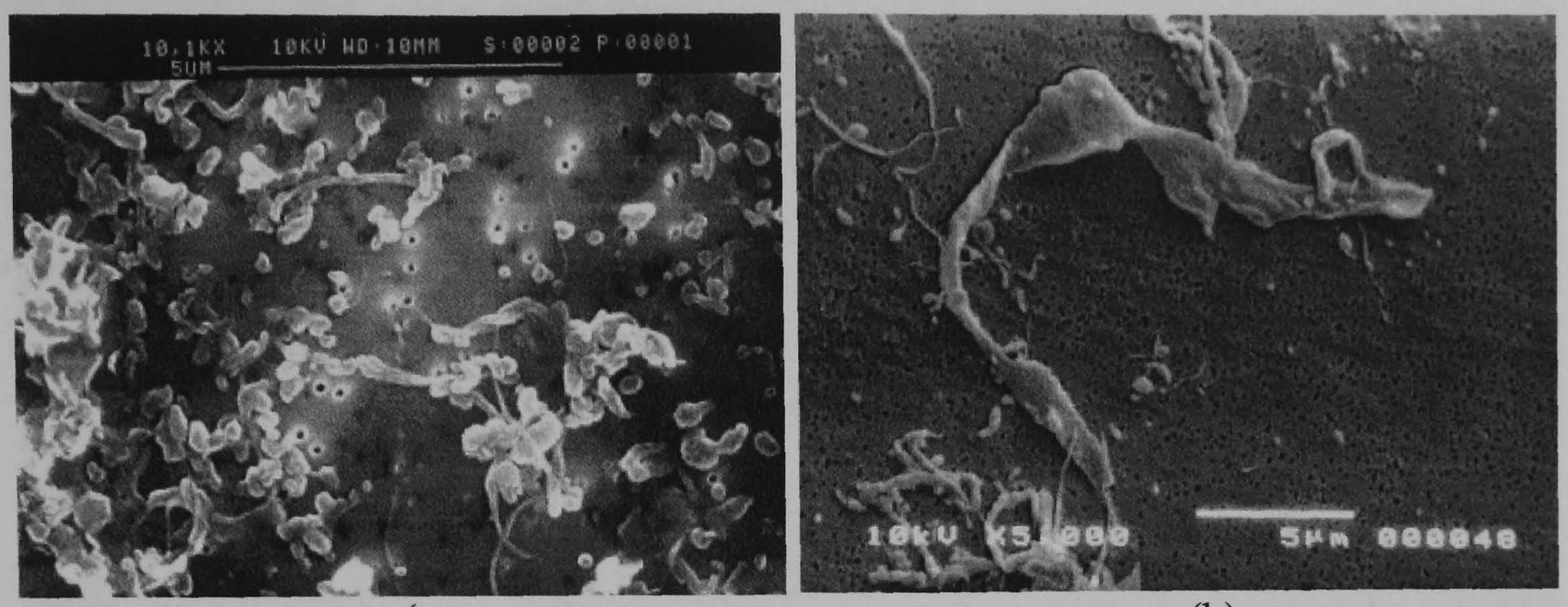


(a (b)

Figure 2.9: SEM images of polyethylene particles, (a) agglomeration of particles, (b) an elongated particle surrounded by sub-micron sized particles (All images originally obtained from Affatato *et al.*, 2003)

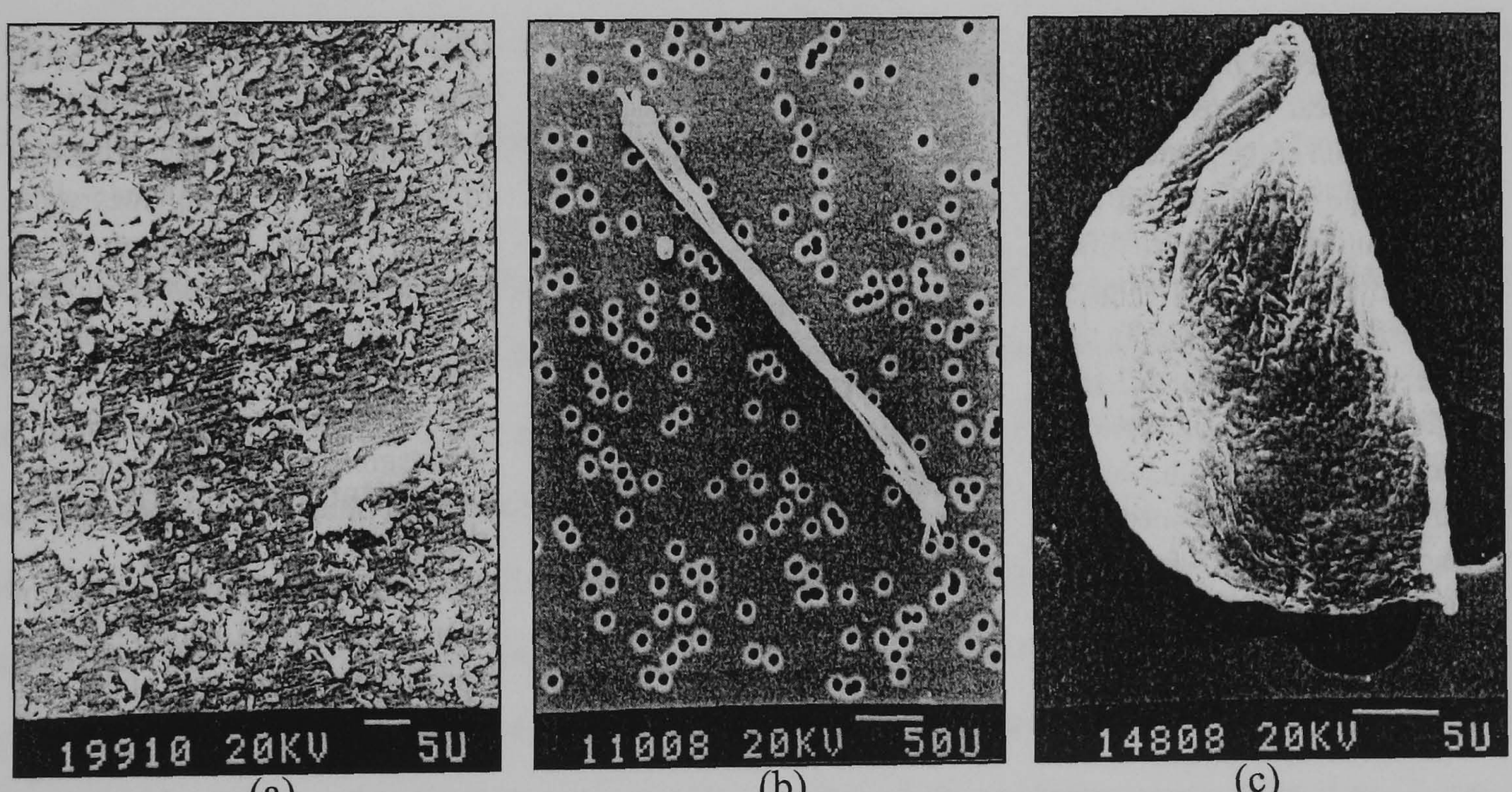


(a) (b) (c)

Figure 2.10: (a) sample of particles, (b) fibril particle, and (c) a large platelet particle (All images originally obtained from Campbell *et al.*, 1996, Hailey *et al.*, 1996, Tipper *et al.*, 2000)

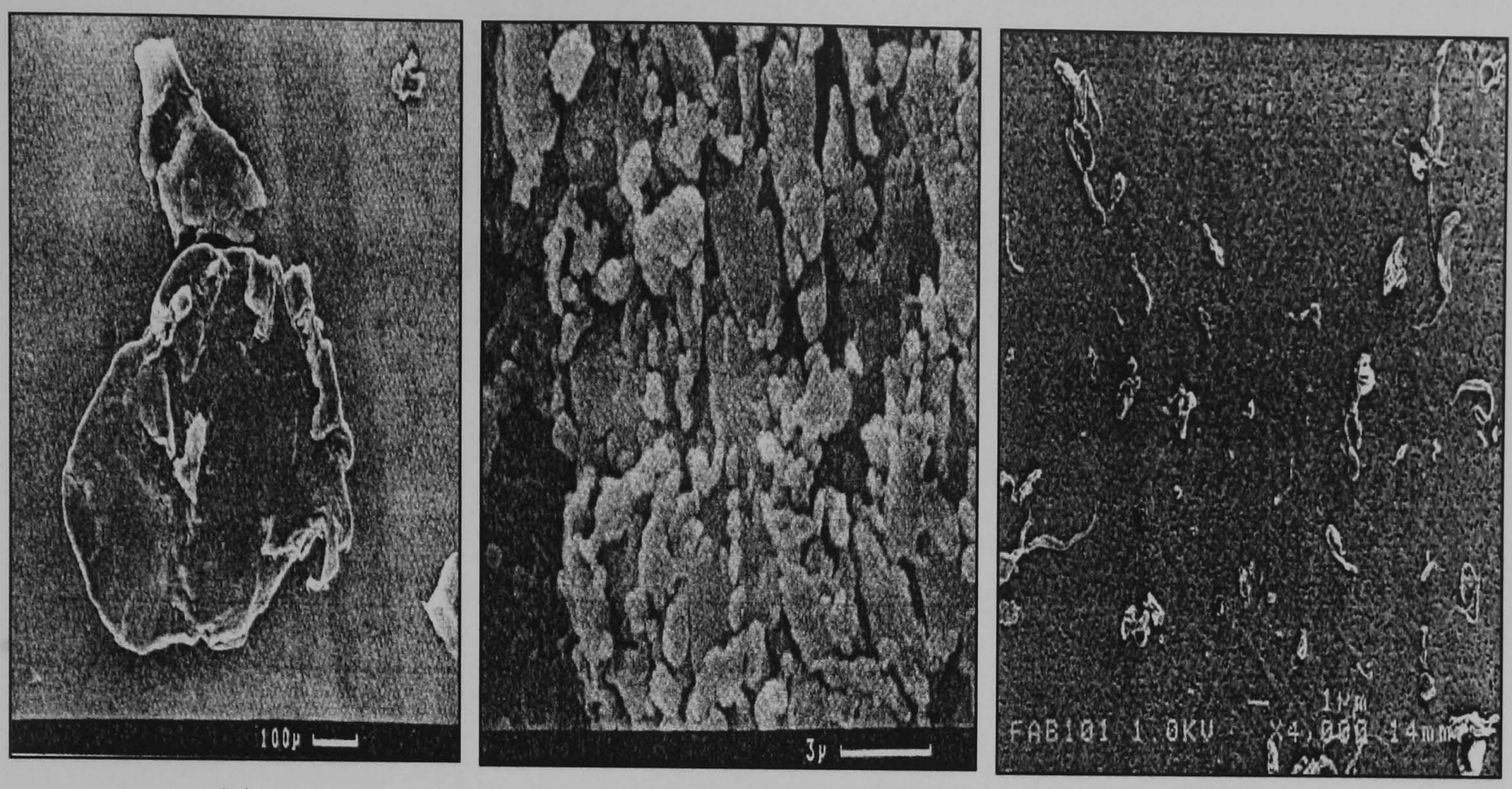


(a) (b) (c)

Figure 2.11: (a) Large platelet particle, greater than 100 μm in size, (b) sub-micron sized particles, (c) sub-micron sized particles (All images originally obtained from Campbell *et al.*, 1996, Hailey *et al.*, 1996, Tipper *et al.*, 2000)

Many studies have been conducted into the size and morphology of UHMWPE particles retrieved from perioprosthetic tissues of which a few are presented in Table 2.3. Tipper *et al.* (1997) isolated, identified and quantified particles ranging from 0.1-0.5 μm from 18 tissues obtained from the acetabulum, which were generated by the Charnley metal femoral head articulating against a non crosslinked UHMWPE. Large particles in the order of 10 μm were also present, consisting of platelets, shards and fibrils, however this was a small percentage of the overall number of particles present. A study by Shanbhag et al (1994) showed that 92 % of polyethylene particles retrieved from tissue were less than 1 μm in size, with a mean particle size of 0.53 μm. This average particle size is similar to many retrieval studies. This data is in good agreement with McKellop *et al.* (1995) who examined retrieved tissues showing similar results.

Table 2.3: Selected studies summarising the size range of UHMWPE particles retrieved from periprosthetic tissue

| Study | Mean particle size (μm) | Range of Majority of Particles (μm) | Largest Particles Observed (μm) |
|---|---|---|---|
| Shanbhag et al (1994) | 0.53 | – | – |
| Campbell et al, 1996 | 0.38 | 0.07–6.3 | 12 |
| Hailey et al, 1996 | – | 0.3–10 | 3000 |
| Hirakawa et al, 1996 | 0.8 | – | – |
| Kobayashi et al, 1997a | 0.7 | 0.3–1.5 | – |
| Kobayashi et al, 1997b | 0.4 | 0.2–1.5 | – |
| Schmalzried et al, 1997 | 0.43 | 0.2–1.2 | 13 |
| Tipper et al, 2000 | – | 0.1–0.5 | 1000 |
| Iwaki et al, 2000 | 0.68 | 0.25–1.28 | |
| Benz *et al.*, 2001 | 0.5 | 0.25–1.28 | 250 |
| Elfick *et al.*, 2003 | 0.69 | – | – |

In terms of wear particle distribution *in situ*, Schmalzried & Callaghan (1999) have suggested that the joint space was a factor in the movement of UHMWPE particles. UHMWPE particles would therefore be dispersed into the fluid in the region of the prosthetic joint, joint fluid flow will then in effect control the rate of osteolysis, as local concentration of wear debris will influence the rate of osteolysis at a given location. Other studies conducted prior to Schmalzried & Callaghan's, have shown the presence of focal-osteolysis in areas of bone loss surround the implant, demonstrating a significant correlation between volume and concentration of wear particles to the amount of bone resorption present (Revell *et al.*, 1997, Kobayashi *et al.*, 1997, Ingham & Fisher 2000).

Studies have also shown that the distribution of wear debris is not even and confined to the perioprosthetic tissue, particles have been found in the draining lymph nodes of patients. Data obtained by Mabrey *et al.*. (2001) suggests that larger particles may get trapped within the hip capsule, whereas smaller particles can migrate to other areas of tissue. Particles

trapped within the hip capsule tended to be larger, more elongated than those found in synovial fluid. Table 2.4 shows the average dimensions of particles found in three different locations surrounding the hip joint, showing the difference in particle size as particles migrates away from the articulating surface.

Whilst the sample size was small compared to other retrieval studies, there was a statistically significant difference between morphology of particles found in the hip capsule in comparison to particles found in synovial fluid, although there was no significant difference between the synovial fluid particles and the particles in the femoral canal. A possible explanation for the increased size of polyethylene particles found in the femoral canal "could be that the capsule acts as a physiological trap that holds the particles, while the smaller and rounder particles have the freedom to migrate" (Mabrey *et al.*, 2001).

The data presented by Mabrey *et al.* shows good agreement with data presented by Elfick *et al.* (2003) who also showed that particle mobility was dependent on the size of a particle. Small particles, less than 50 μm in size, were easily diffused from the articulating surface to the surround tissues, where as larger particles tended to remain near the source of particle production.

Table 2.4: Size and shape descriptors for hip capsule, synovial fluid and femoral canal tissue showing the size difference between irradiated PE particles found in synovial fluid and surrounding tissues (ECD: Equivalent Circle Diameter, AR: Aspect Ratio, R: Roundness, all dimensions are in μms, (Mabrey *et al.*, 2001))

| | ECD (μms) | AR | R |
|---|---|---|---|
| **Hip capsule** | 0.914 ± 0.019 | 1.764 ± 0.025 | 0.0642 ± 0.006 |
| **Synovial fluid** | 0.763 ± 0.012 | 1.700 ± 0.029 | 0.681 ± 0.006 |
| **Femoral canal** | 0.697 ± 0.009 | 1.577 ± 0.016 | 0.715 ± 0.005 |

Other factors, which may possibly affect particle morphology, could be the properties of the polyethylene itself. A study by Oonishi *et al.* (1992) on the effect of gamma irradiation on the clinical wear of UHMWPE acetabular cups indicated the positive effect of

irradiation in reducing wear. This is in agreement with a study conducted by Wang *et al.* (1996), who also supported the view that gamma irradiated acetabular cups showed much greater wear resistance than the unirradiated cups under a multi-directional hip simulator. The debris produced during wear simulation tended to be either fibrillar or equiaxed in shape. The fibrous wear particles were approximately 0.1-0.5μm in diameter and 1-10μm in length whilst the equiaxed particles were sub-micron in size. More recent studies by Oonishi *et al.* (2000) have shown that the size of the particle were influenced by the degree of crosslinking within the UHMWPE, irradiated PE particles tended to smaller and more rounded in shape. Yamamoto *et al.* (2001) found that in general the size and frequency of surface fibrils on the acetabular cups and the size of retrieved polyethylene particles decreased with increasing radiation. An unexpected find was the presence of large flakes of UHMWPE in the 50-150 MRads cups, thought to be a by-product of the brittle surface, this may also be due to the weakening of the crosslinking between the molecular chains in the material.

### 2.5.3 Inflammatory Response to UHMWPE wear debris in vivo

Inflammation is a response to the damage of tissue (Black, 2000), a physiological response to trauma, infection or the incursion of materials alien to the body; wear debris from UHMWPE would thereby be classed as a material alien to the body. After THA, a pseudosynovial membrane is produced around the area of articulation, a fibrous membrane may also form at the bone-cement interface (Fisher *et al.*, 2000), it has been suggested that the formation of the membrane is usually complete within two years of implantation (Bullough *et al.*, 1988). Although, on revision due to aseptic loosening, the fibrous tissue membrane tends to be thick and highly vascularised with heavy presence of macrophages, multi-nucleated giant cell and some lymphocytes, there is a direct association between the number of macrophages present and osteolysis. The likelihood of osteolysis is also increased if the number of particles exceeds $1\times10^{10}$ (Revell et al, 1997, Elfick *et al.*, 2003).

Macrophages and giant cells are a part of the phagocyte system, the principal function of the mononuclear phagocytes is in the detection of foreign material, which would then lead to phagocytosis and the eventual breakdown of the foreign material. Micro organisms are encapsulated by the macrophage and broken down, it also mediates the process of

inflammation and tissue repair. During this process cytokines are released along with other mediators of inflammation, which stimulate other cells in the defence of the host tissue and repair. Figure 2.12 shows the process of osteolysis as elicited by a foreign object.

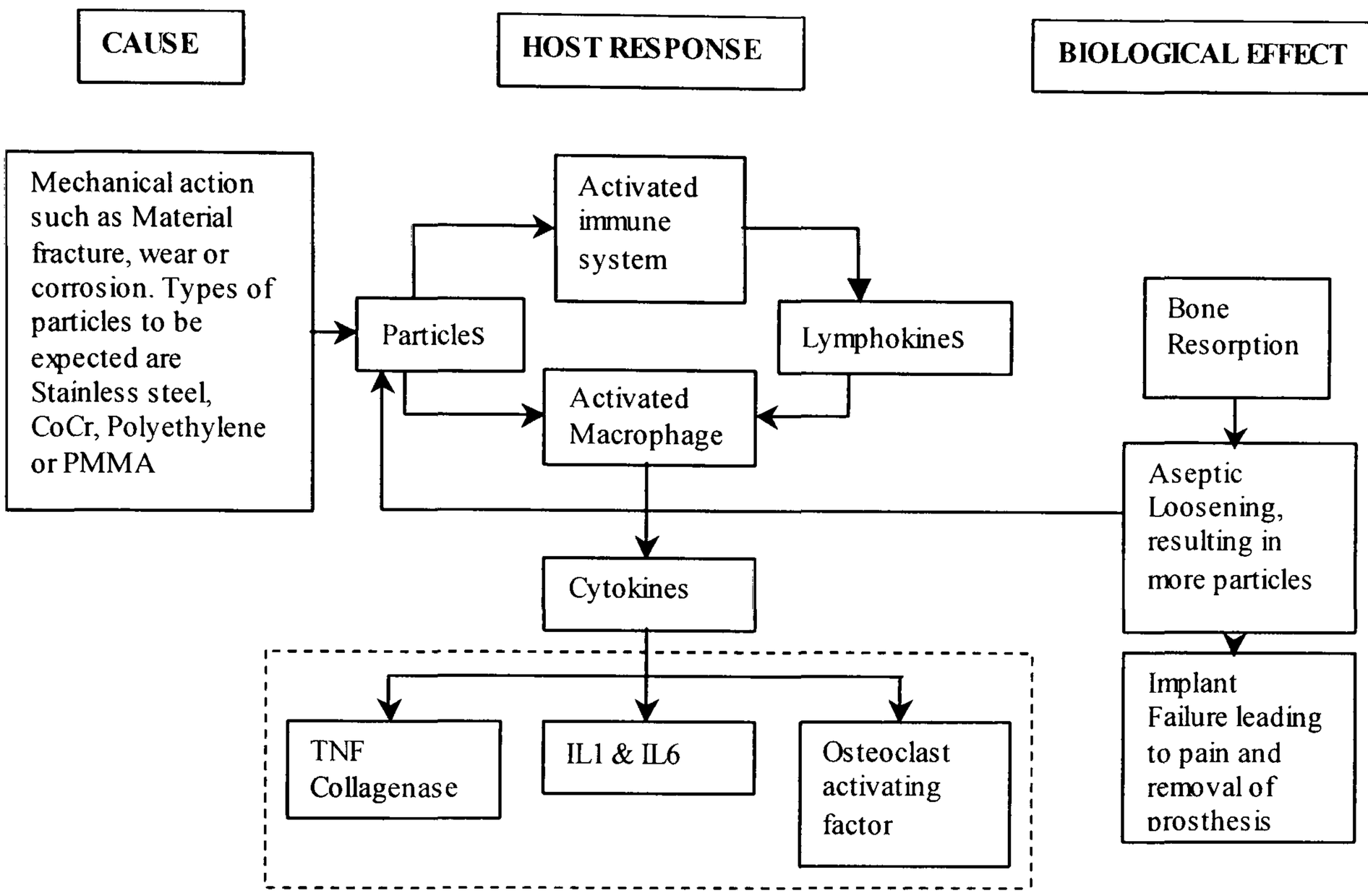


Figure 2.12: Schematic showing the process of osteolysis (Black, 2000, Fisher 2000)

The tissue will try to phagocytose or digest and degrade the particles, but this will not be possible as the particles are bio-inert, and mono-nuclear phagocytes can only combat micro-organisms. This will then lead to the release of other cytokines and mediators, which will cause the formation of a granulomatous reaction and giant cells, in effect removing the particle from its surrounding environment. The primary effect of the cytokines released as a result of the UHMWPE particles, would be the mediation of osteoclasts to resorb bone (Black, 2000). The increase in osteoclastic activity stimulated by cytokines released by phagocytes, but without the production of osteoblasts results in bone loss. Subsequently a loss of structural integrity around the implant, chiefly at the implant-bone interface, will occur leading to loosening, pain and eventual failure.

Many of the cytokines released by the macrophages influence the generation and activation of osteoclasts (Ayers, 1983, Black, 2000). Interleukin-1 (IL-1), interleukin-3 (IL-3), interleukin-6 (IL-6), tumour necrosis factor α (TNF-α), granulocyte-macrophage colony stimulating factor (GM-CSF), macrophage colony stimulating factor (M-CSF), stem cell factor (SCF) and platelet-derived growth factor (PDGF) influence osteoclastic growth and activity (Fisher, 2000). It is apparent that some form of macrophage is present in almost all tissues surrounding an implant (Goodman *et al.*, 1996). Analysis of retrieved tissues have also shown evidence of bone resorption that is non-osteoclastic, where macrophages, not osteoclasts have been identified as the principal cells in the regions of osteolysis (Revell *et al.*, 1997, Curtis & Revell, 2001).

### 2.5.4 In vitro study of UHMWPE wear particles

Biological performance has two aspects: materials response and host response, the long-established method of defining biological performance (biocompatibility) has been to monitor material degradation that occurs during *in vivo* and *in vitro* testing and the host tissue response (Black, 2000). Whilst *in vitro* tests offer a way of investigating the behaviour of cells in response to UHMWPE wear debris, it is still a limited method as it does not provide a full picture of other biological and mechanical interactions between cells and tissues in the clinical situation to be investigated (Fisher & Ingham, 2000). It has already been shown from research that UHMWPE particles of different sizes stimulate macrophages to cause bone resorption, IL-1β, IL-6, IL-8 and TNF-α have all been identified through *in vitro* tests as some of the mediators of osteolytic response (Murray & Rushton, 1990, Shanbhag *et al.*, 1995). However many investigators have failed to take into account the significance of using sterile endotoxin free particles during *in vitro* analysis, which may produce false results.

This led Mathews *et al.* (1997) to devise a more stringent method of obtaining clinically relevant UHMWPE particles, by using a tri-pin-on-disc tribometer confined in a laminar flow cabinet. Particles were collected and separated according to their size, using a sequential filtration process and cultured using mouse peritoneal macrophages in agarose gel. The study showed that the particles induced the macrophages to mediate the release of

interleukins, with a high proliferation of TNF-α cytokines. Particles within the size range of 0.1-10 μm were found to be the most biologically active (Mathews *et al.*, 1997, Tipper *et al.*, 2001). In human cell culture studies the most biologically active particles were found to be within the size range of 0.2-0.8 μm, this is not surprising since macrophages have evolved to detect and phagocytose micro-organisms, which vary in size from 0.5 μm (small bacteria) to 10 μm (yeast cells) (Fisher & Ingham, 2000).

Studies have also indicated that the neutralisation of TNF-α and other mediators significantly reduced the extent of bone resorption, which may suggest that IL-1β, IL-6 and $PGE_2$ may not be directly responsible for bone resorption and that other mediators may be involved. This is in agreement with a study carried out by Schwartz *et al.*, where mice without the presence of TNF-α in their systems showed no inflammation or osteolysis (Schwartz *et al.*, 1999).

Although studies have identified what the causes of osteolysis are, it is still unclear as to precisely how particles cause the process of osteolysis in terms of numbers and volume of debris required to initiate the process of osteolysis leading to aseptic loosening. Since the recognition that the majority of the particles produced are sub-micron in size, new techniques are being developed to allow for the analysis of these particles. Elfick *et al.* (2001) technique of LDPA is one promising technique, but more independent studies are required to verify this method.

### 2.5.5 Wear Debris of Metal-on-Metal Implants

McKee used metal-on-metal THRs in the 1960s, but early failures led to eventual abandonment of these designs in favour of the Low Friction Arthroplasty (LFA) principle developed by Charnley. However there is now a renewed interest in metal-on-metal prostheses as a result of the long-term results of early metal-on-metal designs, namely the McKee-Farrar type, some of which have survived for up to 20 years with very low wear rates (Semlitsch & Willert, 1997). Early failures of the McKee-Farrar hip prostheses were believed to have been caused by poor design, surface finish and loosening within the body,

but manufacturing techniques have improved over the years, with greater understanding of material properties and process of lubrication and wear, which has fuelled the renewed interest.

The original design of the McKee-Farrar prostheses (shown in Figure 2.13) was manufactured from CrCo, and the acetabular component was fixed into the acetabulum with screws. Due to the generation of high friction in the femoral head, cobalt-chromium-molybdenum (CoCrMo also known as Vitallium™) was later used as a result of its high wear resistance properties. Initially the acetabular cups were manufactured with the same diameter as the head, but the need for a clearance became clear so as to limit equatorial binding and excessive friction (Dowson, 2000).

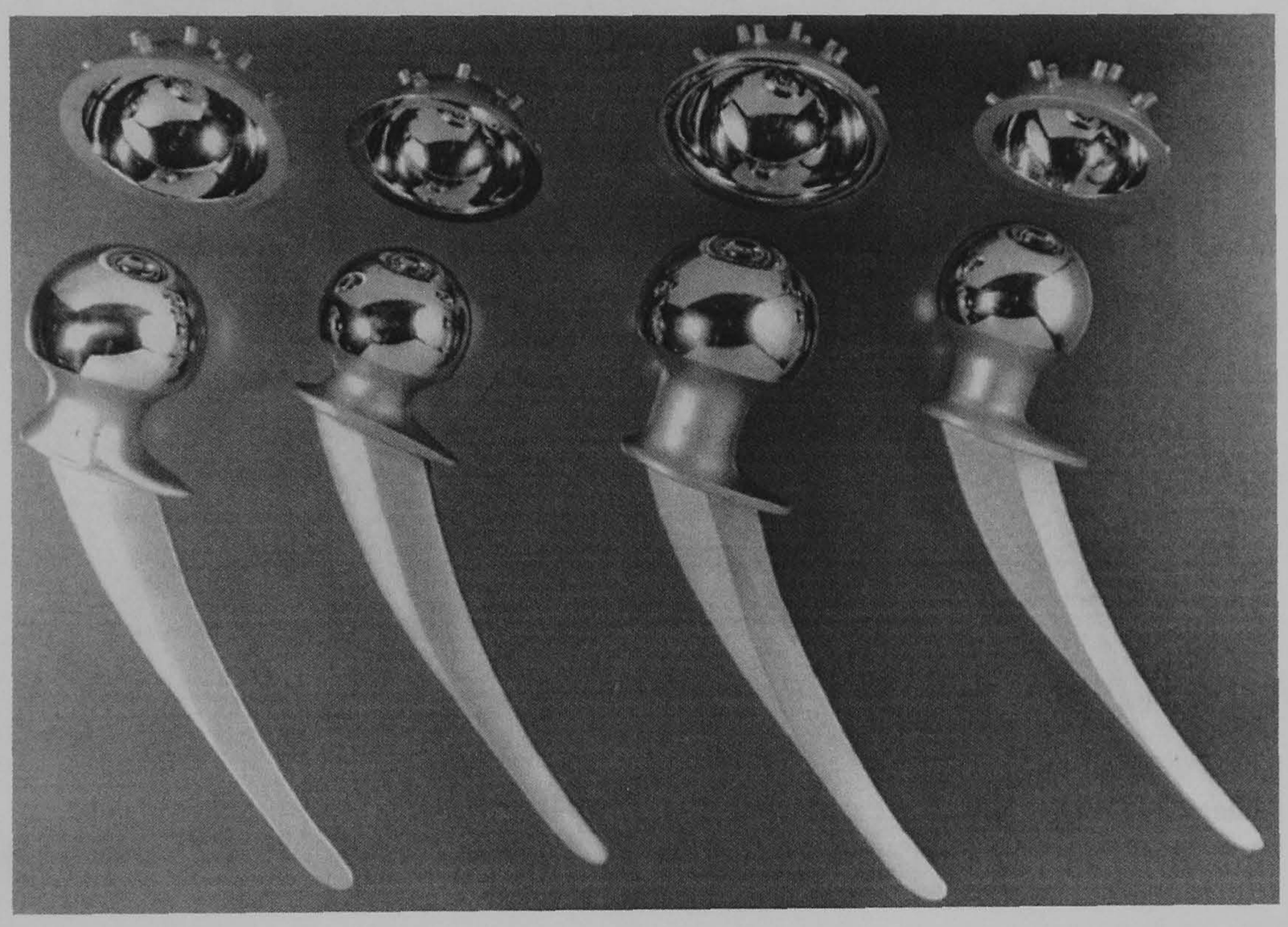

Figure 2.13: Metal-on-metal McKee-Farrar hip replacements (from http://www.midmedtec.co.uk/total_hip_history.htm)

Around the same time, Huggler and Muller started using metal-on-metal THRs in Switzerland, manufactured from cast CoCrMo alloy, initially without any clearance, but later with a clearance of 200 μm.

The long life of some metal-on-metal implants led to an investigation of revised THRs in the late 70's, studies have shown wear rates at 2-5 μm per year for Muller prostheses after 10-20 years use. Second generation metal-on-metal implants, such as the Metasul™ and the Weber-Sulzar THR, Figure 2.14, have shown a mean wear of 0.3 $mm^3$ per year (Seiber *et al.*, 1998). Although metal-on-metal have shown low wear rates in comparison to UHMWPE, it has now become clear that it is not the volume of wear that is the cause of osteolysis, rather the number of particles produced and volume concentration within a cell (Germain *et al.* 2003). Developing techniques for the measurement of distribution and number of particles will now be more important (Elfick, 2000) as this will provide a more accurate picture of what is occurring *in vivo*.

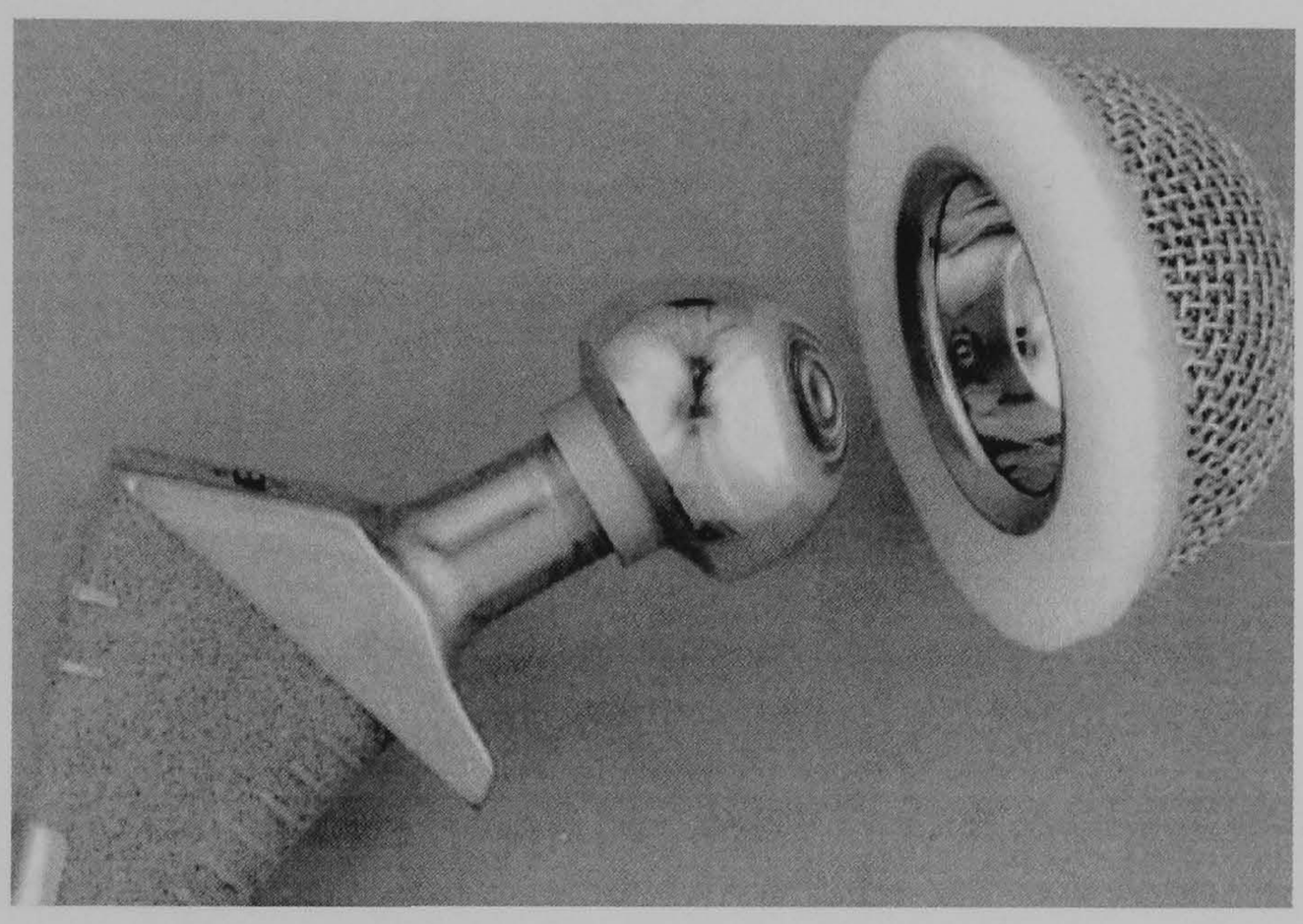

Figure 2.14: A Weber acetabular component with a CoCr Metasul articular surface and a Metasul CoCr head (Hilton *et al.*, 1996)

## 2.5.6 Metal-on-Metal Wear Debris In Vivo

The isolation of metallic wear debris is a much more difficult task compared to the isolation of UHMWPE particles. Particles can be lost through the isolation procedure, dissolution and also from the formation of particle agglomerates, making individual particles undistinguishable from one another. Catelas *et al.* has developed a technique were the particles are centrifuged and the pellets are imbedded in a resin, the advantage with this method is that the particles remain dispersed and there is a reduction in particle loss in comparison to the filtration process (Catelas *et al.*, 2001). As part of the characterisation procedure many researchers employ transmission electron microscopy (TEM), as the

resolution is much higher due to the lower beam spread of 40 nm, whereas SEM has a beam spread of 1 μm. Studies using TEM have shown particles in the size range of 10-50 nm and 10-400 nm (Doorn *et al.*., 1996, Catelas *et al.*, 2001) An example of a metal particle is shown in Figure 2.15 (Tipper, 2001). Various range of sizes have been reported for metal particles found in retrieved tissue some of which are shown in Table 2.5.

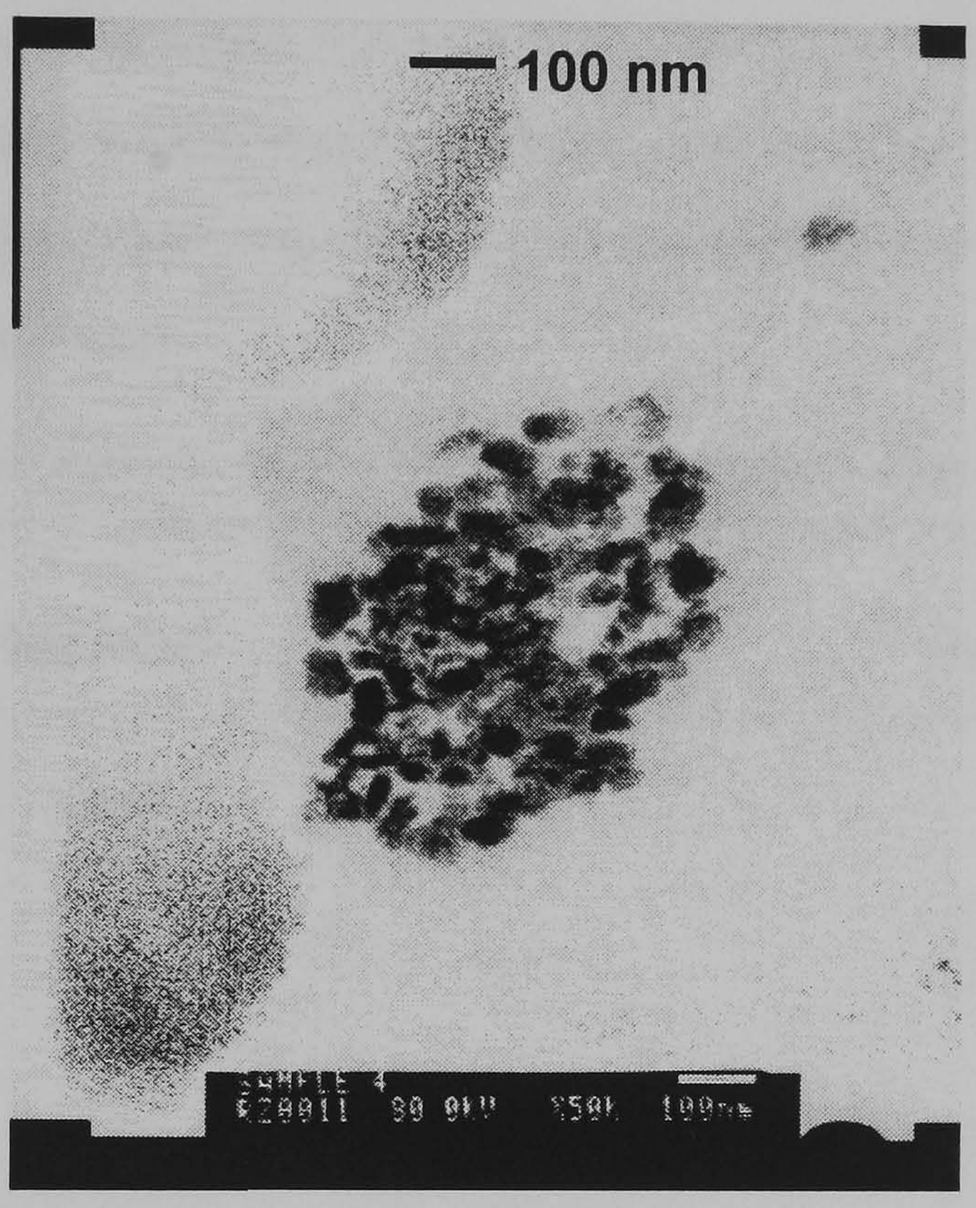


Figure 2.15: A TEM micrograph of metal particles, the majority of the particles are less than 100 nm in size (Tipper, 2001)

A recent study by Doorn *et al.* used TEM and enzymatic isolation procedures to isolate and characterise particles. Particles retrieved from tissue were found to be mostly rounded with a small percentage elongated, all within the size range of 51-116 nm. Following this it was estimate that the number of particles produced could be up to $2.5\times10^{14}$ per year, nearly two orders of magnitude greater than the UHMWPE particles produced in a typical metal-on-polyethylene prostheses (Doorn *et al.*, 1998). However TEM travels through the specimen as opposed to SEM, which provides a projected image of the particle, therefore some particles may be misclassified in their shape and size. In a recent study by Catelas *et al.*, the majority of the particles for McKee & Wright implants were more oval in shape (Catelas *et al.*, 2001a, Catelas *et al.*, 2001b).

It might therefore be inaccurate to assume that metal-on-metal particles are of a uniform size and shape (Ingham & Fisher, 2000), particles may also change shape *in vivo*, Shahgaldi *et al.* has shown that cobalt was lost at the debris site, but chromium was still present (Shahgaldi *et al.*, 1995), indicating that some form of corrosion or an oxidative process is occurring. The body fluid consists of an aerated and warm solution containing approximately 1% weight fraction of sodium chloride (NaCl), other salts and organic compounds are also present in minor concentrations. Therefore the environment into which the implant is being placed is very corrosive, in the case of metal alloys, this could lead to uniform corrosion, crevice and pitting corrosion of the implant as well the particulate debris in terms of size and morphology.

Table 2.5: Reported metal particle sizes retrieved from periprosthetic tissue.

| Study | Method | Isolation Protocol Used | Particle Size |
|---|---|---|---|
| Yamac *et al.*, 1996 | SEM | Yes | 0.3 μm |
| Soh *et al.*, 1996 | TEM | No | 0.01 to 0.4 μm |
| Doorn *et al.*, 1996 | TEM | Yes | 0.094 μm (0.02-0.958 μm) |
| Doorn *et al.*, 1996 | TEM | No | 0.08 μm (0.006-1.2 μm) |
| Doorn *et al.*, 1998 | TEM | Yes | 0.42 μm (0.006-0.744 μm) |

The estimation of particle size provided by Doorn *et al.* may also be low due to the distribution of metal-on-metal particles to other parts of the body via the lymphatic system, also found in the liver, spleen and bone marrow (Elfick *et al.*, 200, Jacobs *et al.*, 1996).

### 2.5.7 Host Response to Metallic Wear Debris

There is still a lot of debate as to whether metal-on-metal wear debris can cause osteolysis. Toxicity from metal corrosion does not seem to be a problem, metals used in orthopaedic implants have very low corrosion rates and are found as trace elements within the body, and therefore the body is able to deal with them. Increased Co and Cr levels have been observed

in patients, but well below the toxic range, indicating that the correct function of metal-on-metal implants can be observed by evaluating the Co and Cr levels in urine and serum for patients with metal implants. It is still unclear as to whether metal THRs can cause cancer, as there is no conclusive evidence linking metal THRs with carcinogenecity (Wagner & Wagner, 2000, Heisel *et al.*, 2003).

To date there has been no direct link between the second generation of metal-on-metal prostheses with osteolysis (Seiber, 1998). Osteolysis in metal-on-polyethylene prostheses is usually detected five years from implantation, and some Metasul$^{TM}$ implants have been in use for up to 10 years. Manley and Serekian (1994) have reported the presence of metal particles in osteolytic lesions, but it is still uncertain as to whether the metal particles were a factor in the formation of the lesions. The only evidence of osteolysis was in two hips with calcar resorption, from a study of 56 Metasul$^{TM}$ THRs (Manley & Serekian, 1994). Osteolysis in metal-on-metal implants seems to be a secondary effect.

Metal-on-metal prostheses used by Muller showed no signs of migration but the roof of the acetabulum was often sclerotic. Histological samples obtained from the capsule did not indicate the presence of macrophages or giant cells, which are often associated with polyethylene wear debris. The capsule surrounding the implant was described as of normal thickness and showed no signs of inflammation during surgery (Muller, 1995).

Histological studies of tissues retrieved from revised metal-on-metal prostheses have shown a mild to moderate macrophage penetration by metal debris within macrophages as agglomerates or singly in the cells, and tissue areas of necrosis associated with small amounts metal particles have also been observed (Seiber *et al.*, 1991, Fisher & Ingham, 2000).

Another concern that has arisen is the distribution of metallic debris throughout the rest of the body. Metal debris dispersed to lymph nodes is not inert and causes changes within those organs (Bauer *et al.*, 1993). There have also been reports of necrosis and some

fibrosis in lymph nodes in response to the presence of metal particles. Tissues with a high concentration of metal particles, such as the lymph node, the heavily laden macrophages might become necrotic. This has led to some concerns of an increased risk for the development of tumours of the lymphatic and haematopoietic system from metallic wear particles (Athanasou, 2002)

Another issue of concern is the development of hypersensitivity to the metal ions released, namely metal associated hypersensitivity with types IV (slow reaction over a 48 hours period) and I (immediate response). For either to occur the metal ion must bind to a protein or cell. The immune response begins with the processing of the organometallic complex by an antigen-processing cell. An antigen-antibody reaction may cause local or systemic reaction, with symptoms, such as wheal-and-flare reaction on skin contact. There is evidence that link metallic debris with hypersensitivity in some individuals, but fortunately this is a very low percentage (Petty, 1991)

### 2.5.8 Metal-on-metal wear debris in vitro

In light of the inflammatory response of UHMWPE particle both *in vivo* and *in vitro*, studies have been carried on metallic particles since the re-emergence of metal-on-metal implants.

A study by Bendall *et al.* (1996) has been shown that cobalt-chromium (Co-Cr) particles (0.5-5.0 μm) can elicit the production of TNF-α by human synoviocytes. Although the study indicates that Co-Cr can cause an inflammatory response, it did not taken into account that metallic particles from metal-on-metal prostheses are on the whole sub-micron in size going into the nanometer range. The bioreactivity of particles has been shown to depend on their size, composition and concentration (Archibeck *et al.*, 2000). The size of the metal particles show that they have the potential to enter many different cell types, as well as being phagocytosed by macrophages. Therefore it is necessary to consider the effects of metal wear debris on the range of cells in the perioprosthetic environment (Fisher & Ingham, 2000).

A recent *in vitro* study by Germain *et al.* (2003) showed that cell response is dependent upon the size of the particle and volume concentration, particle volumes of 50 and 5 $\mu m^3$ per cell were found to be cytotoxic. Assuming that a particle is a sphere, 30 nm in diameter, a 50 $\mu m^3$ volume of metal wear debris in a single cell would in theory contain an estimated number of particles in excess of 3.5 million, however the majority of particles will disseminated throughout the body, therefore a single cell is unlikely to contain so many particles. Although the number of particles generated *in vivo* is in excess of this number and in light of the research conducted by Germain *et al.*, it would be safe to assume that metal wear debris has the potential to cause osteolysis at a given concentration and number.

*In vitro* tests have looked at fibroblasts, osteoblasts, endothelial cells, macrophages and lymphocytes. Cobalt has been shown to produce more cellular toxicity than other elements (Petty, 1991) and led to altered phagocytic activity and cell death (Archibeck *et al.*., 2000). Cobalt at high dosage leads to an increase in cell death. Haynes *et al.*. (1998) showed that cobalt-chromium particles, at physiological concentrations, caused human mononuclear phagocytes to produce low levels of TNF-α, M-CSF, osteoclast differentiation factor (ODF-regulates osteoclast lifecycle), osteoclast differentiation factor receptor (ODFR) and osteoprotogerin (Opg-essential for bone resorption, inhibiting the differentiation and activation of osteoblasts). This study showed that cobalt-chromium wear particles might stimulate macrophages leading to the release of mediators of osteoclast differentiation, ODF, ODFR and Opg. Opg generated *in vivo* in response to wear particles will have an effect on the extent of osteoclastic differentiation and bone resorption. The secondary effect of that would be aseptic loosening.

These studies do not provide any conclusive evidence as to whether metallic particles have a carcinogenic effect on the human body, but they do indicate that cobalt ions may constitute a hazardous risk for cobalt-chromium metal-on-metal implants (Archibeck *et al.*, 2000).

## 2.6 Ceramic-on-Ceramic

Alumina-on-alumina total joint replacements have been in use since 1972. Alumina ceramic THRs have now been in clinical use, mainly in Europe, for more than 25 years, and have been improving ever since. Problems such as femoral head fractures and breakage of the ceramic cups have been reduced by improvements in design and the quality of the alumina ceramic used in production. Impingement between the acetabular cup and the femoral neck have been associated with wear and osteolysis, and stripes have been found on the femoral head (Stewart *et al.*, 2001)

### 2.6.1 Distribution and morphology of Ceramic-on-Ceramic wear debris in vivo

In comparison to the study of metal-on-metal wear debris, very little is known about the accumulation of ceramic wear debris in perioprosthetic tissues and the distribution of alumina particles to sites surrounding ceramic prostheses. Histology studies that have been carried out on the pseudo synovial membranes and soft tissues retrieved from the acetabular cup-bone interface and the femoral stem-bone interface of both cemented and non-cemented ceramic on-ceramic prostheses, have shown sharp-edged polygonal yellow-brown particles. Particles of up to 5 μm in diameter and smaller granular debris have been observed inside macrophages. A study carried out by Lerouge *et al.* (1996) identified particles by SEM highlighted a mean size of 0.44 ± 0.25 μm. Analysis carried out Yoon *et al.* (1998) of particles isolated from three soft tissue samples from loosened Mittelmeier non-cemented acetabular cups confirmed submicron sized alumina particles, of mean size 0.71 μm. Alumina ceramic wear particles generated *in vivo* are variable in their size and range from about 0.1 to 7 μm.

### 2.6.2 Host response to Ceramic-on-Ceramic wear debris

Very little information is available concerning osteolysis with ceramic articulations, and generally osteolysis has been limited to cases of massive wear. Huo *et al.* (1995), found no indication that would indicate the presence of osteolysis after a mean implantation time of 9 years for non-cemented components. This is in contrast to finding by Yoon *et al.* (1998)

who concluded that ceramic wear particles could stimulate a foreign body response, leading to peri-prosthetic osteolysis. Articulating surfaces of failed prostheses showed cracking and wear scars on the weight-bearing surface. In light of this it is still unclear as to whether there is definite connection between ceramic particles and osteolysis, or rather the volume of ceramic particles that would lead to osteolysis. Particles will elicit a host response, but at what stage of the prostheses lifetime is still a point of debate and research. A recent literature review by Campbell *et al.* (2004) has shown that the incidence of osteolysis is rare, however if there is a catastrophic failure of the ceramic replacement, then the chances of osteolysis are substantially increased. Other studies reviewed by Campbell *et al.* that have reported Osteolysis in ceramic implants, have shown that Osteolysis was linked more closely with loosing of implants rather than the particles generated during wear.

## 2.7 Wear

### 2.7.1 Mechanisms of Wear

Wear can be defined as the material lost as a result of fatigue, or motion between two counterfaces, and importantly it is recognised that wear, with regards to THRs, is a function of use, not time (Schmalzried *et al.*, 2000).

The two main mechanisms of wear occurring in THRs are known as adhesive and abrasive wear, occurring microscopically (0.1-1 μm) and macroscopic wear (1-100 μm). Microscopic wear would lead to sub-micron sized particles, where as macroscopic wear would result in large particles such as fibrils and large plate like particles. Other forms of wear can also occur through fatigue and oxidative corrosion, which is a chemical process rather than a mechanical process. All the above mentioned forms of wear can occur successively or through a combination of all four modes (Wang *et al.*, 1995)

Abrasive wear is damage to a counterface caused by motion with a surface comprising of hard asperities or particles trapped between the two counterfaces. In the case of metal on polyethylene THRs, cutting or ploughing as a result of scratches present upon the articulating surface would remove material from the polyethylene counterface.

Additionally, third body particles trapped between the two articulating surfaces can also further cause damage the femoral head. Damage to the femoral head by third body particles, would result in rough counterface, shown in figure 2.17(a), which in turn would lead to more abrasive wear thereby increasing the volumetric wear, in turn increasing the number of wear particles (Rieker *et al.*, 2001).

Metal-on-polyethylene THRs function in a boundary or mixed lubrication regime, where asperity contact is unavoidable resulting in wear at the counterface. Under these conditions load transmission is achieved by asperity contact and by the hydrodynamic action of the fluid film. Prediction of lubrication regimes can be achieved by using the soft elastohydrodynamic lubrication theory proposed by Jin *et al.* (1997). Results using this theory are presented in Figure 2.16, which shows the influence of varying radial clearance on the film thickness for metal-on-metal and metal-on-polyethylene counterfaces. The figures show that the film thickness decreases as radial clearance increases, and are similar for both combinations of materials. These results suggest that radial clearance is an important parameter for the lubrication of THRs. As implants wear, radial clearance becomes more important, particularly metal-on-metal implants, where high radial clearances can result in increased wear.

Figure 2.17(a) is an example of damage to the femoral head as a result of third body particles. Figure 2.17(b) shows an SEM image of damage to the femoral head, note the multidirectional nature of the scratches observed (Bragdon *et al.*, 2003, Wang & Essner, 2001). Abrasive wear has been reported to be the most common form of wear experienced by metal-on-metal implants, it is believed that this form of wear is caused by hard particles such as carbides that may have been removed from the articulating surface and become trapped and may also cause the elevated levels of wear seen during the wear in phase (Medley *et al.*, 1996, Wang & Essner, 2001, Bragdon *et al.*, 2003, Cawley *et al.*, 2003).

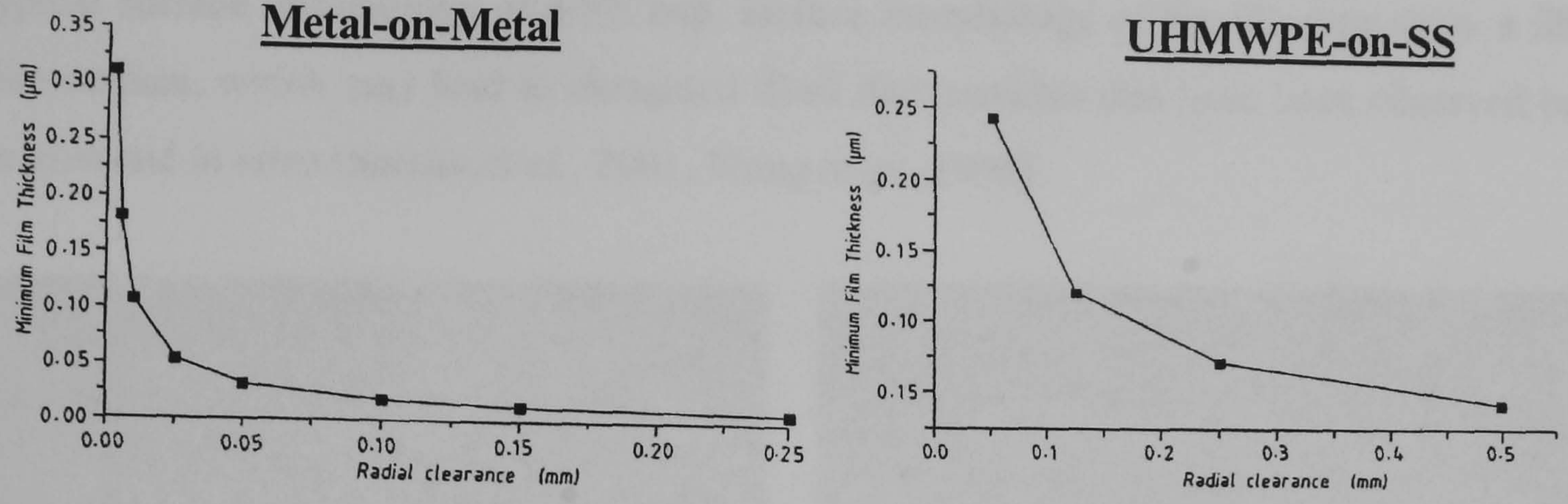


Figure 2.16: Predicted film thickness for metal-on-metal and metal-on-metal hip implants (Jin *et al.*, 1997)

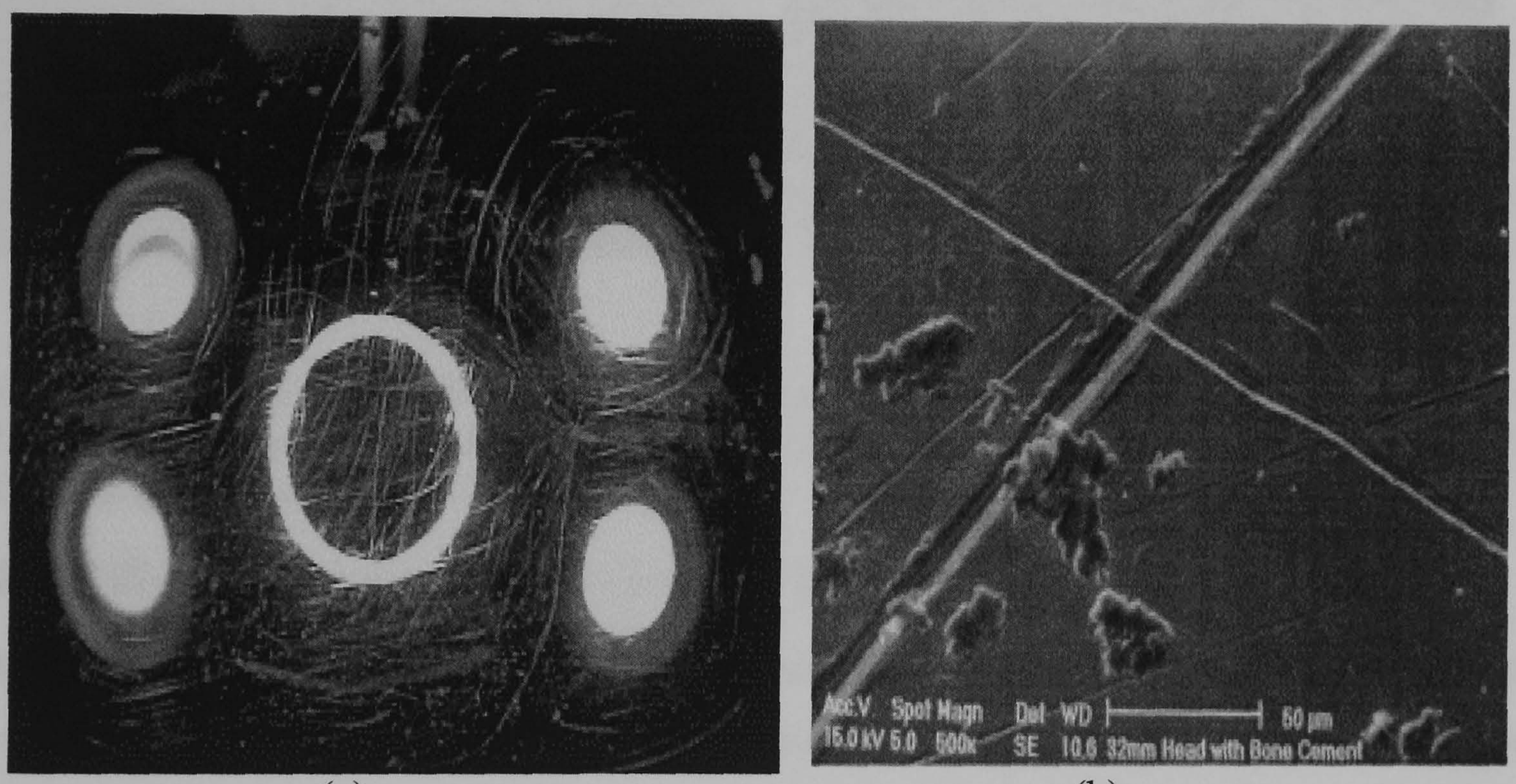


(a) (b)

Figure 2.17: (a) shows damage to a femoral head as a result of third-body wear, and (b) SEM image of a CoCr head damaged by PMMA particles (Bragdon *et al.*, 2003, Wang, 2001 respectively)

Adhesive wear occurs when asperities adhere together, if the contact pressure is high, a layer of the soft material, such as PE, in metal-on-UHMWPE THRs, can deform plastically and asperities may bond to the harder counterface. Therefore once the shear stress at the interface becomes greater than the shear strength of the softer material, adhered asperities can be removed, becoming third body particles. Adhesive wear along with abrasive wear is

a common feature polyethylene based TJRs. Figure 2.18(a) and Figure 2.18(b) show the typical surface morphology of a PE cup, surface morphology of the PE cups show a fibril like surface, which may lead to elongated fibril like particles that have been observed both *in vivo* and *in vitro* (Saikko *et al.*, 2001, Wang *et al.*, 1995)

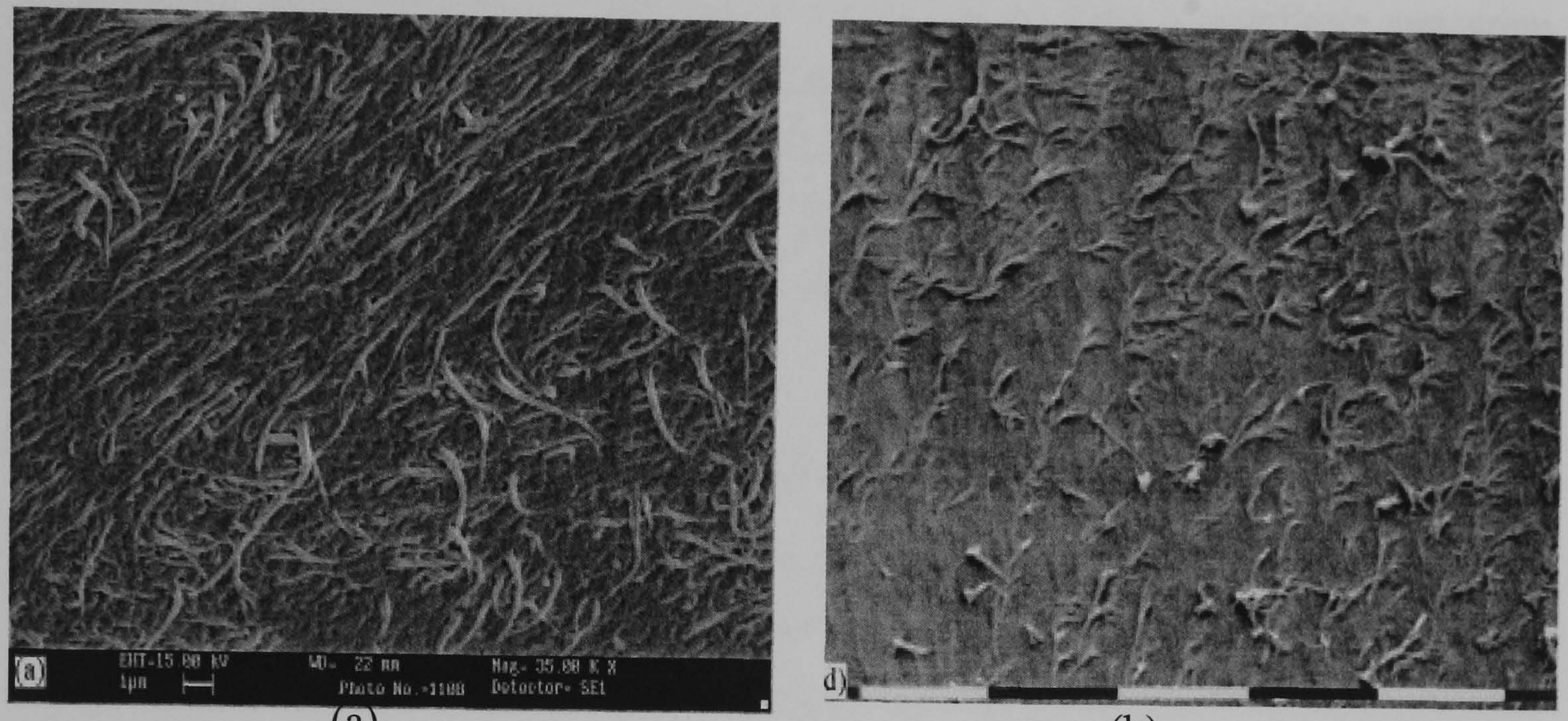


(a) (b)

Figure 2.18: (a) SEM image of PE cup worn against a CoCr head for 3 million cycles in a hip simulator and (b) an SEM image of PE cup worn against CoCr head *in vivo* for 97 months. (Saikko *et al.*, 2001)

## 2.7.2 Wear Measurement in vitro and in vivo

Wear rates are measured in terms of linear wear and volumetric wear, both are required in order to understand the aspects of aseptic loosening. Linear wear is measured through the understanding of penetration depth and is useful in the investigation of mechanical failure of THRs *in vivo*.

Also important is the gravimetric wear measurement, which is an indicator of the amount of wear debris produced. *In vivo* calculations of wear must be calculated from linear penetration of the femoral head into the acetabular cup. Weight loss measurement techniques are not possible for *in vivo* cups, as soak controls cannot be used, this technique is only possible for *in vitro* tests. In gravimetric wear calculations, a loaded and unloaded soak control must be maintained during tests, to take into any account any differences in

absorption that will occur, due to the hydrophilic nature of UHMWPE (Saikko, 1996). Using soak controls eliminates further errors in calculations of wear as fluid absorption can be accounted for, through changes in weight for the loaded and unloaded soak controls.

Volumetric wear measurements can also be carried out by using a coordinate measuring machine (CMM) or shadowgraphs. The volumetric wear is calculated by subtracting the average volume changes from the average volume changes in the creep stations (Bowsher, 2001). A comparative study carried out by Smith & Unsworth (1999) showed that there was no statistically significant difference between gravimetric and volumetric techniques in measuring wear rates for *in vitro* tests.

### 2.7.3 Reported clinical wear of Metal-on-Polyethylene implants

UHMWPE has been paired with metal femoral heads for a number of years now. This combination has been shown to be more wear resistant than conventional PE, crosslinking techniques have also improved wear resistance and reduced the effects of oxidation (Buford & Goswami, 2004). A number of studies have investigated wear of metal-on-polyethylene of which a few a shown in Table 2.6.

Table 2.6:Wear rates for metal-on-polyethylene *in vivo* (Buford & Goswami, 2004)

| Study | Femoral Bearing | Head Diameter (mm) | Average wear rate (mm/yr) |
|---|---|---|---|
| Ohashi *et al.*, 1989 | CoCr | 32 | 0.04 |
| | Stainless steel | 28 | 0.04 |
| Okumura *et a.*, 1989 | Stainless steel | 22 | 0.14 |
| Livermore *et al.*, 1990 | Stainless steel | 22 | 0.13 |
| | CoCr | 32 | 0.10 |
| | Stainless steel | 28 | 0.08 |
| Woolson & Murphy, 1995 | CoCr | 28 | 0.14 |
| Bankston *et al.*, 1995 | CoCr | 28 | 0.05 |
| Madey *et al.*, 1997 | Stainless steel | 22 | 0.09 |

Although reported clinical wear rates are important they must however be viewed as a general comparison between the different forms of THRs, since the recognition that wear is a function of use rather than time as previously thought. Therefore it would be useful for the future study of wear to take into account not only the patients general details such as weight, age and implantation time, but also the types of activity a particular patient may be involved in, as this will no doubt affect wear and success of the THR in the long term.

### 2.7.4 Reported clinical wear of Metal-on-Metal implants

Assessment of wear of metal-on-metal implants is very difficult *in vivo* due to the extremely low wear seen in retrieved metal-on-metal implants. Many rely on implant retrieval and tissue samples from revisions to evaluate the performance of MoM implants, other studies have also looked at the levels of ion release in patients to assess the performance of MoM implants (Jacobs *et al.*, 1996, Lhotka et al, 2003)

A study by Weber (1999), presented the results of 865 Metasul™ THRs that were implanted between 1988 and 1997. Out of the 865 implants, 2.5% of them had failed at 10 years. The reasons for failure were put down to the incompatibility of the cement used with the titanium stems and also concluded that poor surgical technique may have been a factor in the failure of the implants that failed, nonetheless the results show that there is a 97.5 % survival rate after 10 years of implantation.

Wagner & Wagner (2000) reported the results of 70 MoM implants, with a follow up time of 2 to 5 years, reporting that 96 % were still performing well according to the Harris hip score. No osteolysis was found either at the stem region or cup region. An earlier study by Dorr *et al*. (2000), showed similar results to that of Wagner and Wagner, however analysis of retrieved tissue did indicate the presence of metal debris, although no sign of osteolysis was detected. Schmidt *et al.* (1996) reported that out of 40,000 metal-on-metal implants, 0.1 % had to be revised due to loosening. The maximum time *in situ* was 5 years with an average linear wear rate of 2-5 μm/year, early revisions showed a linear wear rate of 15-20 μm/year, indicating that there is initial wear in phase, where wear is significantly higher than during steady state conditions.

## 2.8 Role of Surface Topography

### 2.8.1 Surface Topography in Relation to THRs

Surface profiles are most commonly mapped out by using a surface profilometer, with a stylus to obtain a profile of the counterface. Measurements are taken over a defined cut-off length and an average of various parameters are obtained, which characterise the surface, providing information of the surface at a macro level. The most common parameters used are $R_a$ (arithmetic mean of the roughness height) Ra is used for detecting general variations in overall profile height. $R_q$ (root mean square of the roughness height), $R_t$ (maximum roughness height between a peak and a valley) and $R_p$ (the distance between the mean line and the highest peak present). Although $R_a$ provides a useful measurement of the surface roughness, this parameter alone will not itself provide a meaningful picture of what is occurring at the counterface, and when it changes, it usually signifies that something in the process has changed.

Because Ra is an average, defects in the surface do not greatly influence the results, therefore this is not useful in detecting defects. However $R_a$ combined with $R_p$ would provide a more detailed representation of surface texture. $R_p$ in such cases would be the most important parameter as it is the peak scratch height that is measured, and therefore comes into contact with the acetabular component, creating the greatest damage. Care must be taken as to which parameters are best used to describe the surface, Hall *et al.* (1997) has shown that profile peak area along with $R_p$ and $R_a$ provide a better understanding of the scratches found on explanted femoral heads and the effects of surface texture on the upon wear.

Surface topography of the femoral head will have a direct effect on the wear volume, wear rate and the type of wear that occurs both *in vivo* and during *in vitro* tests. Many studies have been carried out to determine the extent and effects of surface topography of the femoral head upon the acetabular component. Table 2.7 shows a summary of recent studies where retrieved heads were examined and measured for the levels of surface roughness present. The most severe case of roughness reported is by Tipper *et al.* (2000) with an $R_a$ of

4.3 μm for stainless steel heads, however this is not representative of the bulk of retrieved THRs. A comprehensive review by Bowsher has shown that femoral head roughness does not usually exceed 0.4 μm (Bowsher, 2001).

Table 2.7: summary of published surface topography of retrieved heads from metal-on-polyethylene prostheses (Bowsher, 2001)

| Study | No. of cases | Mean implant time (yrs) | Roughness range or max. | $R_p$ Range or maxima |
|---|---|---|---|---|
| Wroblewski et al, 1992 | 4 | 20 | $R_a$ 0.008 μm to 0.102 μm | – |
| Isaac et al, 1992 | 71 | 9 | $R_a$ 0.013 μm to 0.4 μm | 0.30 μm |
| Jasty et al, 1994a | 23 | 4.3 | 0.1 to 2 μm deep scratches | – |
| Bauer et al, 1994 | 45 | 2.6 max | $R_a$ 0.002 μm to 0.47 μm | – |
| Hall et a, 1996 | 129 | 10.7 | $R_a$ 0.02 μm to 0.19 μm | – |
| Hall et al, 1997 | 35 | 12 | $R_a$ 0.08 μm, $R_t$ 1.55 μm | 0.40 μm to 0.69 μm |
| Kusaba and Kuroki, 1997 | 36 | 9 | $R_a$ 0.006 μm to 0.06 μm | – |
| Minakawa et al, 1998 | 10 | 14.4 | – | 0.05 μm to 2.3 μm |
| Sychterz et al, 1999 | 20 | 8.5 | $R_a$ 0.022 μm to 0.098 μm | – |
| Tipper et al, 2000 | 18 | 12.9 | $R_a$ 0.01 μm to 4.3 μm | 4.1 μm |
| Raimondi et al, 2001 | 5 | - | - | 0.3 μm to 1.3 μm |

Further analyses using SEM have also been used in many studies to determine the type of damage that can occur *in vivo*, providing information at a micro level as to what is actually occurring at surface of the femoral head or acetabular cup. With regards to femoral heads, scratches tend to be multi-directional in nature with varying $R_a$ and $R_p$, see Figure 2.19. Peak height ($R_p$) would appear to be the critical factor when considering damage to polyethylene cups, resulting from damage in the femoral heads. Abrasive wear as a result of third body wear appears to be the cause of most damage that occurs *in vivo*. Surface examination of polyethylene cups, revised due to loosening, show extensive abrasive wear, pitting and fatigue fracture (Willert *et al.*, 1991).

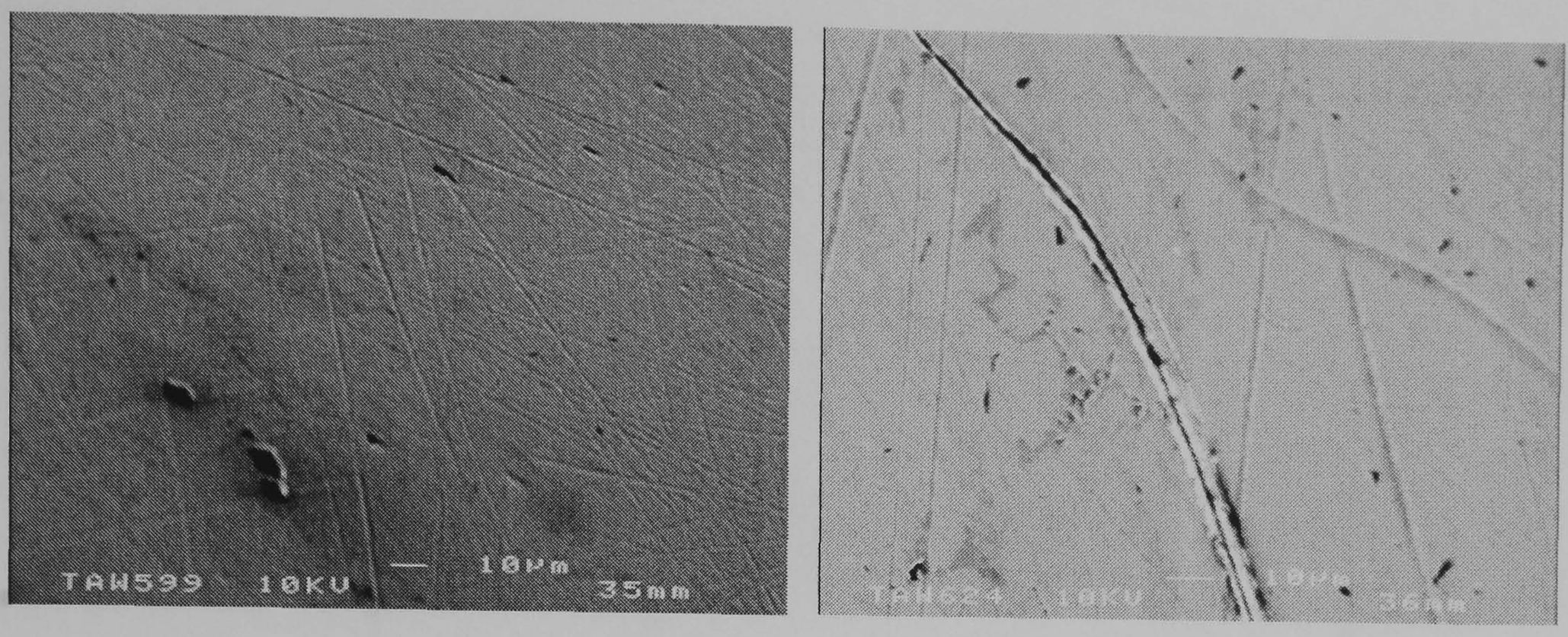


Figure 2.19: Surface examination of a retrieved CoCrMo femoral head, showing multi-directional scratches, both straight and curved, ranging from approximately 1-100 μm in length and 0.1-5 μm in width

Hall *et al.* (1997) noted that material(s) build up on either side of scratches was the major cause of the increased wear observed; this was especially true if the scratches were orientated perpendicular to the direction of wear. Wear, in particular, abrasive wear can be reduced to a certain extent by the use of highly crosslinked polyethylene as demonstrated by Yamamoto *et al.* (2001), where highly crosslinked polyethylene cups showed reduced wear rates, scratching, delamination and less abrasive wear.

### 2.8.2 Surface Topography and its Influence In vivo

There has been much debate as to whether the surface topography has any effect on the wear of acetabular cups. Many studies have concluded that the counterface roughness has no adverse effect of the wear of the cup (Isaac *et al.*, 1992, Elfick *et al.*, 1999) *in situ*, through the analysis of retrieved prostheses. Hall *et al.* (1996) on the other hand showed a positive correlation between the surface topography and the clinical wear factor, K. Elfick *et al.* (1999) however concluded that although a relationship exists between the surface topography and the rate of wear, the relationship is very weak, as there is a high degree of scatter of K versus $R_a$, shown in Figure 2.20.

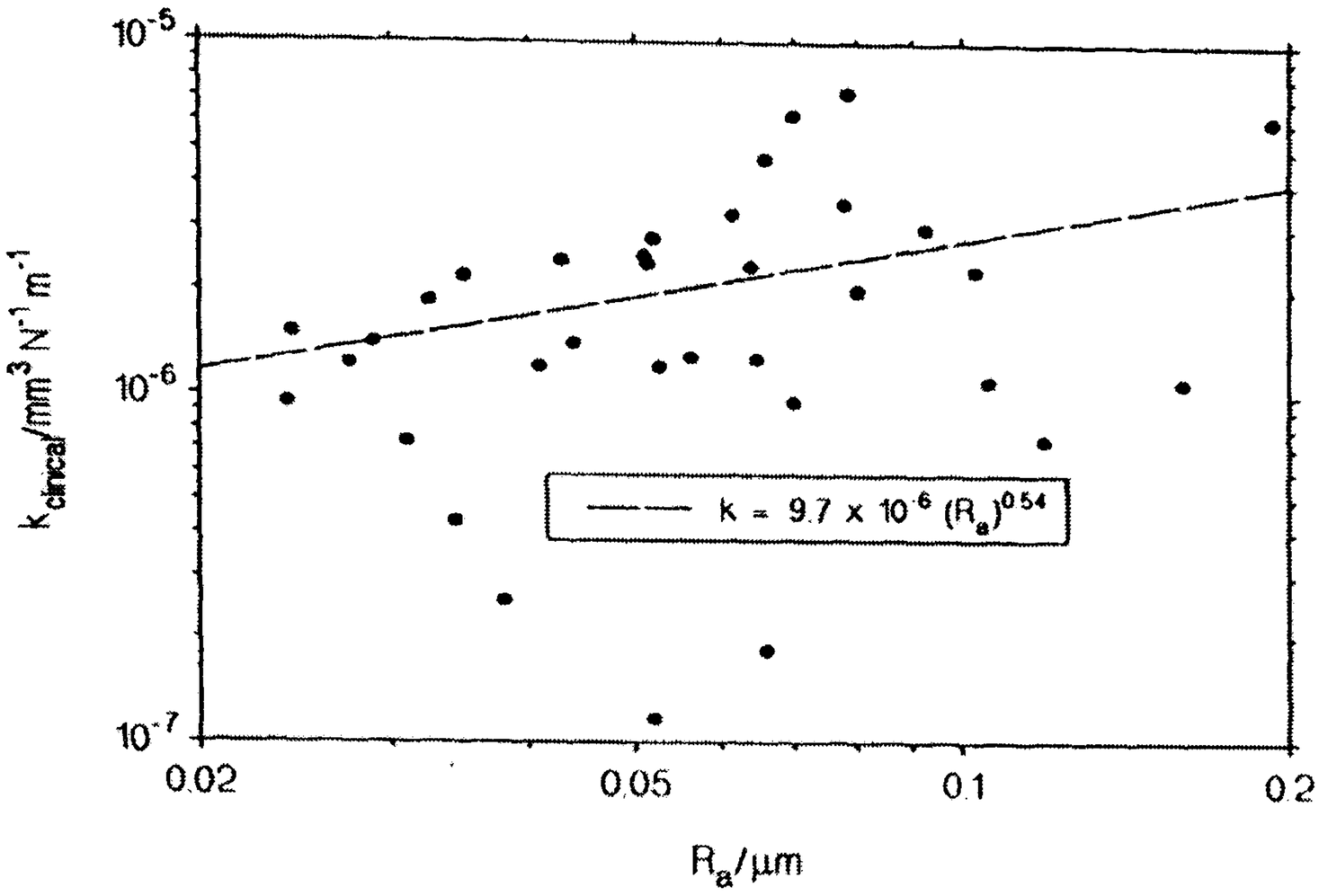


Figure 2.20: Variation of the clinical wear factor K versus $R_a$ for retrieved Charnley prostheses (Hall *et al.*, 1996)

Although the relationship between the wear rate and roughness may be weak according to Elfick *et al.*, studies conducted by Wang *et al.* (1998), McKellop *et al.* (1999), and Endo *et al.* (2000) have shown an increase in the volumetric wear through *in vitro* testing in hip simulators. Wang *et al.* (1998) has carried out a comprehensive study using a hip simulator on the effect of the roughness of a femoral head and the lubricant (in this case bovine serum) against UHMWPE, and reported that the wear rate of the UHMWPE is approximately proportional to the square root of the femoral head roughness.

Early studies have shown the effect of femoral head roughness is significantly less when compared to pin-on-disc studies (Wang, 1996, McKellop *et al.* 1999). However, these studies have used relatively low physiological loads, a peak load of 2500 N, based upon previously published data (Paul, 1966). Thus, when considering increased patient activity such as jogging (Bergmann *et al.*, 1993), femoral head surface damage may be more influential when considering the wear rate and morphology of polyethylene wear debris generated under these conditions.

A study by Bowsher & Shelton (2001) using a fully roughened head under normal walking produced a six-fold increase in wear, agreeing with Wang *et al.,* (1998). Nevertheless, the wear is considerably less than that which is produced when using linear pin-on-disc wear machines. Bowsher & Shelton's study also looked at the effects of increased patient activity on the wear of lightly crosslinked polyethylene using a fully roughened femoral head. Under simulated jogging (105 rpm, 4500 N max) a fully roughened femoral head, with an $R_a$ of 0.4 μm and maximum $R_p$ of 3.0 μm, produced a massive influence on the wear rate, generating wear greater than 2000 $mm^3/10^6$ cycles for 5 MRads gamma irradiated lightly-crosslinked polyethylene.

Multi-directional hip simulator studies, using bovine serum as the lubricant, have shown a reduced influence of the femoral head roughness against the wear of UHMWPE cups. Pin-on-disc studies using bovine serum as a lubricant showed a 30-fold increase in wear (Fisher *et al.*, 1995), where as studies using a hip simulator, under a physiological load, only showed a 2-3 fold increase (Wang *et al.*, 1998). This result is matched by McKellop *et al.* (1999) who studied both crosslinked and non-crosslinked UHMWPE cups, against smooth and rough femoral heads. Reporting a small increase in the wear rates for both types of cup, with the crosslinked polyethylene performing better. McKellop *et al.*. also reported a reduction in the wear rate on subsequent test intervals, attributing this to a polishing of the surface scratches on the ball by the polyethylene.

Figure 2.21 shows the wear of PE against smooth and rough femoral heads showing a direct link with wear and counterface roughness.

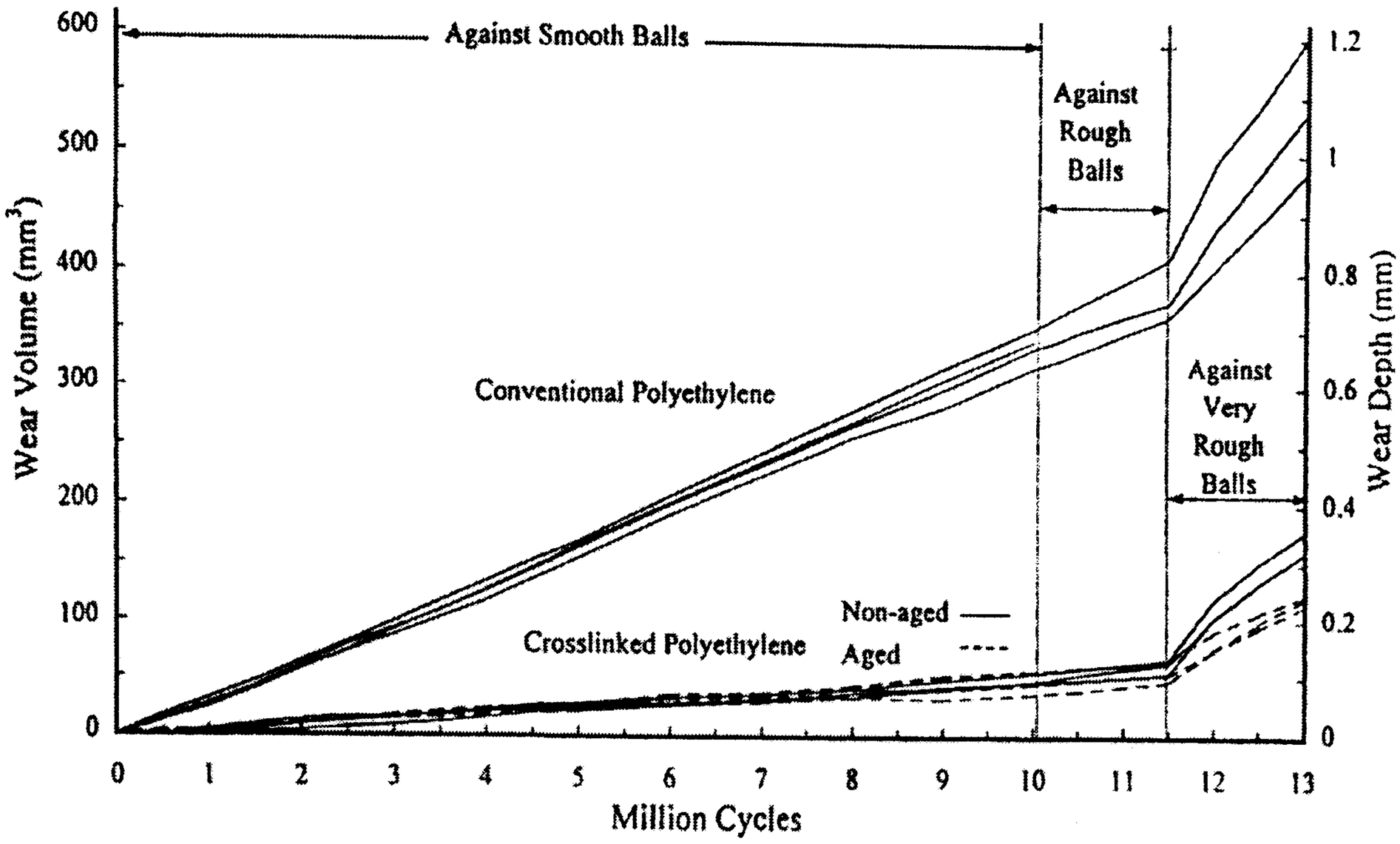


Figure 2.21: *In vitro* comparison of wear of crosslinked and non-crosslinked cups with smooth and rough femoral heads (McKellop *et al.*, 1999)

*In vitro* studies are in good agreement with retrieval investigation such as Hall *et al.* (1997), which show a weak correlation between roughness and wear of the polyethylene cup. Single prominent scratches also have little influence on the wear rate, indicating that the process of wear is multi-factorial and roughness alone cannot explain high clinical wear (Bowsher, 2001). Factors such as patient activity, surface finish, bone and cement debris must be taken into account when considering future tests, as these parameters will no doubt influence the wear rate and also particle morphology.

## 2.9 Project Aims and Objectives

Early clinical studies of crosslinked polyethylene based THRs have shown significant reductions in wear compared to non crosslinked polyethylene and has become the material of choice for acetabular components, with second generation metal-on-metal implants making a comeback. However, aseptic loosening remains the major cause of failure regarding polyethylene based implants. Wear debris has been identified as one the major parameters which can lead to aseptic loosening, and numerous studies have shown that wear debris of a particular size and morphology can induce osteolysis. Most studies have only considered walking as the major activity undertaken by patients; which may not be appropriate for the younger and more active patients who require hip replacements. For these people activity rather time *in situ* maybe the main controlling factor in terms of wear. The aim of the current work is to evaluate THRs in *in vitro* tests under adverse conditions, such as walking and jogging, to determine improved clinically relevant data. In addition the work aims to establish the effect of rough femoral heads on the wear, particle size and morphology of the particles generated.

The hypothesis for this research is that activity as well as surface topography can affect the performance of THRs, in turn affecting the type of debris produced.

Ultimately this will lead to the generation of a model for the prediction of wear under high activities and assist in the selection of an appropriate implant that suits the patient lifestyle in terms of activity.

The aims will be achieved through a series of objectives namely to understand:

- the influence of surface damage under increased activity on the wear and particle morphology of metal-on-polyethylene implants

- the influence of the size of the damaged area on the wear process of metal-on-polyethylene implants

• the influence of bearing diameter on the wear rate and particle size and morphology for metal-on-metal implants.

• the influence of activity combined with bearing diameter on the wear rate and particle size and morphology for metal-on-metal implants.

# Chapter 3 Materials & Methods

## 3.1 MTS 8-Station Hip Joint Wear Simulator

### 3.1.1 Hip Wear Simulator

All wear tests were performed using an 8-station hip joint simulator (MTS Systems, USA), utilising a sun and planetary gear system, producing eight synchronised and repeatable load and wear paths. This type of simulator has been previously described in detail and used successfully in many previous studies (Wang *et al*, 1998, Bowsher & Shelton, 2001).

Each actuator is attached to a mounting block inclined at 23° from a vertical alignment to provide a biaxial rocking motion, 46° in total, when in rotation. The simulator applies a single joint force in one axis, in this case vertically. The combined application of force and rotation replicates the kinematics of walking, simulating both the flexion-extension and abduction-adduction of the human gait cycle during normal walking. A servo hydraulic motor is used to drive the gear assembly system located below the actuator pistons, which provide the simultaneous axial and rotational movement for the inclined block. A proximity switch, triggered at every cycle load, insures synchronisation of the walking action and the preset loading profile for all stations.

Control of the hip simulator is provided via the TestWare SX control system connected to a PC and TestStar II control software, which can be used to run any pre-programmed loading profile up to 5000 N, shown in Figure 3.1(a). This allows constant monitoring of speed, torque, displacement during testing and collection of data for further analysis, which can be viewed via Excel. A schematic showing the configuration of the test chamber and tests specimens in a physiological configuration are shown in Figure 3.1(b), showing how the force is applied and the rotational movement that combines to produce force profile that represents one complete human gait cycle.

(a)

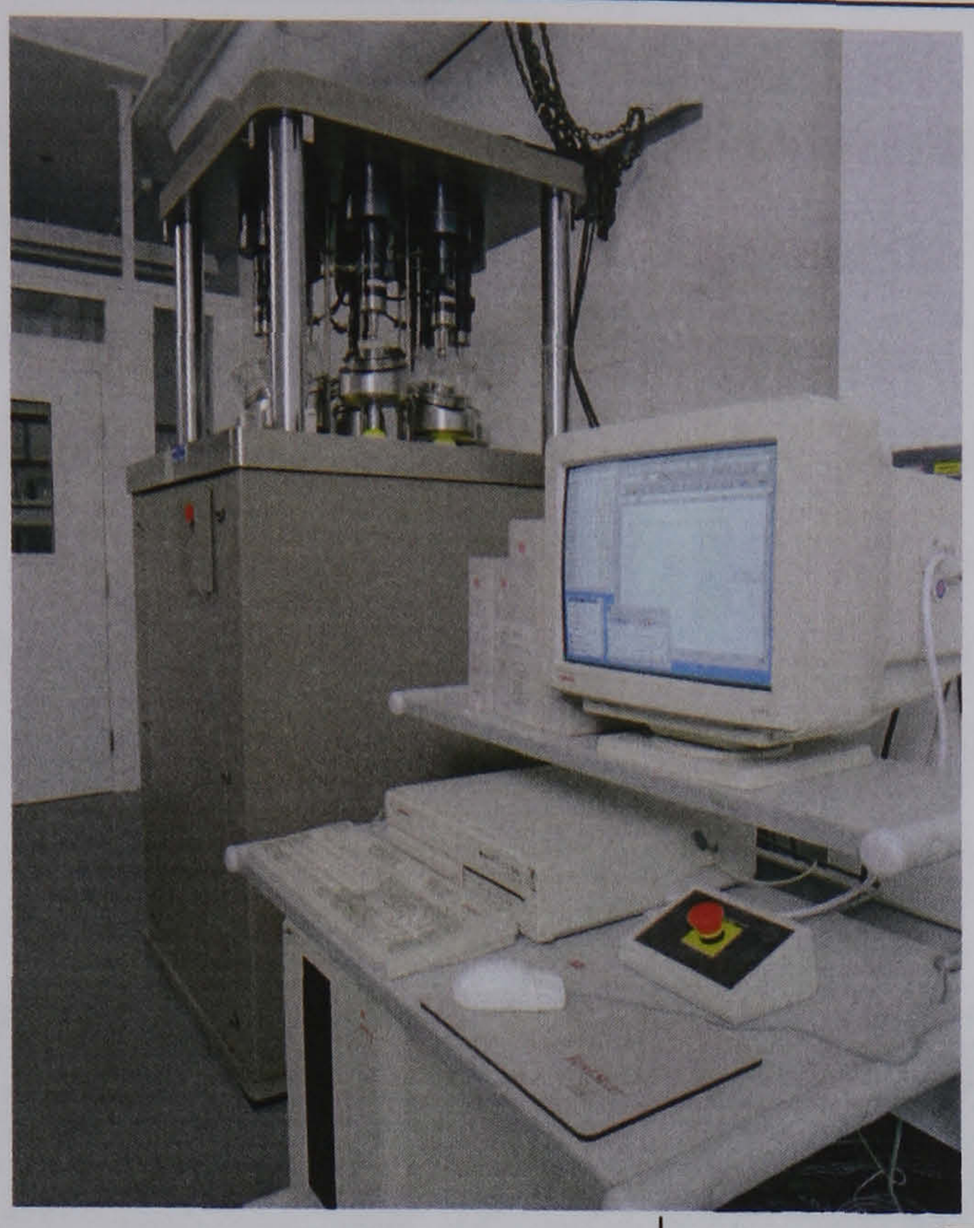

(b)

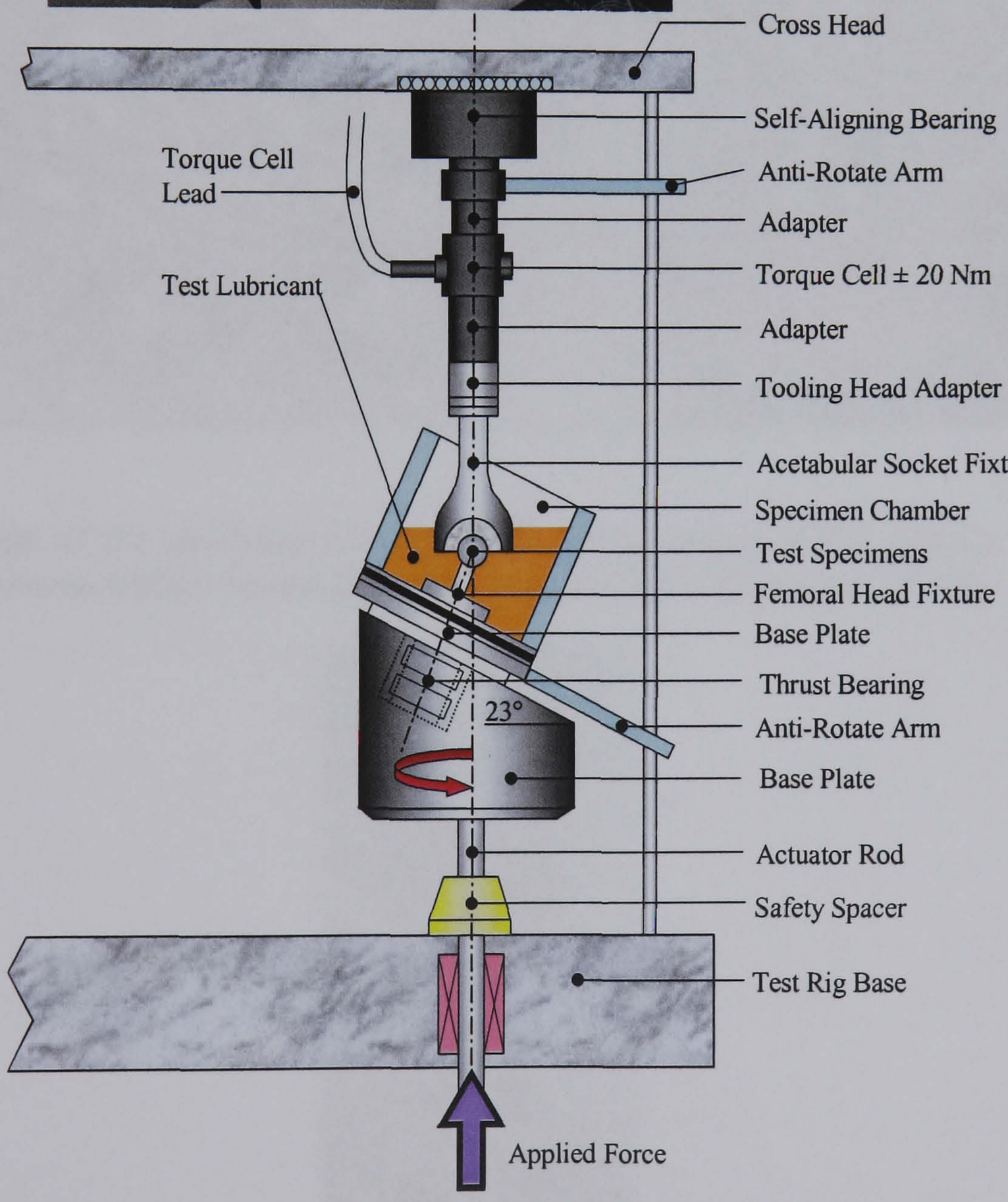


Figure 3.1: (a) Photograph of the MTS hip simulator with the TestWare SX control system, and (b) a schematic diagram of the MTS 8-station hip joint simulator shown in a phyisological configuration (Bowsher, 2000)

The specimen fixtures used in securing the acetabular cups during testing are also shown in Figure 3.2 and Figure 3.3. The partially constraining fixtures used during PE testing clamped 2 mm of the outer diameter of each socket. Each station has a test chamber mounted upon a stainless steel base plate, which is then mounted upon the inclined block. The femoral head was fixed onto a taper and placed within the chamber, as shown in Figure 3.2. In order to prevent rotation of the socket within the socket fixture, two flat faces were machined on each side of the socket, which matched the profile of the clamping plate, providing a secure fit, allowing no movement of the socket during testing

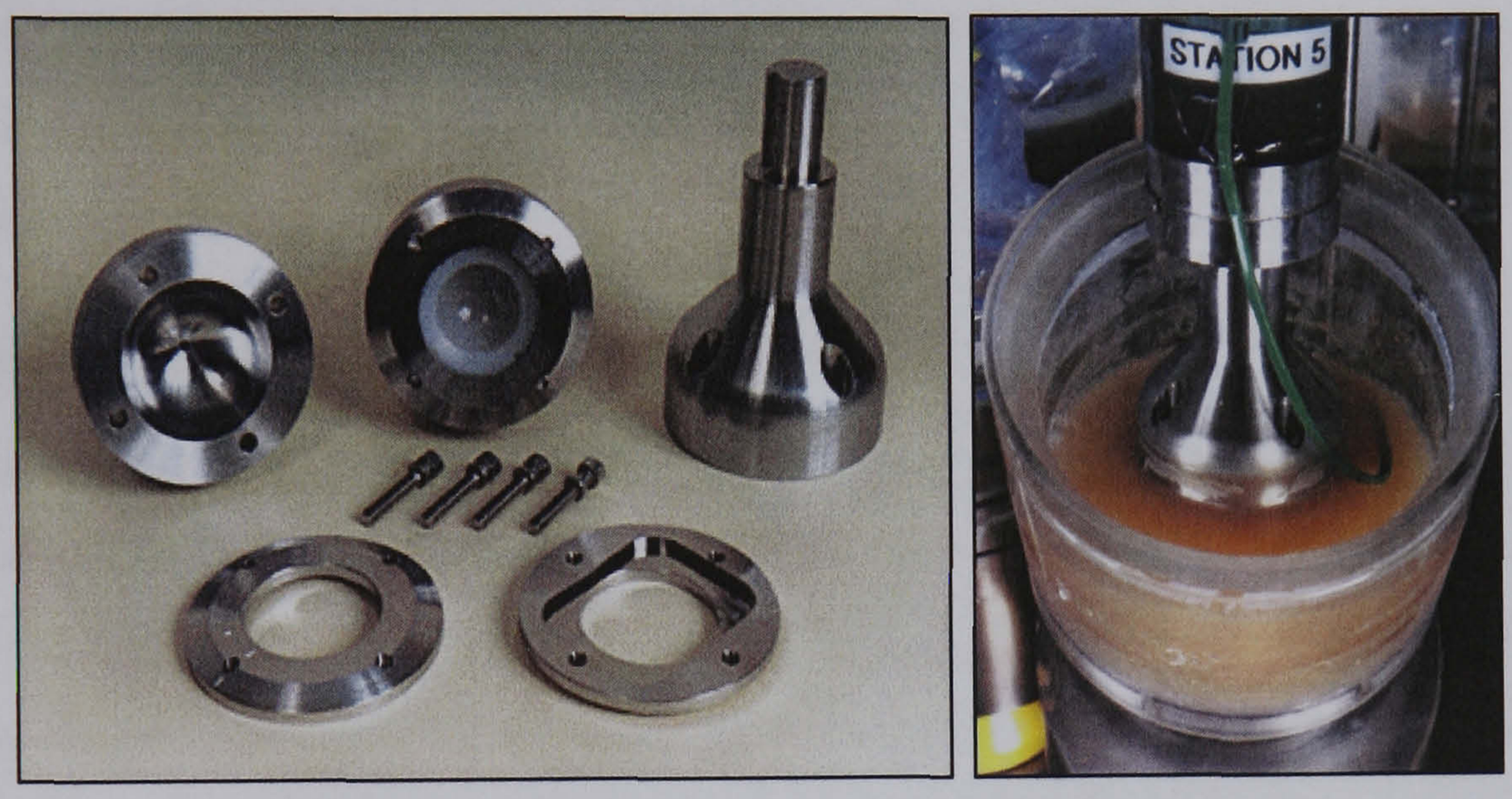


Figure 3.2: Image of the specimen fixtures used during testing of PE, and the assembly of the specimen fixtures within the test chamber with lubricant (Bowsher, 2000)

Figure 3.3: Image of the specimen fixtures and assembly used during testing of MoM

### 3.1.2 Lubricant

For wear tests each chamber was filled with a lubricant. The lubricating medium contained new born calf serum (Sigma UK, C-6278) diluted to 25% using 0.05 μm filtered deionised water with 0.1% sodium azide for bacterial retardation, additional water was used to compensate for serum evaporation during testing through daily checks of lubricant volume, ensuring that lubricant volume was maintained at a constant volume of 500 ml. To prevent any contamination and minimise evaporation of the serum, the chambers were sealed with polyethylene bags. Each test was run for $0.5\times10^6$ cycles after which gravimetric measurements of sockets would be taken, for the calculation of volumetric wear and wear rates, and the lubricating medium changed. All tests were carried out at a constant laboratory temperature of 24° C.

### 3.1.3 Loading Profiles

Walking tests used a Paul-type physiological loading profile, shown in Figure 3.4, with a maximum peak load of 2450 N and a minimum load of 50 N applied at 60 rpm (1 Hz cycle time). A minimum load was maintained at 50 N so as to maintain the hydraulic pressure that drives the planetary gear system, in turn allowing for accurate application of the force profile for all stations simultaneously. For jogging tests a profile was used according to data presented by Bergmann (1992), shown in Figure 3.5, with a maximum peak load of 4500 N applied at 105 rpm (1.75 Hz cycle time). Jogging tests were run for 14400 and 28800 cycles equating to jogging for 2 and 4 hrs respectively.


Figure 3.4: Walking profile (a) used in simulated walking tests on the MTS hip simulator (inverted) and (b) walking profile obtained by Paul, with variation of bodyweight against time (1966)

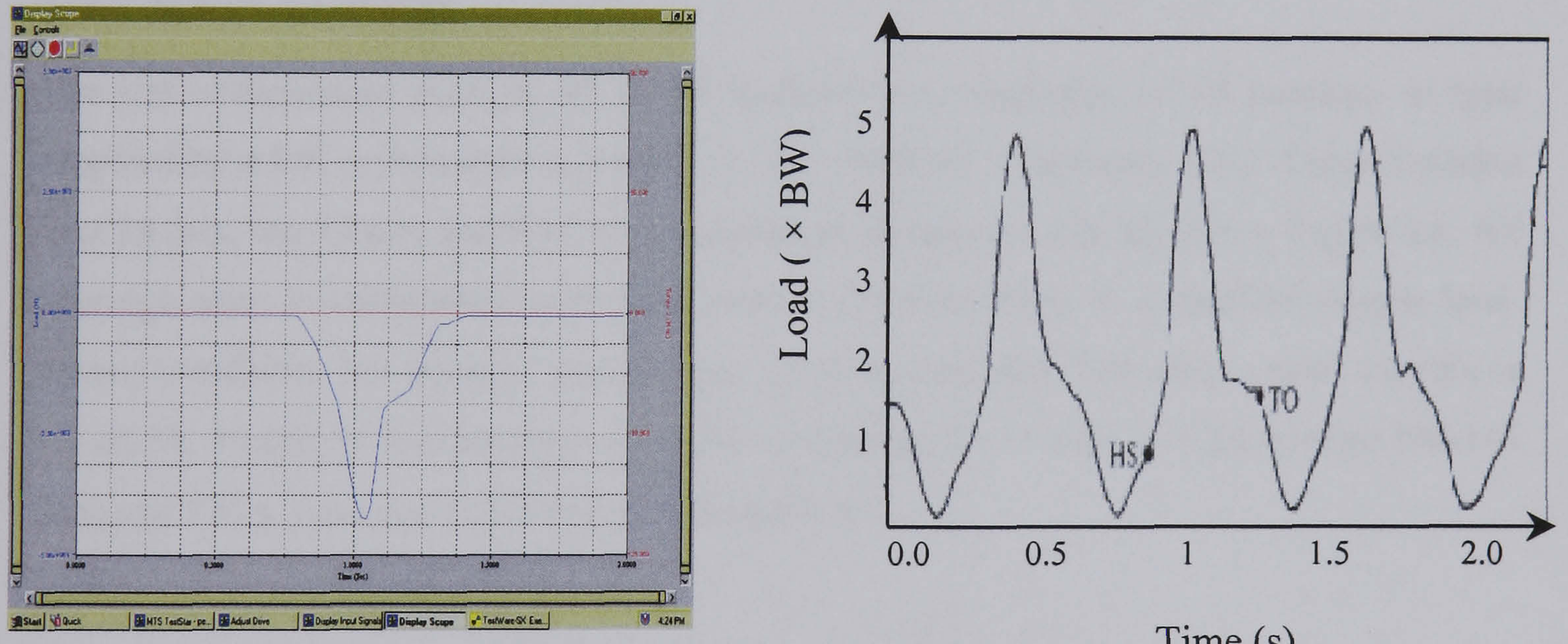


Figure 3.5: Jogging profile (a) used in simulated jogging test on the MTS hip simulator (inverted) and jogging profile (b) obtained by Bergmann (1993) from an instrumented hip replacement. HS and TO indicate the points of Heel Strike and Toe Off respectively

## 3.2 Components Used

The materials used in all wear tests were components that had been supplied by major manufacturers of orthopaedic implants ready for implantation.

### 3.2.1 Metal on Polyethylene

The tests components used in all metal-on-polyethylene tests consisted of 28 mm diameter CoCrMo femoral heads (ULT*FEM) and lightly crosslinked (5 MRads) UHMWPE cups, supplied by a major orthopaedic manufacturer (Depuy Ltd, a Johnson & Johnson Company). All test components were supplied in sealed packages ready for clinical implantation. The acetabular sockets were machined from extruded cylindrical rods of GUR 1020. After machining, all sockets were cleaned and vacuum foil pouched, followed by gamma irradiation in an inert atmosphere (nitrogen), with a maximum dose of 50 KGy (5 MRads). Once opened, all test sockets were first weighed, and then soaked in deionised water at 37°C for a period of approximately one-year prior to testing.

### 3.2.2 Metal on Metal

The test components used in all metal-on-metal tests consisted of 18 bearings in total supplied by a UK orthopaedic company (Corin, Medical, Cirencester UK). These included four 28 mm, ten 40 mm and four 56 mm diameter metal-on-metal hip joints, Figure 3.6. All bearings were manufactured from high carbon CoCrMo alloy in a standard double heat-treated condition, hot isostatic pressed and solution annealed. The mean radial clearances for all 28, 40 and 56 mm bearings were; 42 μm (range 35-53 μm), 119 μm (range 104-144 μm) and 142 μm (range 131-149 μm) respectively.

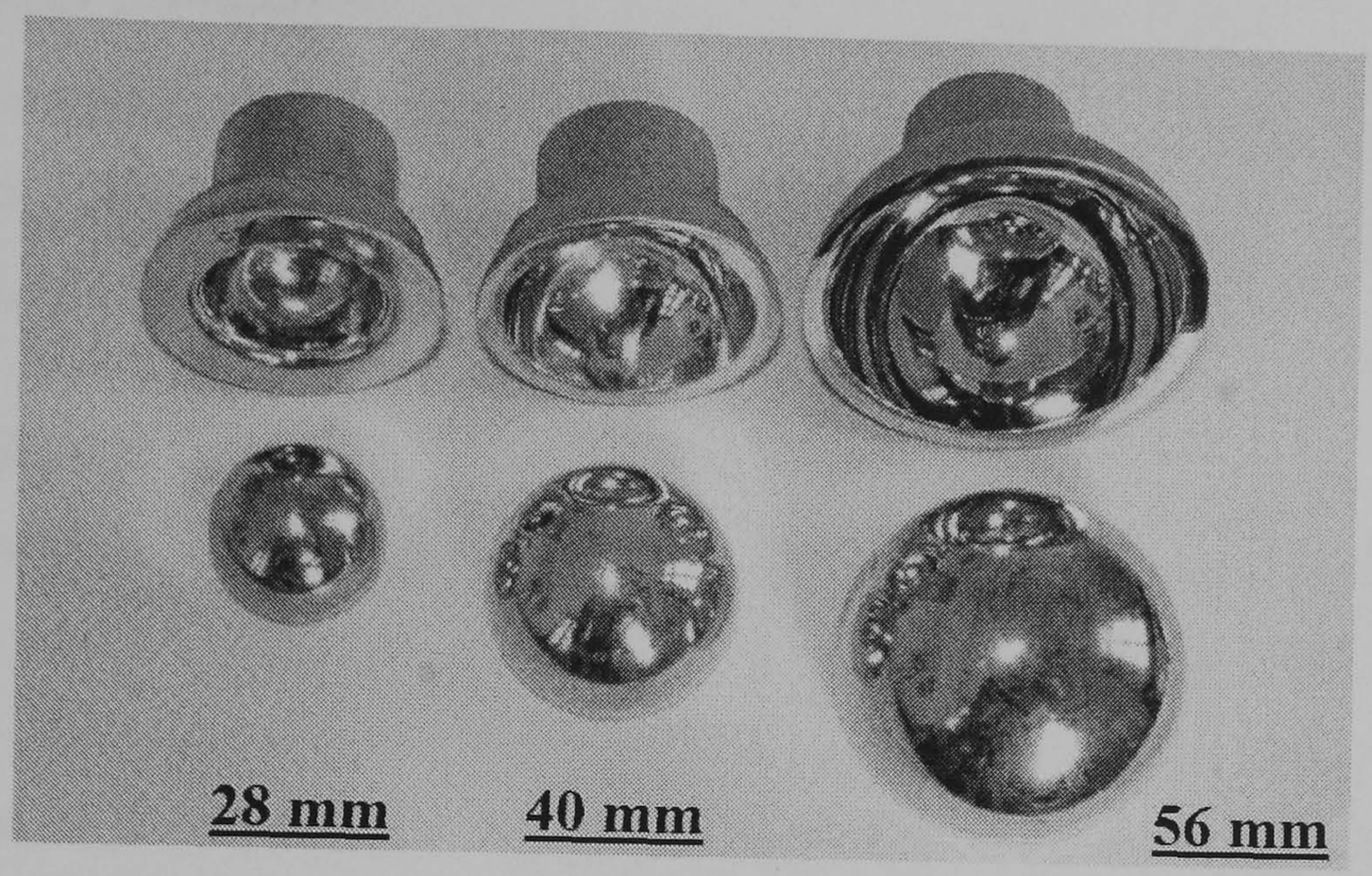


Figure 3.6: Image showing 28, 40 and 56 mm diameter metal-on-metal tests components used during testing

### 3.2.3 Surface Topography Measurement

Surface topography measurements of femoral heads were measured before and after wear tests using a surface contact profilometer (Surftest SV-400, Mitutoyo, Japan), with a cut-off length of 0.4 mm. Measurements were taken at eight locations, two measurements at each location, 90° apart, providing a total of sixteen measurements from which mean values were obtained, two roughness parameters were measured, $R_a$, and $R_p$, defined in appendix 1.4. Figure 3.7 shows the location of the points at which surface topography measurements were obtained from the femoral heads.

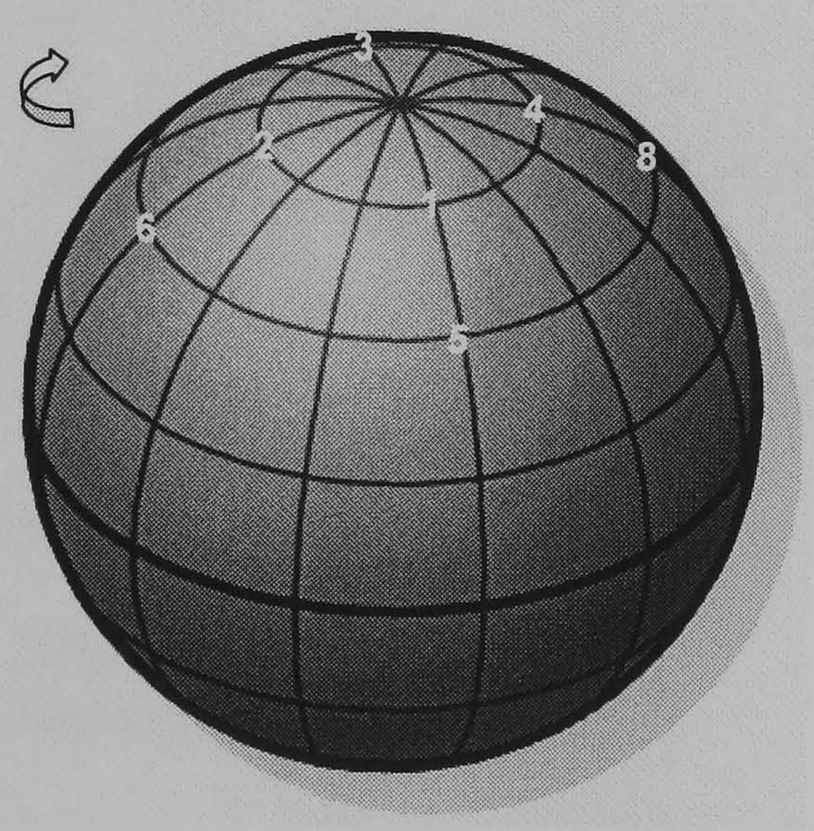


Figure 3.7: Location of surface measurements on the femoral head

### 3.2.3.1 Smooth Conditions

The highly polished CoCrMo heads had a mean head diameter of 27.99 mm, with an initial surface roughness ($R_a$) of 0.012 μm. For test purposes all femoral heads were mounted on 12/14 tapered 316L stainless steel fixture.

### 3.2.3.2 Roughened Heads

For tests conducted under simulated damaged conditions, each femoral head was scratched in such a way as to create the levels of roughness and damage that has been recorded from retrieved metallic femoral heads (Wroblewski et al, 1991, Isaac *et al*, 1992 Hall *et al*, 1997, Sychertz *et al*, 1999), described in detail in appendix 1.3. When simulating damaged femoral head conditions, damage to the femoral head was located at the area of maximum sliding velocity on the acetabular socket. Figure 3.8 shows the location of damage to the femoral head in relation to the acetabular cup. Scratched areas were created using 400 grit SiC paper, applied to the femoral head in a circular motion, producing multidirectional scratches, representing conditions that have been found on retrieved femoral heads, see Figure 2.17. All scratches were located in the upper hemisphere of each femoral head, with the fully roughened head covering damage over the entire upper hemisphere (Figure 3.9 (c).

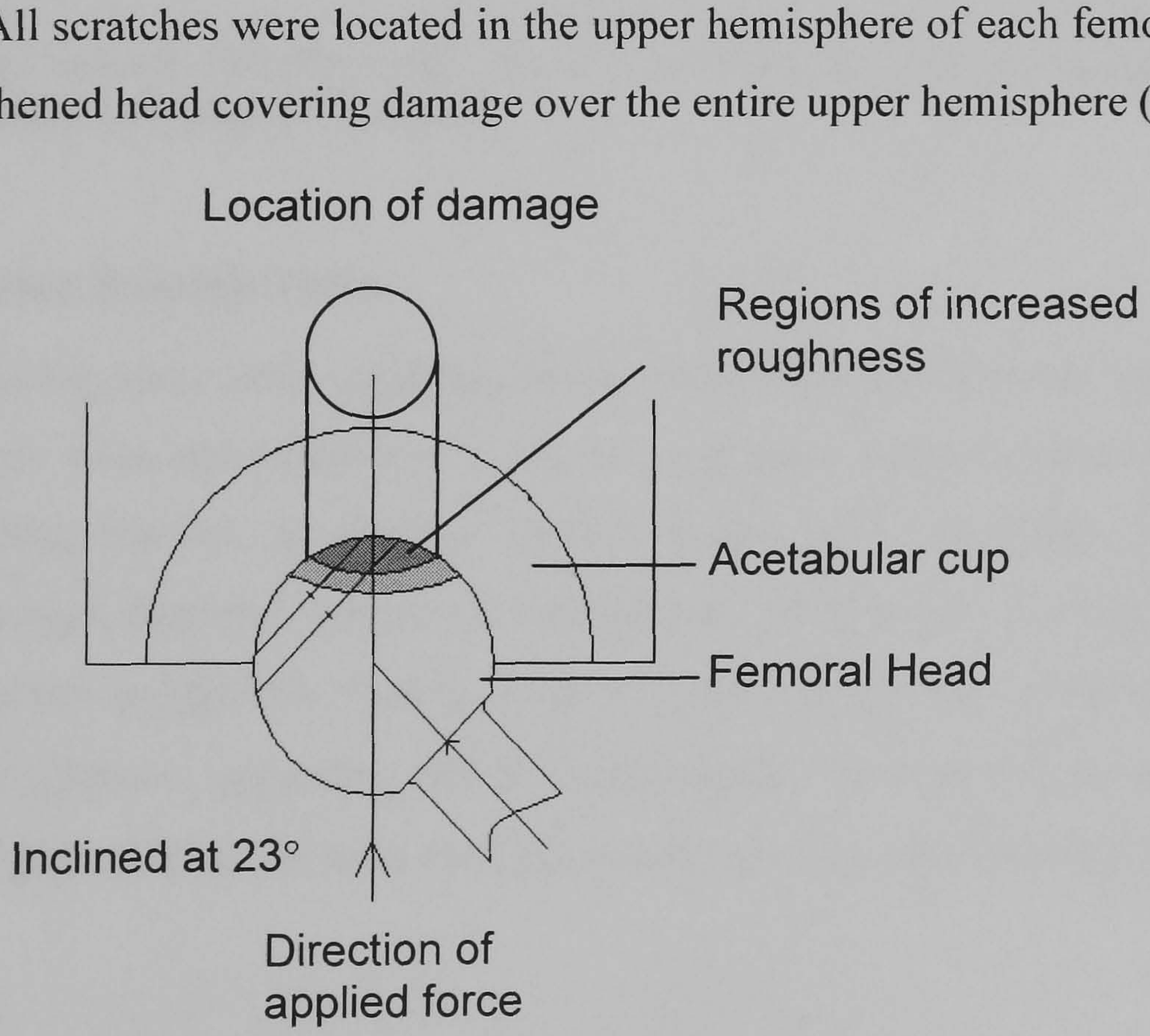


Figure 3.8: Location of damaged areas on the femoral head in relation to the position of the acetabular cup

Figure 3.9 (a) to (c) show the visual comparison of virgin femoral heads and roughened femoral heads, Figures 3.9(b) and 3.9(c) show the differences in surface finish, from smooth to rough. Femoral heads with partially roughened areas covered damage over an area of 5 mm diameter (20 $mm^2$), 10 mm diameter (80 $mm^2$) and 15 mm diameter (176 $mm^2$), initial topography of each roughened femoral head whether fully or partially rough was controlled to a median surface roughness $R_a$ of 0.4 μm, with a maximum scratch height of 1.5 μm $R_p$. This was achieved through the regular measurements of the surface finish following the application of the grit paper to roughen the surface.

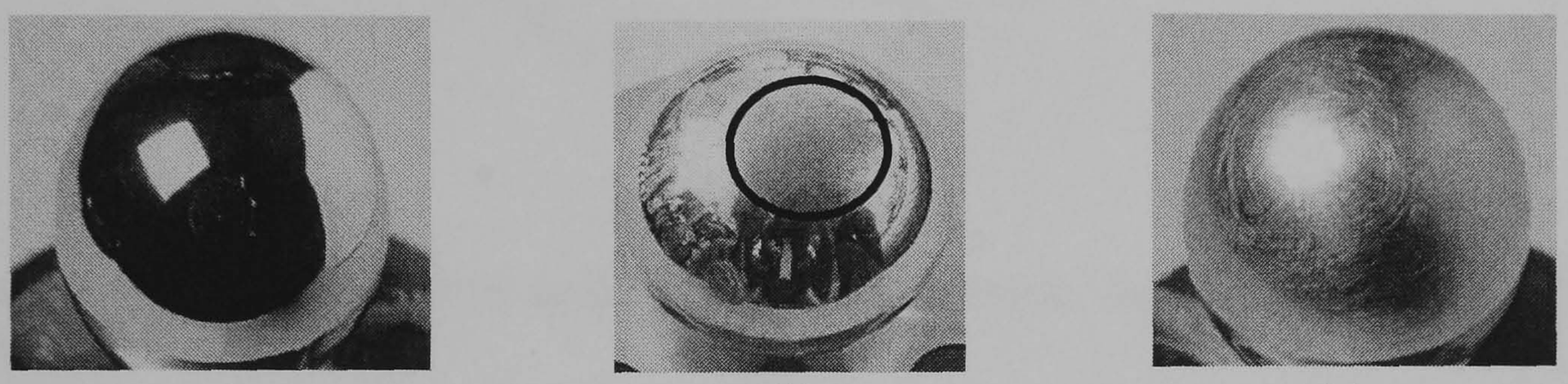

(a) (b) (c)

Figure 3.9: (a) Smooth femoral head, (b) 10 mm diameter partially roughened femoral head, and (c) fully roughened femoral head

### 3.2.3.3 Discrete Scratch Tests

As well conducting tests under rough conditions that represented damage similar to *in vivo* conditions, tests were also conducted using three single scratches applied to the area of maximum sliding velocity, to form an asterisk, Figure 3.10 and Figure 3.11. This was achieved by using a diamond indenter, which applied a scratch over a specified length with a maximum scratch height of 1.5 μm $R_p$. One femoral head was also scratched covering the entire upper hemisphere, extending 180° from the equator, through the pole and back down to the equator, this method has been used previously and described in detail by (Barbour *et al.* (2000).

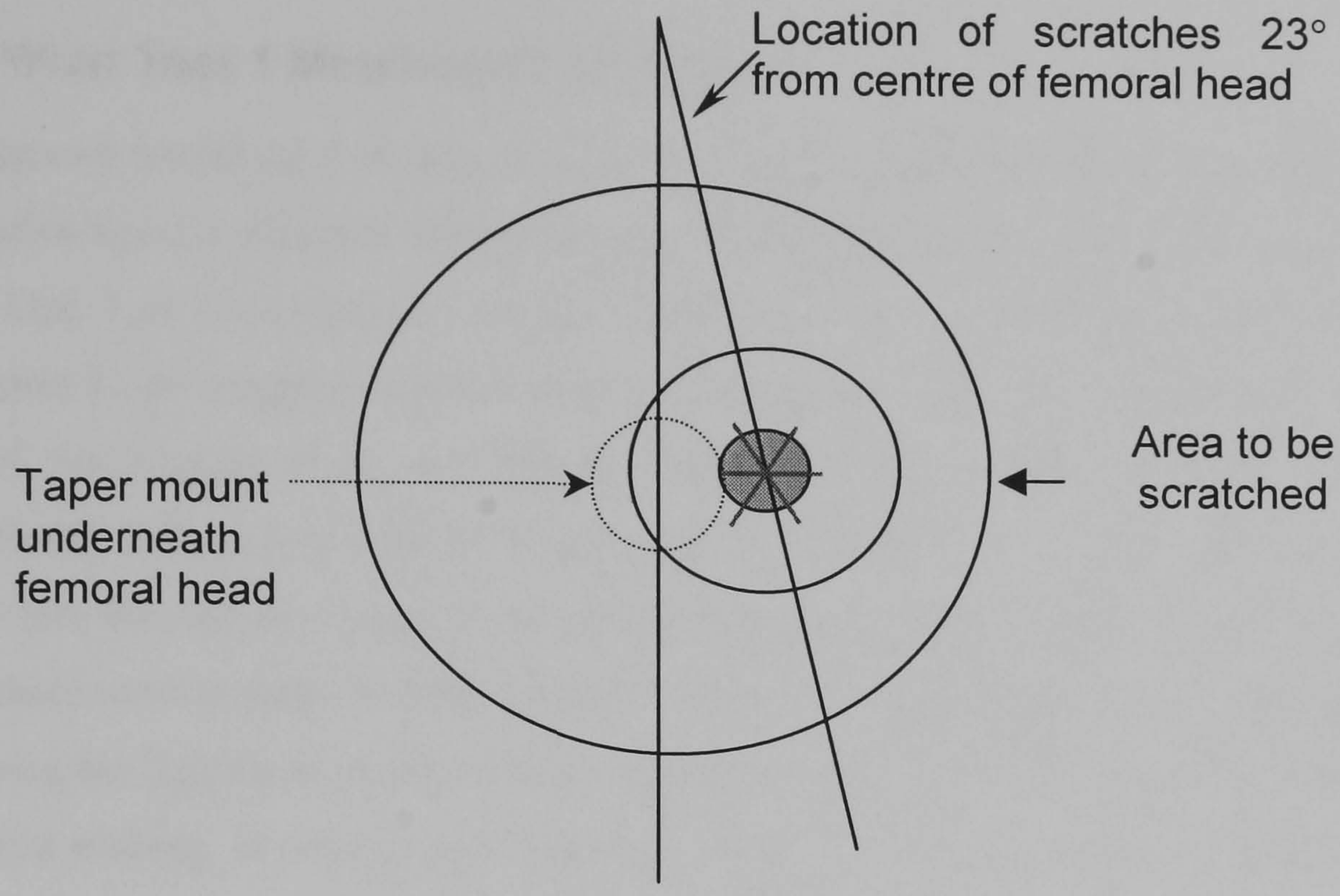


Figure 3.10: Top view of femoral head showing the location of scratches in the form of an asterix

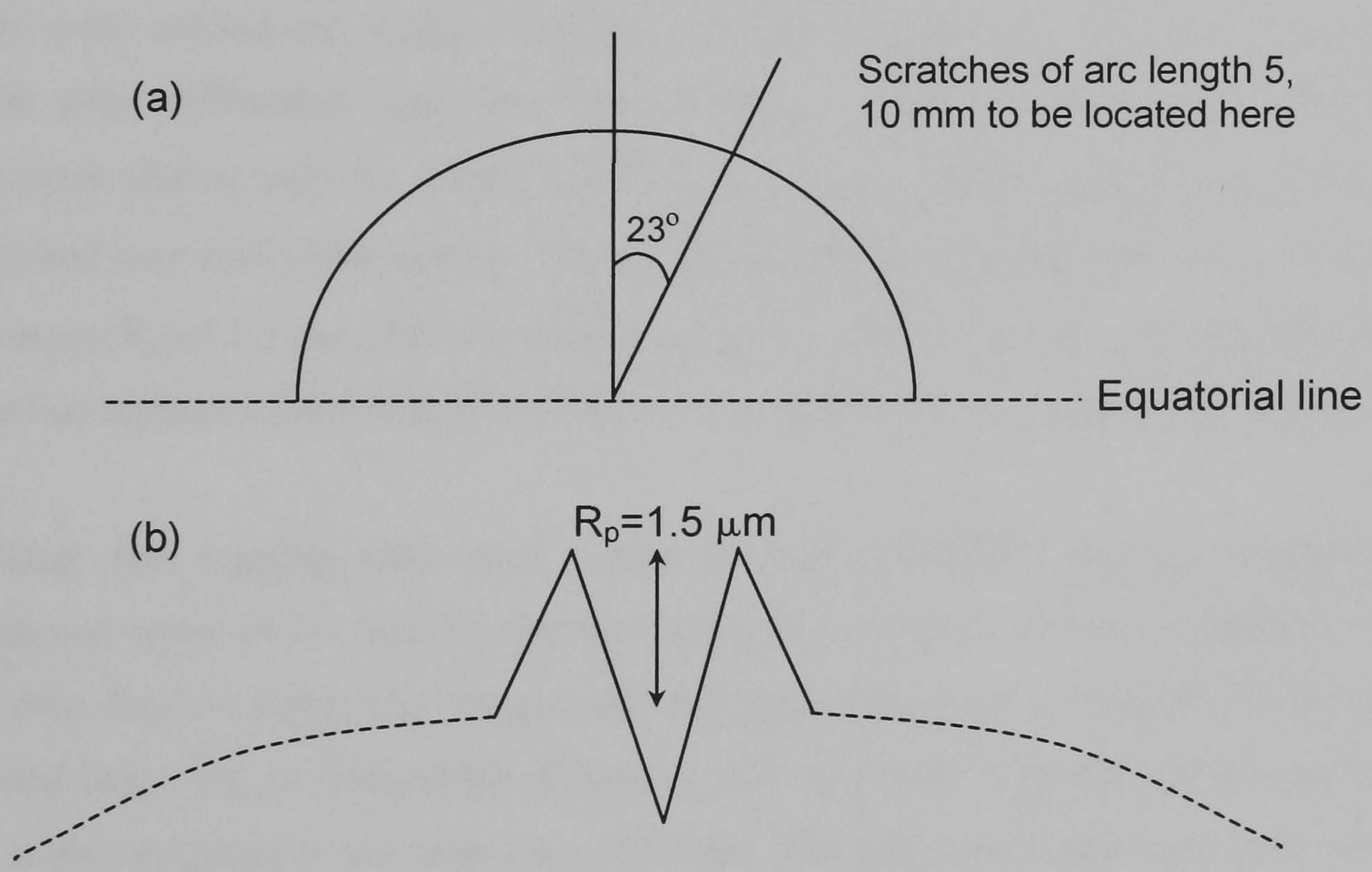


Figure 3.11: (a) Side profile femoral head showing location of scratch and (b) side profile of a single scratch, with a maximum height of 1.5 μm $R_p$

## 3.3 Wear Testing

### 3.3.1 Wear Test 1 Metal-on-Polyethylene

Five stations contained CoCrMo femoral heads articulating against UHMWPE cups, and one station used a Zirconia femoral head articulating against UHMWPE. Initial walking tests (Test 1.1) consisted of 442,390 cycles per test, in total 2,654,340 cycles were completed. Upon completion walking tests, jogging tests were carried out (Test 1.2). At the start of the jogging tests, the sockets were run for 0.2 million cycles of walking, immediately followed by 2 hrs of jogging. The 0.2 million cycles were carried out in order to take into account any creep or deformation that may have occurred during the time that the sockets were in soak. In total, 129,600 cycles were completed for smooth jogging tests. Following the jogging tests, the sockets were then run for a further one million cycles under simulated walking, to observe any long-term influence of jogging upon volumetric wear.

#### 3.3.1.1 Wear testing under rough conditions

Tests were carried out under simulated damaged conditions. In this case three femoral heads were deliberately scratched over an area of a specified diameter at the point of maximum sliding velocity, which is 23° off the centre of the femoral head, with one head scratched over half of the sphere. The median $R_a$ of this scratched area was 0.4 μm with a maximum $R_p$ of 1.5 μm. The scratches were applied in such a way as to simulate scratches found on retrieved femoral heads, which show multidirectional scratches (Wang, 1999).

Walking and jogging tests were repeated under simulated damage conditions with roughened areas of 20 $mm^2$ (5 mm diameter), and 80 $mm^2$ (10 mm diameter), with one CoCrMo femoral head fully roughened. Attempts were made at roughening the Zirconia femoral head, but no discernible difference was measured using the surface profilometer, this is also reflected in the wear rates observed. The fully roughened head from test period 1.5 to 1.8 was not re-roughened.

Table 3.1: Summary of tests for Wear Test One. Identical tests were carried out for the fully roughened head, however surface roughness covered an area of 1230 $mm^2$ under simulated damaged conditions

| Test | Test type | Femoral head condition | Number of Cycles (million) | Activity level (N) | Frequency (rpm) |
|---|---|---|---|---|---|
| 1.1 | Walking | Smooth | 0.0 - 2.7 | 2450 | 60 |
| 1.2 | Jogging | Smooth | 2.7 - 3.0 | 4500 | 105 |
| 1.3 | Walking | Smooth | 3.0 – 4.0 | 2450 | 60 |
| 1.4 | Jogging | Smooth | 4.0 – 4.1 | 4500 | 105 |
| 1.5 | Walking | Partially rough 20 $mm^2$ | 4.1 – 5.1 | 2450 | 60 |
| 1.6 | Jogging | Partially rough 20 $mm^2$ | 5.1 – 5.2 | 4500 | 105 |
| 1.7 | Walking | Partially rough 80 $mm^2$ | 5.2 – 6.2 | 2450 | 60 |
| 1.8 | Jogging | Partially rough 80 $mm^2$ | 6.2 – 6.3 | 4500 | 105 |

### 3.3.2 Wear Test 2 Metal-on-Polyethylene

Wear test two consisted of two smooth CoCrMo femoral heads and sockets, one rough CoCrMo femoral head with original test socket and one Zirconia femoral head with original test socket head, remaining from wear test one. Walking tests were carried out in order to wear in the two new femoral heads over 5 million cycles. The femoral heads were then roughened over an area of 15 mm diameter (an area of approximately 180 $mm^2$) at three different grades of surface roughness, 0.2 μm, 0.5 μm, and 0.8 μm, which represented the worst case scenario for a damaged femoral head (Wang, 1996). These heads were re-roughened to these values following each test. The Zirconia femoral head was replaced with a fully roughened CoCrMo femoral head with an $R_a$ of 0.39 μm, after five million cycles, and was not re-polished during consecutive tests. Simulated walking and jogging tests were then repeated under damaged conditions. Slow walking at 60 rpm for 0.5 million cycles and fast walking at 105 rpm for 0.1644 million cycles, followed by slow jogging at 60 rpm for 0.1644 million cycles and fast jogging at 105 rpm for 0.1644 million cycles. A summary of the tests conducted during test 2, are presented in Table 3.2.

Table 3.2: Summary of tests for Wear Test Two

| Test | Test type | Femoral head condition | Number of Cycles (million) | Activity level (N) | Frequency (rpm) |
|---|---|---|---|---|---|
| 2.1 | Walking | Smooth | 0.0 – 5.0 | 2450 | 60 |
| 2.2 | Walking | Partially rough 176 $mm^2$ | 5.5 – 6.0 | 2450 | 105 |
| 2.3 | Walking | Partially rough 176 $mm^2$ | 6.0– 6.5 | 2450 | 60 |
| 2.4 | Jogging | Partially rough 176 $mm^2$ | 6.5 – 6.66 | 4500 | 105 |
| 2.5 | Jogging | Partially rough 176 $mm^2$ | 6.66 – 6.82 | 4500 | 60 |

Table 3.3 : Table of samples collected for PSA and SEM analysis

| Sample ID | Test Type | Femoral Head Condition |
|---|---|---|
| 1 | Walking | Smooth |
| 2 | Walking | Smooth |
| 3 | Walking | Smooth |
| 4 | Jogging | Smooth |
| 5 | Jogging | Smooth |
| 6 | Walking | 5 mm rough patch |
| 7 | Walking | 10 mm rough patch |
| 8 | Walking | Fully roughened |
| 9 | Jogging | 5 mm rough patch |
| 10 | Jogging | 10 mm rough patch |
| 11 | Jogging | Fully roughened |

### 3.3.3 Wear Test 3 Metal-on-PE Discrete Scratch Tests

Wear test 3 consisted of six 28 mm diameter femoral heads articulating against UHMWPE sockets. The test consisted of walking and jogging tests under both smooth and rough conditions. Initial phase of the testing consisted of a wear in phase for 1.5 million cycles followed by steady state wear for 1 million cycles for all femoral heads. Following tests under smooth conditions, tests were conducted under rough conditions. Two femoral heads were damaged using single scratches to form an asterix at the point of maximum sliding velocity (see Figure 3.10), 5 mm in length, and one head fully scratched, scratches to form an asterisk covering the entire upper hemisphere. Three more heads were damaged by scratching that represented physiological conditions *in vivo*, over an area of 15 mm diameter (see Figure 3.9). Following damage further tests were then carried out, at one million cycles of walking followed by 4 jogging tests, alternating between 2 and 4 hours respectively. Subsequent to this, the heads were then re-scratched, extending the scratch length to 10 mm at the same location and the tests repeated. The fully scratched head was not re-scratched, although the same tests were carried for this particular head.

Table 3.4: Summary of tests for Wear Test Three

| Test | Test type | Femoral head condition | Number of Cycles (million) | Activity level (N) | Frequency (rpm) |
|---|---|---|---|---|---|
| 3.1 | Walking | Smooth | 0.0 – 2.5 | 2450 | 60 |
| 3.2 | Walking | Damaged | 2.5 – 3.5 | 2450 | 60 |
| 3.3 | Jogging | Damaged | 3.5 – 3.58 | 4500 | 105 |
| 3.4 | Walking | Damaged | 3.58 – 5.58 | 2450 | 60 |
| 3.5 | Jogging | Damaged | 5.58 – 5.66 | 4500 | 105 |

### 3.3.4 Wear Test 4 Metal-on-Metal

The test specimens were divided into two groups. Group one consisted of four 28 mm and four 56 mm bearings, and group two consisted of ten 40 mm bearings. Initially, all components in groups 1 and 2 were subjected to 6 and 3 million cycles of standard walking

respectively, to generate steady state wear conditions. During testing, all bearing couples were positioned physiologically, i.e. cup above a moving femoral head, thereby creating similar *in vivo* wear conditions. Following all walking tests, both groups were then subjected to one million cycles of simulated fast jogging at 105 rpm (1.75 Hz).

A one-hour stationary rest period every 8,000 cycles was incorporated into all jogging tests to prevent unphysiological joint temperatures, temperature of laboratory was increased to 37 °C from 24 °C, qualitative measurements of serum temperatures during previous tests showed temperatures to be in the physiological range. Increasing the laboratory temperature to a more physiological relevant temperature, more closely simulates the temperatures that may be experienced *in vivo*. Since all jogging tests were undertaken at an increased speed of 1.75 Hz, all jogging cycles were adjusted to synchronise the load/loci pattern per cycle, thereby ensuring that the same point on the cup received the same load vector each cycle. Following normal walking and fast jogging tests, samples of used bovine serum were collected and immediately frozen to –25 °C for storage prior to wear particle extraction. After all fast jogging tests, both groups were then further subjected to one million cycles of normal walking to establish if the wear rates would then return to steady-state values.

Table 3.5: Summary of tests for Wear Test Four

| Test | Test type | Femoral head condition | Number of Cycles (million) | Activity level (N) | Frequency (rpm) |
|---|---|---|---|---|---|
| 4.1 | Walking | Smooth | 0.0 – 3 & 6 | 2450 | 60 |
| 4.2 | Jogging | Smooth | 6-7 | 2450 | 105 |
| 4.3 | Walking | Smooth | 7-8 | 4500 | 37 |
| 4.4 | Jogging | Smooth | 8-9 | 2450 | 60 |

## 3.4 Measurement of Wear

### 3.4.1 Gravimetric Analysis

Following each test, sockets were weighed using a balance (Precisa Balance 92SM-202A) accurate to within five decimals places, ± 0.00005 g. This required the removal of the socket from its fixture and cleaned according to the steps outlined in the standard cleaning protocol, appendix 1.1, this ensured that all contaminants were removed from the test cups. Following cleaning, cups were dried and weighed. The unloaded and loaded soak controls allowed fluid absorption, during testing, to be taken into account. This enabled accurate calculation of the wear rates and volume loss. Volume loss was calculated by dividing the weight loss by 0.938 kg/m$^3$, the density of the test sockets (GUR 1020, ISO 5834, Part 1, ISO 5834, Part 2). The equation used to calculate the mass lost during testing is based on ISO standards (ISO/TR 9326:1989) and is shown in equation 1.

$$\delta M_t = (M_{t1} - M_{t2}) + (M_{s2} - M_{s1}) \qquad \text{Equation 3.1}$$

Where: $M_{t1}$= initial mass of test specimen

$M_{t2}$= final mass of test specimen

$M_{s1}$=average initial mass of soak controls

$M_{s2}$=average final mass of soak controls

Soak controls were required as it has been shown that cyclic loading of polyethylene can increase the rate of fluid absorption during hip simulator wear tests (Saikko *et al*, 1992).

Acetabular cups were typically weighed before and after each test, where the tests ranged from $0.0144 \times 10^6$ to $0.5 \times 10^6$ cycles. In general, for accurate weight measurements of PE cups the following protocol was used.

The balance was allowed to equilibrate for at least 6 hours prior to the end of the test. All extraneous flows of air were eliminated and heaters were turned off. The air temperature of the laboratory was maintained at 24 ˚C. A minimum of 5 weight measurements were recorded per cup, ensuring that readings obtained from the balance are repeatable, complete protocol described in detail in appendix 1.2.

Queen Mary
University of London

# Store Material Application

Check the **Catalogue *BEFORE*** making your request and write legibly

| | | | | | |
|---|---|---|---|---|---|
| Periodical ☐ | Book ☐ | Thesis ☑ | Report ☐ | Newspaper ☐ | Other ☐ |

Periodical or Book Title: Characterisation of wear particles generated during accelerated testing of total hip replacements

Author: Azad Hussain

| Vol | No | Year | Pages |
|---|---|---|---|
| | | | 280 |

Location/Bay No (Check Catalogue): ZTH4109 HUS

Date & Time of Request: 26/11/2010 13:00

| Please Tick | UG ☐ | PGT ☑ | PGR ☐ | STAFF ☐ | Other ☐ |
|---|---|---|---|---|---|
| | Store ☑ | | Pre-1980 | Octagon ☐ | |

**Please note** **Restriction times on Octagon collections may apply**

| Name | Barcode | Department |
|---|---|---|
| Oscar Lancaster-Jones | 02333370086 | SEMS Biomedical Eng. |

Materials are retrieved **Monday - Friday, only** and may be collected from ***The Issue Counter.***
Hand in by 10.00am for collection from 10.30am
or
Hand in by 2.30pm for collection from 3.00pm

**Staff Use Only**
Loan ☐
Reference ☐
Caroline Skeel ☐

Date Issued

Signed

---

**terials & Methods**

erroneous balance
Consequently any
atic discharge line
eby removing any
ue with regards to
e the same problem
here was any static
ce.

**ze Analyser**

ving each test. All
5 °C. Polyethylene
estion method, an
f sodium hydroxide
adients of 0.96 and
1 sample, described
samples were then
alvern Instruments,
in the isopropanol
2 nm and a LED at
crete bands spaced
orts the data in the
d from the volume
f particles, with the
the bandwidth the
lar bandwidth. For
alculated for each

contribution from the total solid matter contained within the suspension passed through the PSA. The volume determined for a particular bandwidth is then divided by the volume of

an individual particle as determined by the PSA for any given bandwidth. This can be worked out for all bandwidths and the total number of particles contained within that sample can be determined.

The circulating suspension that is carried past the laser light is isopropanol at 0.93 $kgm^{-3}$, with added nonidet surfactant (BDH, UK) to stop any agglomeration (Elfick *et al*, 2001). Following Mastersizer analysis, the isopropanol samples containing the volume of PE particles were vacuumed filtered through 47 mm diameter, with pore sizes of 0.05 μm, polycarbonate membrane filters (Nucleopore Filters, Part number 111103, Whatman, UK).

### 3.5.2 UHMWPE Particle Isolation & Analysis-SEM

The filter membranes covered with PE particles were subsequently mounted on an aluminium stub, gold coated using a sputter coater and visualised using a Field Emission Microscope (Jeol JSM 6300F, Japan). Images were obtained under three levels of magnification, ×250, ×2500, and ×5000, with the 20 images captured at each level of magnification. Captured images of particles were then characterised using digital image analysis software (Image Pro Plus, Media Cybernetics, USA), using the mean diameter, perimeter, length, width, area, roundness and the aspect ratio as the parameters to be measured, a custom protocol was established in order to semi-automate the process of analysis. In brief the process of analysis required images to be binarised, in other words, converted to black and white images from the original bright field view image (Figure 3.12).

This allowed bright objects, PE or metal particles, to be isolated from the background, overlaying the original image on top of the binarised image allowed accurate sizing of the particle, by obtaining the correct threshold (0-256) for the binarised image, in order to verify that what is seen is the true border around the particle and not the border that the software has extrapolated. The required parameters could then be selected from a table of measurements and the data obtained from analysis could be stored in Excel or ASCII form for further analysis. A complete protocol for image analysis using Image-Pro Plus V4 is described in detail in appendix 1.7.

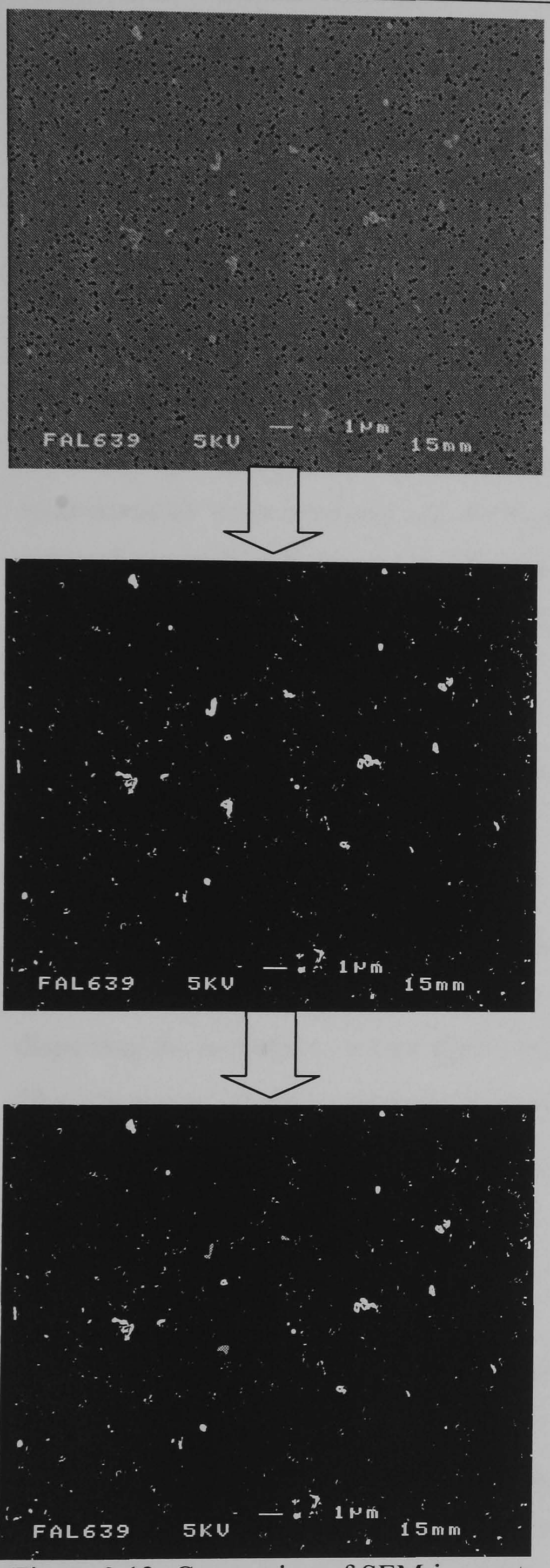


Original image obtained during SEM analysis, showing polyethylene particles on a 0.05 µm pore size, 47 mm diameter polycarbonate filter.

Original image converted to a black and white image using the binaries function in image pro plus.

Once image has been converted, single particles can then be highlighted individually and the parameters can then be measured.

Figure 3.12: Conversion of SEM image to a binarised image highlighting PE particles on a polycarbonate filter.

### 3.5.3 Metal Particle Isolation & Analysis-TEM

Following each test, the complete volume of serum was collected from each station, collected in 500 ml polypropylene bottles, stored at -25°C.

Prior to isolation of wear debris, each sample was removed from the freezer and allowed to defrost at room temperate. Two 40 ml samples of serum were collected and digested from each test station from femoral head prostheses measuring 28, 40 and 56 mm in diameter, with a further 2 samples collected following each jogging test from each station. CoCrMo wear particles were extracted and isolated from used bovine serum (BS) using a similar protocol reported by Doorn *et al* (1996) and Catelas *et al* (2001). This enzymatic protocol has been previously shown to cause less damage to metal particles compared to the use of alkalis, such as KOH or NaOH (Catelas et al, 2001).

In brief, all samples (40 ml) were subjected to a four-loop isolation protocol, which involved centrifugation (16,000 × g), re-suspension in sodium dodecyl sulphate solution (SDS), heating, washing in acetone and a Tris-HCl solution, and incubation in 1) papain and 2) protenaise K (Sigma-Aldrich, Dorset, UK) for 24 hrs at 60°C. Prior to drying on 3 mm carbon coated copper grids for microscopy. Samples were prepared by ultrasonically dispersing the particles to reduce agglomeration, for 30-60 seconds. Following sonication, a 20 µl aliquot of ethanol, containing metal particles was pipetted onto a carbon coated, 200-mesh size, 3 mm diameter copper grid (Agar Scientific, Essex, UK), in 5 µl droplets, allowing the ethanol to evaporate between each consecutive droplet. A complete protocol for isolating metal particles is described in detail in appendix 1.6.

The metallic wear debris were then characterised using a (JEOL JEM 2010, Japan) high resolution Transmission Electron Microscopy (TEM) operated at 200 KeV. Energy dispersive X-ray analysis (EDXA, Oxford Instruments, Oxford, UK) was used to confirm the presence of metal particles, before any images were obtained.

Size and morphology of particles were established from the analysis of micrographs collected as bright field images, which were photographed at 2 levels of magnification. For each sample, 5 images were obtained at ×10 k, for large particles and 10 images at ×50 k for small particles, providing a size range of 10 nm to 3000 nm. This protocol allowed the imaging of 100 or more particles per sample, with an average number of 254 particles for the samples analysed, ranging from 138 to 378 particles.

Images from the TEM were obtained in bright field mode, as this allowed for particles to be imaged at a higher image resolution, which in turn would allow greater accuracy during measurement. Following the development of TEM micrographs, the images were scanned into a computer, and a custom protocol was established in order to semi-automate the process of analysis using image analysis software.

Particles were characterised using digital image analysis software (Image Pro Plus, Media Cybernetics, USA), using the same parameters used to define PE particles, mean diameter, perimeter, length, width, area, roundness and the aspect ratio (Length/Width) as the parameters to be measured. With the information obtained from image analysis, with regards to the mean diameter, and assuming that all particles are spherical, combined with the wear rate experienced by each prosthesis, the total number of particles per unit volume of wear was estimated.

Following image analysis, measurement data was used to calculate the surface area and volume of each individual particle from all samples analysed. Surface area ($S_{PE}$) and volume ($V_{PE}$) data were calculated with the assumption that all particles observed were in the shape of prolate ellipsoids (cigar like), therefore the equations for the surface area and volume for a prolate ellipsoid, as shown in Figure 3.13, was used

A prolate ellipsoid is formed by the rotation of an ellipse around the major-axis (*a*), but ellipsoids are also eccentric, consequently this must be taken into account when calculating

the surface area. Therefore let *a* be the major-axis (length), *b* be the minor axis (width), and $\varepsilon_{PE}$ the eccentricity of a prolate ellipsoid.

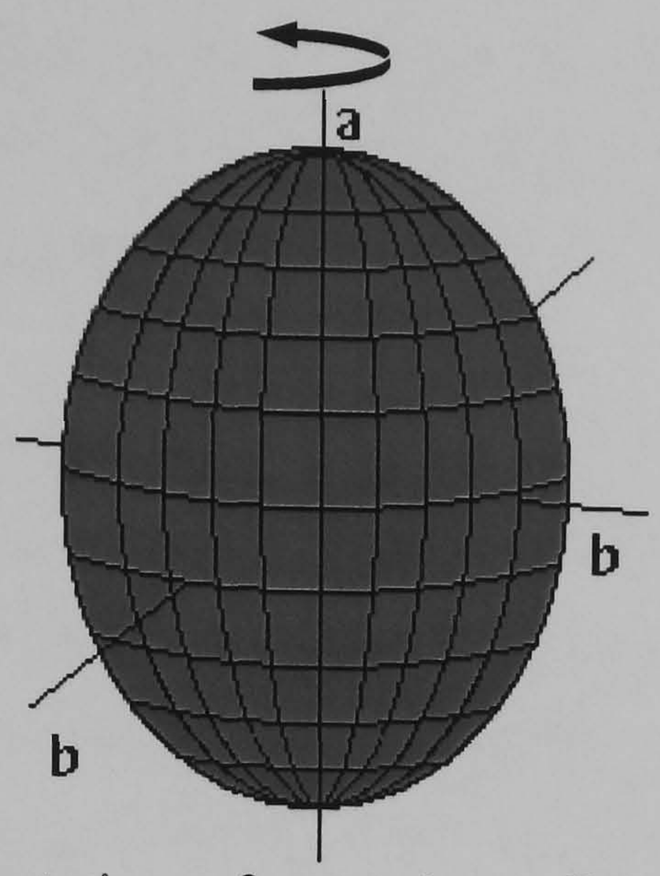


Figure 3.13: Schematic representation of a *prolate ellipsoid* showing the major axis of rotation

Where the eccentricity of a prolate ellipsoid is defined as:

$$\varepsilon_{PE} = \sqrt{1 - \frac{b^2}{a^2}} \qquad \text{Equation 3.2}$$

The surface area for an entire prolate ellipsoid can be found from:

$$S_{PE} = 2\pi a^2 + \frac{2\pi ab \sin^{-1} \varepsilon_{PE}}{\varepsilon_{PE}} \qquad \text{Equation 3.3}$$

and the volume of a prolate is defined as:

$$V_{PE} = \frac{4}{3}\pi ab^2 \qquad \text{Equation 3.4}$$

Parameters *a* and *b*, are measurements obtained during image analysis, representing length and width respectively. This then allows for the accurate calculation of the surface area and volume of each individual particle analysed during image analysis, using equations 3.2 to 3.4. Information gained from the analysis of $S_{PE}$ and $V_{PE}$ was then used to estimate the number of particles and total surface area generated during a test, which can be done as the volume loss has already been calculated using equation 3.1, for  and permits the accurate prediction of the total surface area generated by particles in the long term.

## 3.6 Statistical Analysis

For both volumetric wear and wear particle data, the mean, median and standard errors were calculated using the raw (untransformed) data. To satisfy assumptions of normality and homogeneity of intra-sample variances, and a one-way analysis of variance (ANOVA) (components of variance) was conducted, with $p<0.05$ as the level of significance.

Particle sizes obtained from the PSA were presented as modal particle size due to the nature of distribution, which was presented as normalised data, with a particle size range indicating where the majority of the particles lay within the size bands. Particle size data from SEM and TEM analysis are presented mean particle sizes, as a sufficient number of particles were obtained for image analysis, with the assumption that all distributions observed were normal, justifying the use of parametric statistical analysis.

# Chapter 4 Experimental Results

## 4.1 Walking and jogging with a smooth femoral head

### 4.1.1 Walking

Following walking tests under smooth femoral head conditions, both the metal and ceramic femoral heads articulating against polyethylene cups showed a weak biphasic wear pattern, with a higher wear rate generated in the initial period of walking from 0 to 1.3 million cycles than in subsequent cycles. The initial walking period produced a median wear rate of 21.4 $mm^3/10^6$ cycles, the ceramic head for this period of testing produced a lower wear rate at 13 $mm^3/10^6$ cycles. Once the cups had attained a period of steady state wear, the wear rate for walking with metal heads increased to 26 $mm^3/10^6$ cycles, however the ceramic head produced a lower rate, 11 $mm^3/10^6$ cycles, less than half the wear rate of the metal heads. Accumulated volumetric wear for all tests during smooth conditions are presented in Figure 4.1(a).

### 4.1.2 Jogging

Jogging tests, 1.2 and 1.4, using smooth metal femoral heads produced a median wear rate of 29 $mm^3/10^6$ cycles, an increase in the rate of wear compared to walking. The differences in the median wear rates for metal and ceramic femoral heads was also evident during the jogging tests. For the ceramic femoral head, despite the increase in the activity level, the wear generated was still lower for the metal head, generating a median wear rate of 21 $mm^3/10^6$ cycles. Walking tests between jogging tests produced a normal median wear rate of 24 $mm^3/10^6$ cycles, comparable to the wear rate observed during steady state wear. The accumulated volumetric wear recorded during the jogging tests are presented in Figure 4.1(b), showing both variability in volumetric wear between different metal heads and also between tests for the same heads, due in part to the relatively small changes in volume. The $6^{th}$ jogging test of 4 hours showed a decrease in wear for 3 of the 5 cups. This could have been as a result of climatic changes or charge build up in the polyethylene.

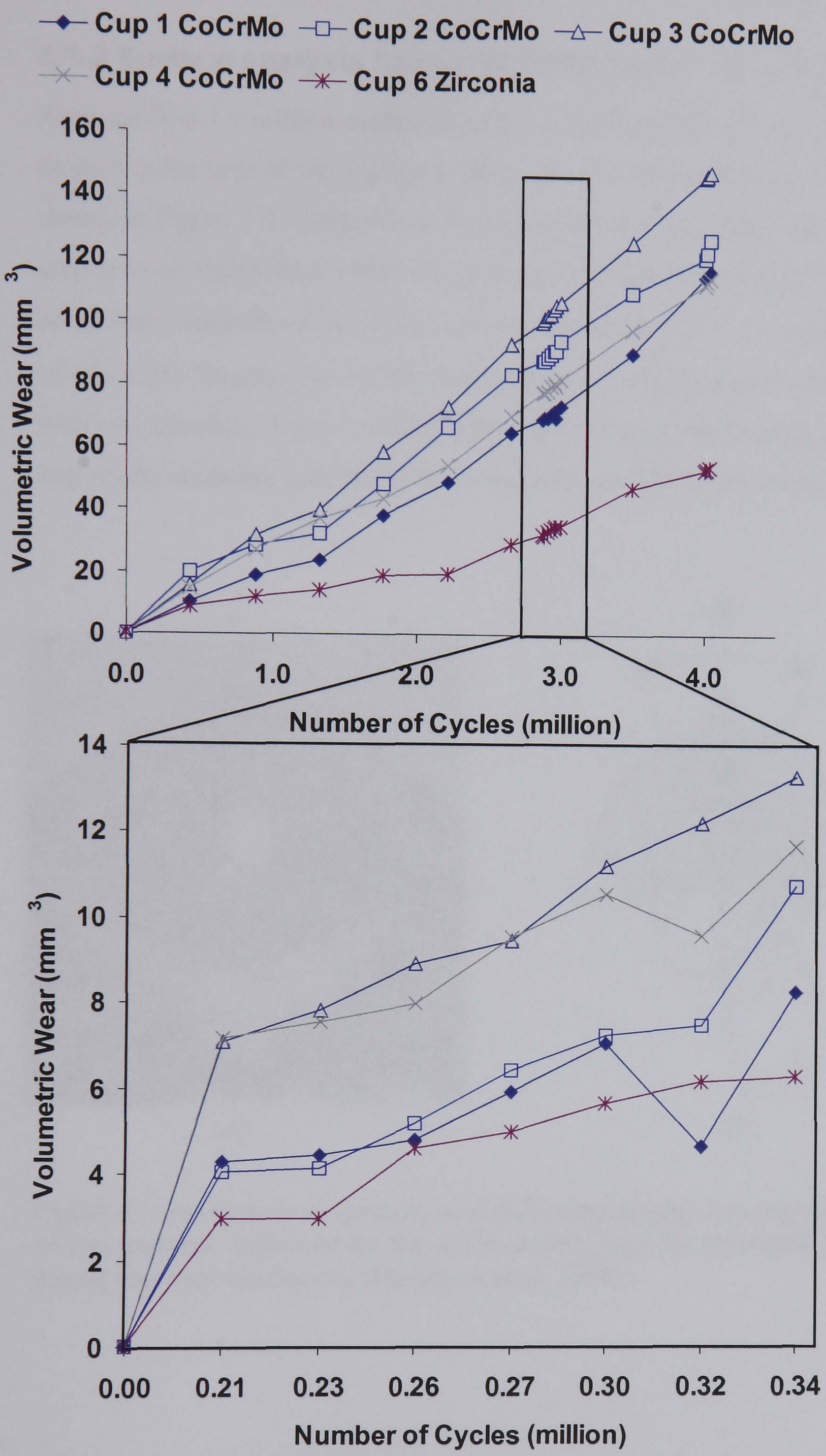


Figure 4.1: Graphs showing volumetric wear following tests using smooth femoral heads (a) shows the accumulated volumetric wear of polyethylene cups following walking and jogging tests and (b) shows the volumetric wear during jogging, as highlighted. The volumetric wear for the ceramic femoral head is consistently lower than metal femoral heads

### 4.1.3 Surface analysis following tests under smooth conditions

After the first 1.3 million cycles of walking visible marks on the metal heads were present, located in the area of the highest sliding velocity. These took on the form of loci patterns, shown in Figure 4.2. Surface measurements taken in this area, locations 1 to 4, in general tended to be higher than surface measurements taken at locations 5 to 8. All metal femoral heads had a mean $R_a$ of 0.019 μm, an increase roughness of 32 % from their initial mean $R_a$ of 0.013 μm. Despite the visible marks present on the heads, all cups were highly polished, with no sign of the initial machine marks present upon the bearing surface of the acetabular cup or any scratches that may have occurred as a result of the marks upon the femoral head.

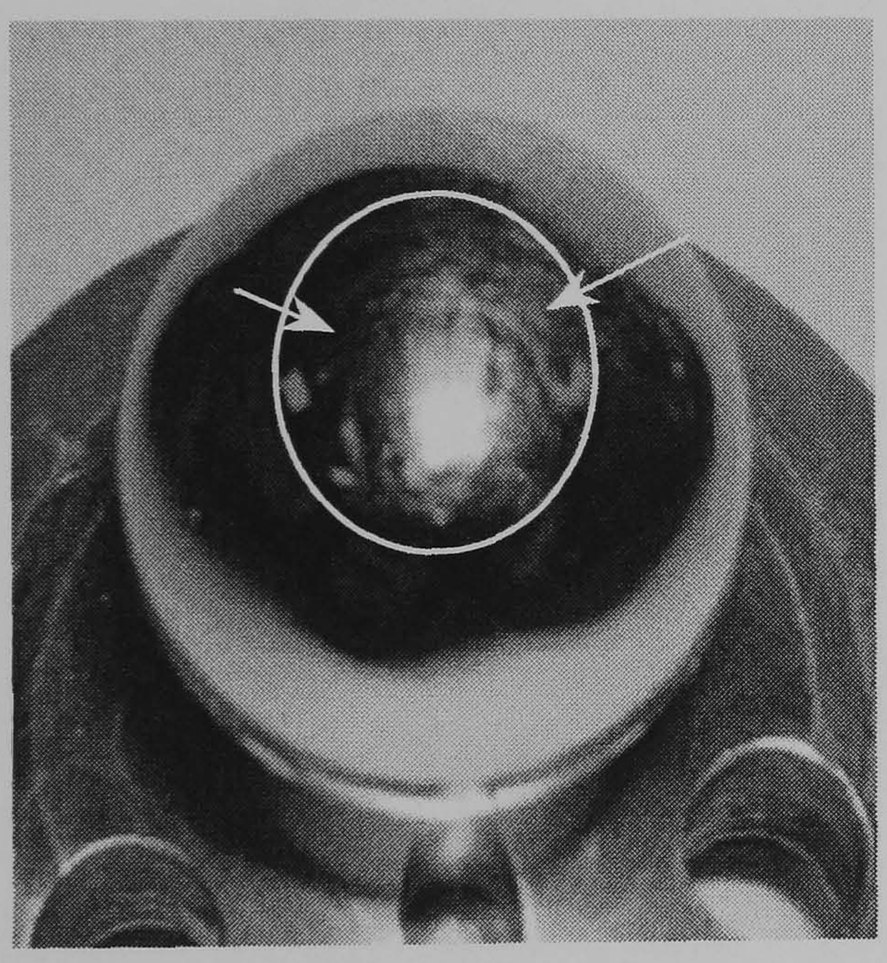

(a)

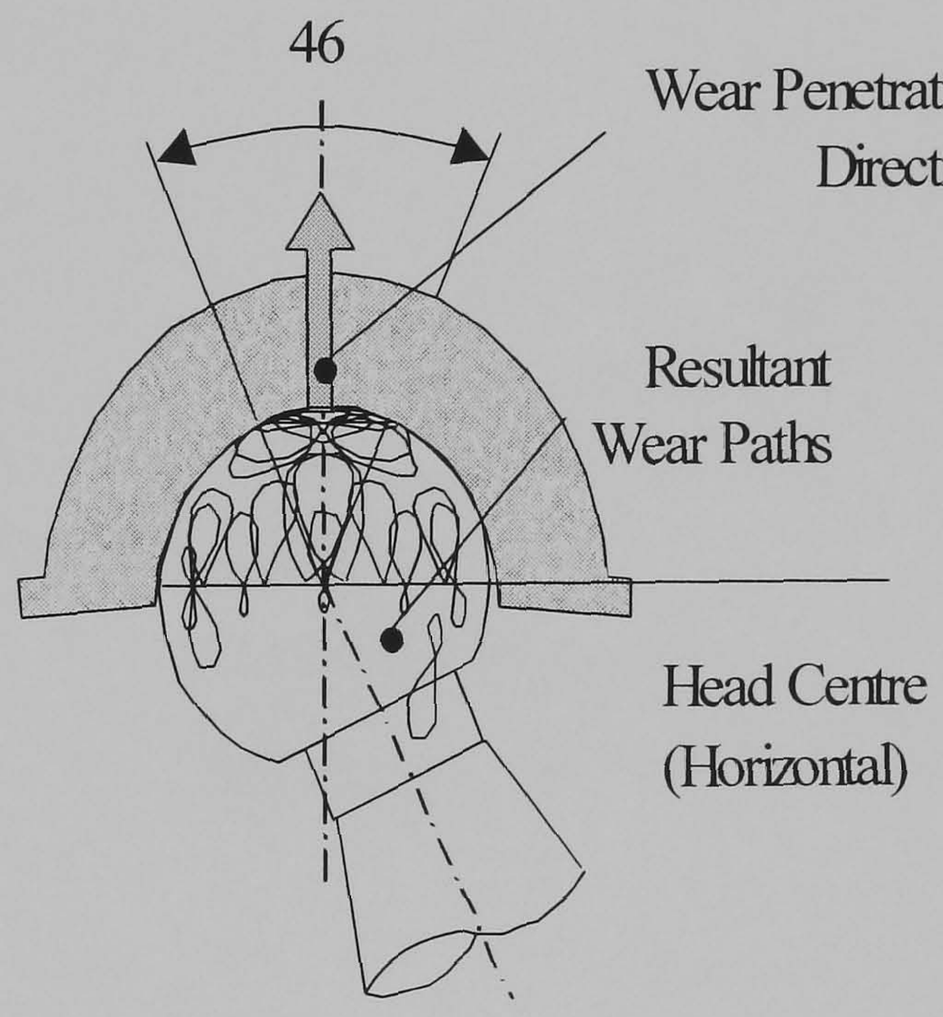


(b)

Figure 4.2: (a) Picture of femoral head following testing showing visible marks in the form of loci patterns, indicated by the white arrows, and (b) schematic of resultant wear paths during hip wear simulation. (Davidson *et al*, 1998).

Figure 4.3 (a) and (b) show a scatter plot of both surface $R_a$ and $R_p$ measurements obtained following 4 million cycles of testing. Both parameters in general show that measurements obtained at locations 1-4 are usually higher than measurements at locations 5-8. Although $R_a$ is a useful parameter for surface analysis, surface $R_p$ will indicate the presence of any scratches that may be present, in Figure 4.4 (b), $R_p$ shows a 10 fold increase in the surface parameter, which would not be indicated by surface $R_a$.

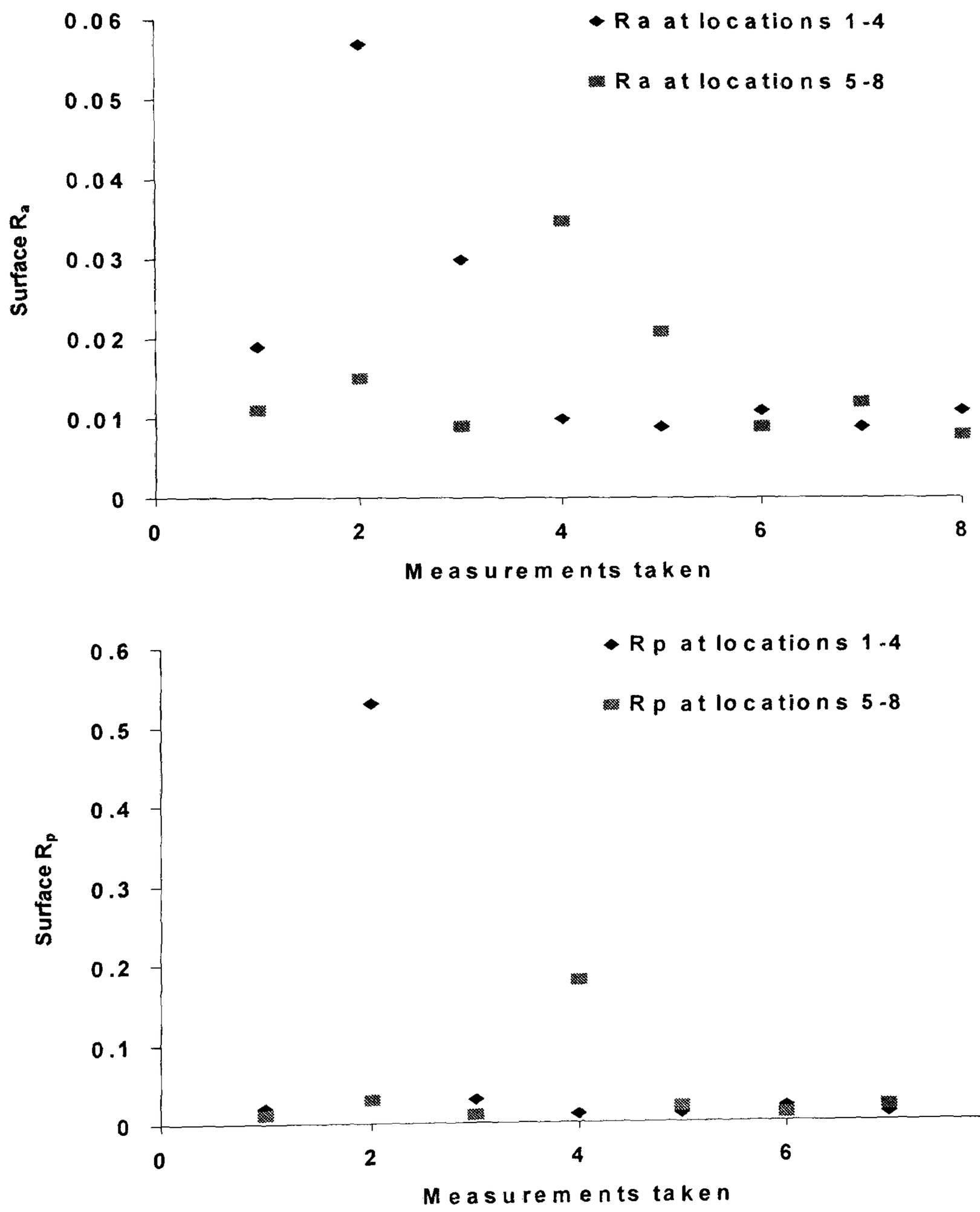


Figure 4.3: Scatter plot of surface $R_a$ and $R_p$ following 4 millions cycles of testing, for positions of surface measurement please refer to Figure 3.7.

Tests conducted under smooth conditions produced slight changes in surface roughness, surface measurements taken after walking showed a reduction in the overall surface topographic features. During the wear in phase (0-1.3 million cycles), surface roughness showed an increase in the metal heads, although subsequent wear created smoother heads. However, following jogging tests, at 3 million cycles, surface roughness showed a statistically significant change, 2-fold increase in the surface topography, $R_a$. The wear rates under smooth conditions did not show any significant difference. However surface measurements between each test and the distance from the pole did show differences for all heads that were measured, they were consistently rougher closer to the area of the highest sliding velocity, Figure 4.4.

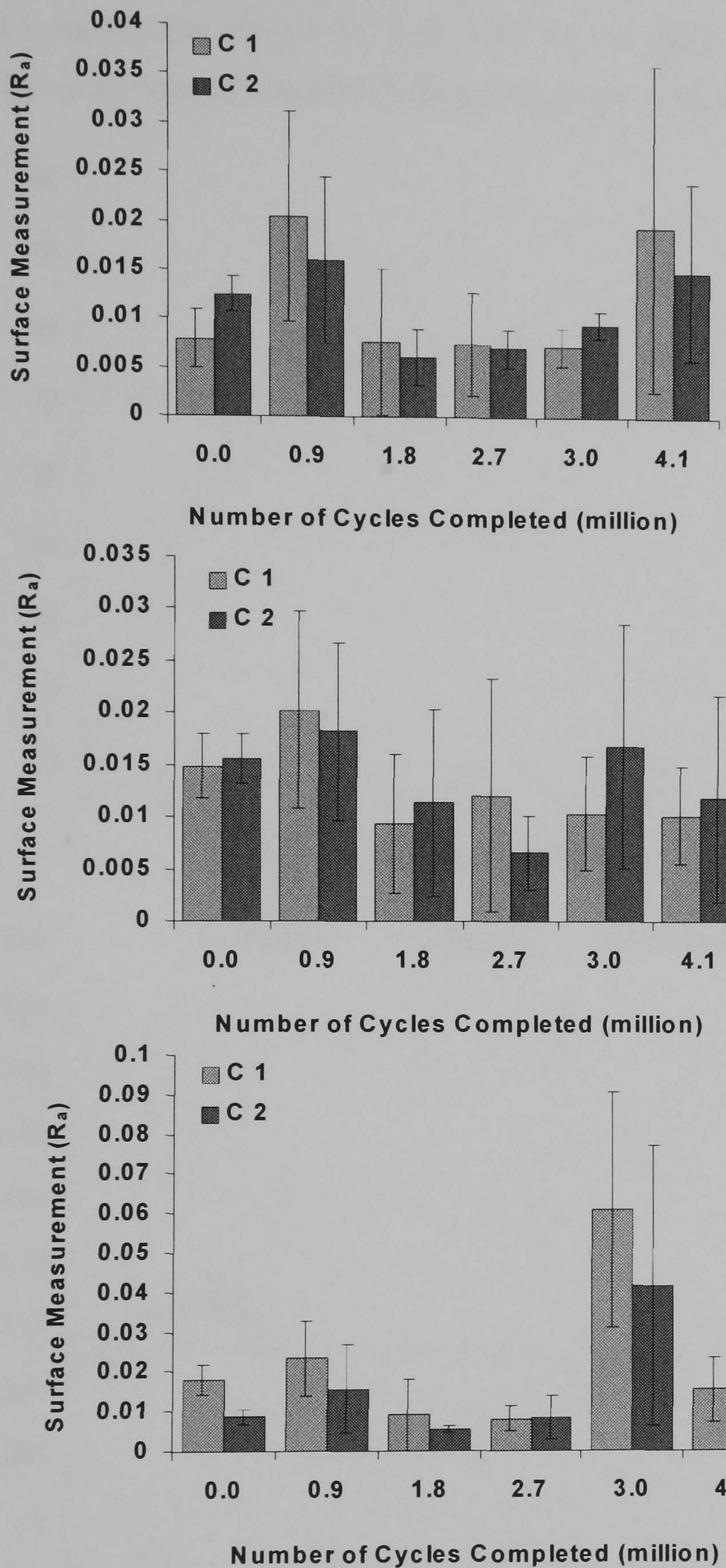


Figure 4.4 Change in surface for femoral heads 1 to 3 under smooth conditions, showing the change in surface topography between measurements at 5 mm (C1) and 10 mm (C2) from the pole

Figure 4.5 shows the change in wear rate for all metal head with changes in surface topography under smooth conditions following both walking and jogging tests.

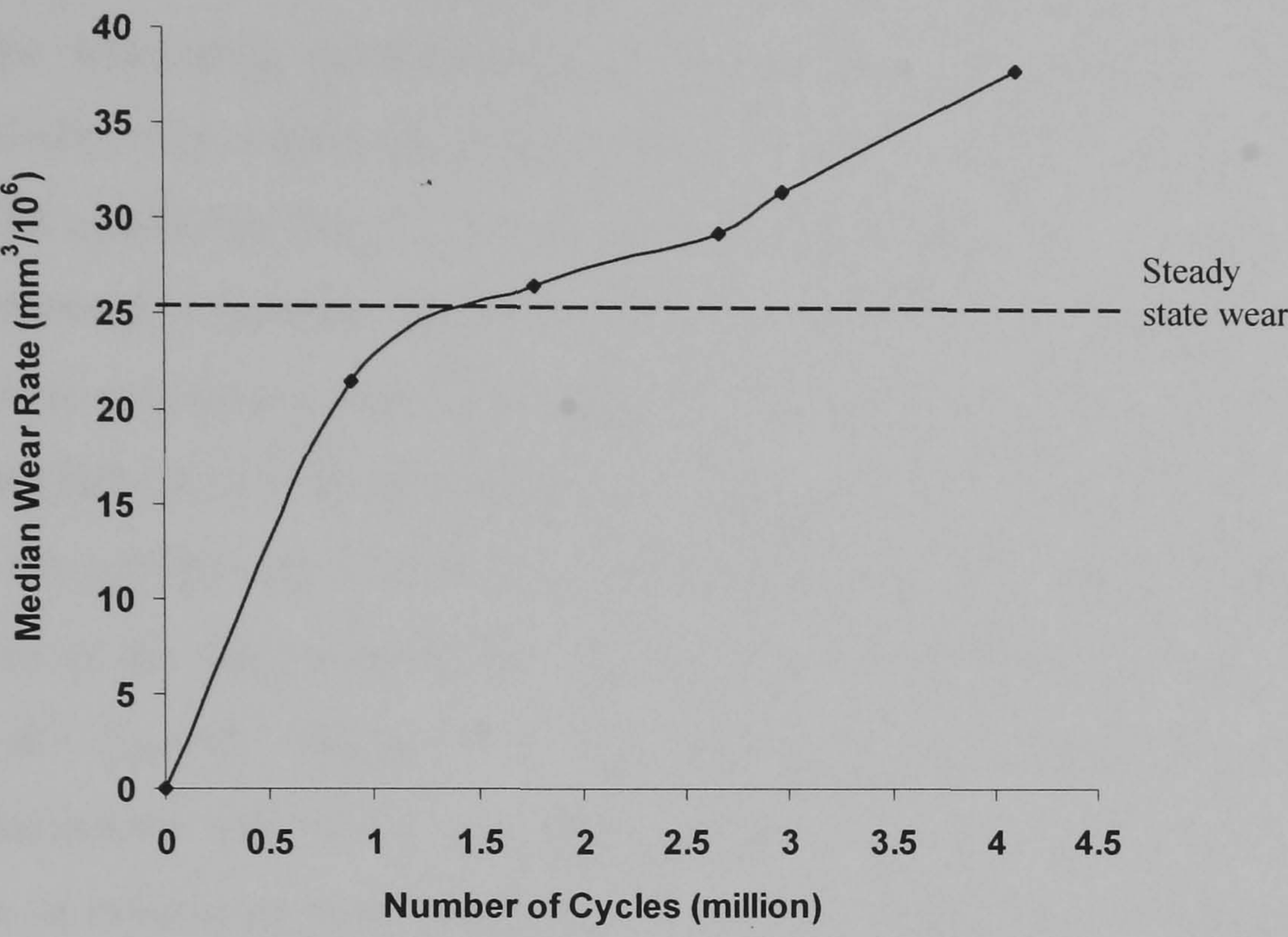


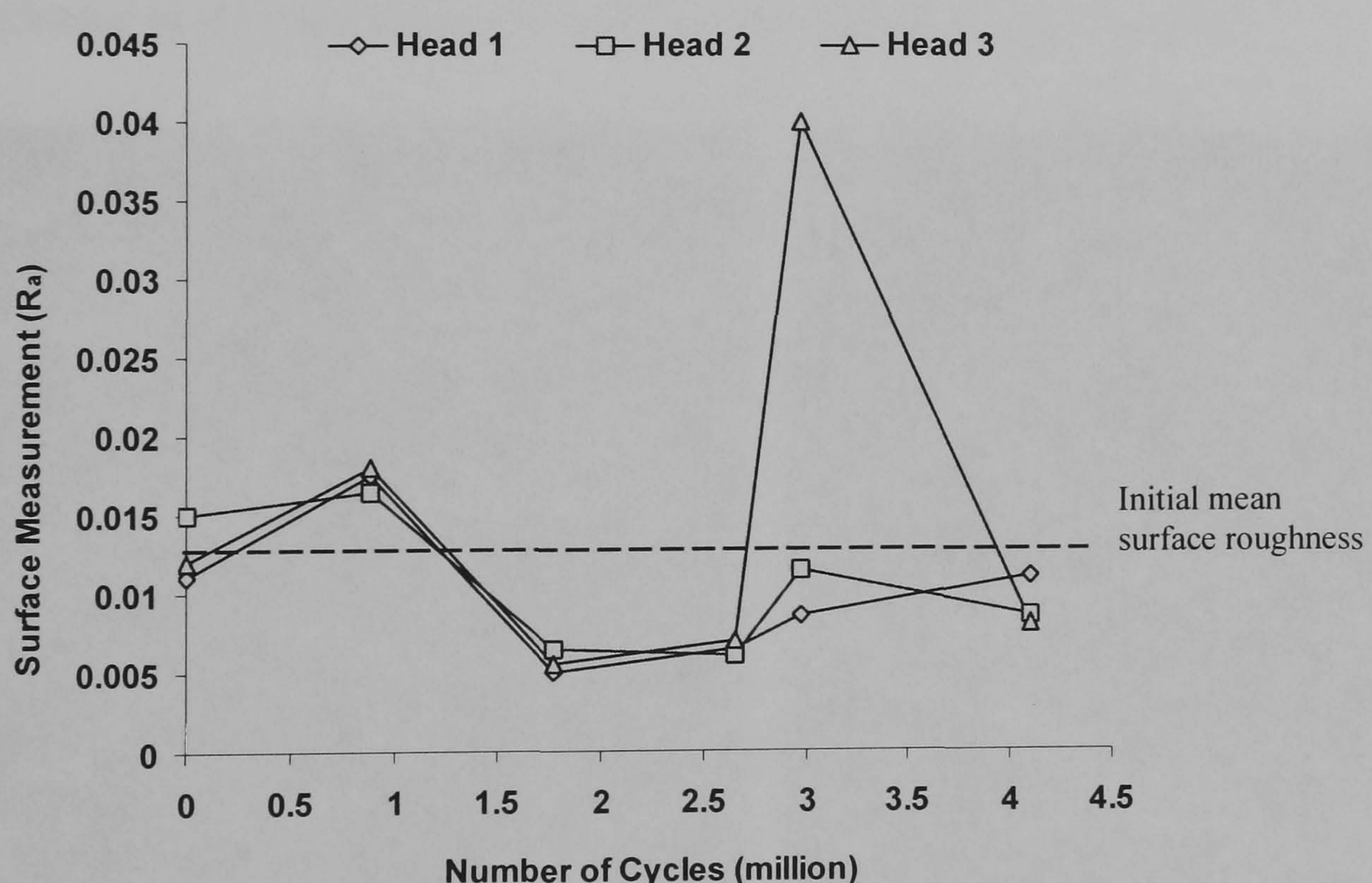


Figure 4.5: (a) the median wear rate obtained from tests under smooth femoral heads and (b) the surface $R_a$ throughout testing under smooth conditions

### 4.1.4 Particle analysis following walking under smooth femoral head conditions

Following walking tests under smooth femoral head conditions, six samples were collected from the lubricating medium used in hip simulator tests at 2, 2.5 and 3 million cycles respectively, two samples per station. Image analysis (Figure 4.7) of the particles viewed on the SEM confirmed that the debris possessed a similar range of sizes, to that which has been reported in previous studies. A variety of particle morphologies were observed, from round/oval particles to plate-like particles. The large particles observed in the course of the SEM analysis tended to be plate-like in shape or in the form of large shreds (Figure 4.6), whilst the smaller sub-micron sized particles tended to be more rounded or oval in shape. Particles in the intermediate size range (1 to 10 μm) were more fibril like, as shown in Figure 4.7 (a), inset Figure 4.7 (b) and submicron sized particles are shown in Figure 4.7 (d). Qualitative analysis during SEM imaging, clearly showed that there were a large number of submicron sized particles that were generated during the tests, which would also be reflected in the total number of particles determined through the PSA.

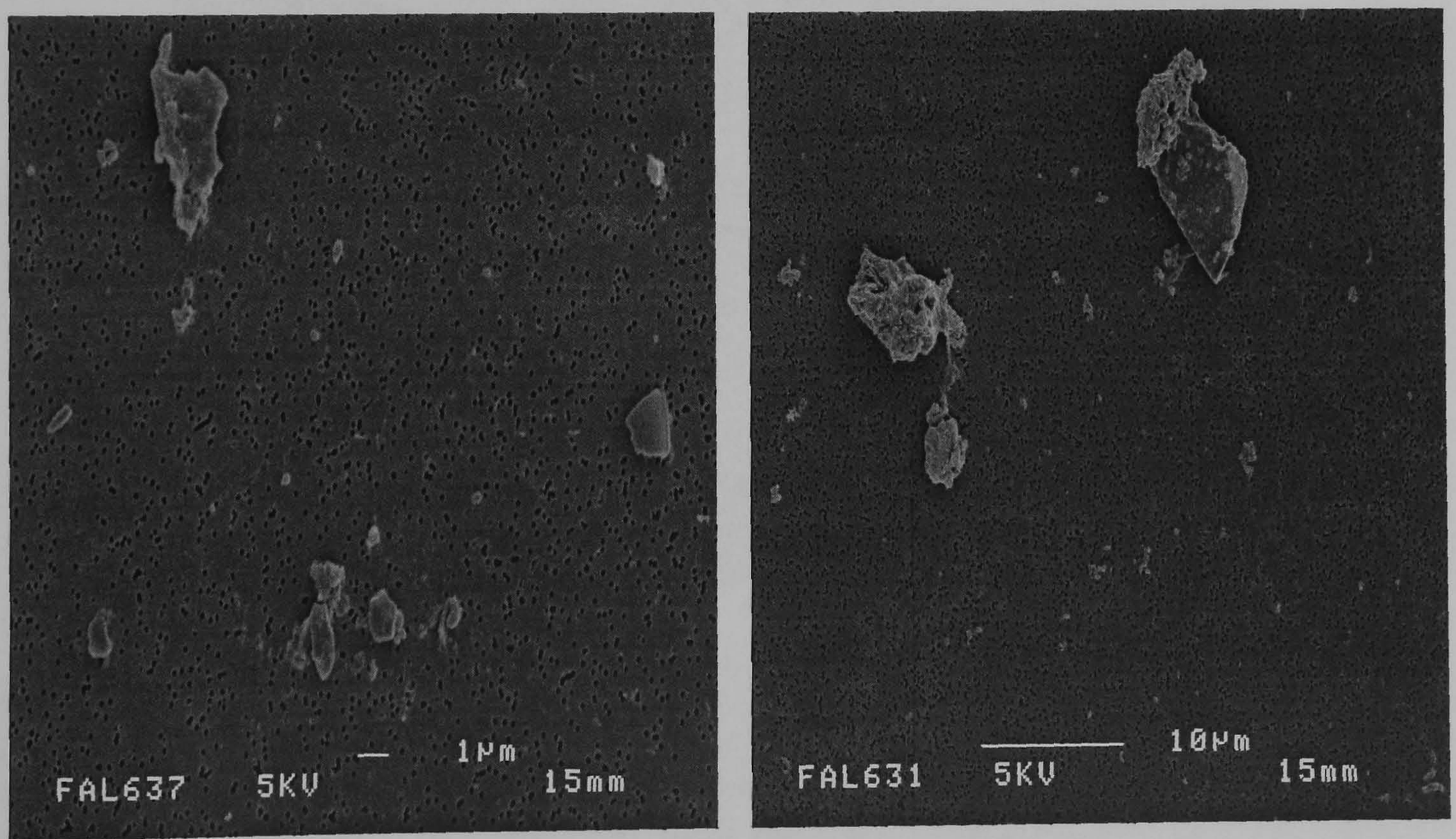


Figure 4.6: Large plate like particles captured on a 0.1 μm pore size filter, ranging in size from 1 to 10 μm in size

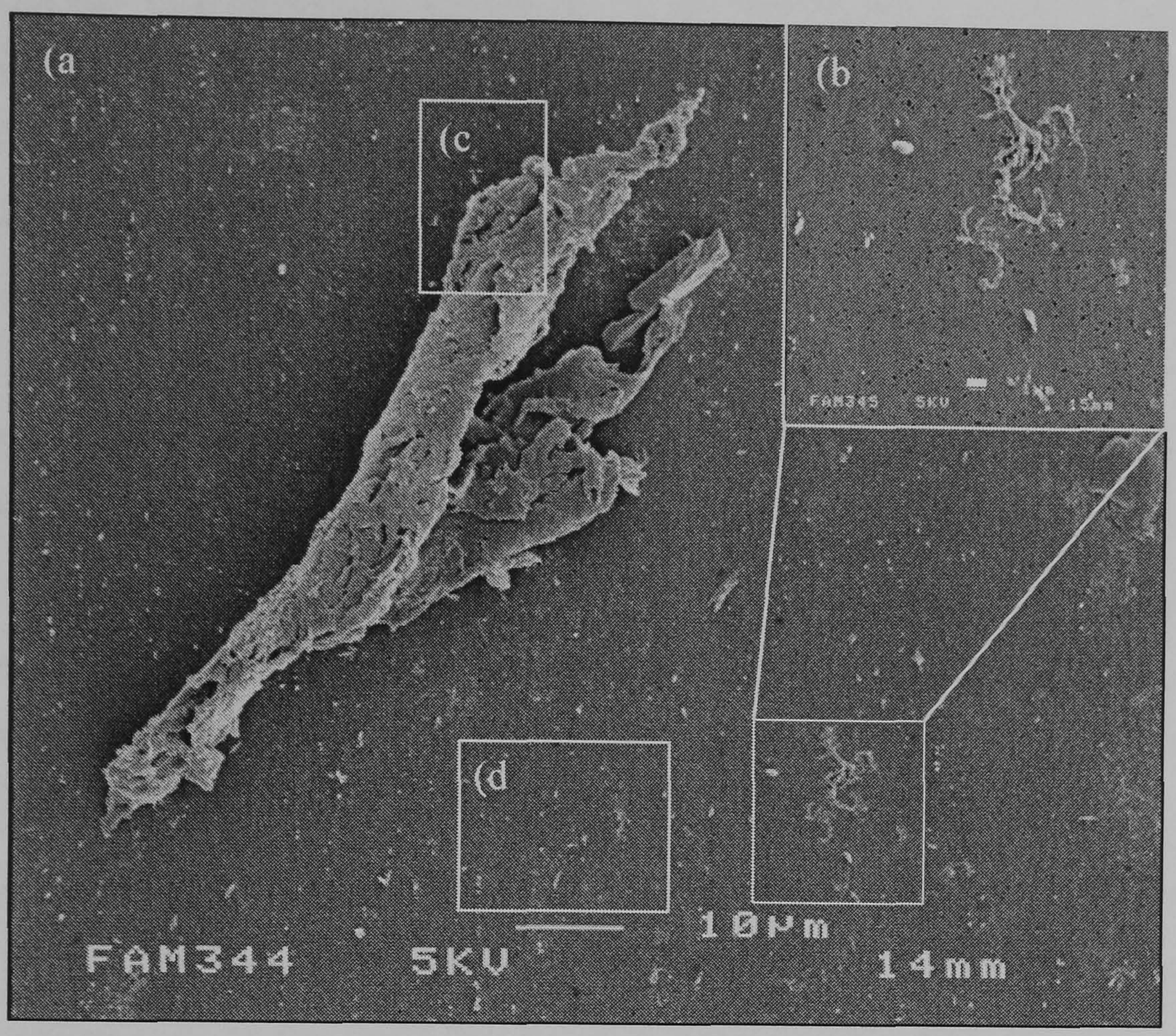


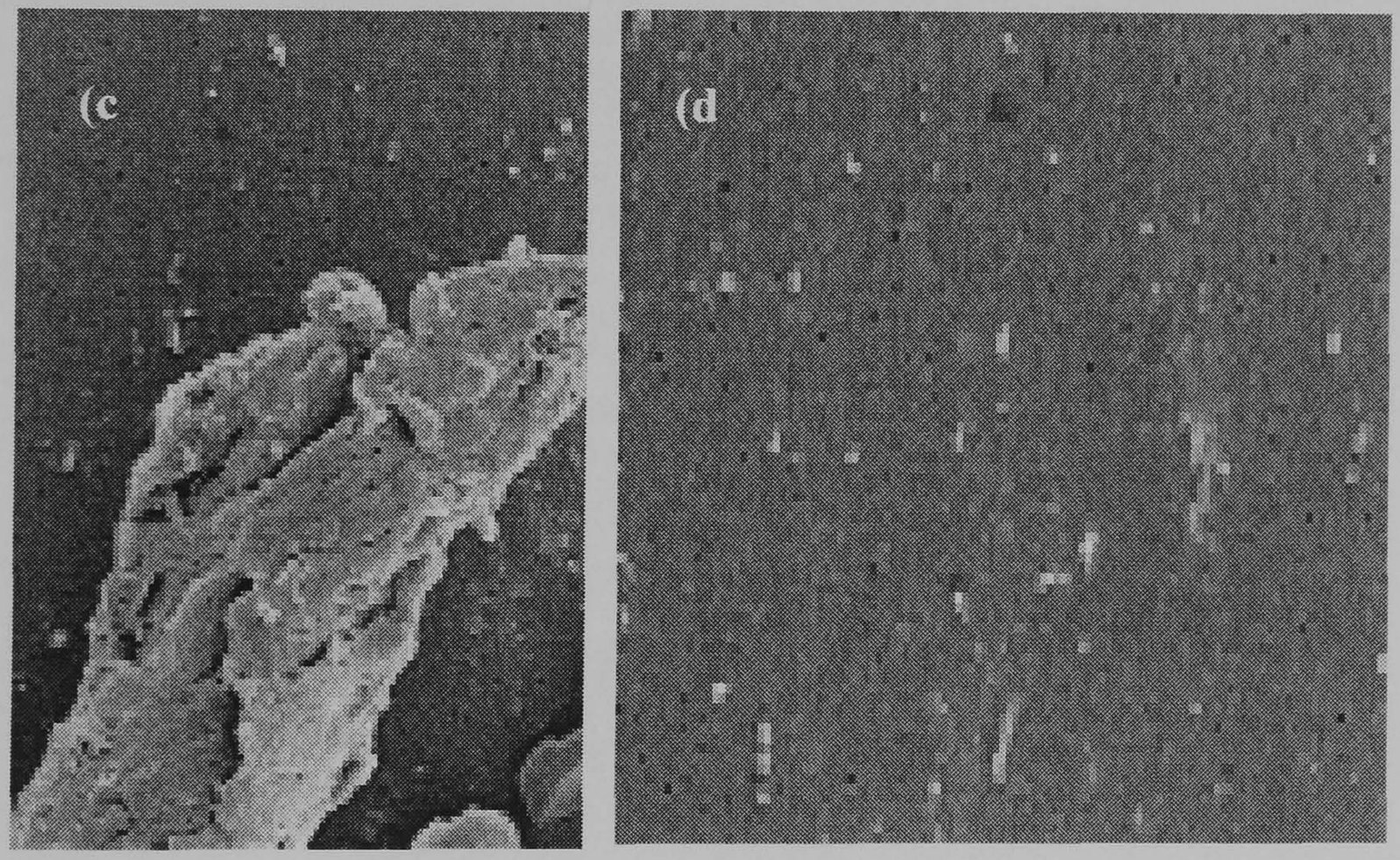


Figure 4.7: SEM images showing polyethylene wear particles produced under normal physiological walking conditions using smooth femoral heads, showing (a) a large shred-like particle greater than 50 μm, with many discrete submicron sized particles and (b) fibril-like particles surrounded by submicron sized particles. Enlargement of insets (c) and (d) from (a), showing many discrete submicron sized particles on and surrounding the large particle. Scale bar indicates 10 μm.

The PSA number distribution for all samples, indicates that the majority of the particles produced during walking tests were in the range of 0.09 to 3 μm. The number distribution showed that the majority of particles lie in the range of 0.08 to 1 μm, Figure 4.8(a), this would therefore indicate that according to the PSA results, the majority of particles are within the bioactive range, i.e. in the range of 0.1 to 10 μm.

Volume distributions for all samples analysed on the PSA are shown in Figure 4.8(b). All the distributions show a bimodal distribution with modal peaks in the range of 0.1 to 400 μm. Both samples at 2.5 million cycles (Sample 2a & b) showed evidence of particles greater than 100 μm, whilst samples at 2 and 3 million cycles (Sample 1a & b, and 3a & 3b) showed that the most frequently occurring particles lay within the size range of 0.1 to 30 μm. The volume distributions of samples 1 and 2 showed two distinct groups of particles, sample 1 showed modal peaks at 1 and 22 μm, whilst sample 2 showed modal peaks at 4.5 and 400 μm. The distributions between the samples showed differences, however, comparisons of samples from a single station showed very similar distributions, indicating that the methodology of sampling and subsequent PSA analysis produced repeatable results.

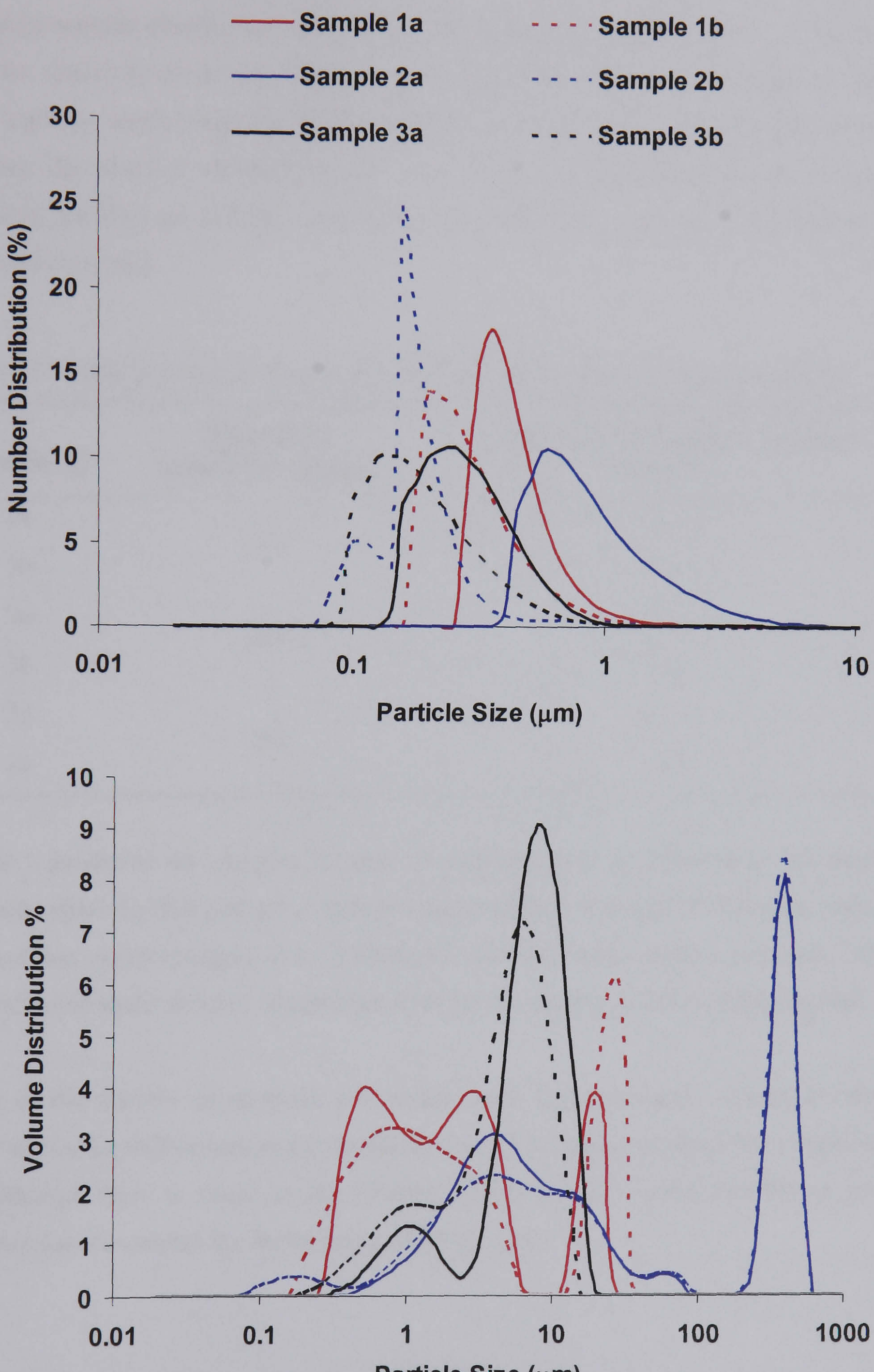


Figure 4.8: Showing (a) number distribution and (b) volume distribution of samples collected at 1, 2 and 3 million cycles.

Percentage number distributions show where the majority of the particles lie within the size band, the distributions do not however provide information on the number of particles within a given sample. Once the number distributions had been obtained, it was possible to determine the absolute numbers of particles. Table 4.1 shows the number of particles counted by the PSA per sample, with the median wear rates observed during tests at 2, 2.5 and 3 million cycles.

Table 4.1: Particle numbers and wear rates for samples analysed following walking

| Sample ID | Wear Rate ($mm^3/10^6$ cycles) | Number of Particles in sample ($\times 10^{12}$) |
|---|---|---|
| 1a | 34.4 | 12.0 |
| 1b | | 33.7 |
| 2a | 28.6 | 5.40 |
| 2b | | 2.69 |
| 3a | 26.4 | 1.39 |
| 3c | | 1.52 |

Sample 1 produced the greatest number of particles, this is reflected in the wear rate observed, which for this particular station was the highest recorded. Subsequent tests at 2.5 and 3 million cycles (samples 2 & 3) showed a decrease in the median wear rate, which is again reflected in the number of particles observed during the analysis of the samples.

A plot of the number of particles per sample with the percentage volume distribution, clearly shows the differences in the number of particles actually counted per sample, Figure 4.9. Although there is range in the volume distribution, the actual number of particles generated for all samples lay in the range of 0.3 to 1 μm

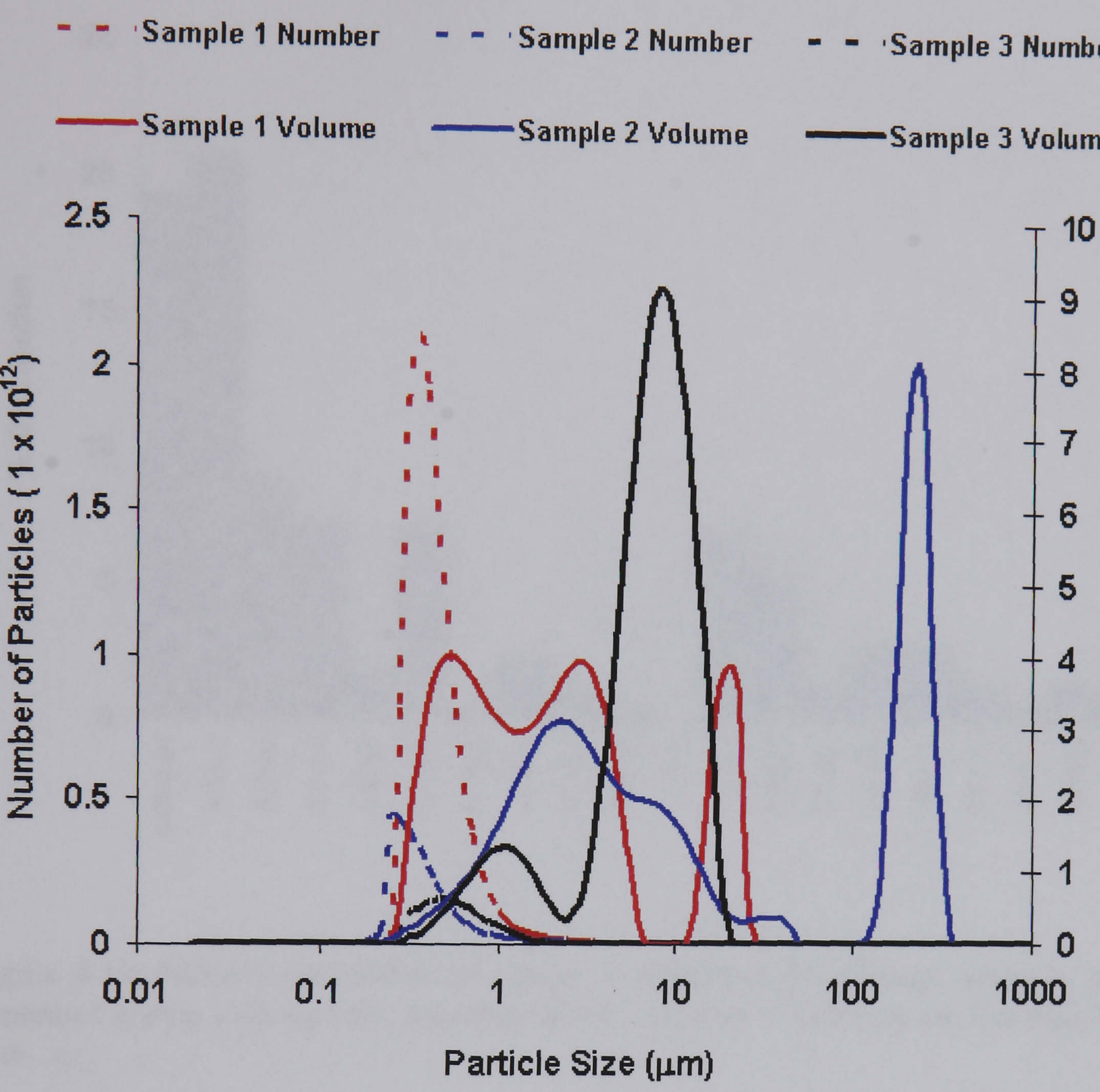


Figure 4.9: A plot of the total number of wear particles with volume distribution of samples following walking tests under smooth conditions.

Following PSA analysis, number distributions were determined using SEM analysis of the same samples. Under smooth conditions, SEM analysis indicated that the majority of particles were less than 1 µm in size, showing good agreement with samples 1 and 3, which also indicated that the majority of samples are less than 1 µm. Figure 4.10 is a percentage number distribution plot as determined following SEM analysis, of particles generated during walking tests under smooth femoral heads conditions.

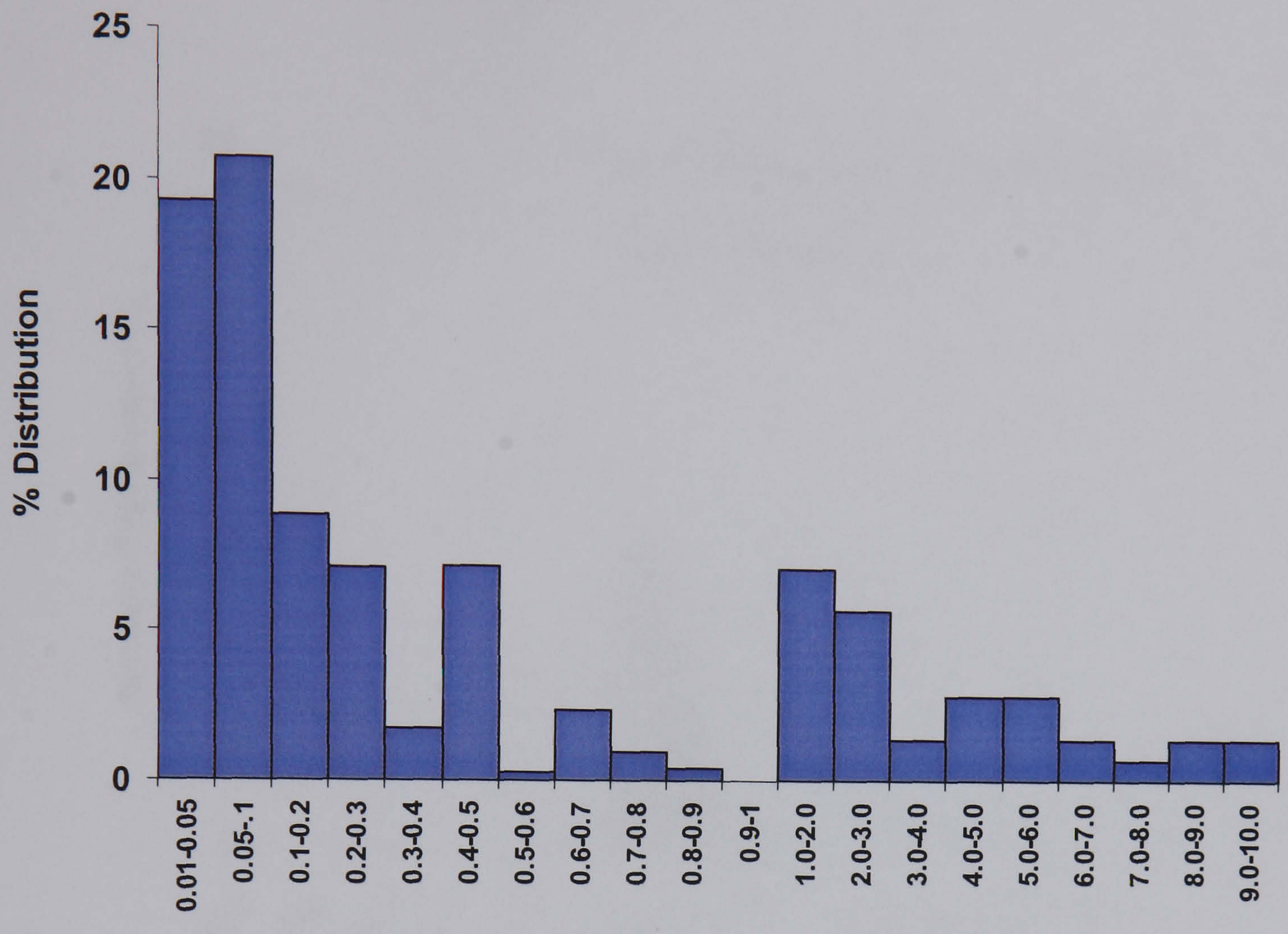


Figure 4.10: Number distribution of sample 1 following SEM image analysis, particles generated during walking tests, showing that the majority of particles are less than 1 μm in size

A comparison of the results in terms of numbers obtained from PSA and SEM analysis, are presented in Figure 4.11. These show some correlation between the number distributions. However PSA results indicate that approximately 90 % of the particles are less than 1 μm in size whereas with SEM results shows this to be at 69 %. Possibly of greater interest are particles less than 0.05 μm in size observed during SEM analysis (Figure 4.7) which were not detected by the PSA.

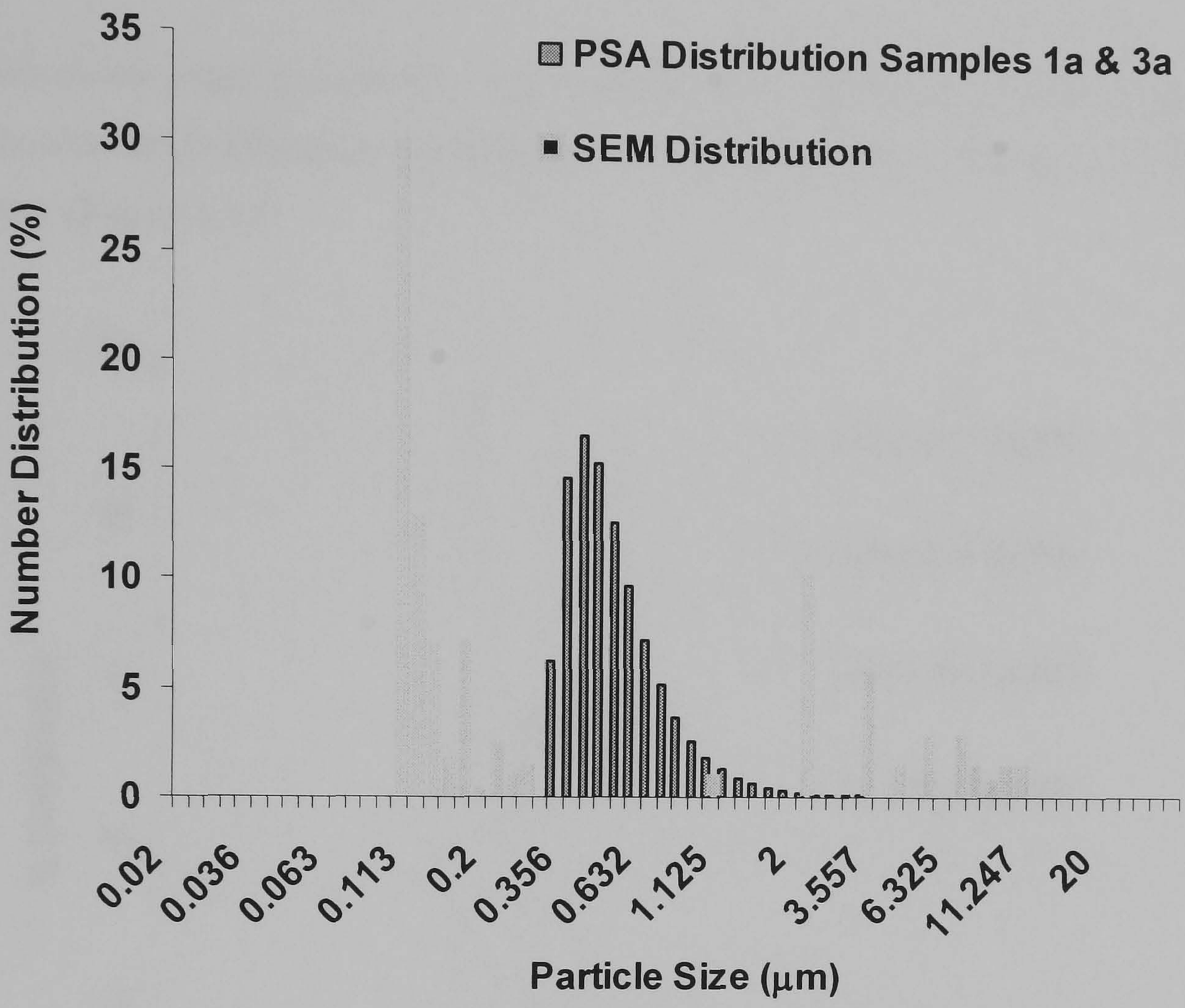


Figure 4.11: Comparison of PSA and SEM number distribution for particles generated during walking tests under smooth femoral head conditions, where the curves show the mean distribution obtained from samples 1a and 3a for both SEM and PSA.

### 4.1.5 Particle analysis following jogging under smooth femoral head conditions

Under simulated jogging activities, two samples were taken from two separate stations. These showed small differences in both the volume and number distribution as determined by the PSA (Figure 4.12).

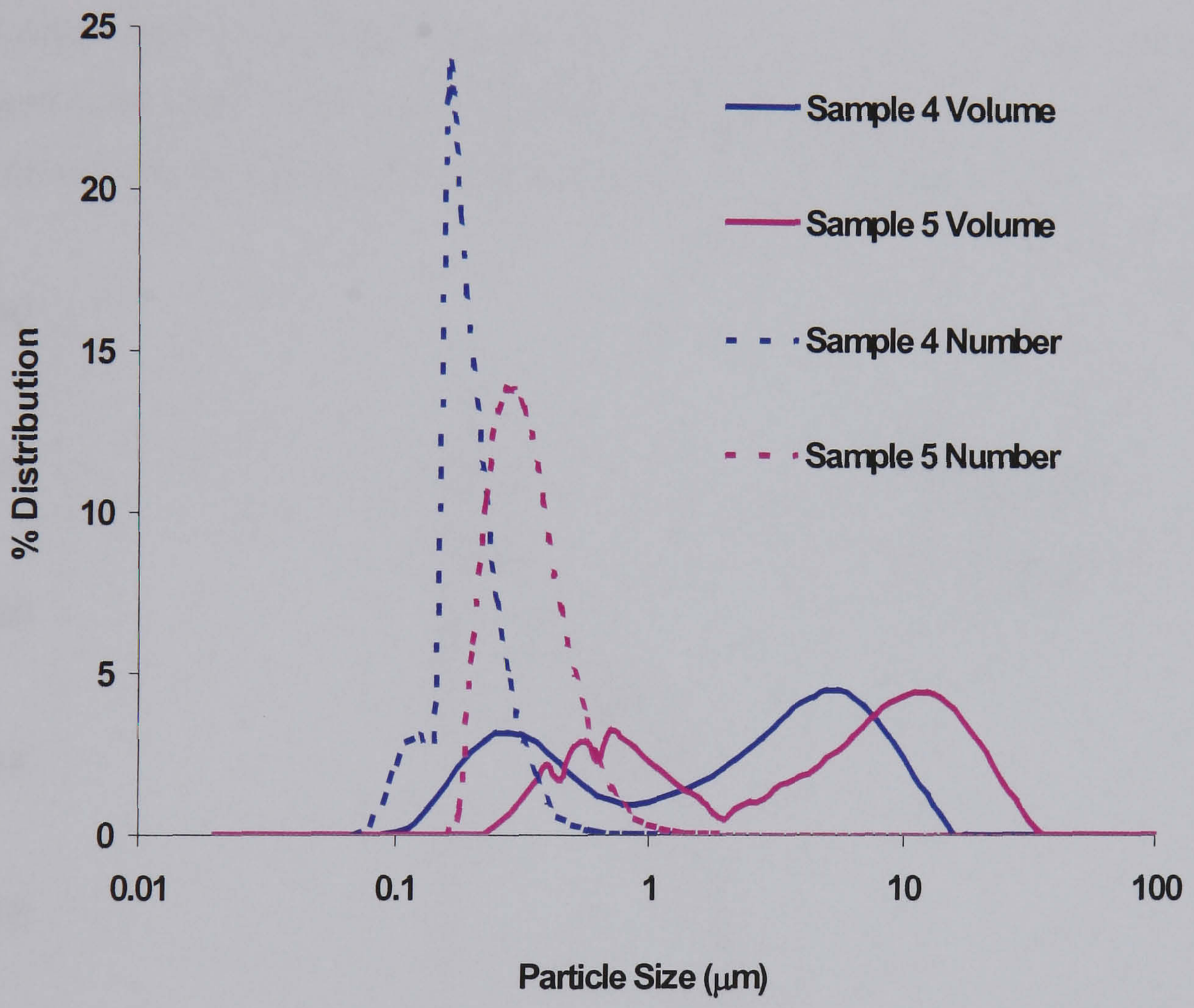


Figure 4.12: Number and Volume distribution of jogging samples (4 & 5) under smooth femoral head conditions

The percentage number distribution of the samples 4 and 5 indicated that the majority of the particles were 0.2 μm in size, ranging from 0.1 to 1.2 μm (Figure 4.12). Although both samples showed similar size ranges and volume distribution, absolute numbers showed that sample 4 produced 8-fold more particles than sample 5 (Table 4.2) in resulting from a higher wear rate.

Table 4.2: Particle numbers for samples 4 and 5 analysed following jogging

| Sample ID | Wear Rate ($mm^3/10^6$ cycles) | Number of Particles in sample ($\times 10^{12}$) |
|---|---|---|
| 4 | 39.2 | 60.8 |
| 5 | 28.9 | 7.19 |

Following PSA analysis, number distribution of samples 4 and 5 were determined through SEM analysis. Figure 4.13, shows the number distribution of these samples, both samples show a good correlation between the two stations, indicating that the results are repeatable between the stations, and the that the sampling method was the same for both.

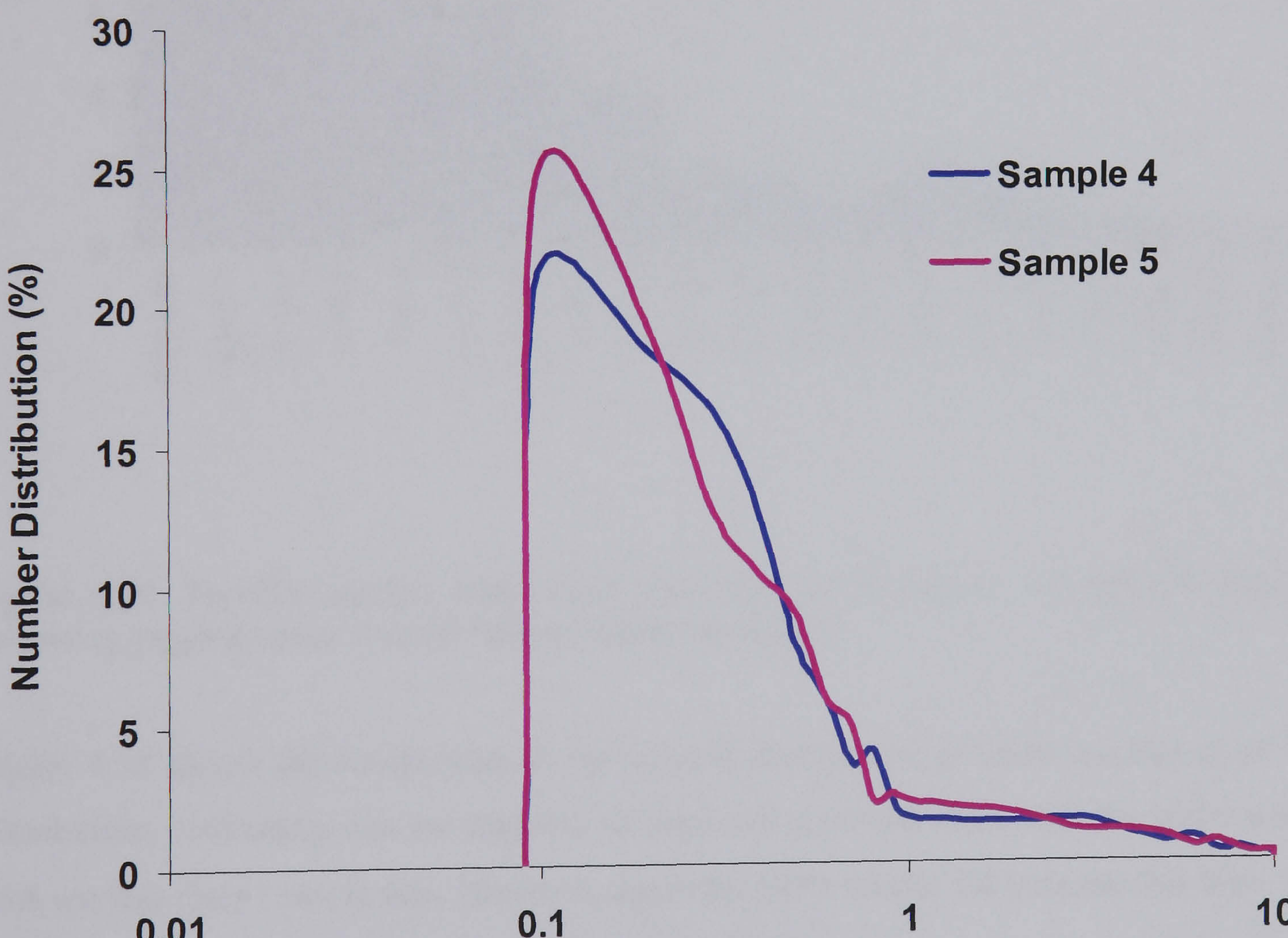


Figure 4.13: SEM number distribution of samples 4 & 5, following PSA analysis plotted on log scale

The overall distribution of particles following SEM analysis are presented in Figure 4.14 showing that the majority of particles (91 %) are less than 1 μm in size.

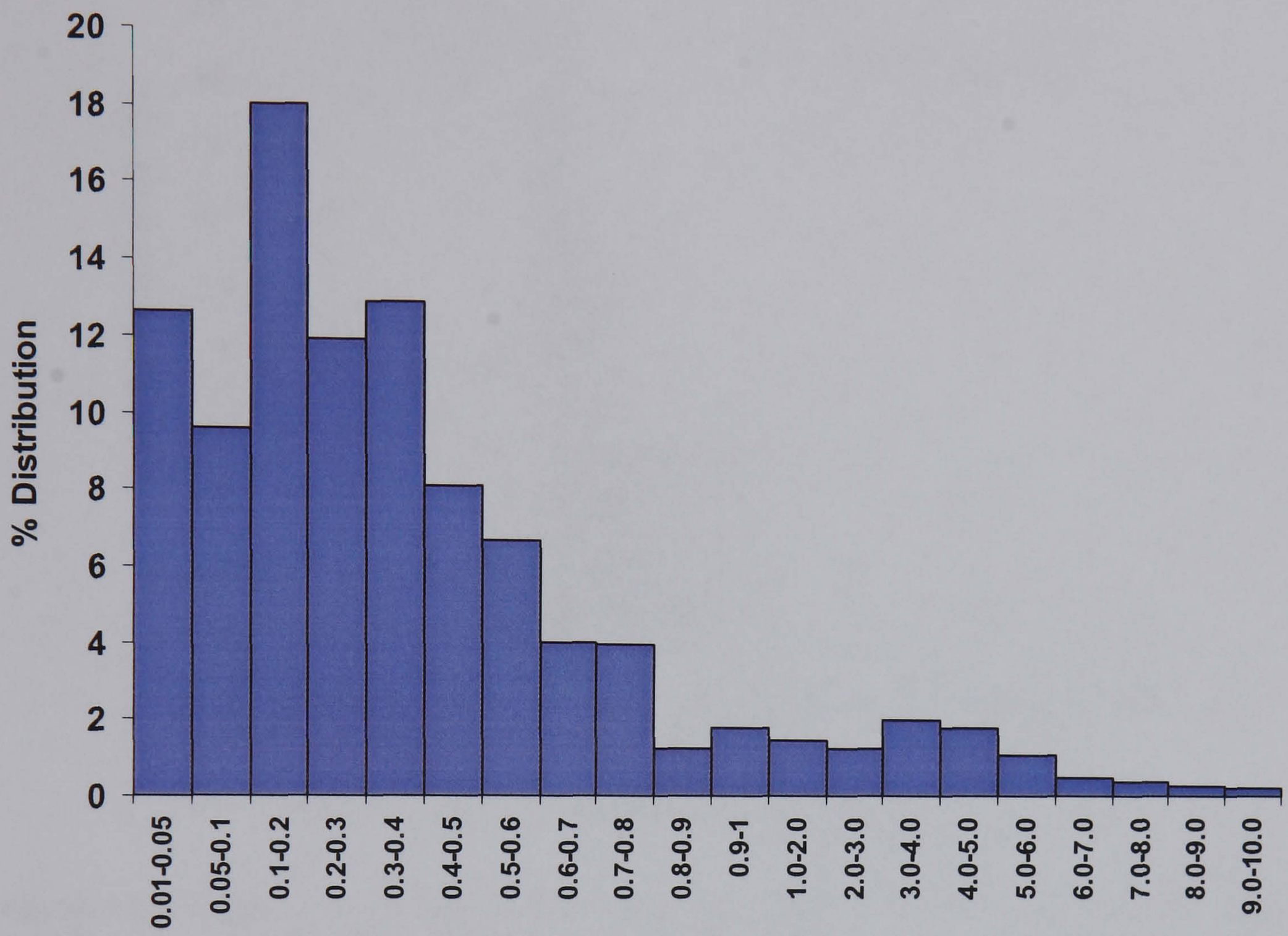


Figure 4.14: Particle number distribution following SEM analysis of particles analysed following jogging under smooth femoral head conditions

Figure 4.15 shows the comparison of the number distribution of SEM and the mean PSA distribution, indicating that the majority of particles observed from both the SEM and the PSA are less than 1 μm in size. However, again the SEM results did indicate that there were particles larger than 1 μm in size, although inevitably there are a very small number of these particles.

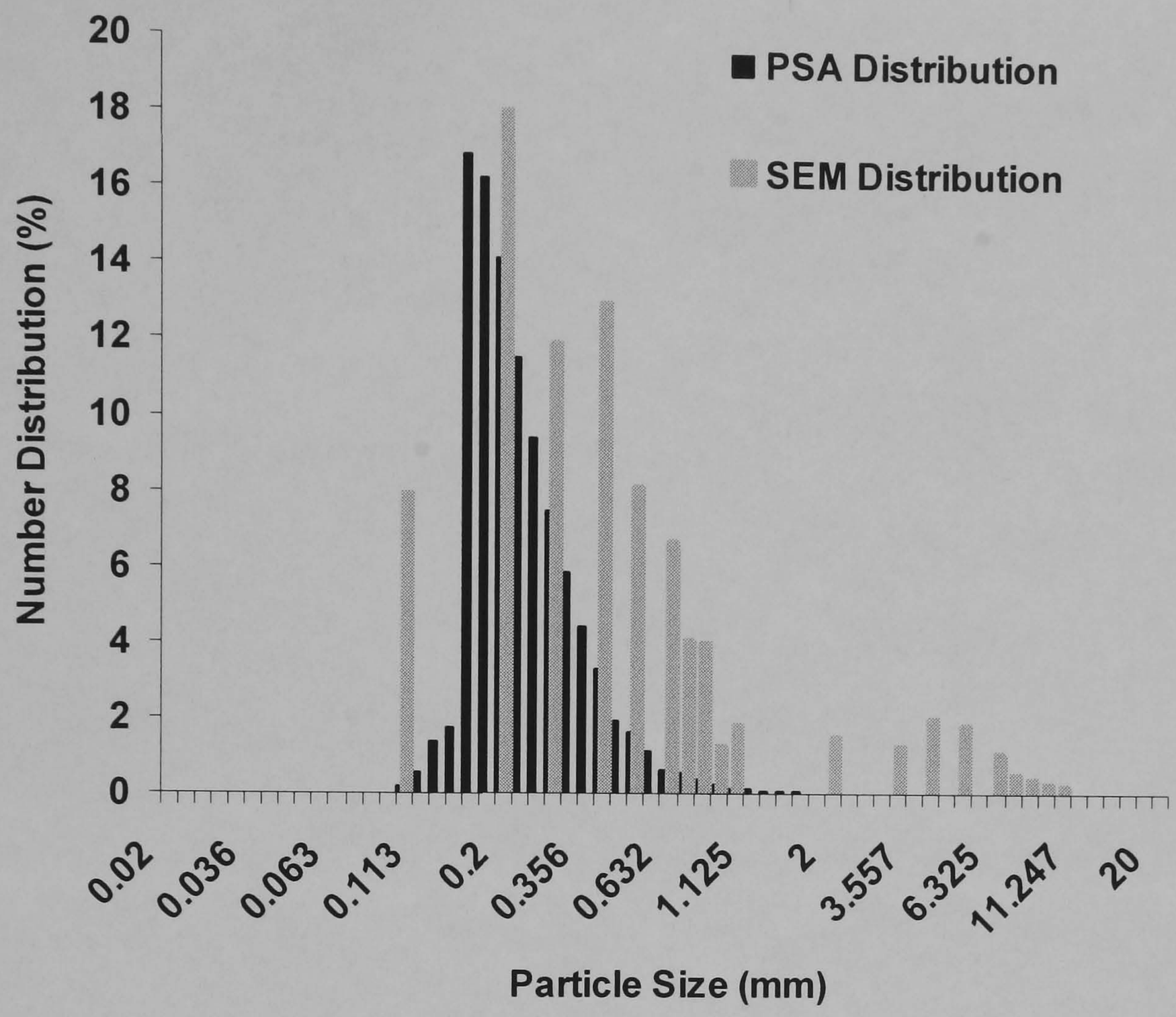


Figure 4.15: Comparison of number distribution from SEM and the PSA for samples 4 and 5, following jogging under smooth femoral head conditions. Presented on a logarithmic axis to allow for comparison of results

The distributions observed following analysis using the PSA and the imaging method using the SEM are very similar (Figure 4.16). The number of particles determined using the PSA may provide a more accurate distribution due to the number of particles the PSA is able to evaluate. However data taken from the SEM images, indicates that there are again a range of very small particles not identified at all by the PSA.

Examples of particles observed during SEM image analysis of sample 4 are shown in Figure 4.16, showing both rounded/oval (submicron sized) and elongated drawn PE particles (1 μm or greater in size).

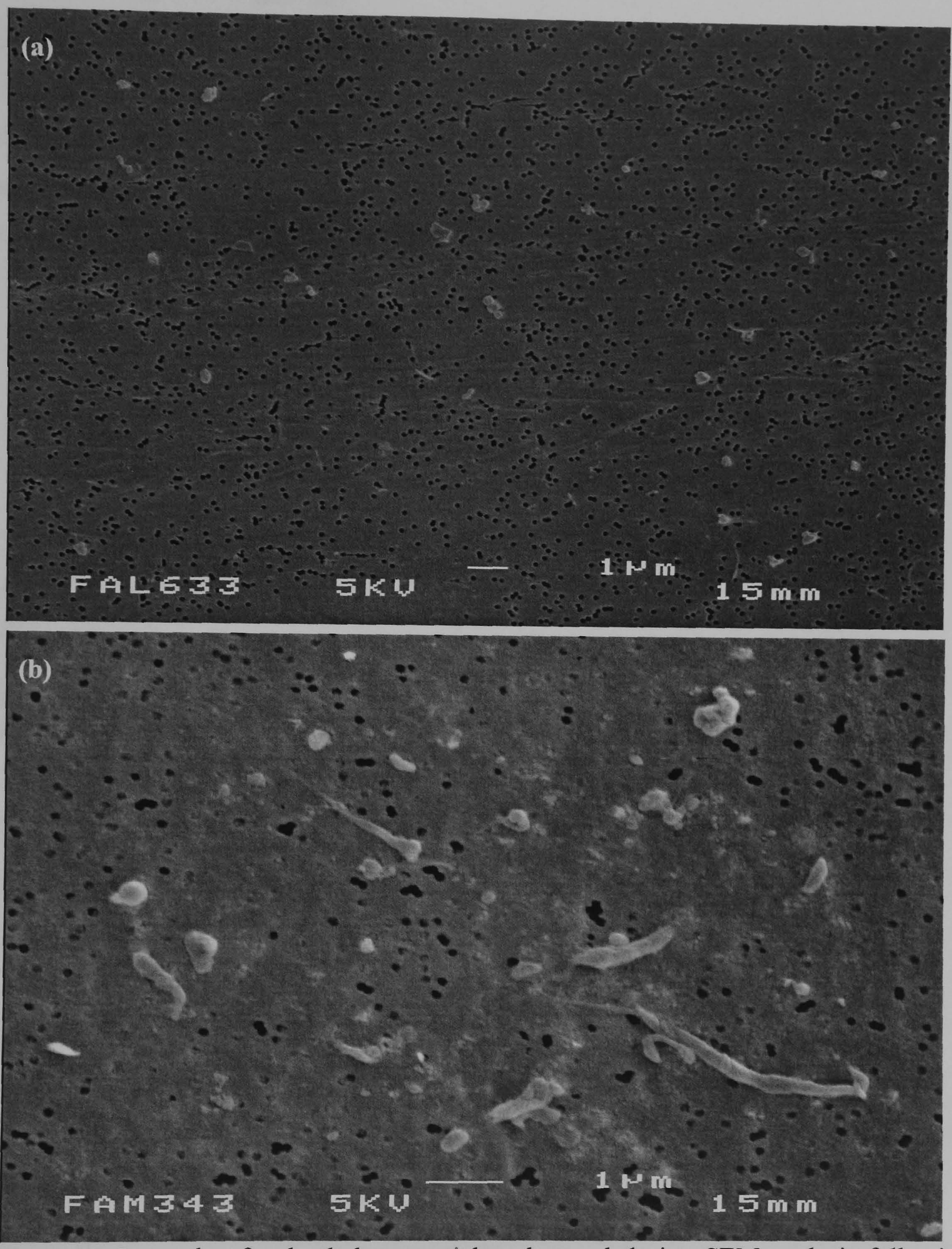


Figure 4.16: Example of polyethylene particles observed during SEM analysis following jogging under smooth femoral head conditions, (a) both rounded and (b) elongated particles can be seen, on a polycarbonate filter with pore size of 0.05 µm.

### 4.1.6 Walking vs. Jogging

A comparison of volume distributions for both walking and jogging samples are presented in Figure 4.17. The volume distribution shows that jogging generally produced smaller particles than walking. Jogging also produced a much larger number of particles due to the increased wear rate when compared with walking. This would therefore suggest that the activity in addition to the duration of activity affects the number of particles generated.

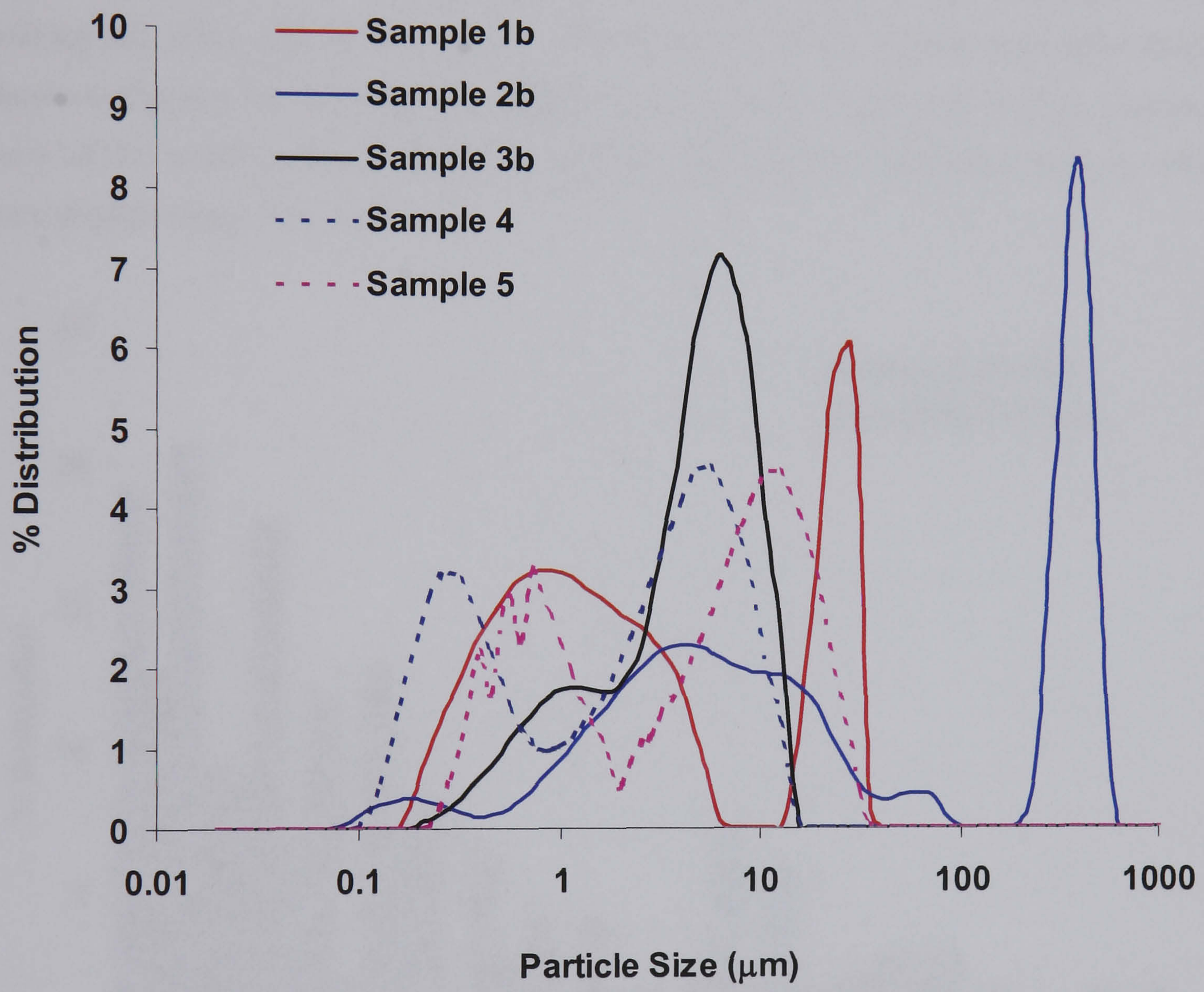


Figure 4.17: Volume distribution of walking (Samples 1b, 2b & 3b) and jogging (Samples 4 & 5)

Walking and jogging samples showed that, the volume distribution of all samples were within similar ranges, however jogging samples did show more particles which were less than 0.25 μm, whereas only one walking sample showed a similar result. Although the number distribution of these samples showed varied results for both walking and jogging,

the mean distributions indicate that simulated jogging produced more bioactive particles than walking with a narrower particle size range (0.08 to 1.1 μm, modal size 0.159 μm). Walking produced particles over a broader range (0.1 to 1.2 μm, modal size 0.25 μm). Both activities would therefore produce bioactive particles, although there would be more particles in total from jogging activity. Although there was no significant difference with the particle range, there was however a significant difference when comparing the modal size of particles produced. Jogging produced no particles greater than 100 μm, whereas walking did, albeit only for one sample. Number distributions obtained from SEM results, shown in Figure 4.18, also suggest a shift in the particle size range, with walking producing more of the smaller particles (0.01-0.1 $\mu$m) and jogging producing more particles which were slightly larger (0.1-0.4 $\mu$m)

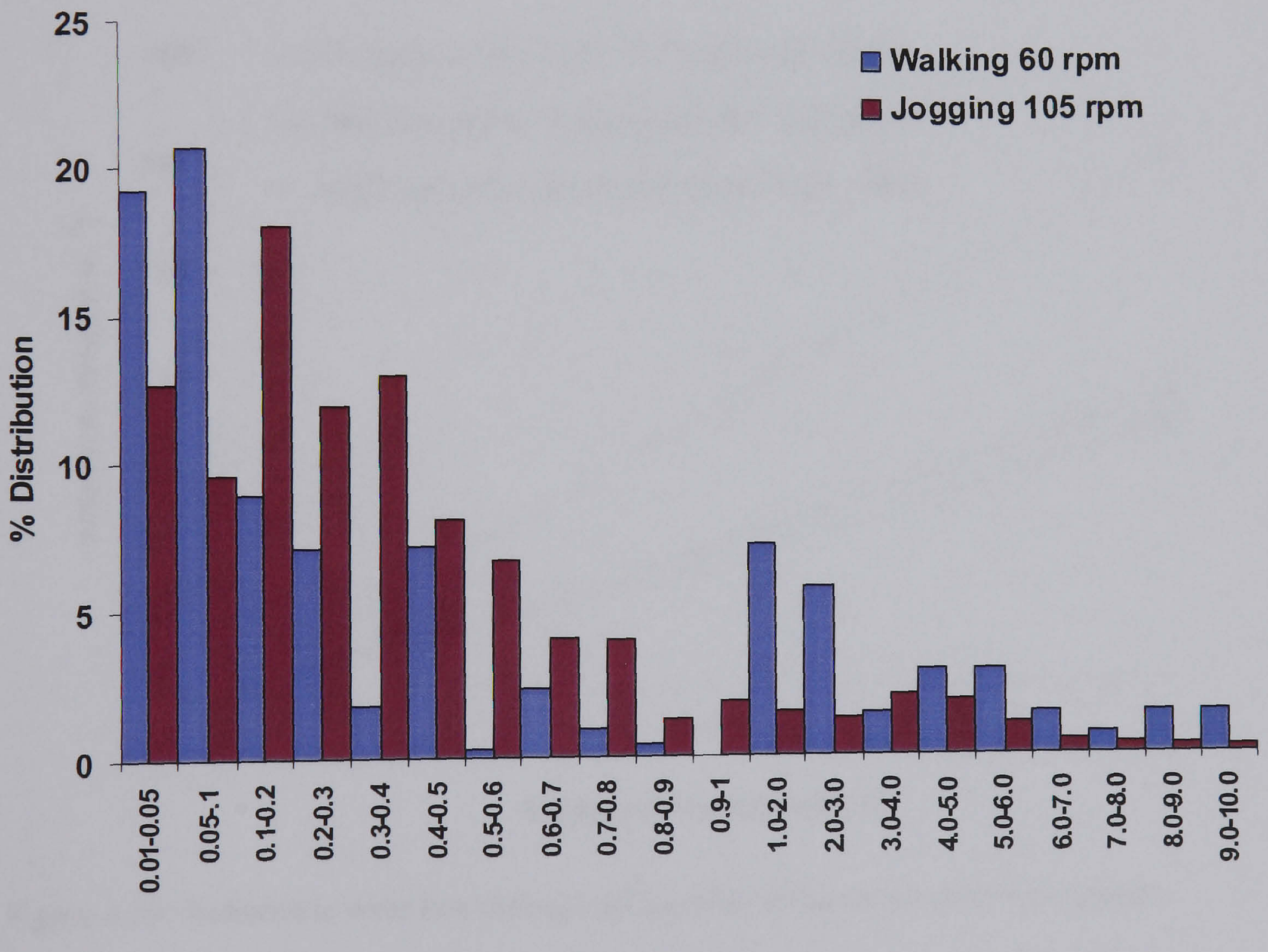


Figure 4.18: SEM number distribution results for both walking and jogging under smooth femoral head conditions

## 4.2 Walking under rough Conditions: Small areas of damage

An increase in femoral head roughness from an $R_a$ of 0.019 μm to 0.4 μm, with a maximum $R_p$ of 1.5 μm, produced slight increases in wear rates experienced by the metal femoral heads. Surface damage covering an area of 20 $mm^2$ (5 mm diameter) produced a median wear rate of 35 $mm^3/10^6$ cycles, with the damage covering an area of 80 $mm^2$ (10 mm diameter) the median wear rate was 39 $mm^3/10^6$ cycles. With the area increased to 176 $mm^2$ (15 mm diameter), again wear rate following walking showed an increase to 65.7 $mm^3/10^6$ cycles. The increase in median wear rate with increasing areas of roughness is also reflected in the volume loss, showing increasing volumetric wear with increasing areas of damage, shown in Figure 4.19.

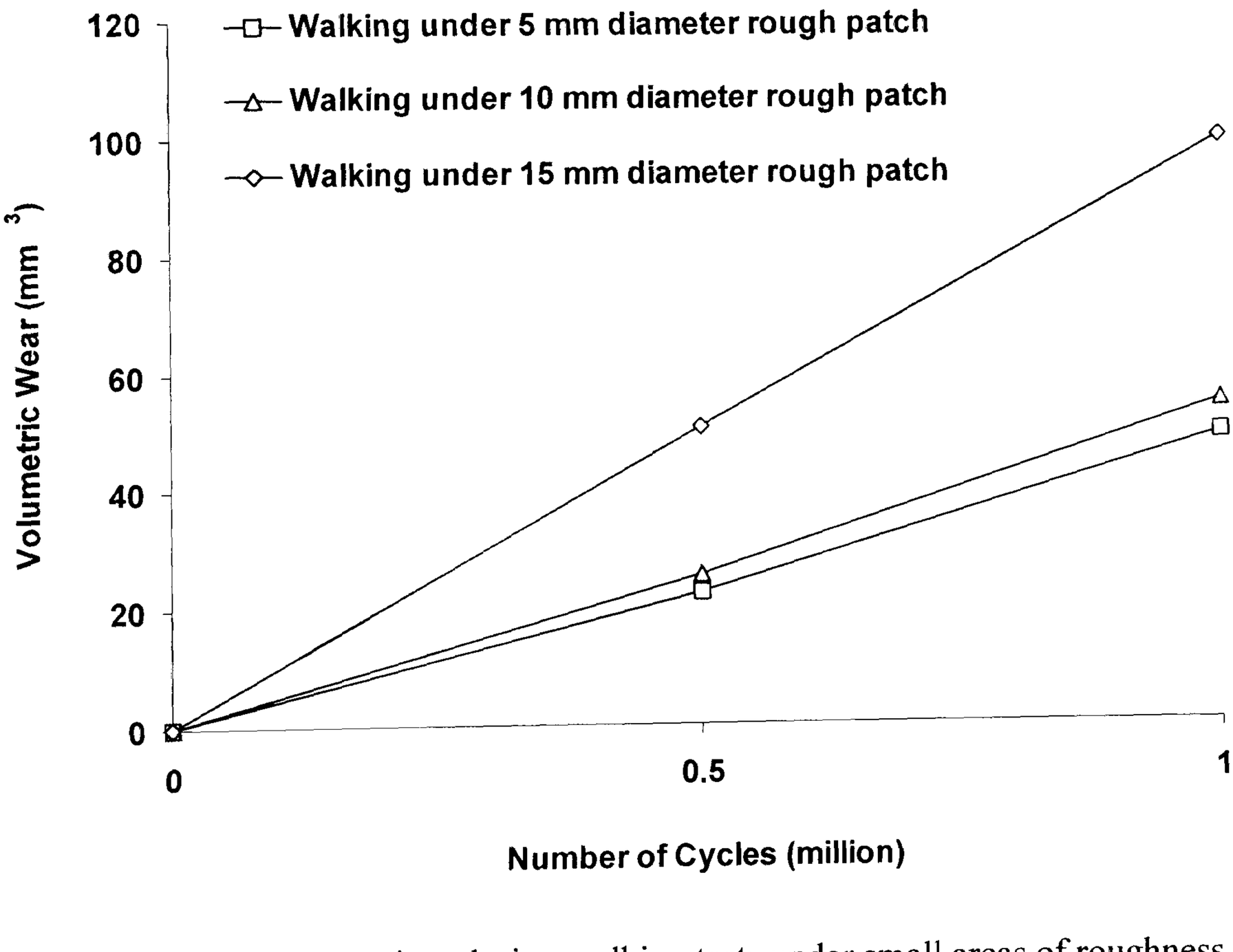


Figure 4.19: Volumetric wear loss during walking tests under small areas of roughness

### 4.2.1 Jogging under rough conditions: Small areas of damage

Following 1 million cycles of walking under rough conditions, jogging tests were conducted. Median wear rate for jogging with surface damage covering an area of 20 $mm^2$ was 39 $mm^3/10^6$ cycles. With surface damage increased to an area of 80 $mm^2$, wear rate showed a subsequent increase, to 41 $mm^3/10^6$ cycles. The increase in wear rate was also observed for surface damage covering an area of 176 $mm^2$, which, following jogging was 204.6 $mm^3/10^6$ cycles, shown in Figure 4.20.

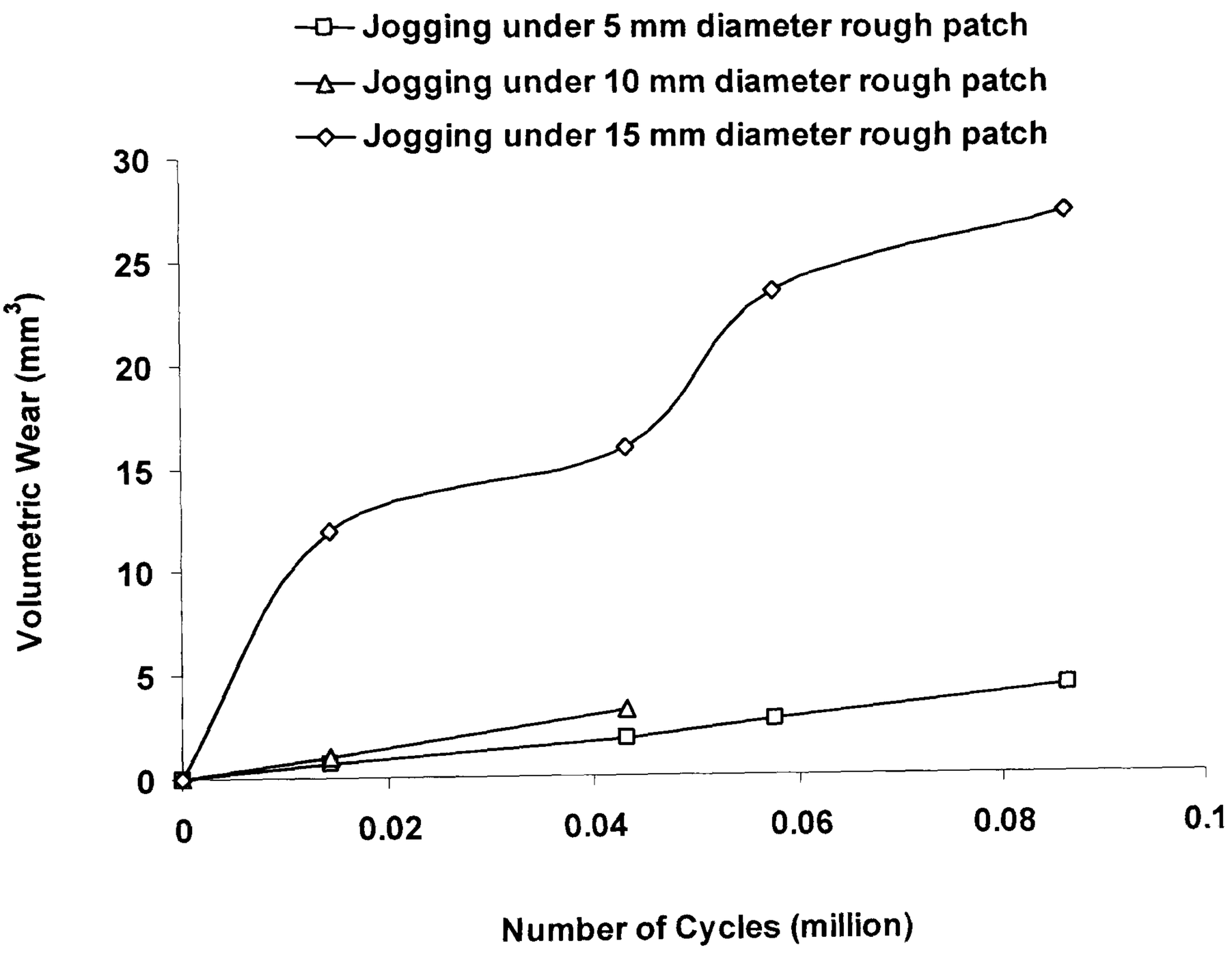


Figure 4.20: Volumetric wear loss during jogging tests under small areas of roughness

The increase in the area of surface damage led to a progressive increase in wear, for walking as well as jogging (Figure 4.21), this is also reflected in the accumulated volume loss which shows a large increase in volumetric wear. However wear rates generated during jogging showed the largest increases in wear and greater variability. A damaged area of 176

$mm^2$ (15 mm rough patch) produced the greatest difference in wear compared to a damaged an area of 20 or 80 $mm^2$ .

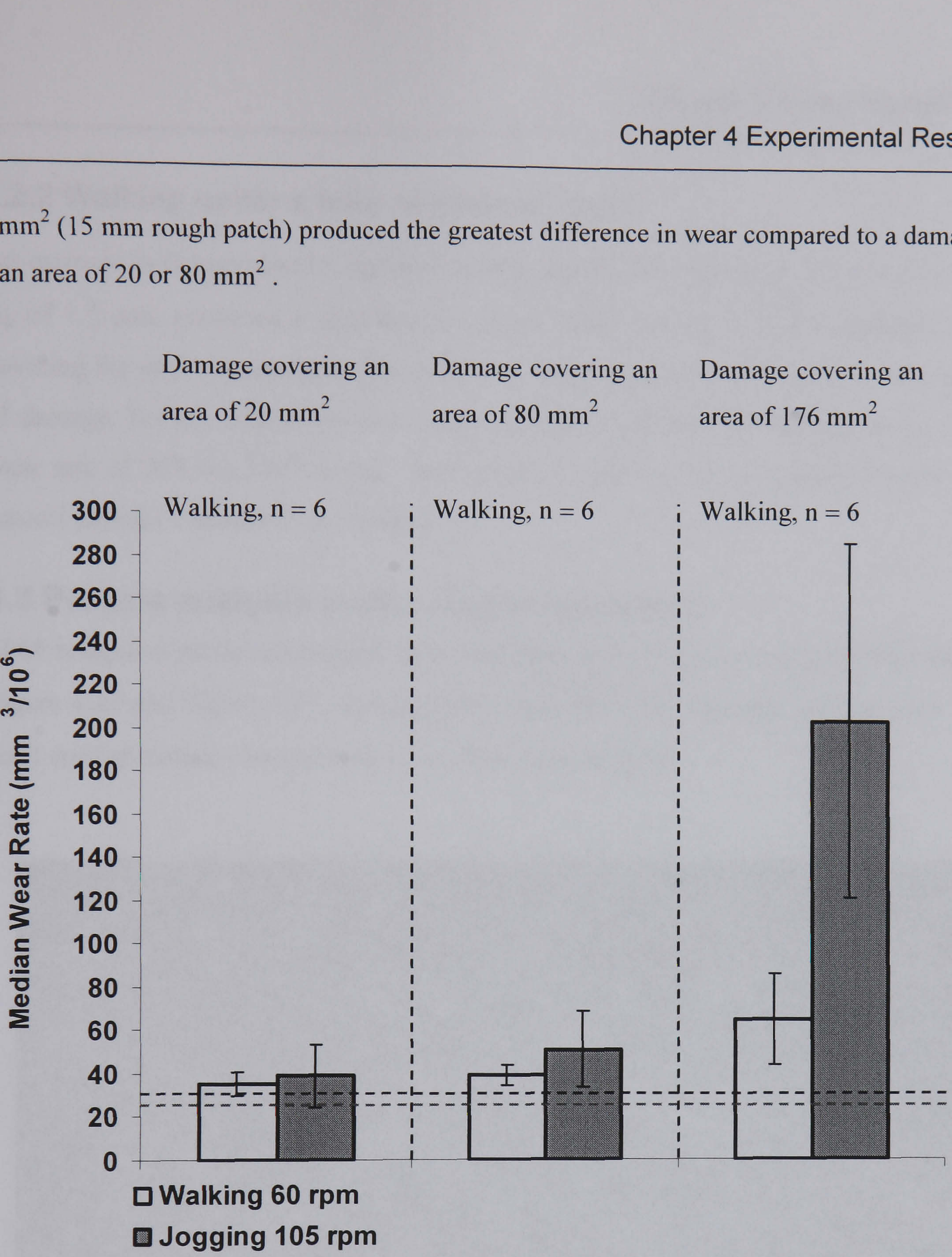


Figure 4.21: Comparison of median wear rates generated during normal walking and simulated jogging with small areas of damage. The red line represents the median wear rate for walking (26 $mm^3/10^6$ cycles) and the blue line represents the median wear rate for jogging (29 $mm^3/10^6$ cycles) under smooth femoral heads, errors bars represent Standard Deviations

### 4.2.2 Walking under a fully roughened head

An increase in femoral head roughness from an $R_a$ of 0.019 μm to 0.4 μm, with a maximum $R_p$ of 1.5 μm, produced a significantly higher wear rate for a fully roughened (damage covering the entire upper hemisphere of the femoral head) than with heads with small areas of damage. For the fully roughened head, wear increased by 1300 %, generating a median wear rate of 369 $mm^3/10^6$ cycles. This however decreased to 111 $mm^3/10^6$ cycles for the second period of intermediate walking.

## 4.3 Particle analysis under roughened heads

SEM images of particles analysed following tests under a roughened head are presented in Figure 4.22 and Figure 4.23, showing both large fibril-like particles (greater than 1 μm in size) and submicron sized particles (less than 1 μm in size).

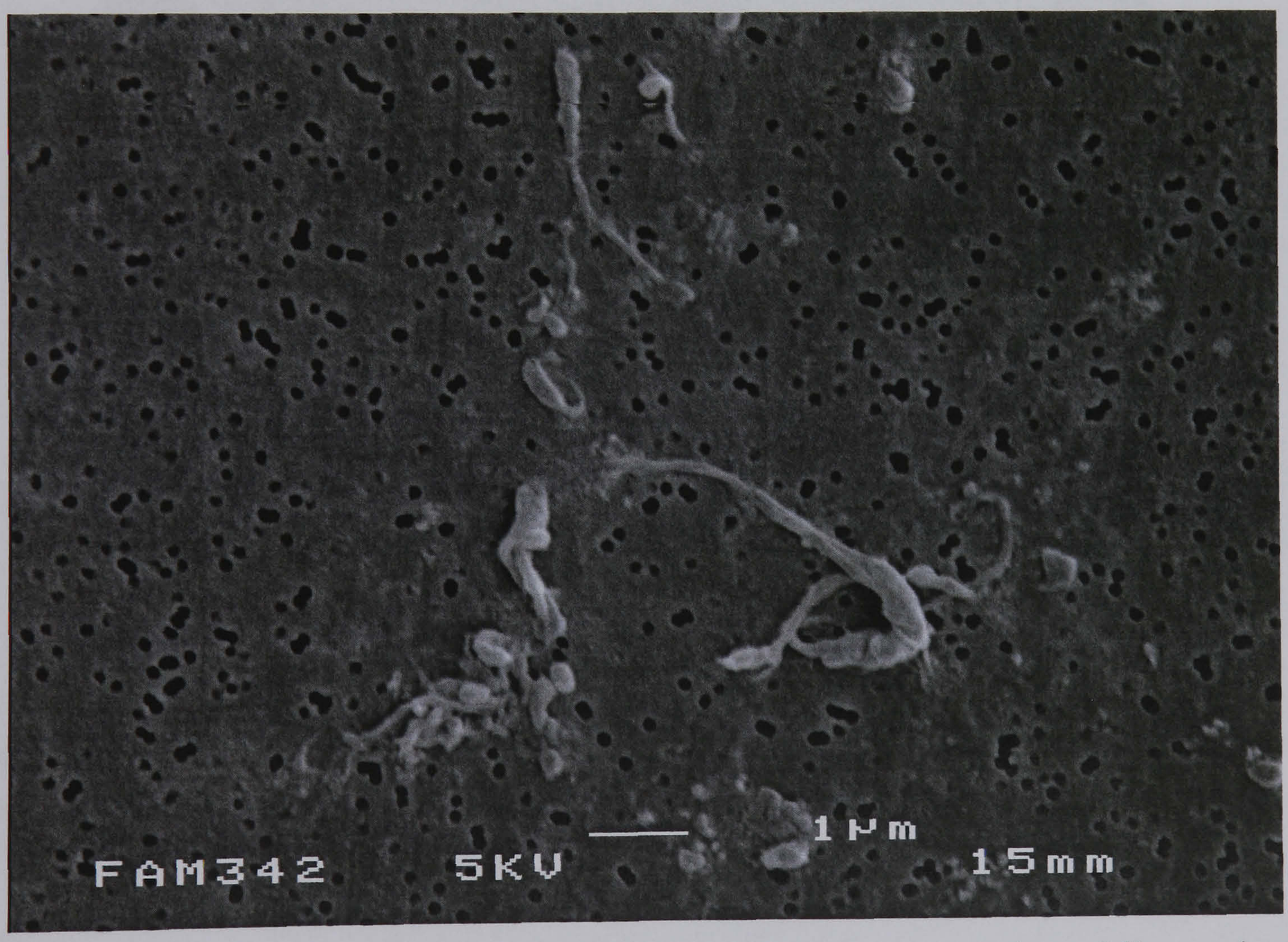


Figure 4.22: SEM images of large particles produced during tests under a fully roughened femoral head. Elongated-fibril particles as well as rounded particles were observed.

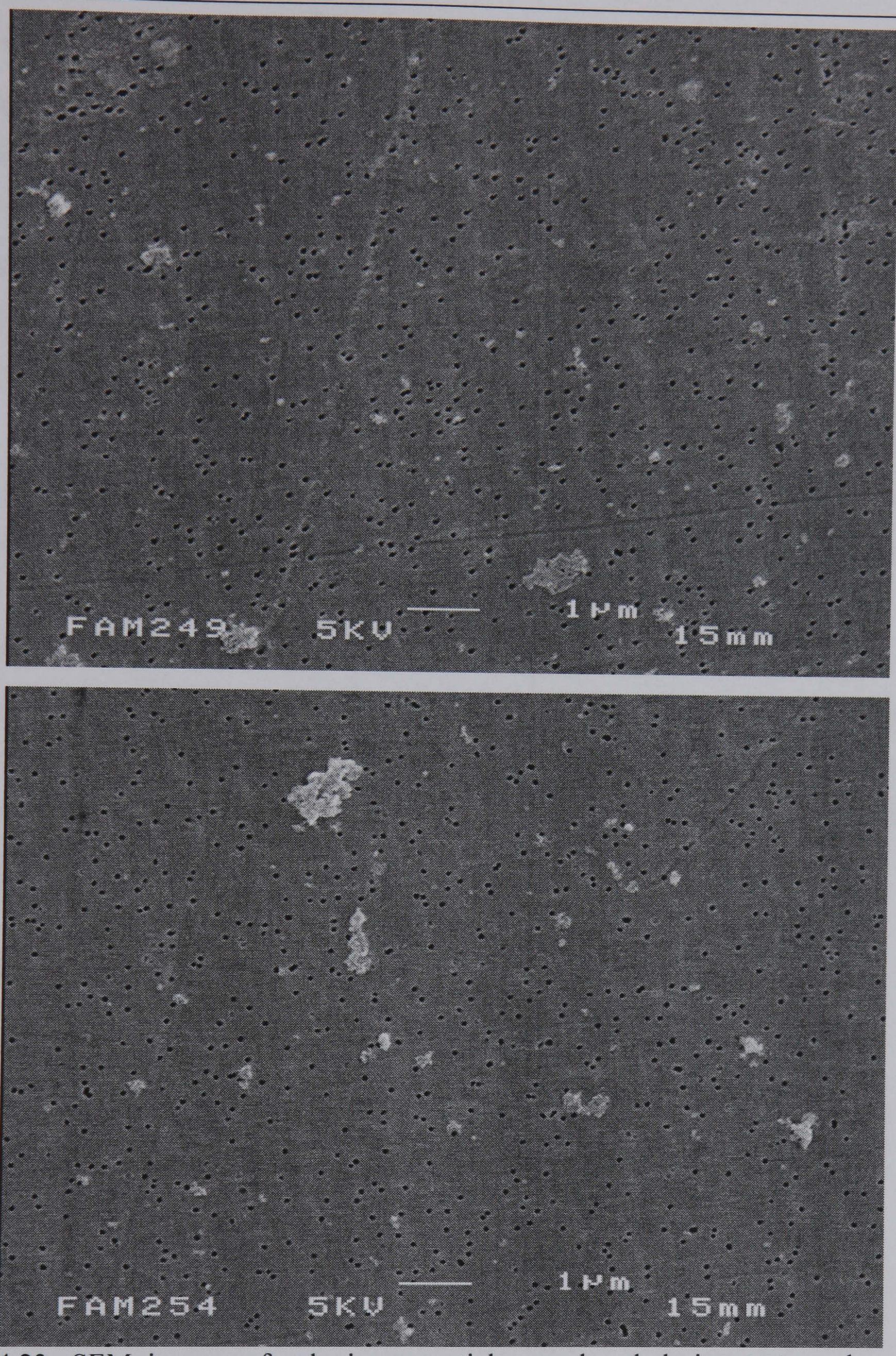


Figure 4.23: SEM images of submicron particles produced during tests under a fully roughened femoral head. The majority of the particles less than 1 μm tended to be round or oval in morphology

### 4.3.1 Particle analysis following tests under small areas of roughness

Following analysis of particles under smooth femoral head conditions, volume and number distribution of particles under rough femoral head conditions were determined. Figure Figure 4.24 (a) and (b) shows the number and volume distribution of particles determined following walking under a roughened area of 20 $mm^2$. One walking sample, sample 6, was produced for this test condition. A smaller particle size range was produced in the range of 0.06 to 12 μm, with a modal size of 0.8 μm.

Figure 4.25 (a) and (b) shows the number and volume distribution of particles determined following walking under a roughened area of 80 $mm^2$, sample 7. Following walking under an increased area of roughness, the volume distribution indicates that particles produced during this test were in the range of 0.1 to 31 μm, with a modal size of 11.3 μm. The number distribution produced a similar result to that of tests under a 5 mm roughened area, however particles less than 0.1 μm were detected for this particular sample, an indication that with an increased area of roughness a greater number of submicron particles may be generated.

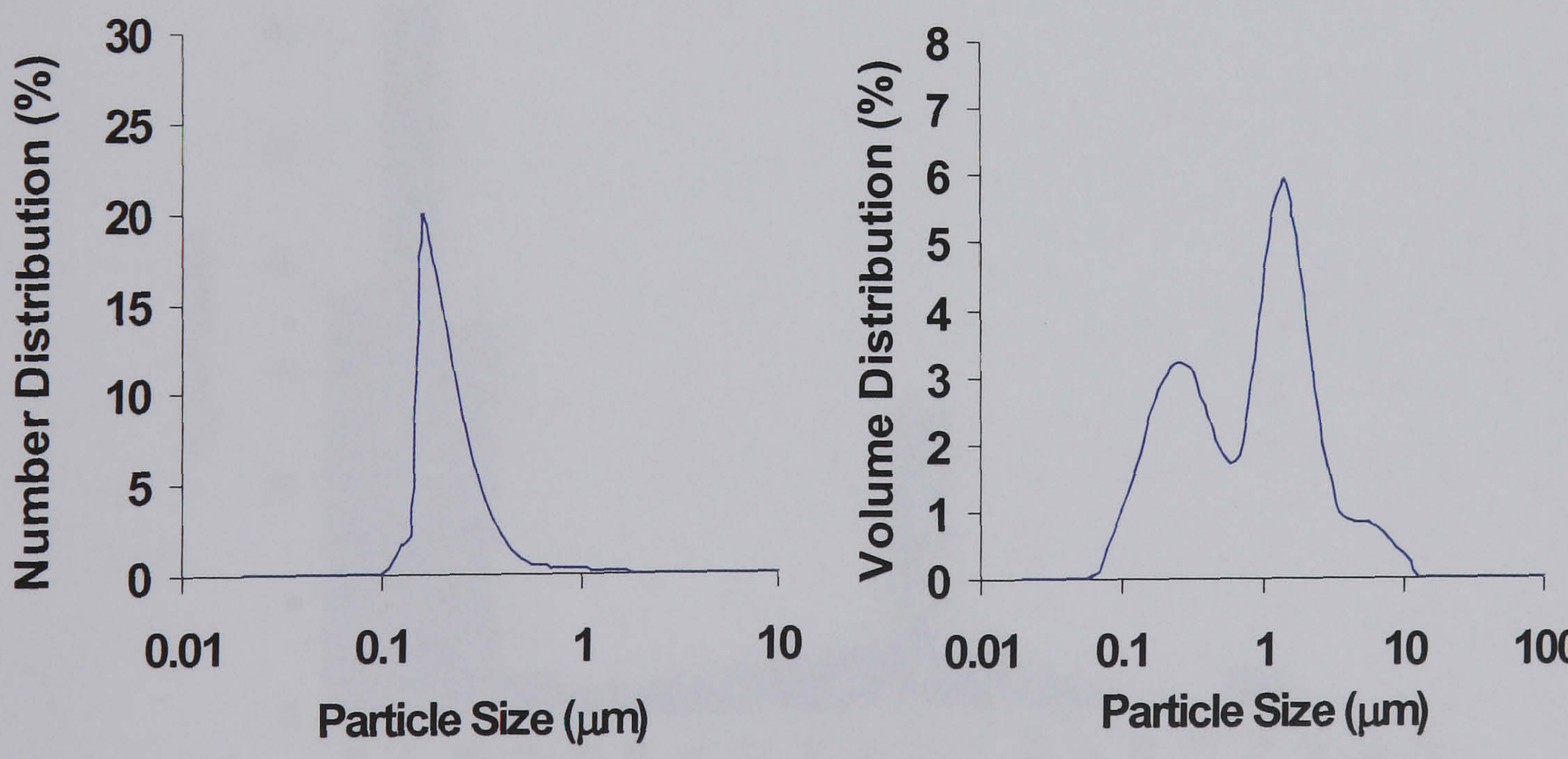


Figure 4.24: (a) Number and (b) volume distribution of sample 6, following walking under a roughened area of 5 mm diameter (20 $mm^2$ rough patch)

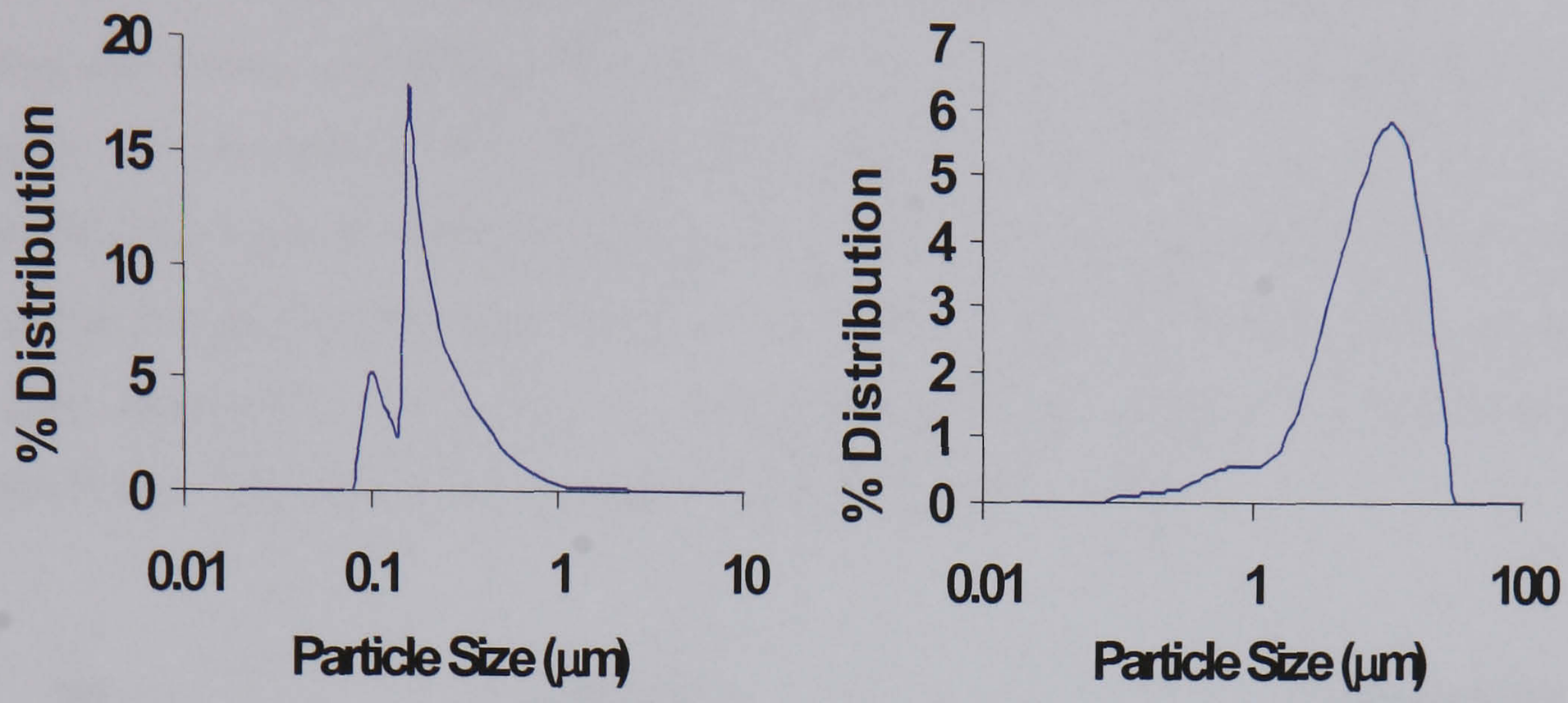


Figure 4.25: (a) Number and (b) volume distribution of sample 7, following walking under a roughened area of 10 mm diameter (80 $mm^2$ rough patch)

SEM analysis, Figure 4.26 following PSA analysis showed that the majority of particles were less than 1 µm in size, 93 %. There was good agreement with the results obtained via PSA, with a modal size in the 0.05 to 0.1 µm size range.

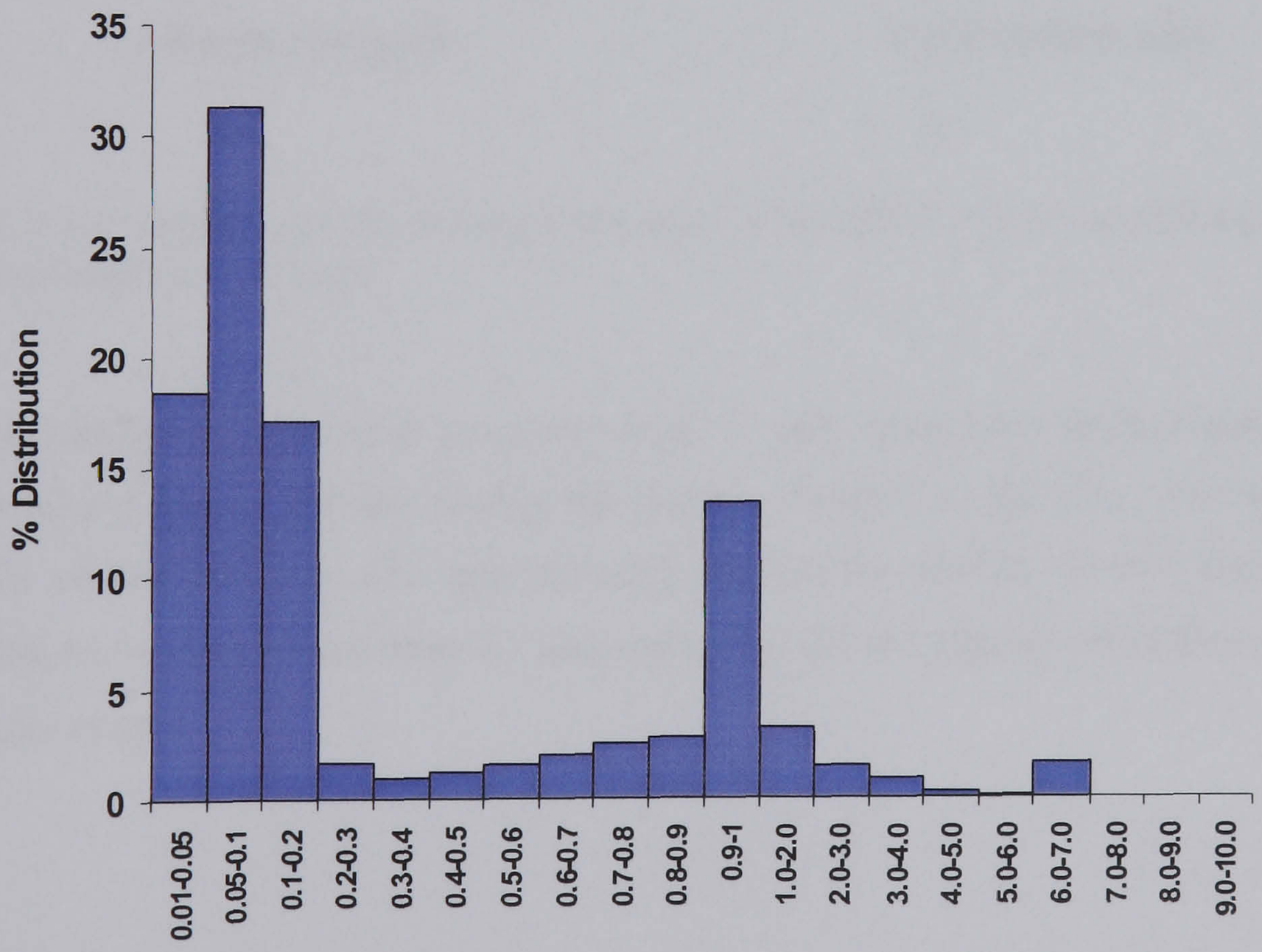


Figure 4.26: Number distribution following SEM analysis for a rough patch of 80 $mm^2$ (10 mm diameter)

### 4.3.2 Particle analysis following tests under fully roughened head

Number and volume distributions for walking under a fully roughened head are presented in Figure 4.27 (a) and (b). The majority of the particles were less than 1 μm in size, with a modal size of 0.2 μm, however the volume distribution indicates that greatest proportion of the volume is composed of particles with a modal size of 3 μm. No particles greater than 8 μm were observed for these samples, indicating that under walking, a fully roughened femoral head would only produce particles within the bioactive range.

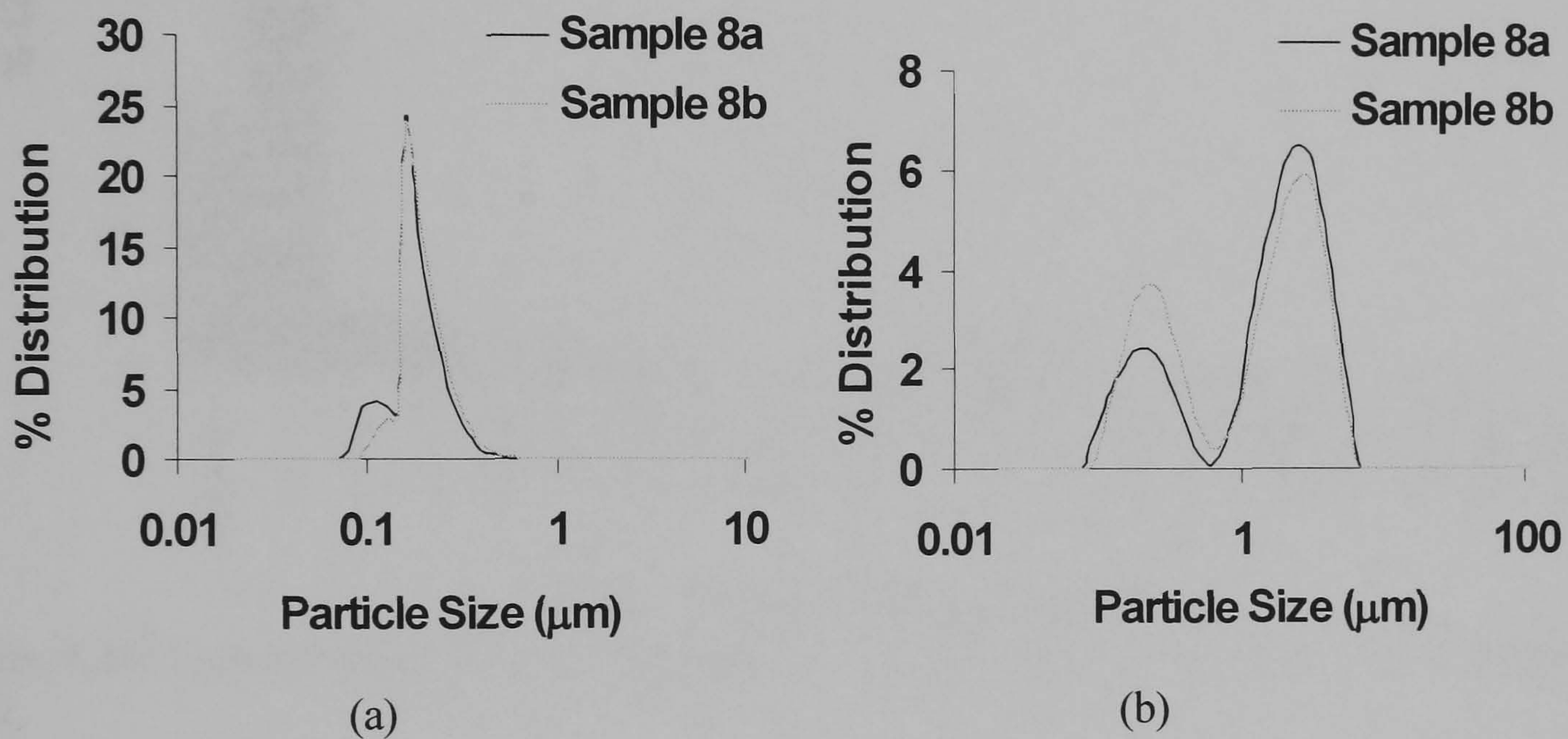


Figure 4.27: (a) Number and (b) volume distribution of sample 8, following walking under a fully roughened femoral head

SEM image analysis of particles generated under a fully roughened head, Figure 4.28 showed good agreement with the number distribution obtained via the PSA. The majority of particles are sub micron in size, approximately 96 % of the particles are less than 1 μm in size, with 81 % particles less than 0.1 μm, indicating that the majority of particles are in the bioactive range.

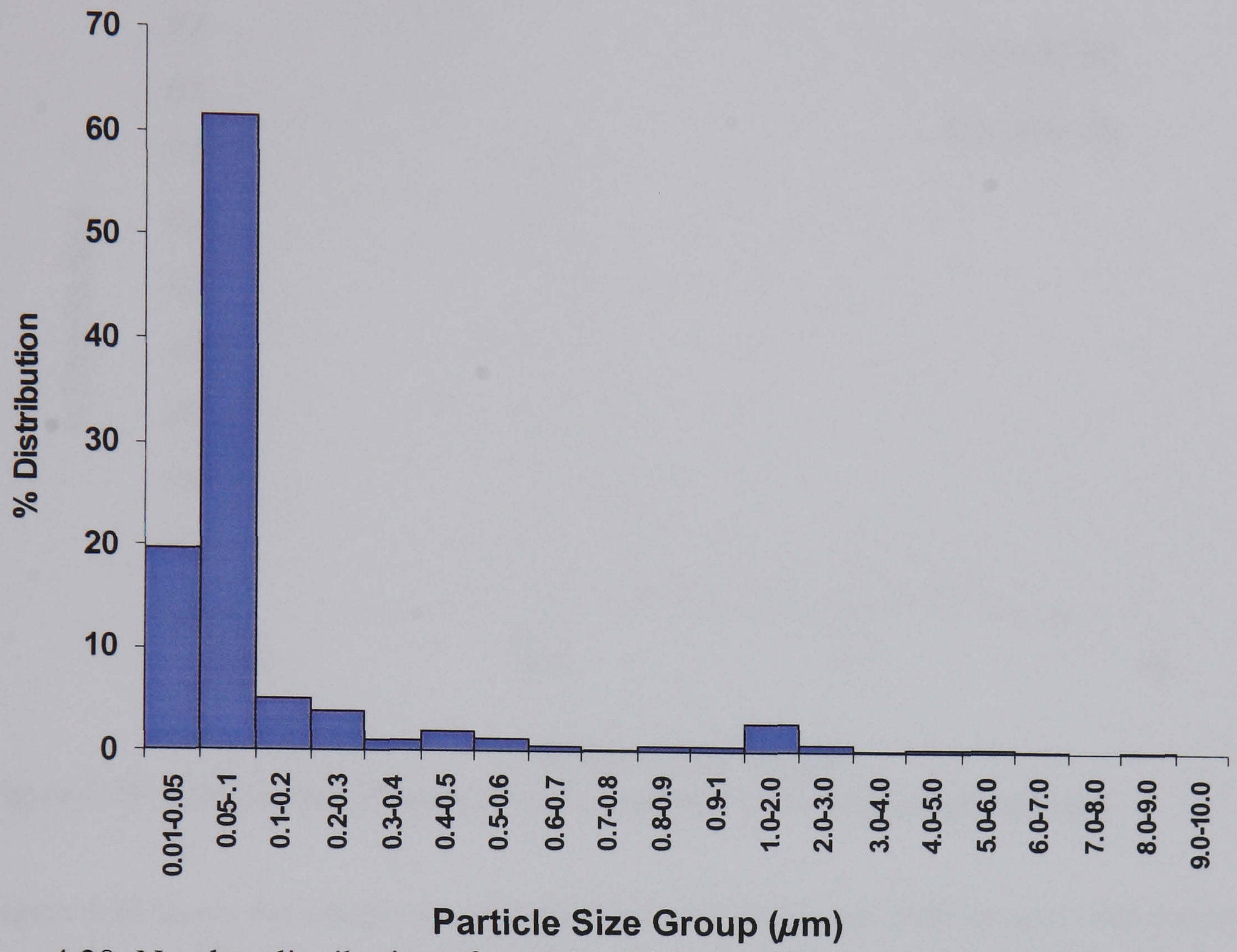


Figure 4.28: Number distribution of particles following SEM analysis for a fully roughened head.

Figure 4.29 shows a comparison of samples 8a and 8b following SEM image analysis, showing good agreement between 2 samples for walking under a fully roughened head, with no significant difference between the two samples.

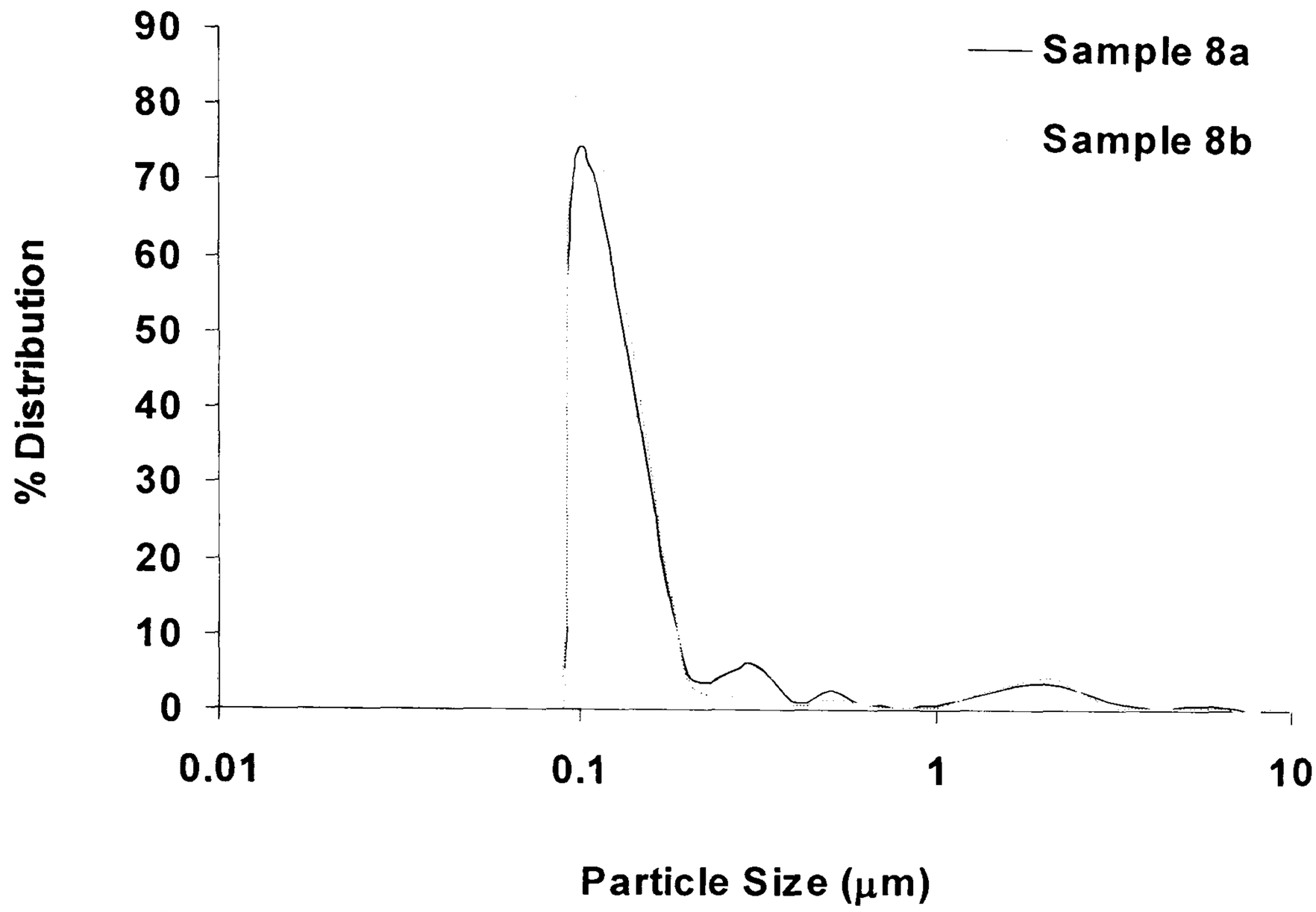


Figure 4.29: SEM number distribution from walking under a fully roughened head

Figure 4.30 shows the comparison of mean PSA distribution and SEM analysis distribution for a fully roughened head. SEM analysis indicates a modal size of 0.1 μm, whereas with the PSA shows a modal size of 0.16 μm. Although the distributions look similar, SEM analysis shows that there were particles present, which were greater than 1 μm, up to 10 μm, whereas this was not identified with the PSA. In addition the SEM analysis also indicated particles smaller than 0.1 μm in size, again not identified by the PSA

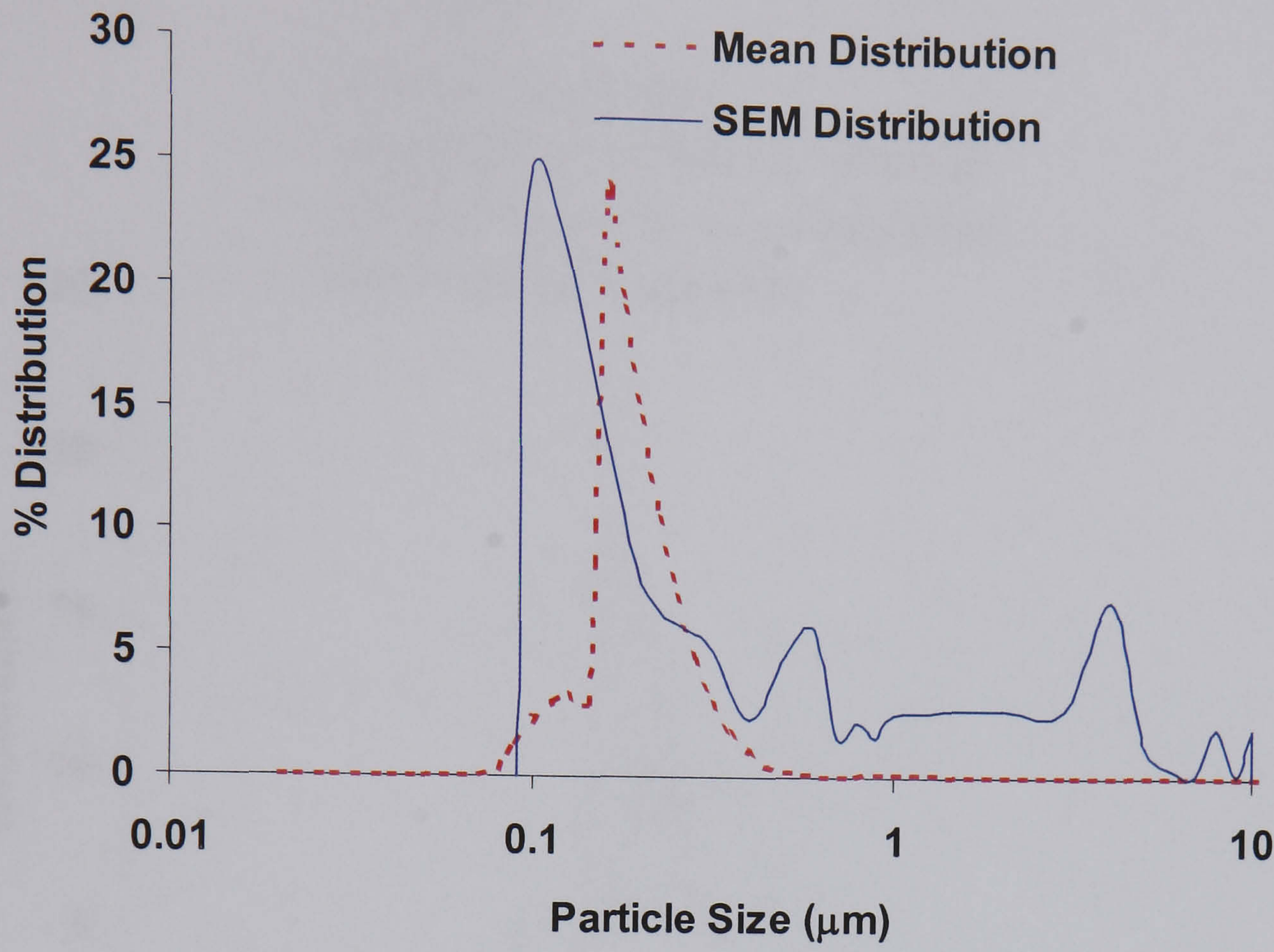


Figure 4.30: Mean number distribution of SEM and PSA debris following walking under a fully roughened head

A comparison of particle debris analysed using the PSA, for tests under various femoral head conditions during simulated walking are shown in Figure 4.31. The samples show an emerging pattern in that as the area of roughness is progressively increased in size, there appears to be an increase in the number of smaller and thereby bioactive particles that are produced, with a concomitant decrease in the range of the particle sizes.

### 4.3.3 Particle analysis following tests under various femoral head conditions

Although there is an increase in the number of bioactive particles, there is little change in the modal size, with the mean number distribution showing a modal size in the range 0.178 to 0.2 μm. Walking under smooth and walking with 5 mm diameter rough patch, however showed a statistically significant difference when comparing the modal sizes.

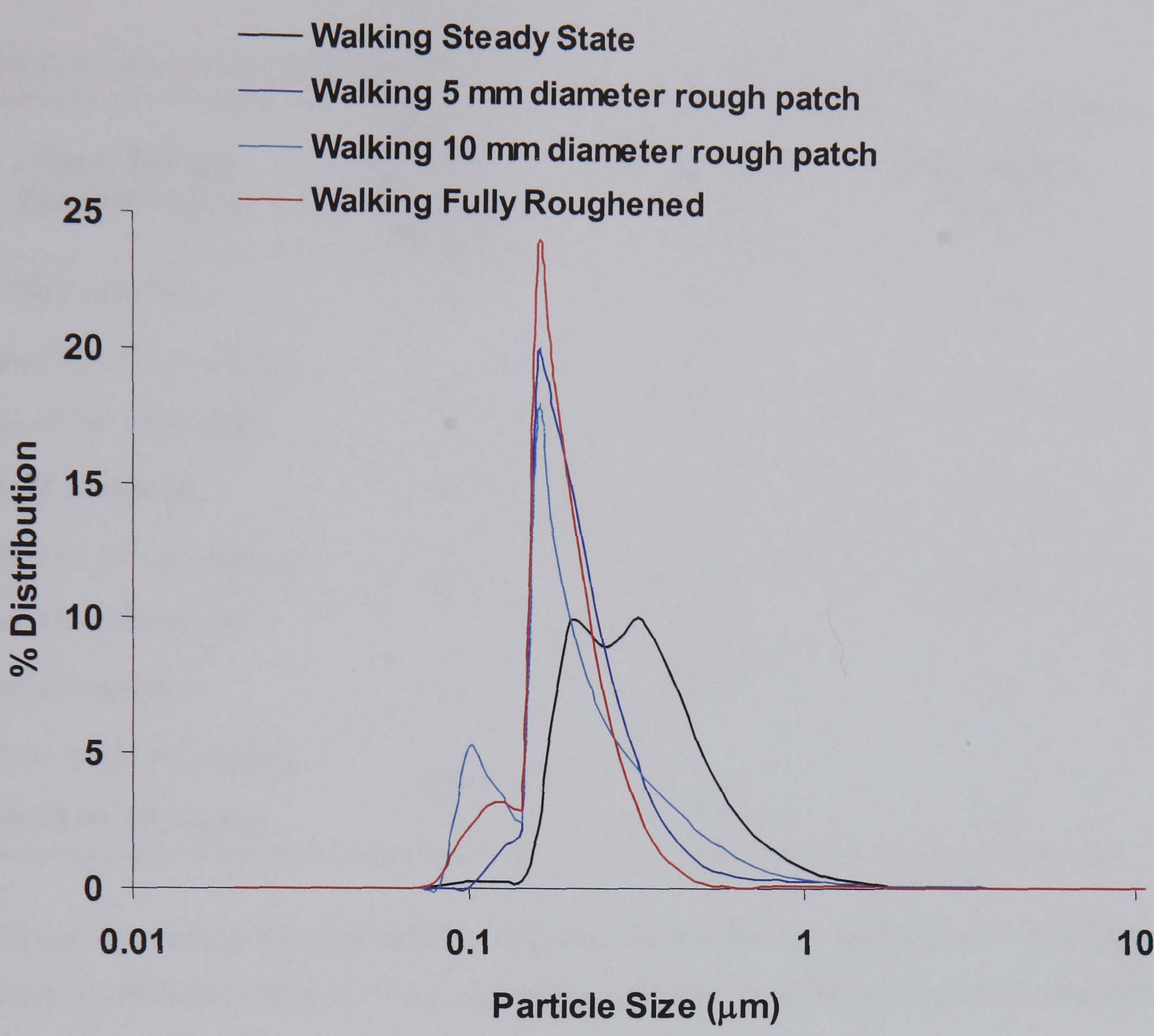


Figure 4.31: Comparison of number distribution during walking under various femoral head conditions

### 4.3.4 Surface Analysis following tests under rough conditions: Small areas of damage

Under small areas of damage, surface roughness had little influence upon the long term wear of lightly cross-linked PE. However the nature of the surface roughness was monitored before and after each test. It was apparent that the surface roughness reduced following walking tests. Changes in surface topography were observed following walking and jogging tests, with a reduction in surface $R_a$ from 0.39 μm to 0.28 μm and 0.34 μm, for 20 $mm^2$ and 80 $mm^2$ of damage respectively, as shown in

Table 4.3.

Table 4.3: Changes in surface topography for femoral heads with damage

| Test: Rough femoral heads | Area of surface damage ($mm^2$) | Metal surface Ra (μm) | Metal surface Rp (μm) |
|---|---|---|---|
| Initial roughness | 20 | 0.39 | 1.42 |
| After $1\times10^6$ of walking and 10 hrs of jogging | 20 | 0.28 | 1.18 |
| Initial roughness | 80 | 0.37 | 1.53 |
| After $1\times10^6$ of walking and 8 hrs of jogging | 80 | 0.34 | 0.67 |
| Initial roughness | 1230 | 0.37 | 1.45 |
| After $2\times10^6$ of walking and 18 hrs of jogging | 1230 | 0.27 | 1.35 |

Although the change in mean surface roughness for damage covering 20 $mm^2$ was large, it did not significantly affect the wear rate when compared to wear under smooth conditions. The $R_p$ showed a slight reduction from the maximum $R_p$ of 1.42 μm to 1.18 μm.

The fully roughened head also showed a reduction in its surface roughness $R_a$, only showed a slight decrease, nonetheless, the results indicate that some self-polishing had occurred, the decrease in surface roughness is reflected in the reduction in wear experienced by the fully roughened head following initial jogging tests. From these results it would seem that significant changes in surface topography tend to occur over short periods of high activity.

The results presented for a fully roughened head combined with results obtained under small areas of damage would appear to support the supposition that the amount of damaged area combined with the type of activity undertaken would be the predominant factor in determining the wear that is experienced by a polyethylene cup.

## 4.4 Jogging under rough femoral head conditions

Figure 4.32 shows the wear particle number distribution data from 20 $mm^2$ partially roughened area during jogging. The modal size of particle from the PSA is 0.15 μm, with a size range of 0.07 to 0.6 μm. All samples produced very similar results

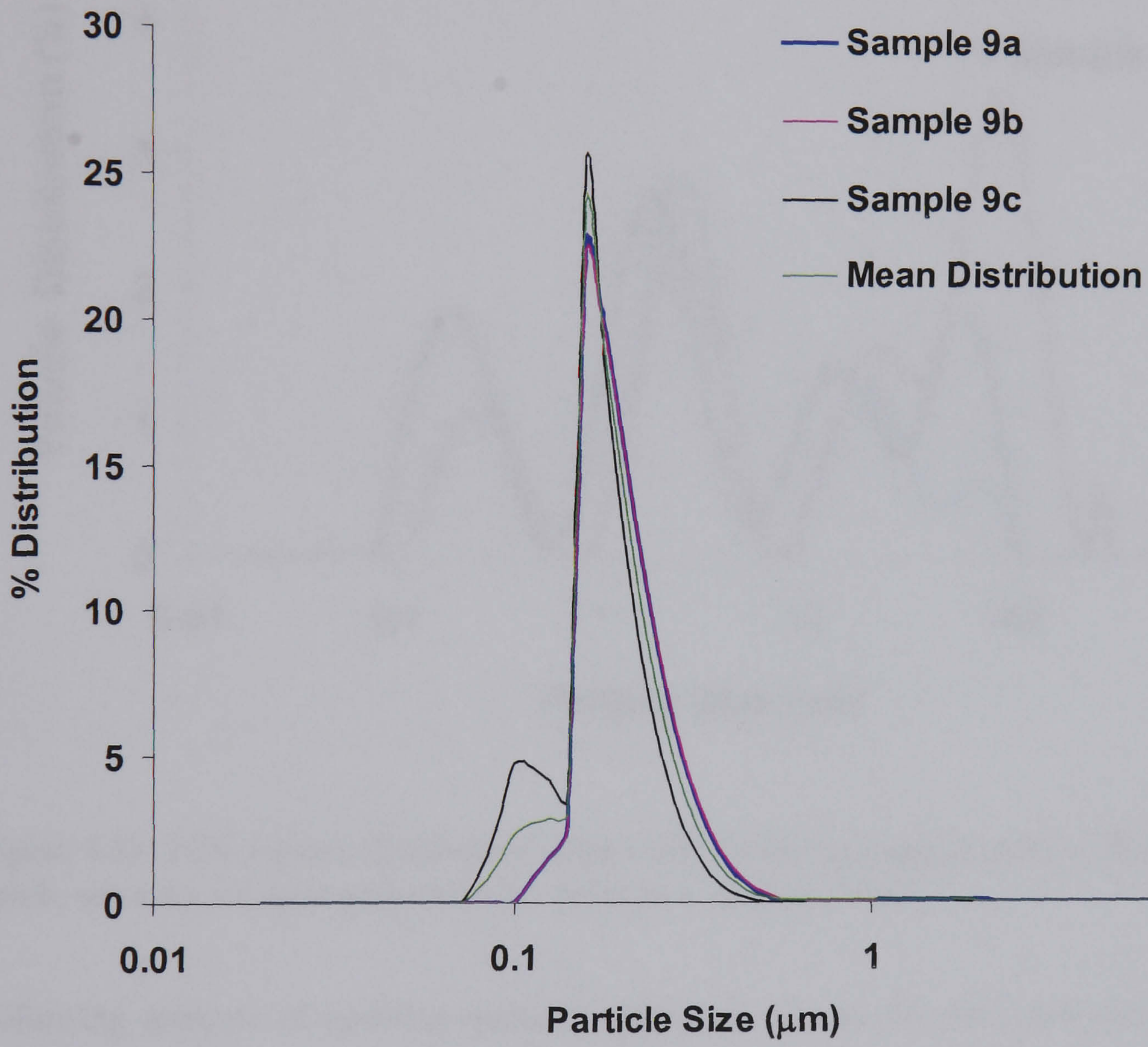


Figure 4.32: Number distribution of particles following jogging under a 20 $mm^2$ rough patch, showing the mean distribution from the three samples

Figure 4.33 shows the volume distribution of samples following jogging under a roughened area of 20 $mm^2$. Unlike the volume distribution obtained for tests under smooth conditions, which showed multiple peaks, tests under rough conditions exhibited bimodal distributions. The results from the number distribution indicate that the majority of the particles are less

than 1 μm, although the major proportion of the volume is composed of particles greater than 1 μm.

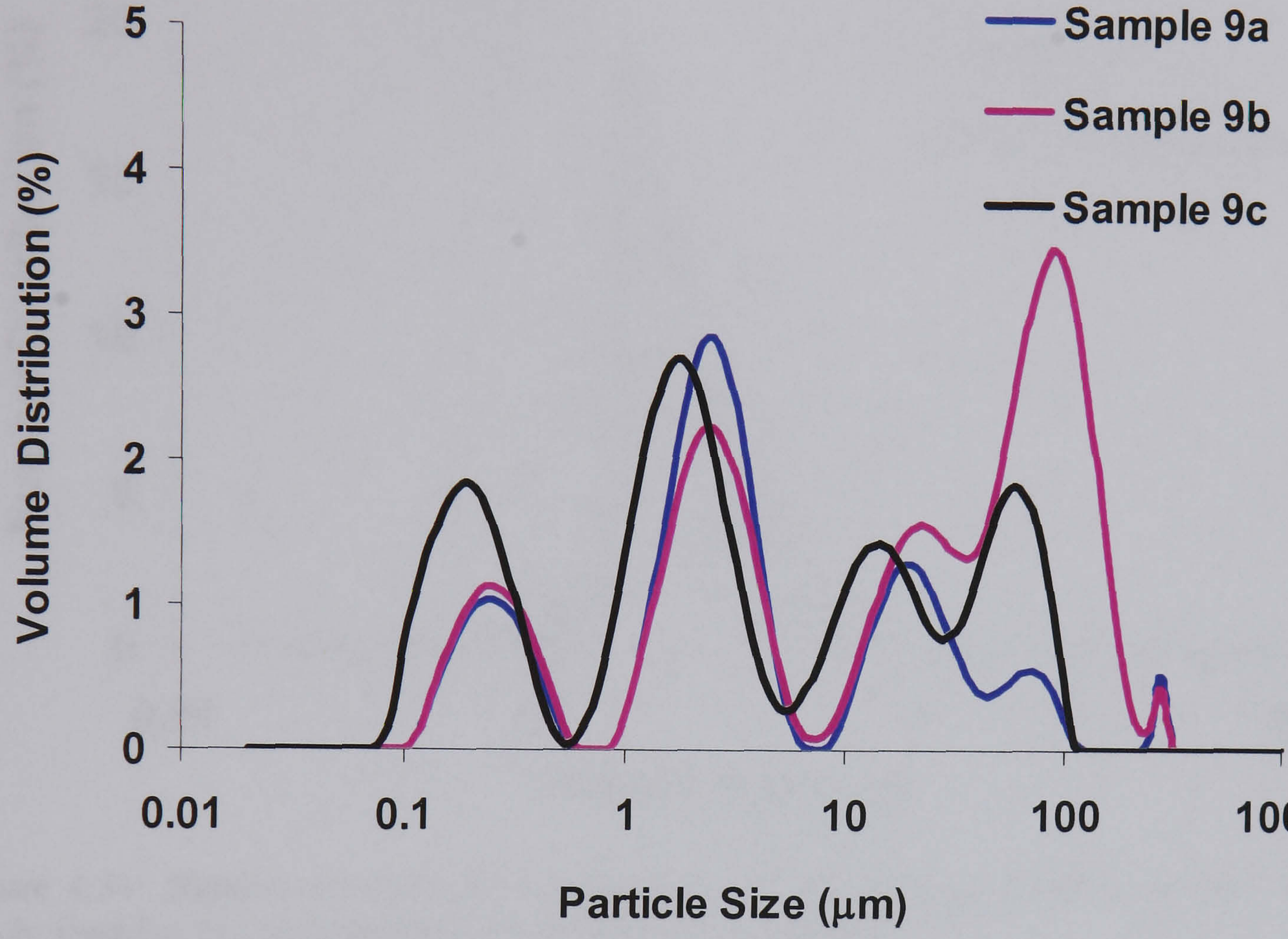


Figure 4.33: PSA volume distribution of particles following jogging under a 20 $mm^2$ rough patch, showing multiple peaks with particles up to 400 μm in size

Following analysis of particles under a roughened area of 20 $mm^2$, particles generated during tests under a roughened area of 80 $mm^2$ were carried out, shown in Figure 4.34. When comparing the number distribution for an area of 20 $mm^2$ roughened area with that of the 80 $mm^2$ roughened area, they are very similar in both distribution and the range particle size that were observed.

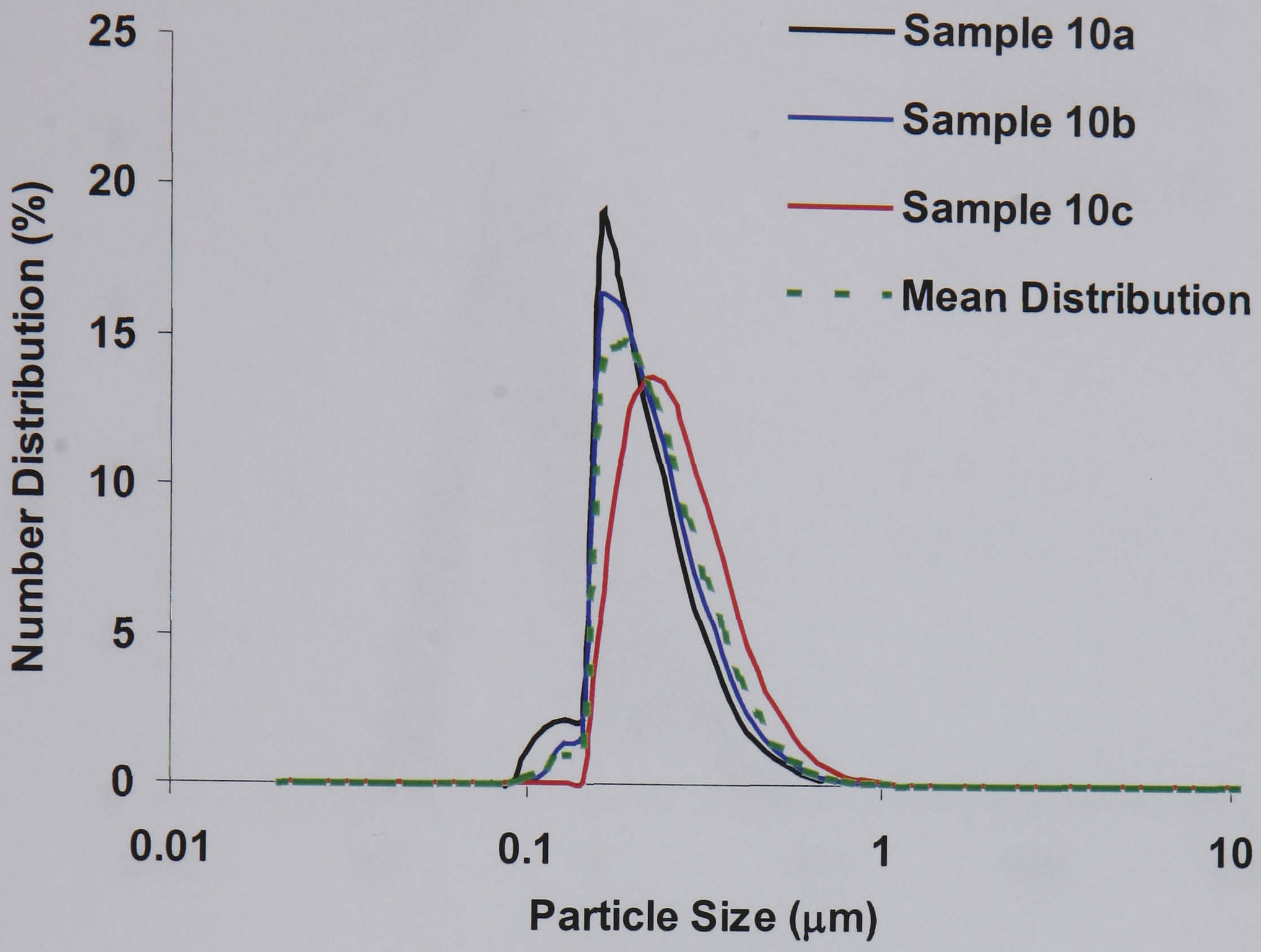


Figure 4.34: Number distribution of particles following jogging under a 80 $mm^2$ rough patch, showing the mean distribution from the three samples

Although number distributions were similar, volume distribution however showed that the distribution under this increased of roughness to be different, generally producing a bimodal distribution. Volume distributions (Figure 4.35) for jogging with a rough patch of 80 $mm^2$, indicated that for all 3 samples, there were no particles greater than 10 μm therefore the majority of the particles generated under this condition would be bioactive and potentially harmfully.

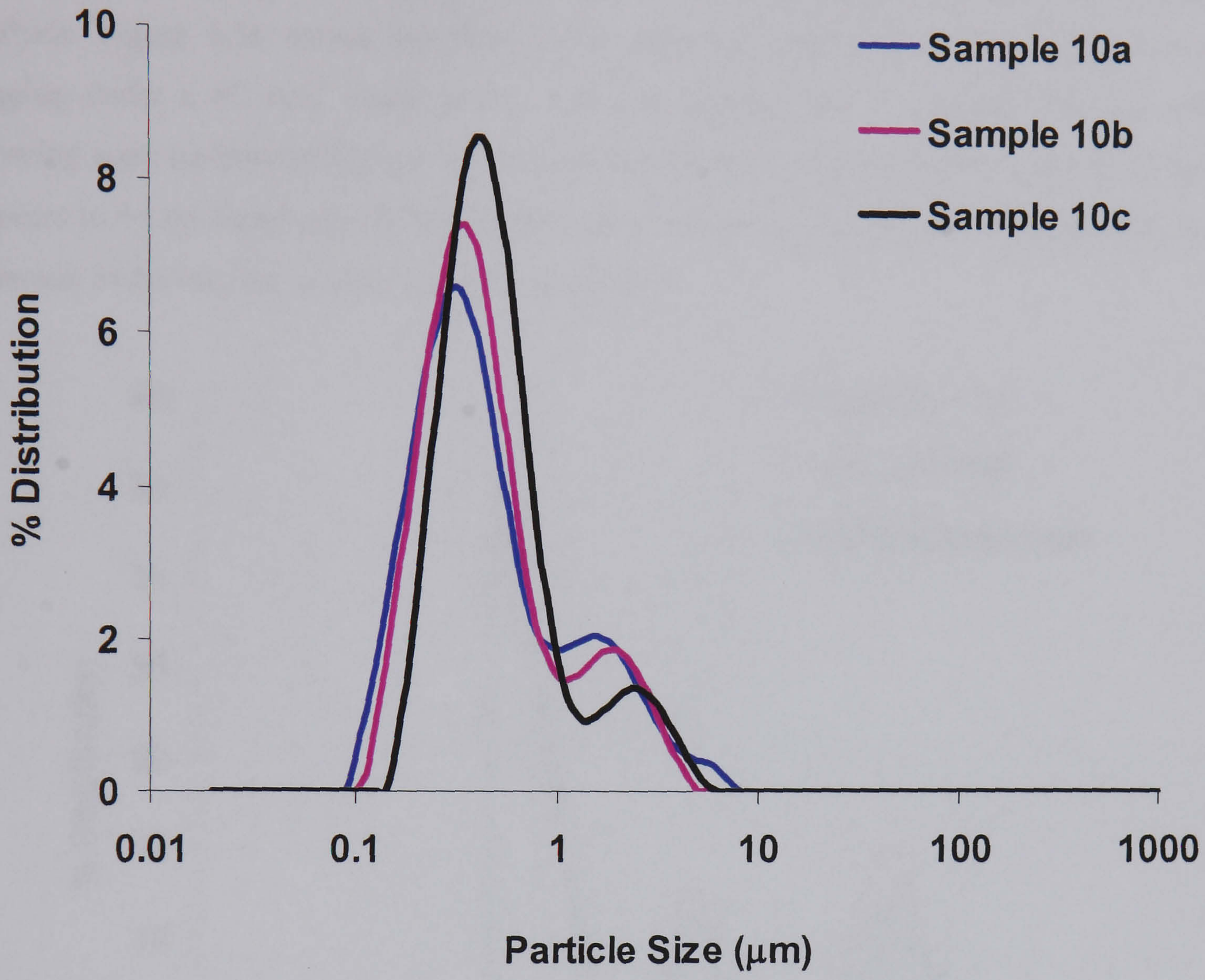


Figure 4.35: Volume distribution of particles following jogging under a 80 $mm^2$ rough patch, showing a bimodal distribution

Following PSA analysis, the number distribution was determined by means of SEM image analysis. Figure 4.36 shows the mean SEM number distribution of particles following jogging under a 80 $mm^2$ rough patch, with the distributions of samples 10a and 10b, showing good agreement between the two samples. When compared with Figure 4.27 there appears to be no significant difference the mean modal size (0.18 μm), although there is a decrease in the numbers produced at the modal size.

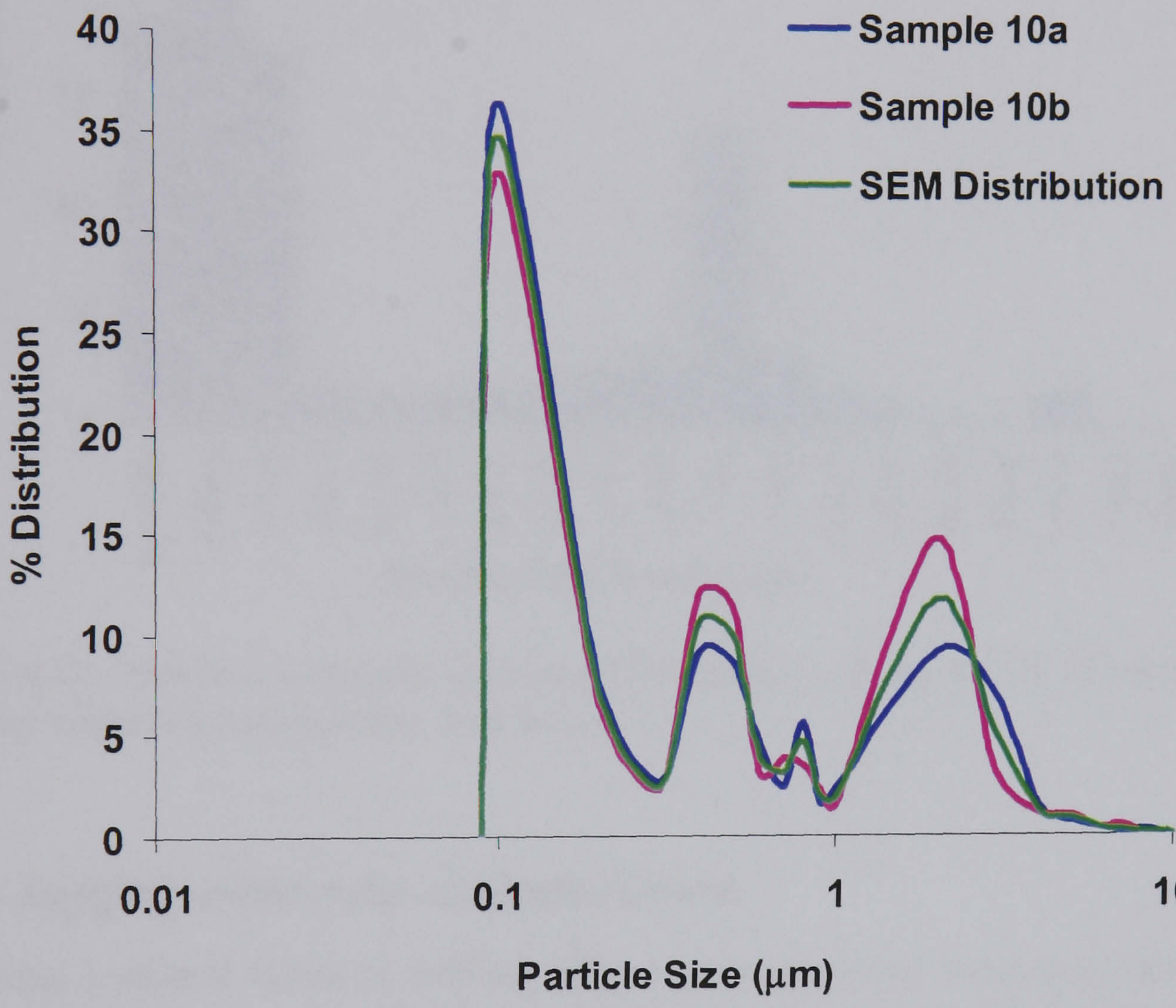


Figure 4.36: Number distribution of particles following jogging with a rough patch of 80 $mm^2$ following SEM image analysis of sample 10.

Mean distribution of sample 10 following SEM analysis are shown in Figure 4.37, showing that the majority of particles are submicron in size, 80 % of the particles analysed are less than 1 μm in size

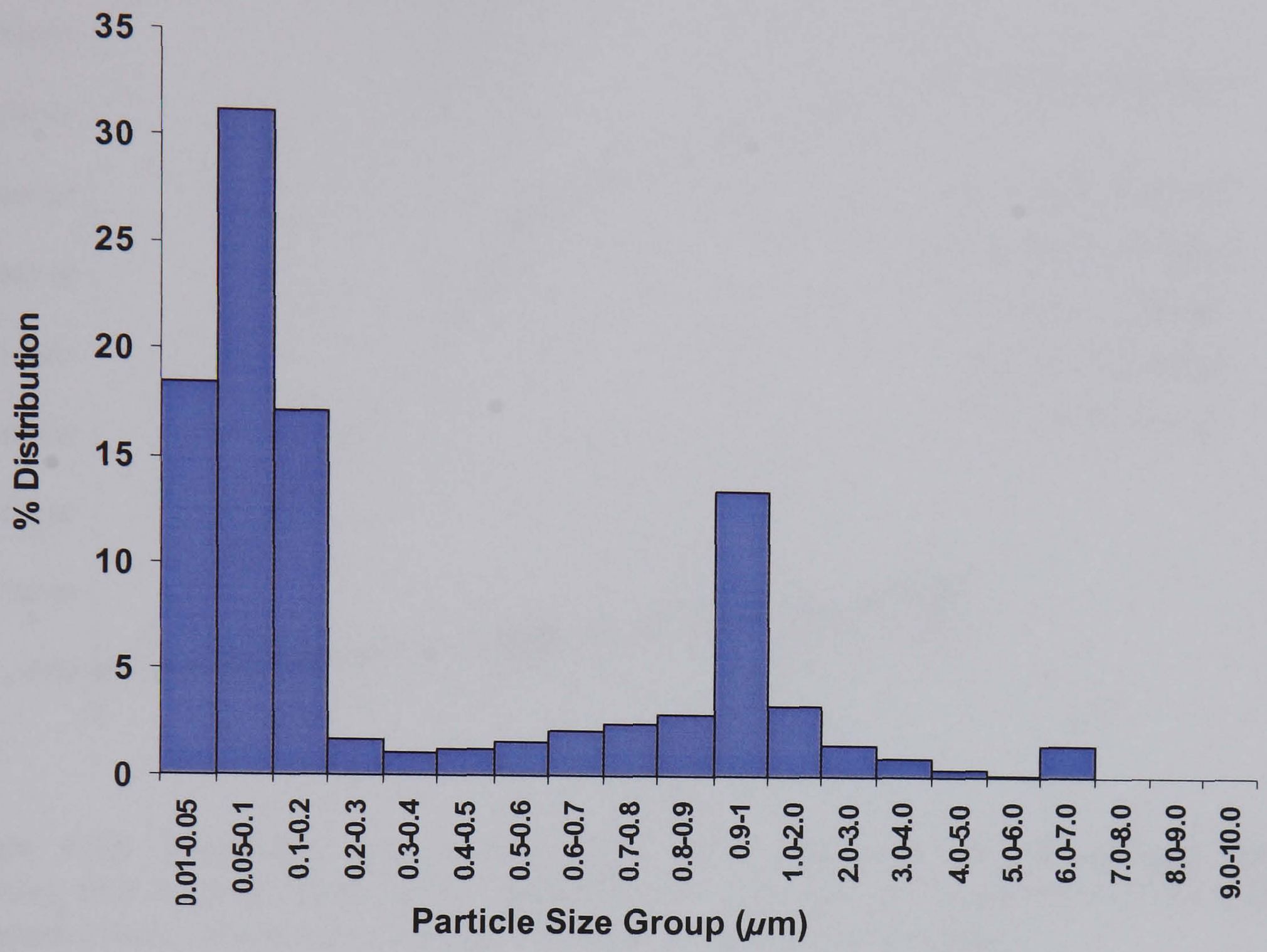


Figure 4.37: Particle distribution following SEM analysis of sample 10, showing that the majority of particles are less than 1μm in size

### 4.4.1 Jogging under fully roughened head

Following 1 million cycles of walking under a fully roughened head, jogging tests were conducted. The median wear rate was 690 $mm^3/10^6$ cycles, showing almost a 2-fold increase in wear compared to walking under a fully roughened head, a statistically significant difference in wear. Following a further 1 million cycles of walking the wear rate showed a subsequent decrease to 250 $mm^3/10^6$ cycles, which can be seen in Figure 4.38, which shows a decrease in gradient for the wear experienced by the polyethylene cup under a fully roughened head. This result once more appears to support the supposition that some form of polishing has occurred during the period of jogging

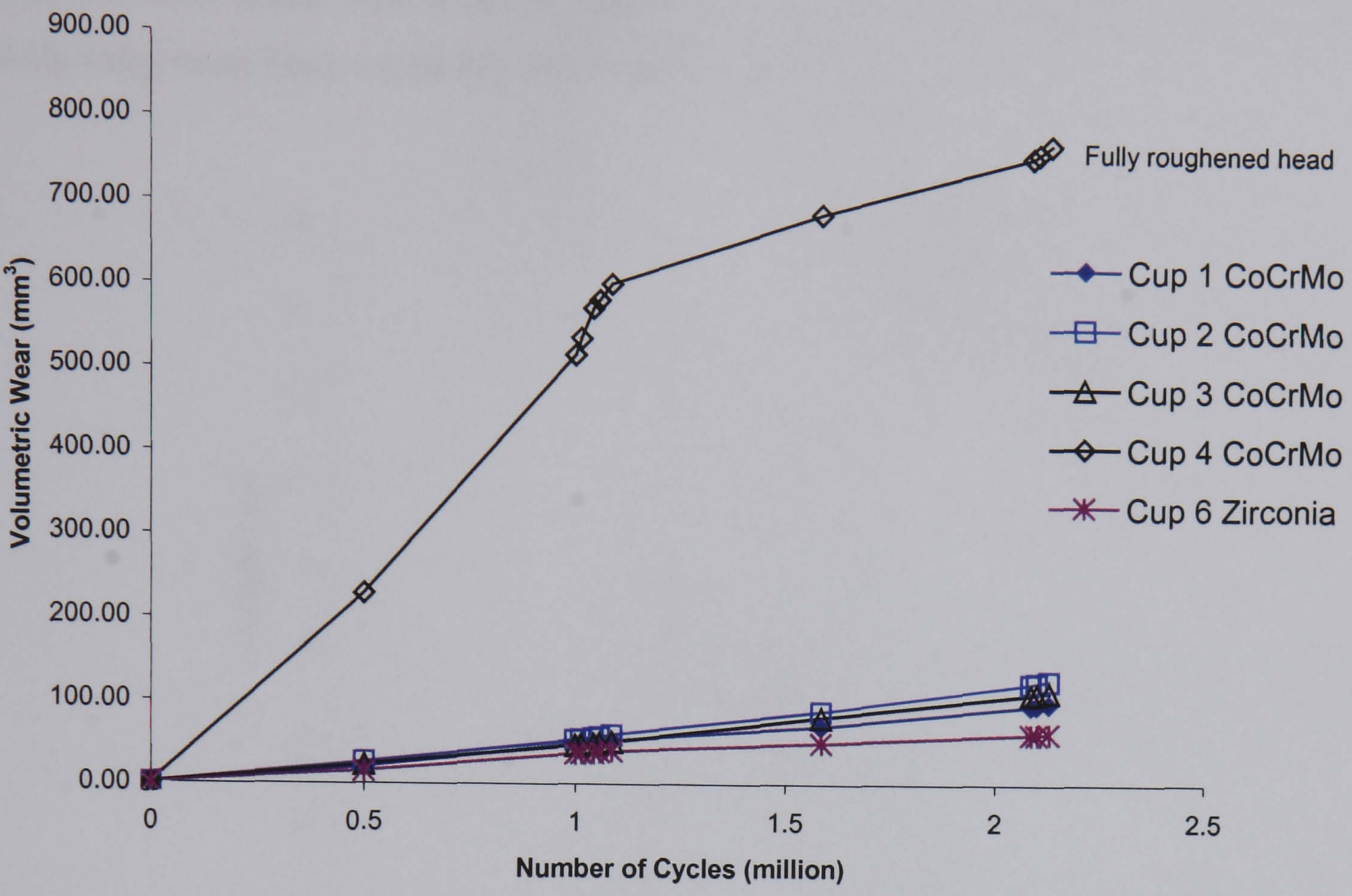


Figure 4.38: Volumetric wear change under small and large areas of damage during walking and jogging. Showing the difference in volumetric wear experienced by a fully roughened head compared to volume loss under small areas of damage

### 4.4.2 Particle analysis following jogging under a fully roughened head

The particle number distributions determined following jogging under a fully roughened head showed wide variability between all samples, shown in Figure 4.39 (a), however this can be explained by the number of particles that were counted for each sample. Samples 11a and 11b produced a lower number of particles, $8.72\times10^{14}$ and $6.41\times10^{14}$ respectively, whereas sample 11c produced a ten fold increase with $111.0\times10^{14}$ particles (Table 4.4). Another major difference between the samples analysed is that both sample 11b & 11c produced a single peak distribution whereas sample 11a produced a bimodal distribution.

Analysis of the particle volume distribution, Figure 4.39 (b), shows that two samples (11a & b) produced particles with a modal size of 2 μm, whereas sample 11c showed that the majority of the volume was composed of particles with a modal size of 0.4 μm, despite the

differences in modal size, it can be said that all the particles generated during tests under a fully roughened head would fall within the bioactive range.

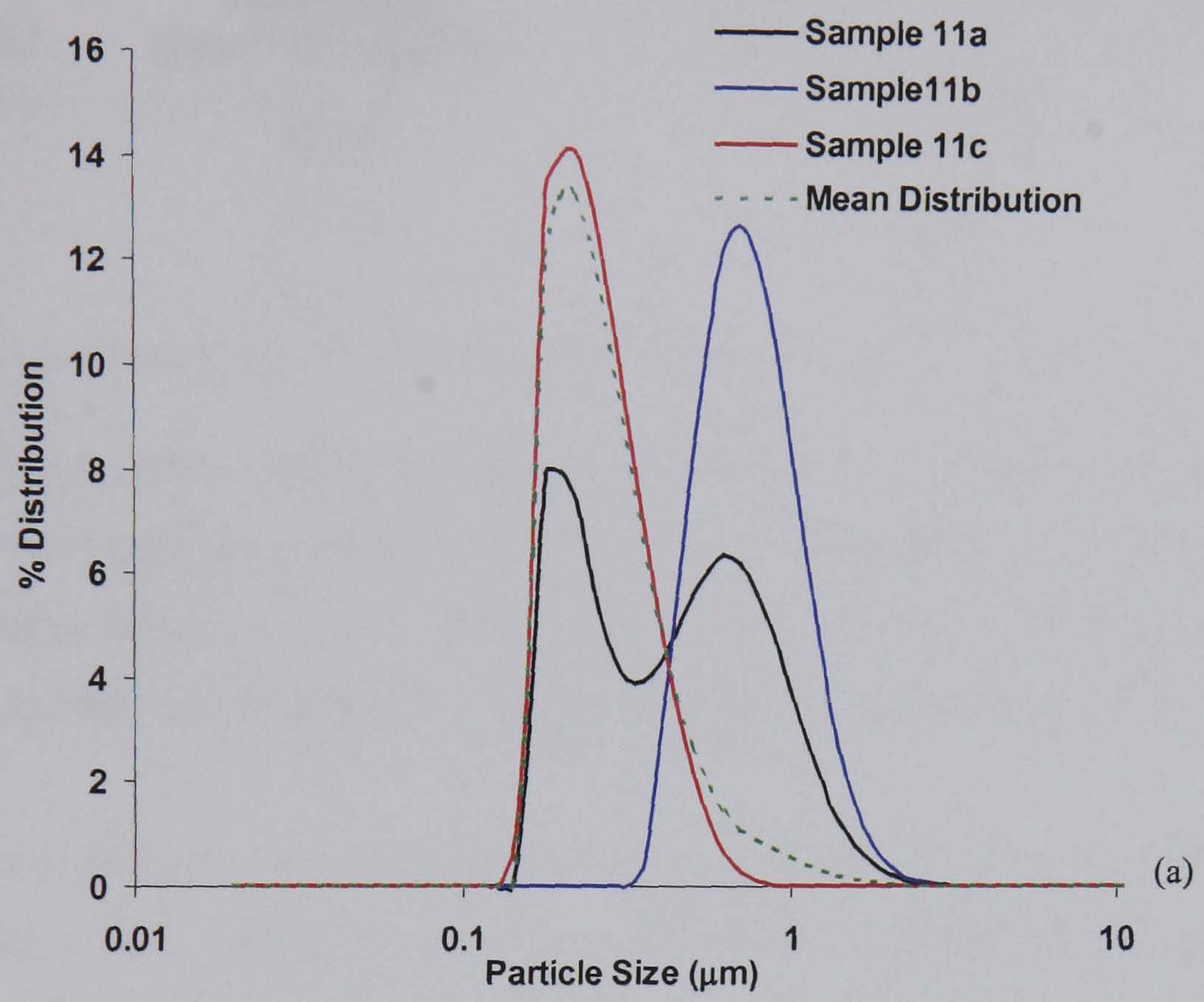


Figure 4.39: (a) Number distribution with the mean distribution, and (b) volume distribution of particles following jogging under a fully roughened head.

Table 4.4: Particle numbers for samples 11a, b and c analysed following jogging under a fully roughened head

| Sample ID | Wear Rate ($mm^3/10^6$ cycles) | Number of Particles in sample ($\times 10^{14}$) |
|---|---|---|
| 11a | 674.6 | 6.41 |
| 11b | 674.6 | 8.72 |
| 11c | 674.6 | 111.0 |

The distribution and the number of particles observed accounts for the mean distribution being skewed towards the smaller particle size. The mean distribution taken over three samples indicates that the modal size of particles is 0.22 μm, ranging from 0.142 to 2.8 μm, showing that the majority of particles generated under this test condition are bioactive.

SEM analysis of particles generated under a fully roughened head are shown in Figure 4.40. Jogging under a fully roughened head showed that the majority of the particles were submicron in size, with 97 % of the particles less than 1 μm in size, with the greatest number of particles in the 0.01-0.05 μm size band. Indicating that almost all the particles generated under this condition would lie in the bioactive range.

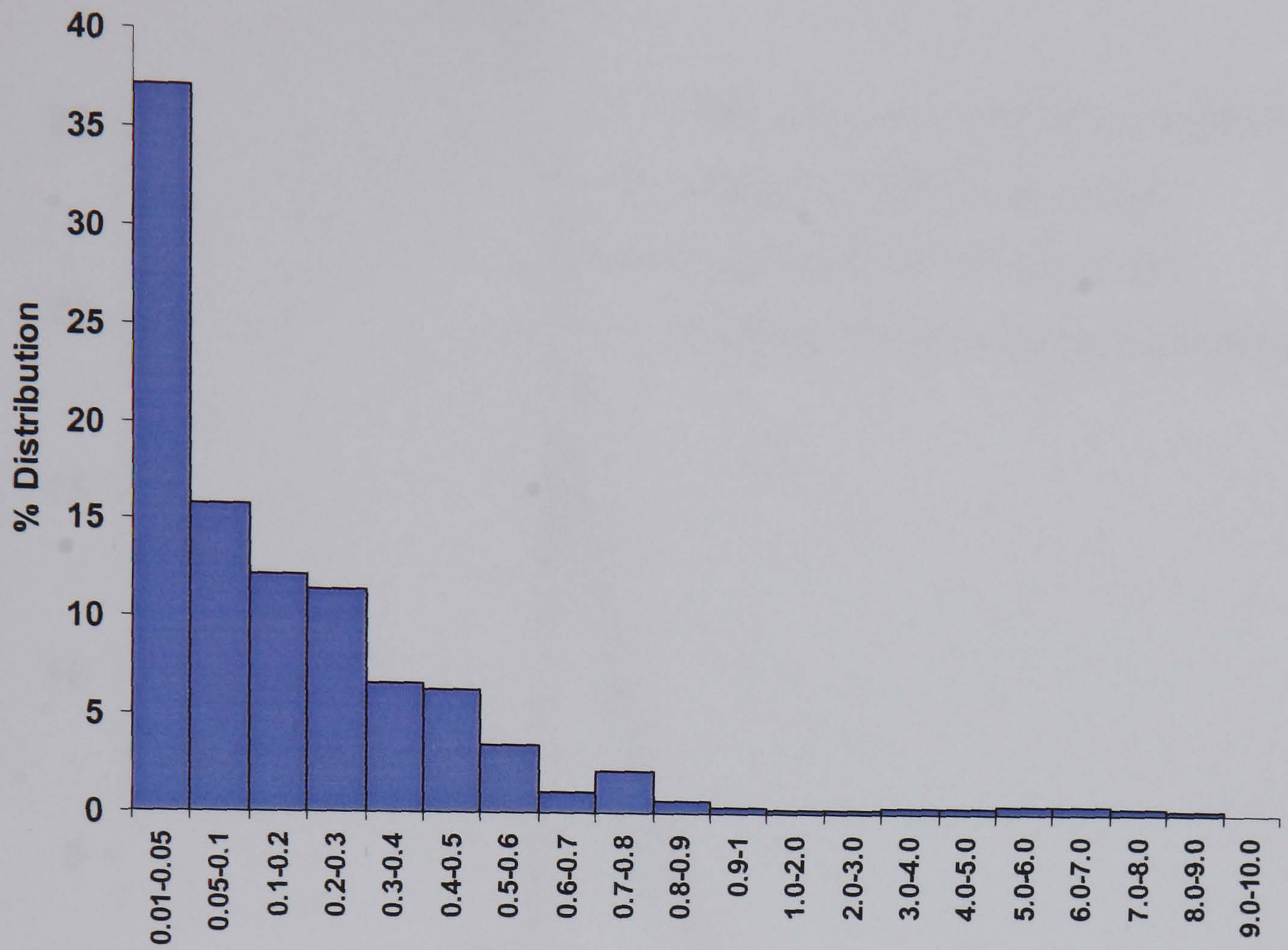


Figure 4.40: SEM number distribution of particles following jogging under a fully roughened head

### 4.4.3 Particle analysis following tests under various femoral head conditions: Jogging

A comparison of the mean number distribution of jogging samples under various femoral head conditions are shown in Figure 4.41. The distributions may be compared to the distributions seen for walking under various femoral head conditions (Figure 4.32). As the size of the area of roughness is increased, there is a decrease in the number distribution, but an increase in size range. There appears to be no significant difference between jogging under smooth conditions and a roughened area of 20 $mm^2$, which suggests that a threshold point exists where roughness would become the determining factor in the type and size of particles produced.

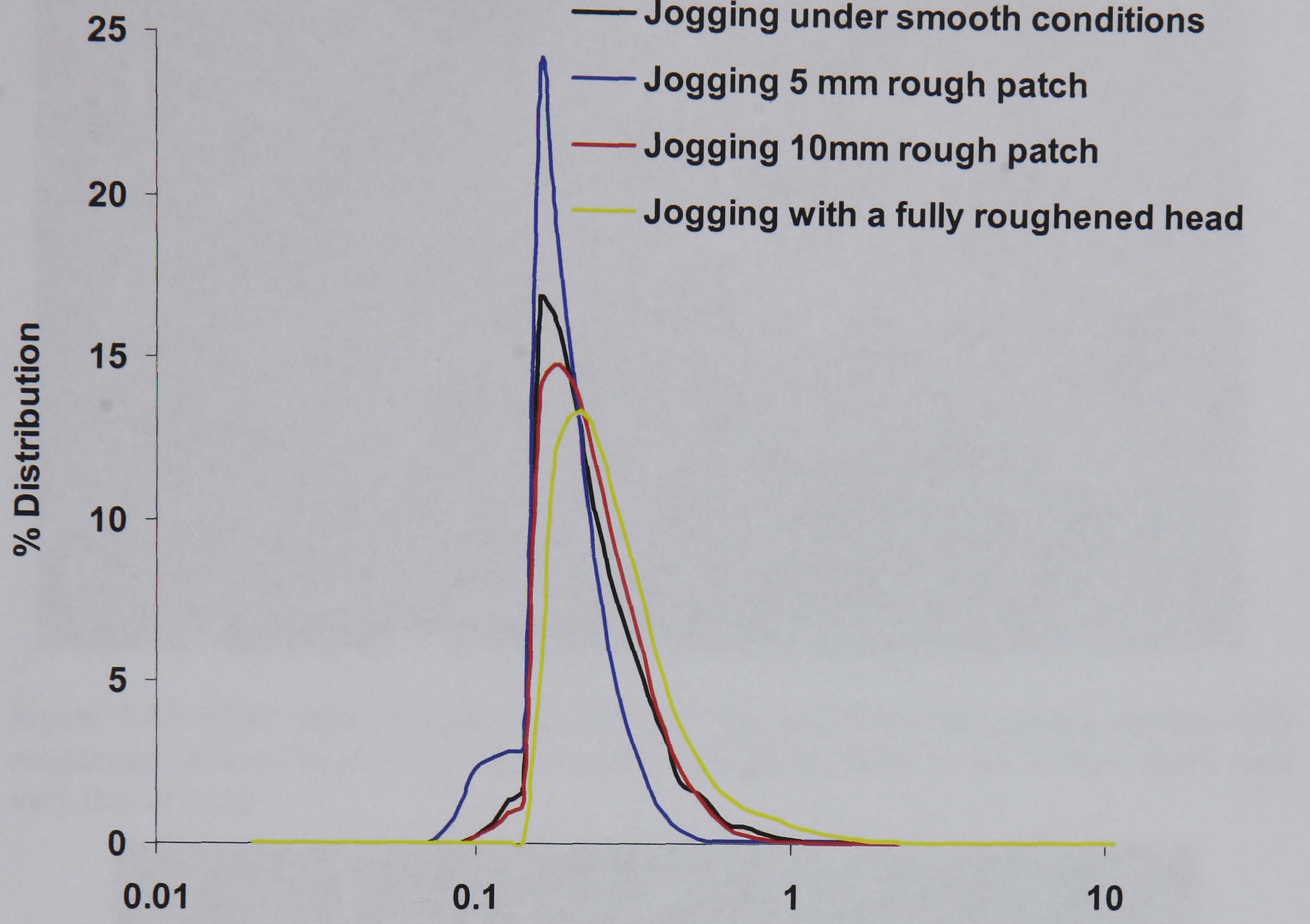


Figure 4.41: Mean number distribution of jogging samples under various femoral head conditions.

Examples of particle morphology observed during SEM analysis of particles following jogging under a fully roughened are shown in Figure 4.42 and Figure 4.43.

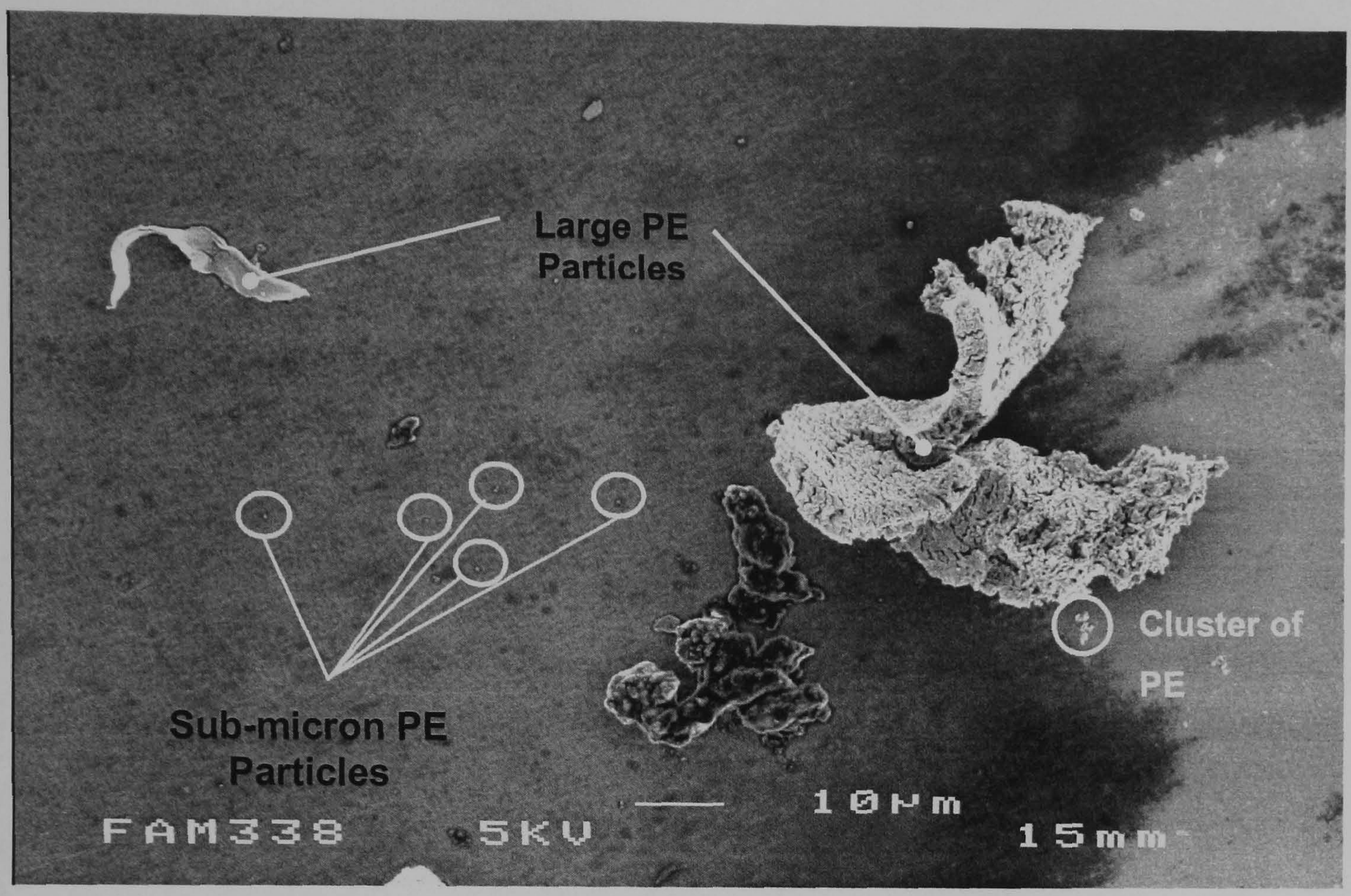


Figure 4.42: SEM image of large PE particles observed following jogging under a fully roughened femoral head, showing some particles greater than 10 μm in size, there were very few of these.

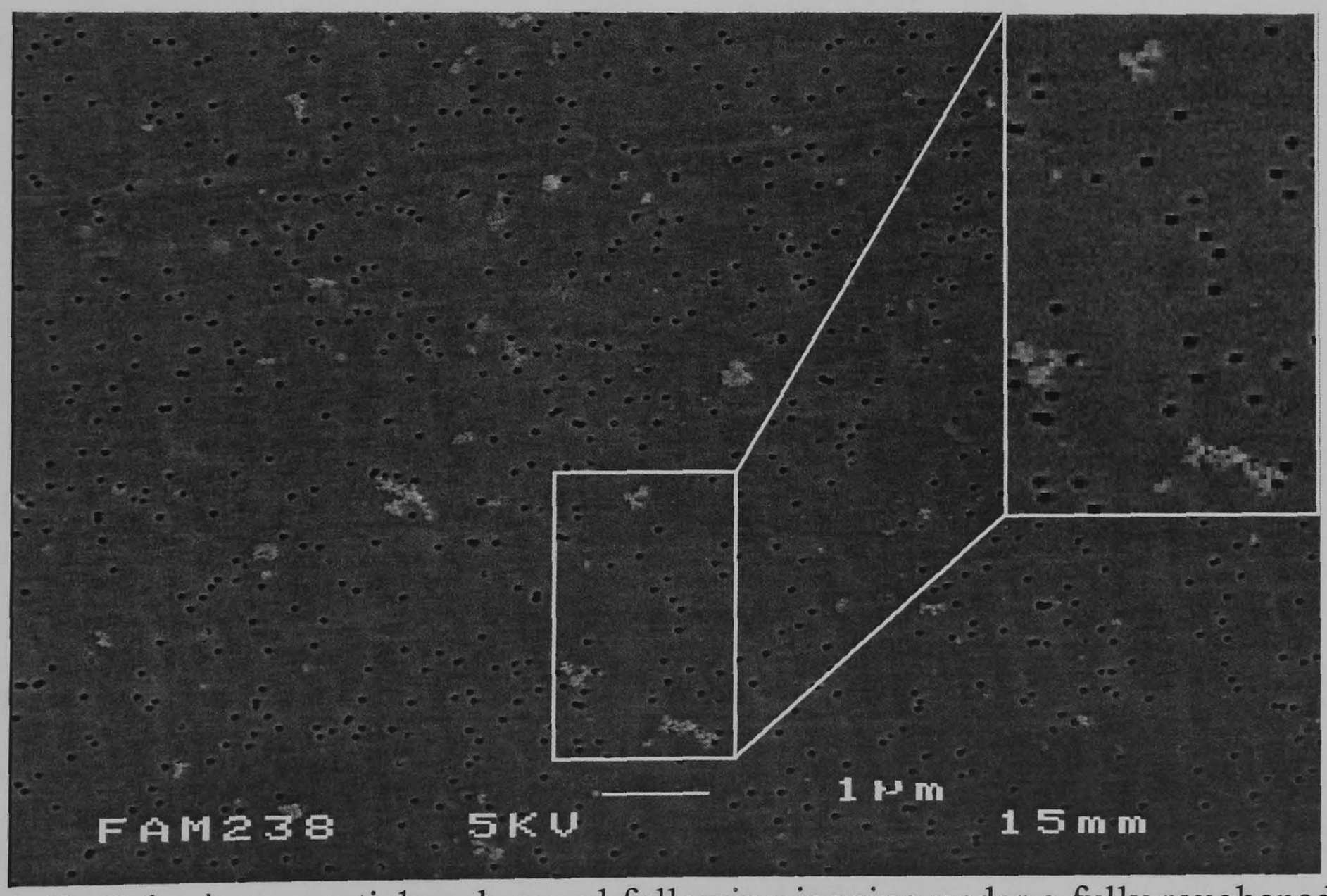


Figure 4.43: Submicron particles observed following jogging under a fully roughened head, majority of particles tended to be round or oval in morphology. Black dots are the pores in the polycarbonate filter, which are 0.05 μm in diameter

### 4.4.4 Summary of wear and surface topography for wear test one

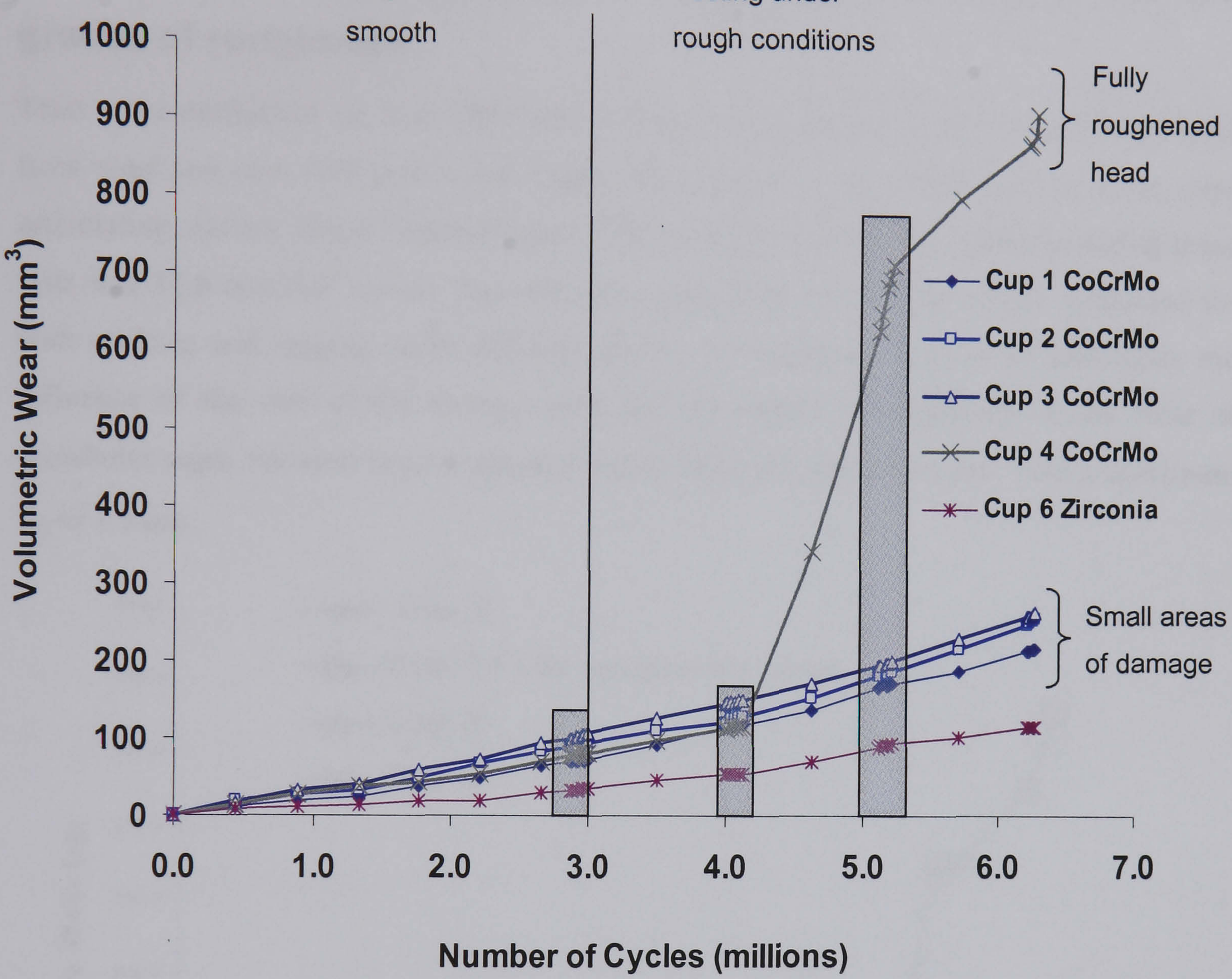


Figure 4.44: Total accumulated volumetric loss following all tests under both smooth and rough femoral head conditions. Highlighted areas indicate jogging tests preceded and followed by walking tests for 1 million cycles.

This study has shown that under smooth conditions, strenuous activities such as jogging can be still be undertaken with minimal effect on the wear of lightly cross-linked polyethylene. The introduction of small areas of surface damage had a moderately low influence on the wear rate of lightly-crosslinked UHMWPE under both high and low patient activities. However, it appears that a threshold point exists, where the area of

surface damage combined with increased activity, reaches a critical value, which would lead to excessive wear and a significant increase in the number of particles produced.

## 4.5 Wear Test Two: Walking and Jogging tests under different grades of roughness

Tests were performed on four new head and cup combinations. Cups 3 and 6 were used from wear test one, with new metal heads, cups B and C were introduced as virgin cups articulating against virgin femoral heads. The median wear rate for walking during these tests was 17.6 $mm^3/10^6$ cycles. Fast and slow tests at 60 and 105 rpm were conducted for both walking and jogging under different grades of roughness, in order to investigate the influence of the size of the damage area and the degree of roughness on the wear of acetabular cups. Femoral head roughness varied from 0.2 μm to 0.8 μm, with a maximum $R_p$ of 1.5 μm.

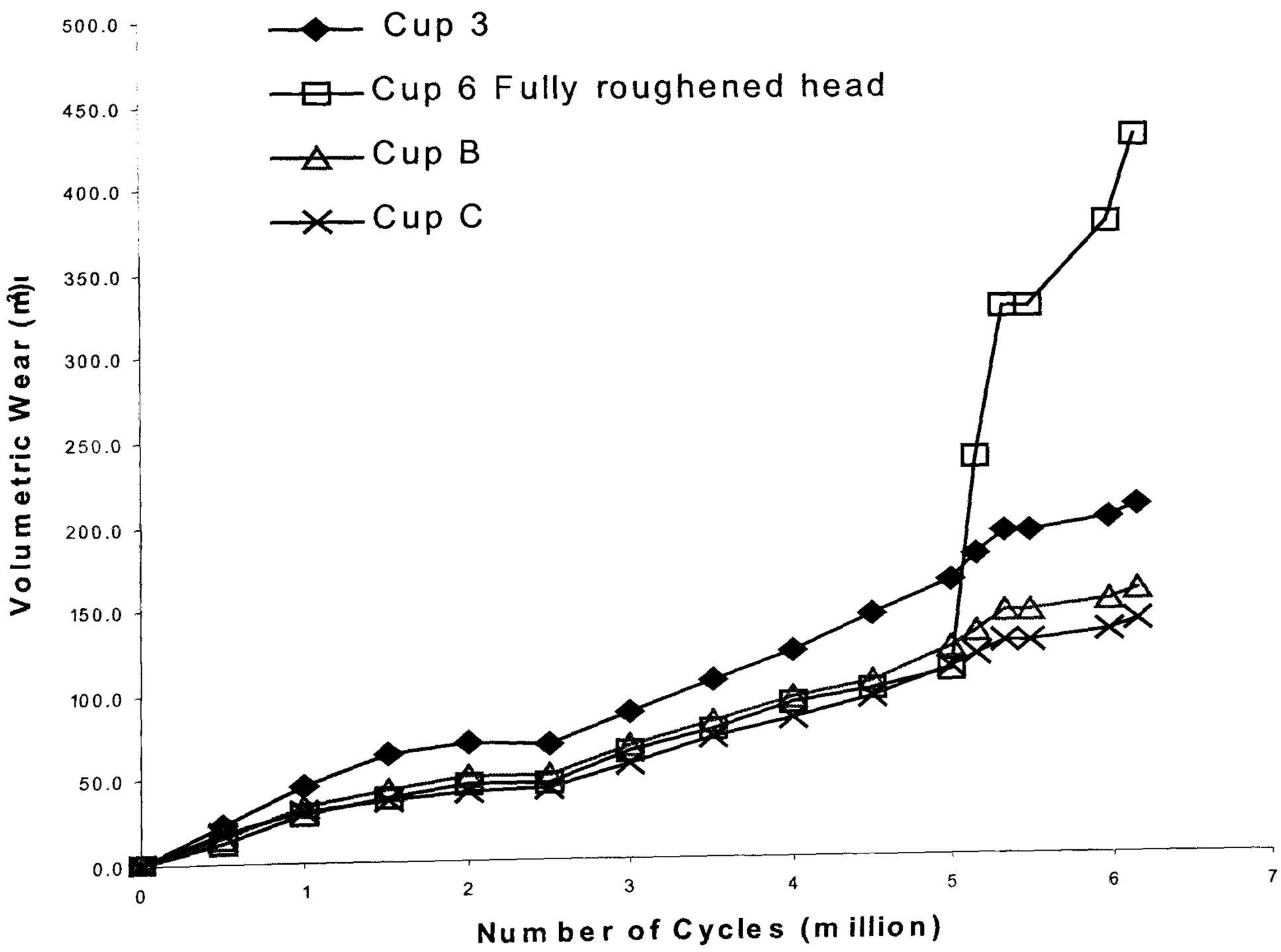


Figure 4.45: Overall volumetric wear for all test conducted during wear test 2

Table 4.5: Summary of wear rates obtained following fast and slow, walking and jogging tests where the roughness was introduced over an area of 80 $mm^2$. * Fully roughened head

| Test | Head C | Head 6* | Head B | Head 3 |
|---|---|---|---|---|
| Initial $R_a$ (μm) | 0.2 | 0.4 | 0.5 | 0.8 |
| Fast jogging ($mm^3/10^6$ cycles) | 35.6 | 551.6 | 42.2 | 65.7 |
| Slow jogging ($mm^3/10^6$ cycles) | 33.6 | 393 | 50.8 | 60.3 |
| Fast walking ($mm^3/10^6$ cycles) | 27 | 231.6 | 27.8 | 33.6 |
| Slow walking ($mm^3/10^6$ cycles) | 23.5 | 220 | 24.9 | 30.6 |

At small areas of roughness, volumetric wear continued in a linear manner, with no long term effect, however with the fully roughened head, there was a rapid increase in the wear experienced by the PE cups (Figure 4.45). The degree of damage experienced by the cups appears to have an influence upon the volumetric wear observed during tests, with fast and slow jogging producing the highest volumetric wear over a roughened area of 176 $mm^2$. Fast and slow walking produced approximately half the wear compared to that of jogging, an indication that activity combined with femoral head damage would increase wear.

The fully roughened head also shows a similar trend in that jogging produced wear that was 2-fold higher than that of walking at both and fast and slow conditions (Figure 4.12). It would also appear that in general activities carried out at slower speeds produced lower volumetric wear to that of activities carried out at faster speeds, whether walking or jogging, Figure 4.46. Fast and slow walking produced low wear rates compared to jogging for all different grades of roughness, showing small increases in wear despite the increase in surface roughness. Jogging on the other hand showed the greatest difference in wear rates whether fast or slow, showing very similar rates of wear with increasing levels of roughness. This suggests that the level of surface roughness combined with increased loads is a major factor in the wear of lightly crosslinked polyethylene.

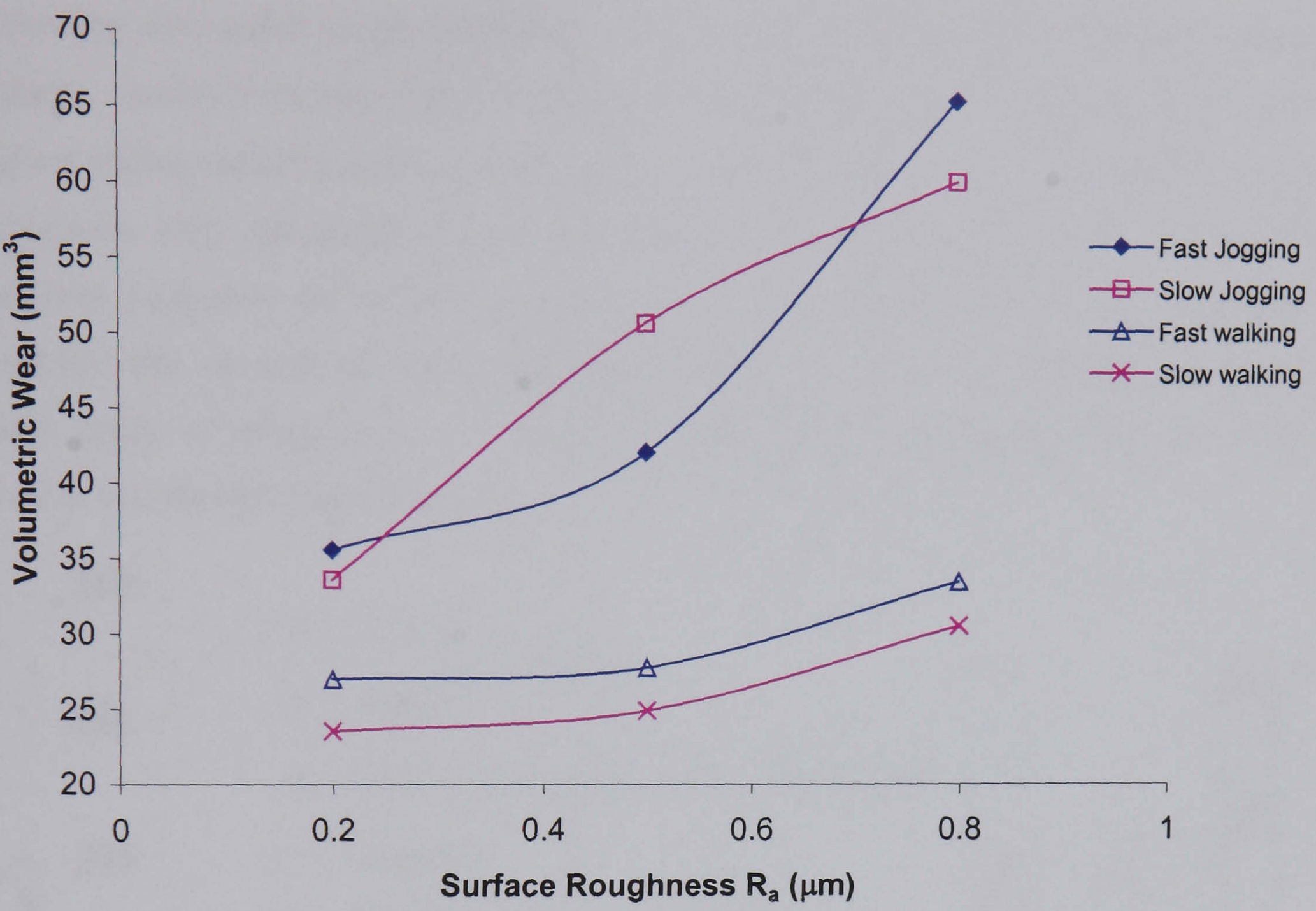


Figure 4.46: Plot of volumetric wear versus surface roughness for $R_a$ values of 0.2, 0.5 and 0.8 μm over an area of 80 $mm^2$ for 1 million cycles.

## 4.6 Wear Test Three: Walking and Jogging with discrete scratches

Following tests under rough conditions where an area of roughness consisted of a patch of damage, similar tests were then conducted using discrete scratches applied in the area of highest sliding velocity with a maximum $R_p$ of 1.5 μm. Figure 4.47 shows the accumulated volumetric wear following walking and jogging tests under a rough patch and discrete scratches applied to the head of length 5 and 10 mm (Cups 1 and 2). Cup 3 had discrete scratches that covered the entire upper hemisphere of the head. Although tests under a rough patch covering an area of 176 $mm^2$ were already conducted, this was only one sample, and the tests were repeated.

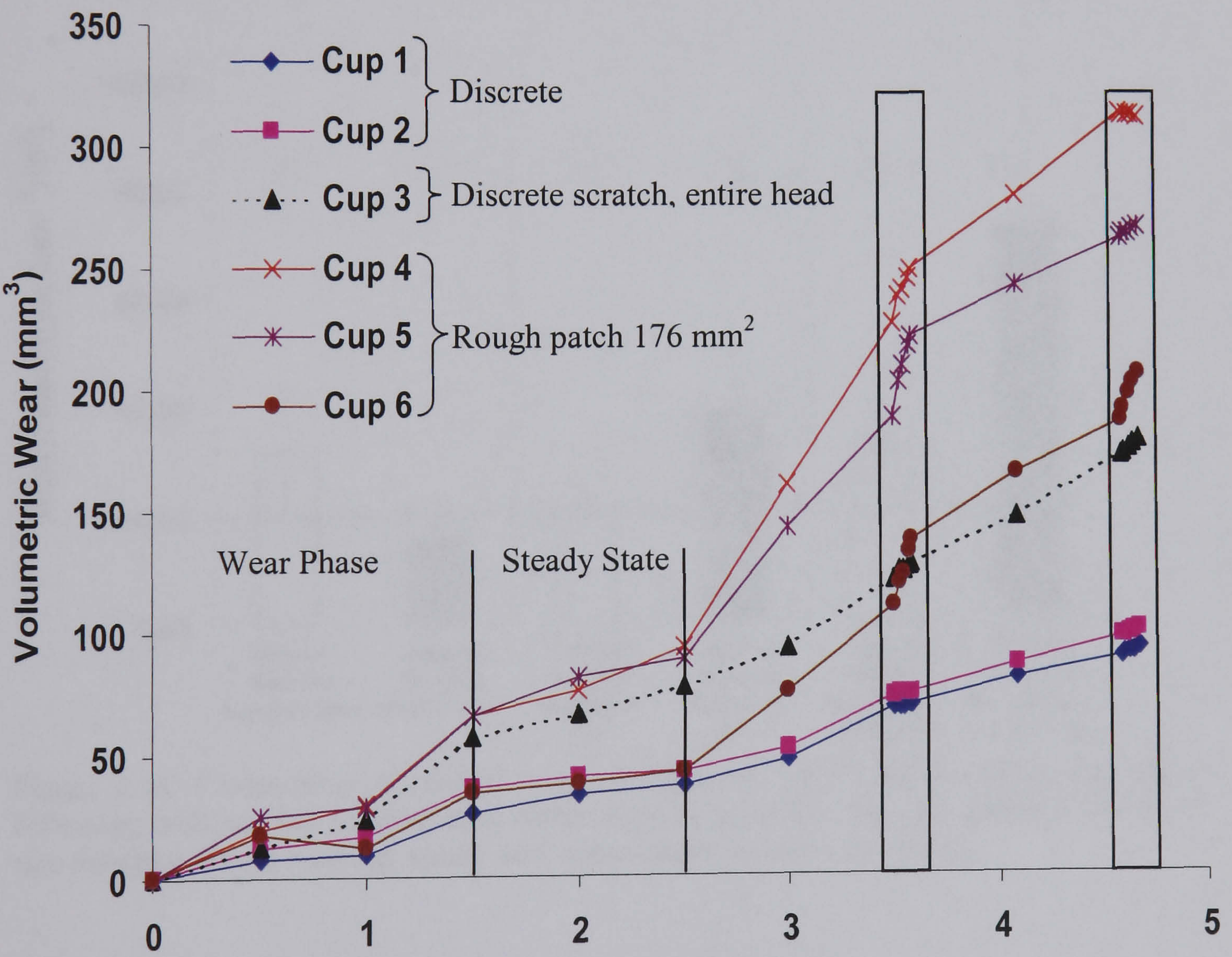


Figure 4.47: Accumulated volumetric wear loss for walking and jogging following tests under discrete scratches.

Tests under scratches showed similar trends to that of tests under rough patches in that wear showed a progressive increase with increased length of scratches. However this trend was only evident for PE cups once the scratch length had reached 10 mm in length.

Under a 5 mm scratch length jogging showed less wear than walking, contrary to all other tests which showed an increase in wear with increased activity. Figure 4.48 shows a comparison of the median wear rates under discrete scratches for differing lengths and activity.

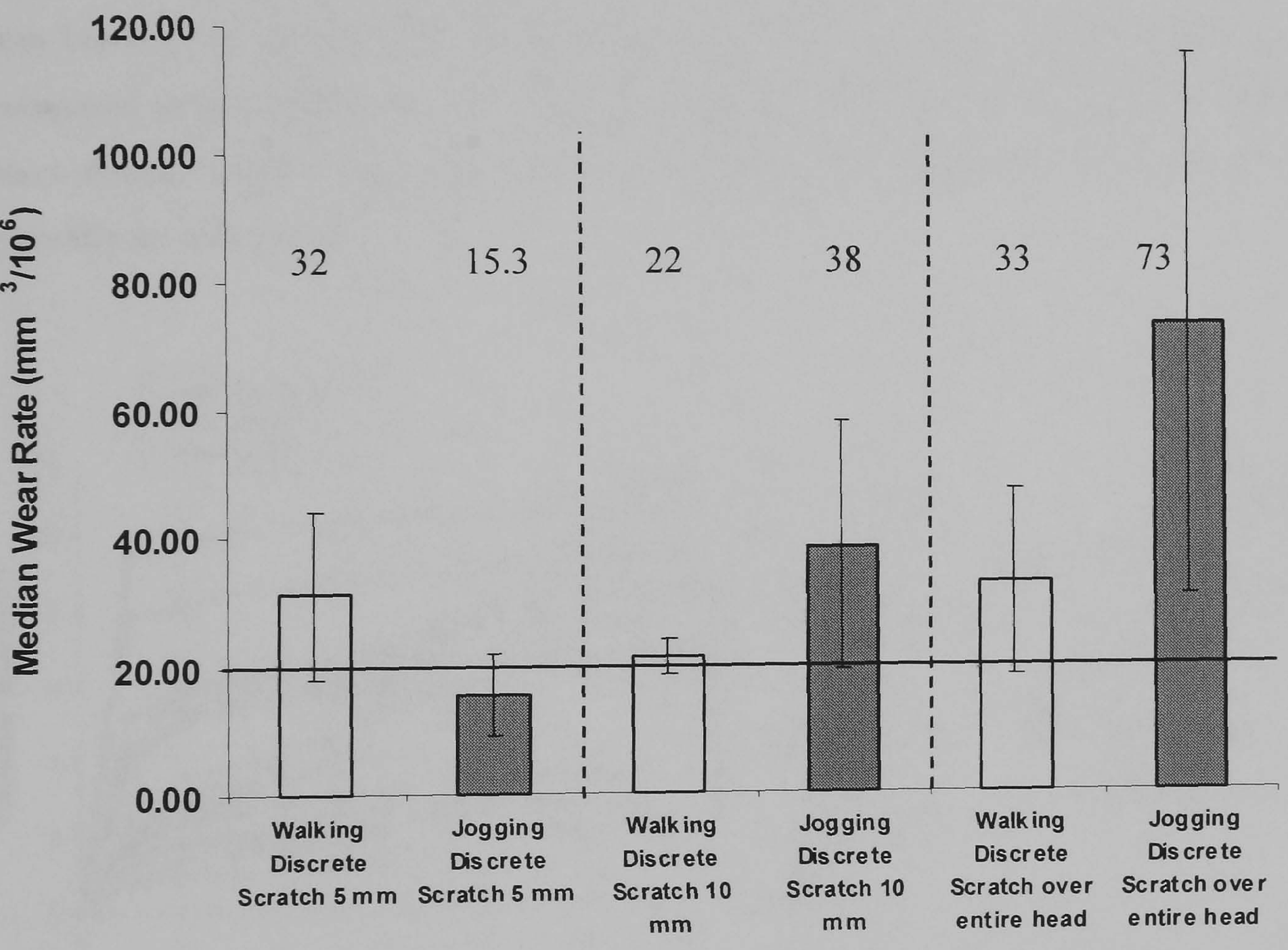


Figure 4.48: Comparison of median wear rates (shown by the figures above bar chart) following walking and jogging tests under discrete scratches, the line indicates the wear rate obtained during walking, steady state wear, under smooth conditions

## 4.7 Wear test 4: Metal on Metal

### 4.7.1 Running-In Wear - Standard Walking Tests

Figure 4.49 (a) and (b) presents the combined (head and cup) volumetric wear results as a function of number of cycles for all 28, 40 and 56 mm MOM bearings. It shows that all bearing couples generated a biphasic wear pattern, producing higher initial wear followed by a reduced steady-state wear, a statistically significant difference in wear rate ($p<0.05$). Figure 4.49 (a) shows the mean combined volumetric wear rates for all bearing sizes during running-in, and highlights that the 56 mm bearings generated by far the greatest running-in wear at 7.0 $mm^3/10^6$ cycles. The lowest mean running-in wear rate was generated by the 40 mm bearings at 2.2 $mm^3/10^6$ cycles, showing a 2–3.5 fold reduction in running-in wear compared to the 28 and 56 mm bearings respectively ($p<0.05$). Additionally, all bearing sizes showed greater wear loss from the acetabular cups compared to the femoral heads, typically by a factor of 2.

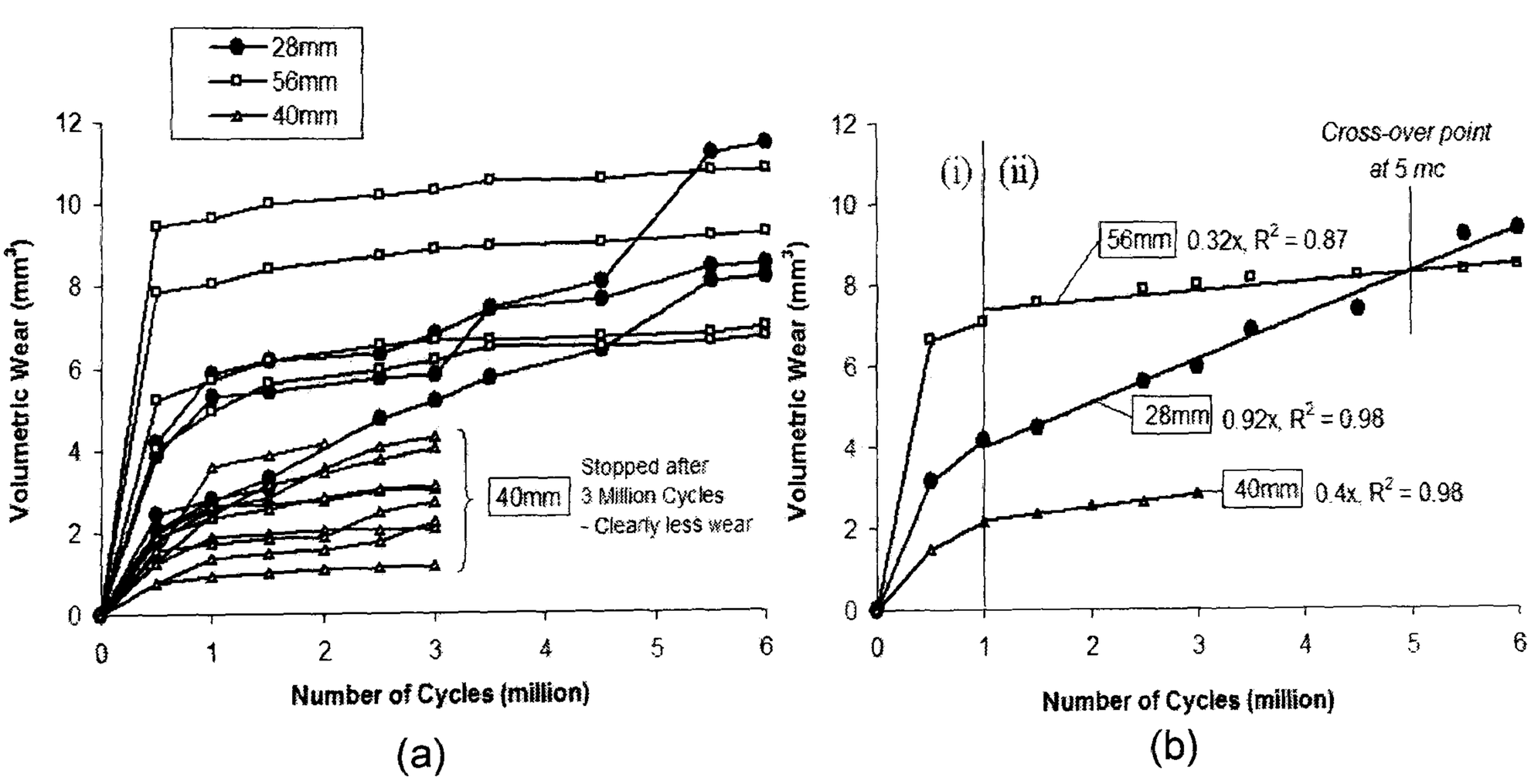


Figure 4.49: Variation of combined (head & cup) volumetric wear verses number of cycles under normal physiological walking, for (a) all 18 bearing couples tested, and (b) the accumulative mean for the three bearing sizes – showing (i) running-in conditions-walking (first $1x10^6$ cycles), and (ii) steady-state (SS) conditions–walking (after $1x10^6$ cycles).

### 4.7.2 Steady-State Wear - Standard Walking Tests

Figure 4.49 (b) and Figure 4.50 (b) present the mean combined (head + cup) steady-state volumetric wear rates for all 28, 40 and 56 mm couples. The results showed that the larger 40 mm bearing typically generated a clear 2–3 fold reduction in mean steady-state wear rate compared to the smaller 28 mm bearing sizes ($p<0.05$). The 56 mm bearings generated a further 20 % reduction in steady-state mean wear rate compared to the 40 mm bearings ($p<0.05$). In general, the wear results for all groups produced low scatter, showing no runaway wear for any bearing tested, Figure 4.50a.

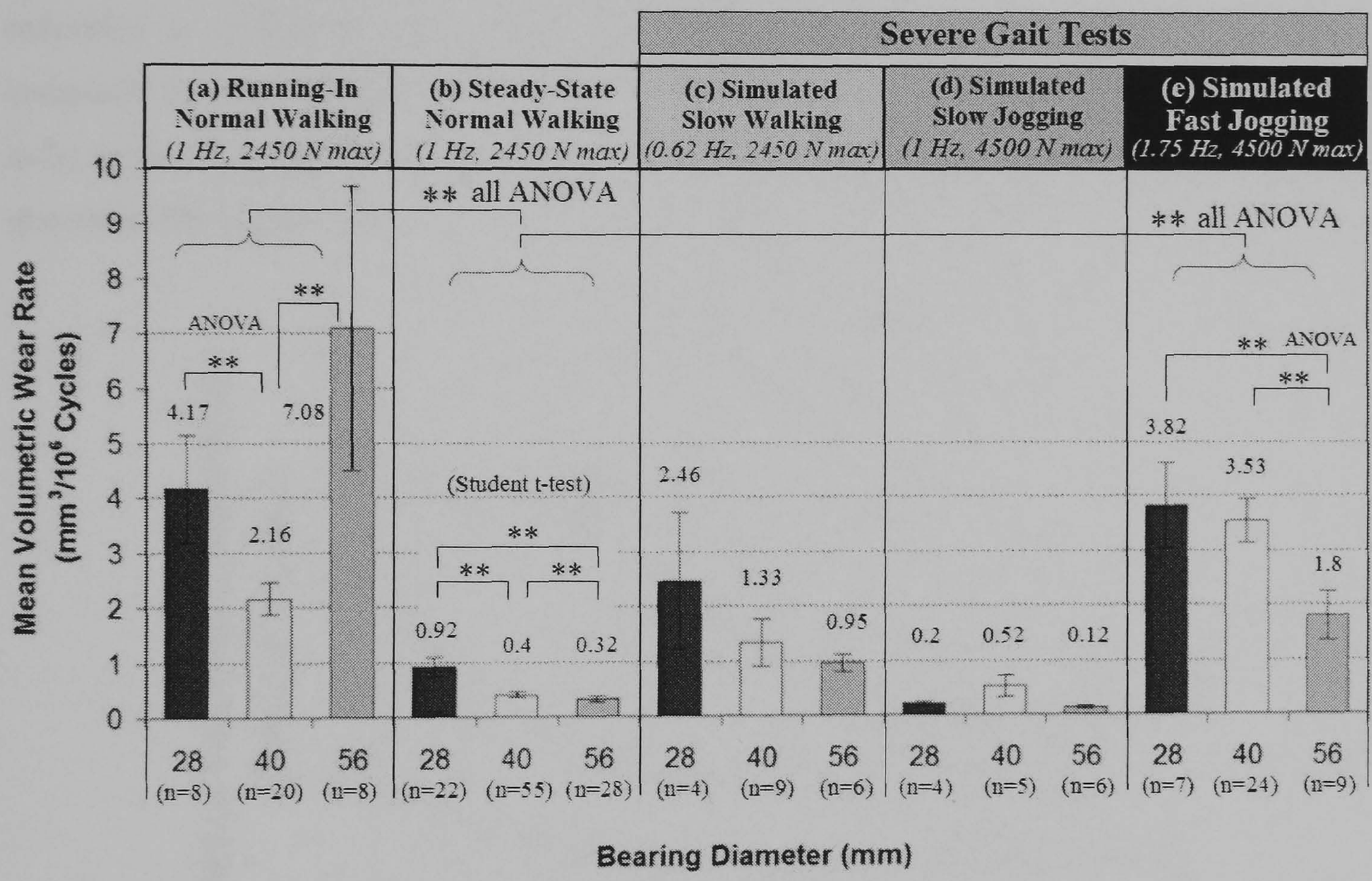


Figure 4.50: Summary of mean combined volumetric wear rates (head & cup) under smooth conditions for (a) running-in wear – normal walking, (b) steady-state wear – normal walking 2450 N max 1 Hz, (c) simulated slow walking 2450 N max 0.62 Hz, (d) simulated slow jogging 4500 N max 1 Hz, and (e) simulated fast jogging 4500 N max 1.75 Hz. The error bars represent ± SE, n = number of wear test results, ** = $p<0.05$

### 4.7.3 Increased Patient Activity Tests

Out of the three severe gait activities simulated, fast-jogging (1.75Hz, 4500 N max) generated the worst wear condition for all bearing sizes, typically showing a 4–9 fold

increase in volumetric wear compared to standard walking (1 Hz, 2450 N max) ($p<0.05$) shown in Figure 4.52. Slow-walking (0.62 Hz, 2450 N max) was the next highest ranked severe activity, typically showing a 3–fold increase in volumetric wear compared to standard walking for all bearings ($p<0.05$) shown in Figure 4.51 (c).

With respect to bearing diameter, the results showed that the 56 mm bearings generated the least amount of steady-state wear under all severe activities simulated, showing greater wear resistance compared to the 28 and 40 mm bearings after the running-in phase. Moreover, the results showed that the more-severe the gait activity simulated, a greater reduction in volumetric wear could be achieved by using the larger 56 mm bearings compared to other smaller sizes (Figure 4.51). Figure 4.51 also shows that under the two most demanding activities simulated, slow walking and fast jogging, the 28 mm bearings generated the highest wear.

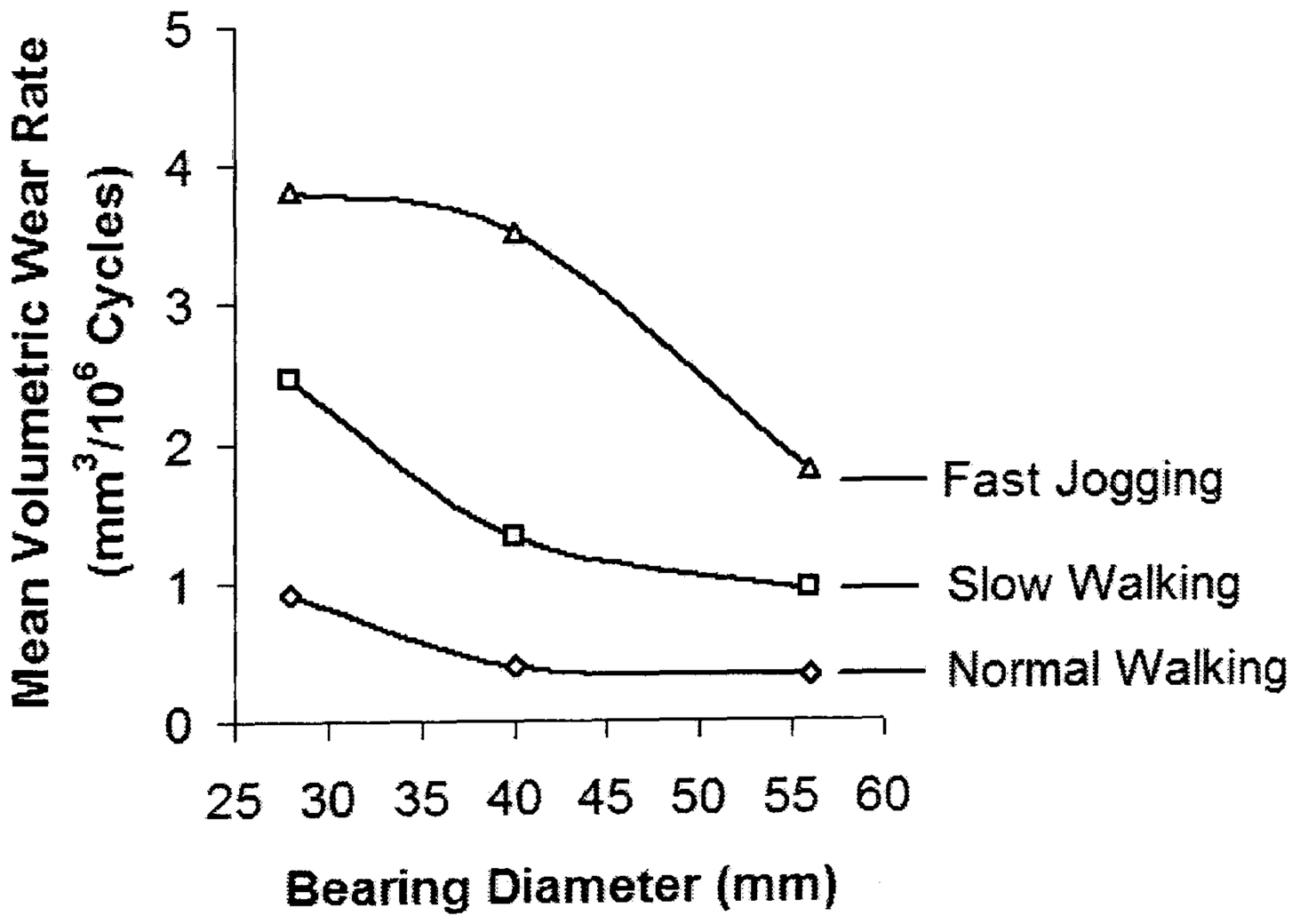


Figure 4.51: The variation in mean combined MOM volumetric wear rate (head and cup) verses bearing diameter for all main patient activities simulated.

Following all fast jogging and slow walking simulations, additional normal walking tests showed that most bearing couples returned to steady-state wear conditions, with only 2

bearings showing a small running-in period for 0.5 million cycles. All wear surfaces showed no visible change in surface roughness as a result of severe gait.

### 4.7.4 Particle Sample Analysis

Initial examination of samples showed various types of contamination from other types of metals present in the samples prepared for TEM analysis. Titanium (Ti), tin (Sn), Nickel (Ni) and Iron (Fe) were observed and confirmed via EDX. The morphology of these particles were very distinct, compared to wear debris particles, contaminating particles were needle like in shape and on the whole larger in size, examples of these particles are shown in Figure 4.52. The length of the contaminating particles ranged from 200 nm to 1500 nm. All particles showed some form of agglomeration, whether it was contaminating particles or wear debris particles.

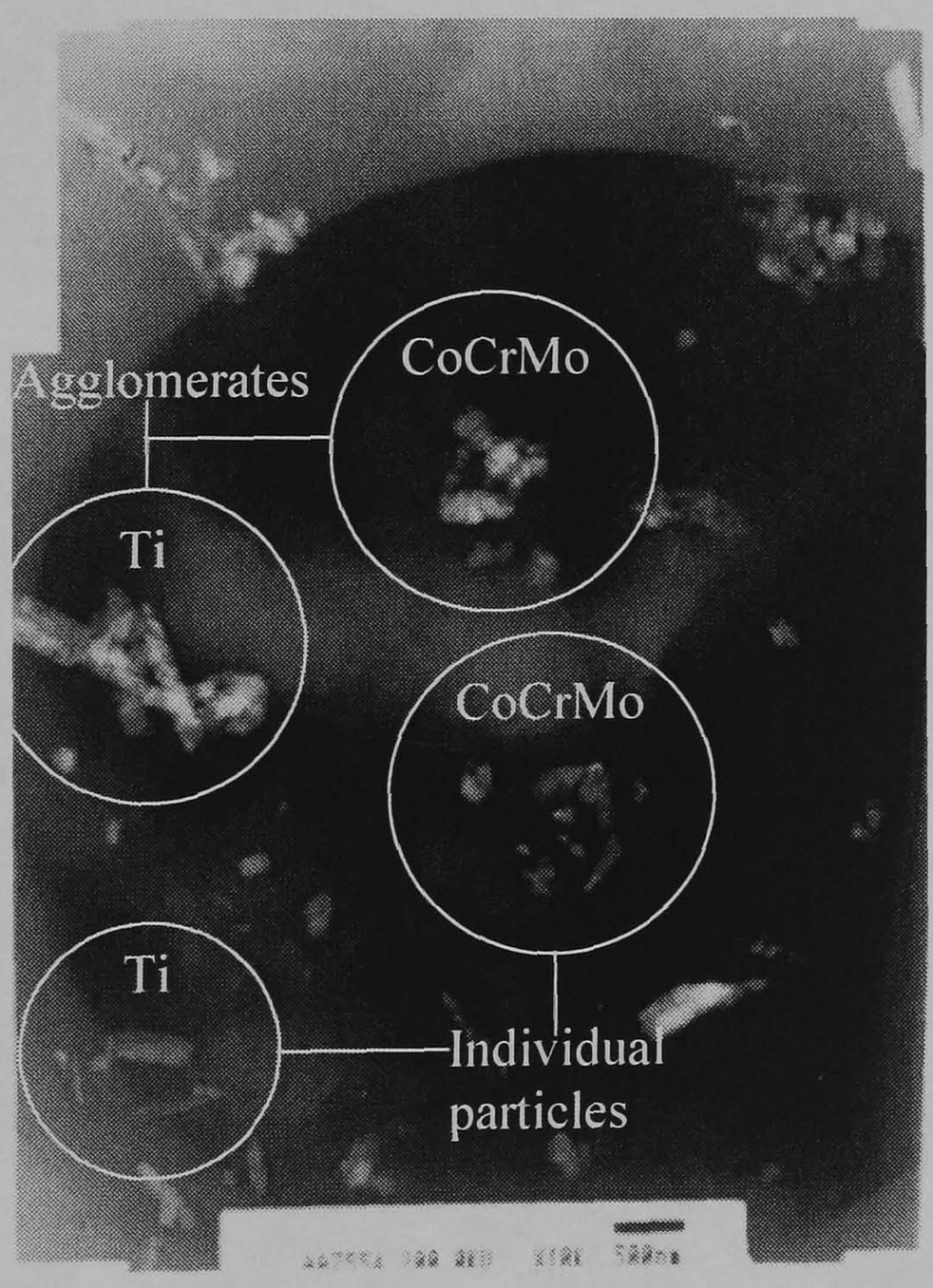


Figure 4.52: A TEM micrograph of Titanium (Ti) and CoCrMo particles taken at ×10 K magnification, note the difference in morphology of Ti and CoCrMo particles, the scale bar = 500 nm.

Composition of the elements within the particles was confirmed via EDX, shown in Figure 4.53 (a) and (b), the EDX scans also provide a qualitative indication of the weighting of the elements within the particle itself.

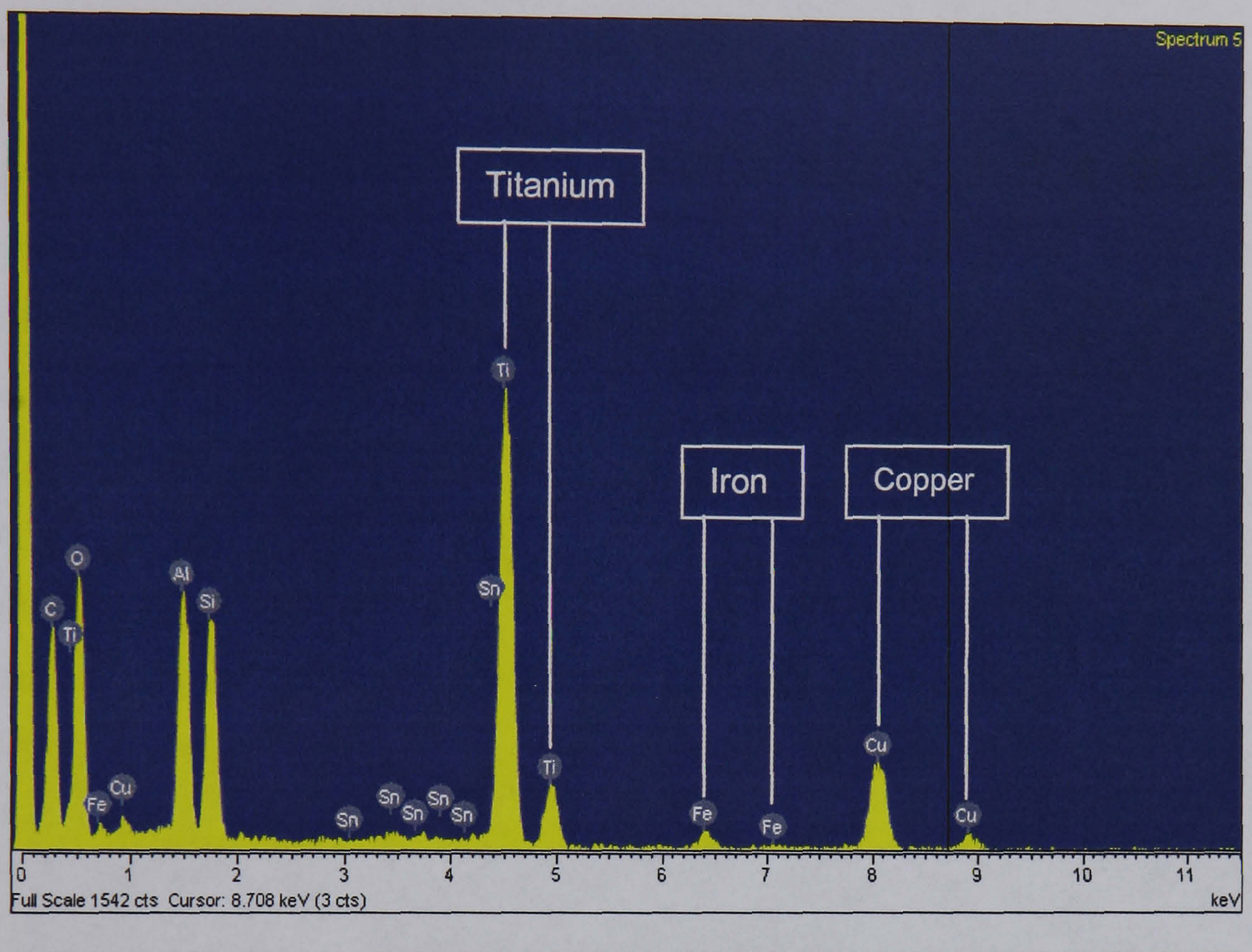


(b)

Figure 4.53: (a) EDX spot analysis of a Titanium particle, highest peak present and (b) EDX spot analysis of a metal particle, showing the presence of Fe and Ni as well Cobalt (Co), Chrome (Cr), and Molybdenum (Mo) elements within the particle

The carbon and copper peaks shown in Figure 4.53 (a) and (b) can be attributed to the grid used in TEM analysis. The grid itself is manufactured from copper and the film that covers the grid is composed of a thin layer of carbon. Silicon (Si) was also found in some EDX scans but not all, again this contamination might be attributed to the silicon sealant used in the test chambers to stop any leakage of serum from the test chambers. The source of the metal particle contamination was traced back to the acetabular cup fixtures used during the wear tests. Metal particles were filed from all the fixtures used in the tests as well as samples of metal filings from the unused components, which were subsequently analysed in the SEM with EDX analysis. A typical scan of the particles obtained from the femoral head and cup is shown in Figure 4.54. From the EDX scan, the spectrum confirms the presence of Co, Cr and Mo. The Fe peak seen in this scan was attributed to contaminating artefacts possibly already present in the TEM sample holder. No other types of metals were seen in the samples analysed from material directly derived from the femoral head and cup.

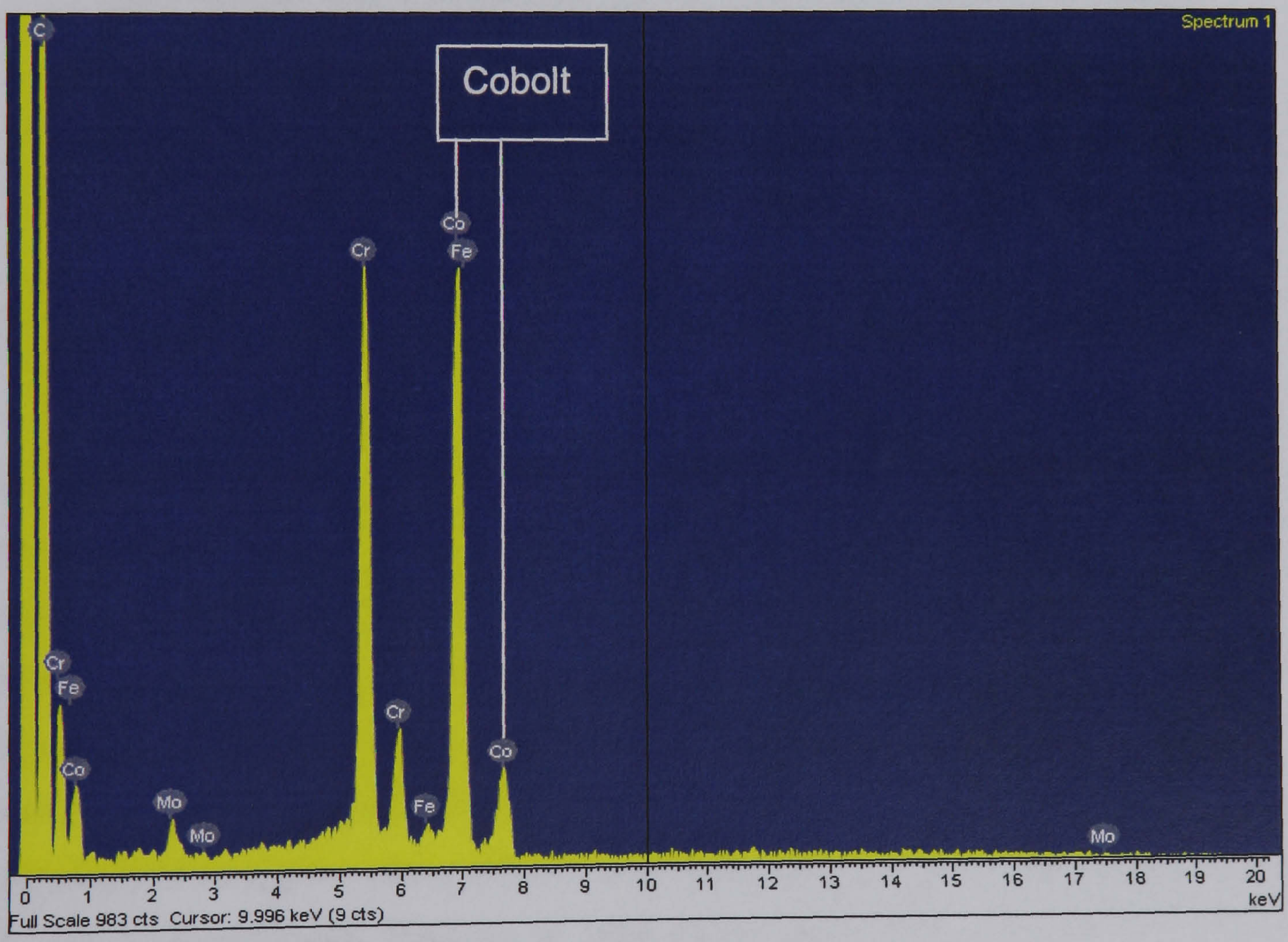


Figure 4.54: Typical EDX spectrum of particles from a CoCrMo femoral head and acetabular cup, showing the major elements that are present within the femoral head and acetabular cup.

than 1 μm (1000 nm) in size were observed but these were few in number. An example of large particles is shown in Figure 4.56, EDX analysis confirmed the presence of metal elements found in CoCrMo femoral heads.

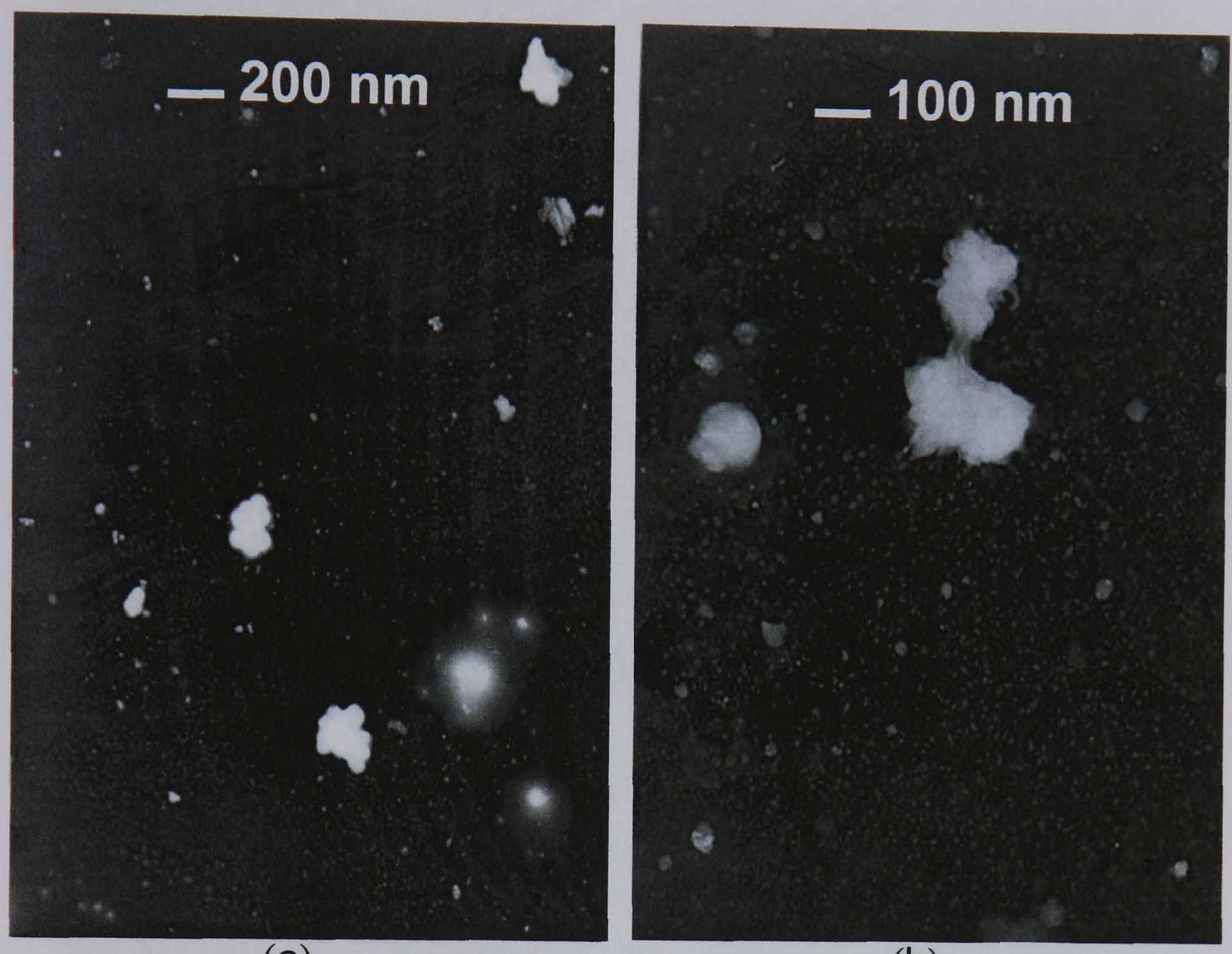


Figure 4.56: Examples of large CoCrMo particles observed during TEM, particles less than 0.5 μm in size are also present

From qualitative observations, particles generated during metal-on-metal articulation appeared to be very uniform in morphology, with the majority of the particles either oval or round in shape, as shown in Figure 4.57. This made the identification of metal wear particles easier due to their distinct morphology, with EDX analysis confirming the particle composition. Occasionally Ti and Fe particles were also observed, needle like in morphology compared to CoCrMo particles. Particles were seen in two different states, either singly or in agglomerates, shown Figure 4.58, which shows various types of particles with varied morphologies. Particles in large agglomerates were not analysed due to the difficulty in separating individual particles from the clusters. However a sufficient number of particles were imaged to provide an accurate indication of the size of the particles

produced during testing. A summary of the raw data collected during image analysis is presented in Table 4.6 (a).

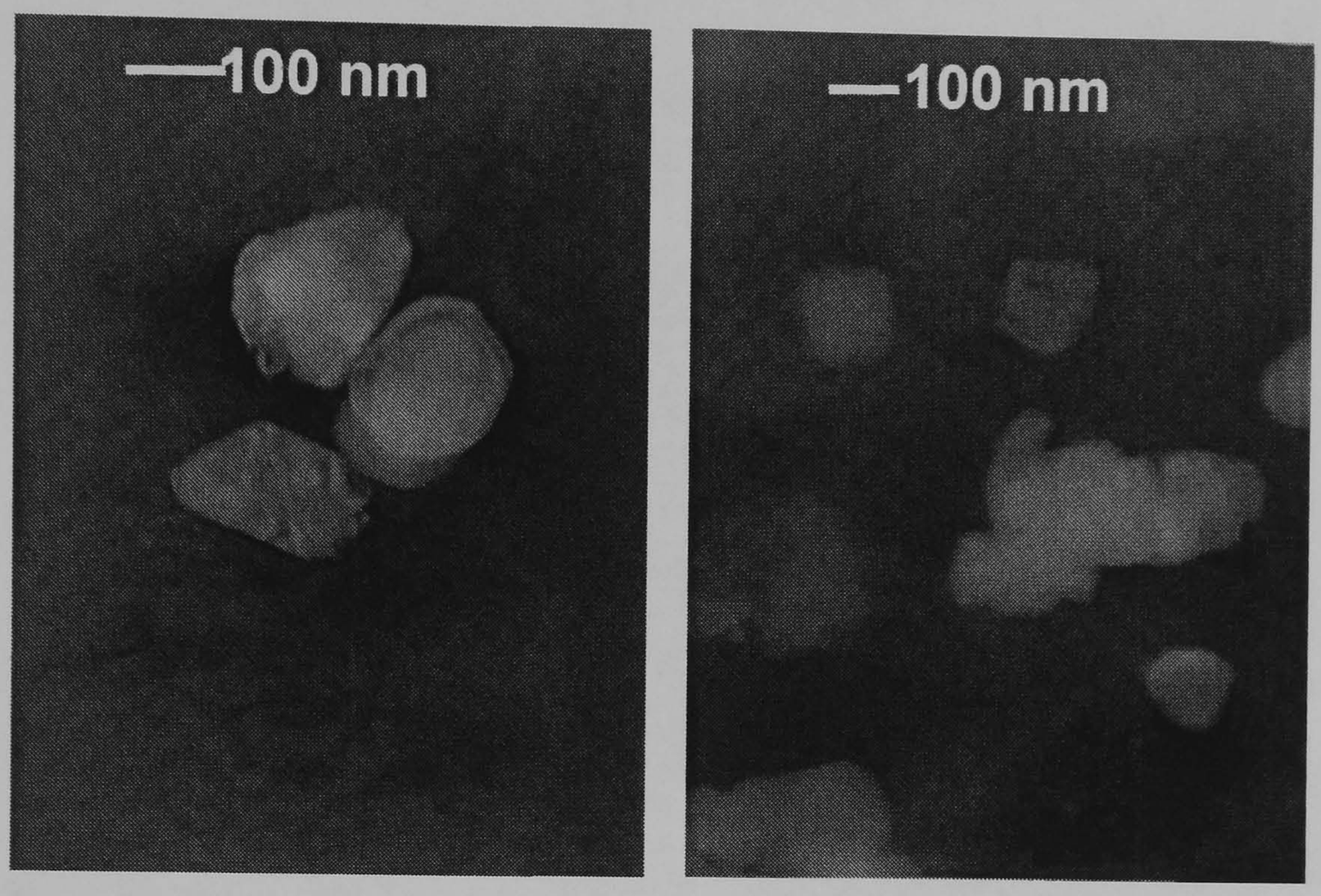


Figure 4.57: Example of small CoCrMo particles, with very distinct morphology, round or oval in shape.

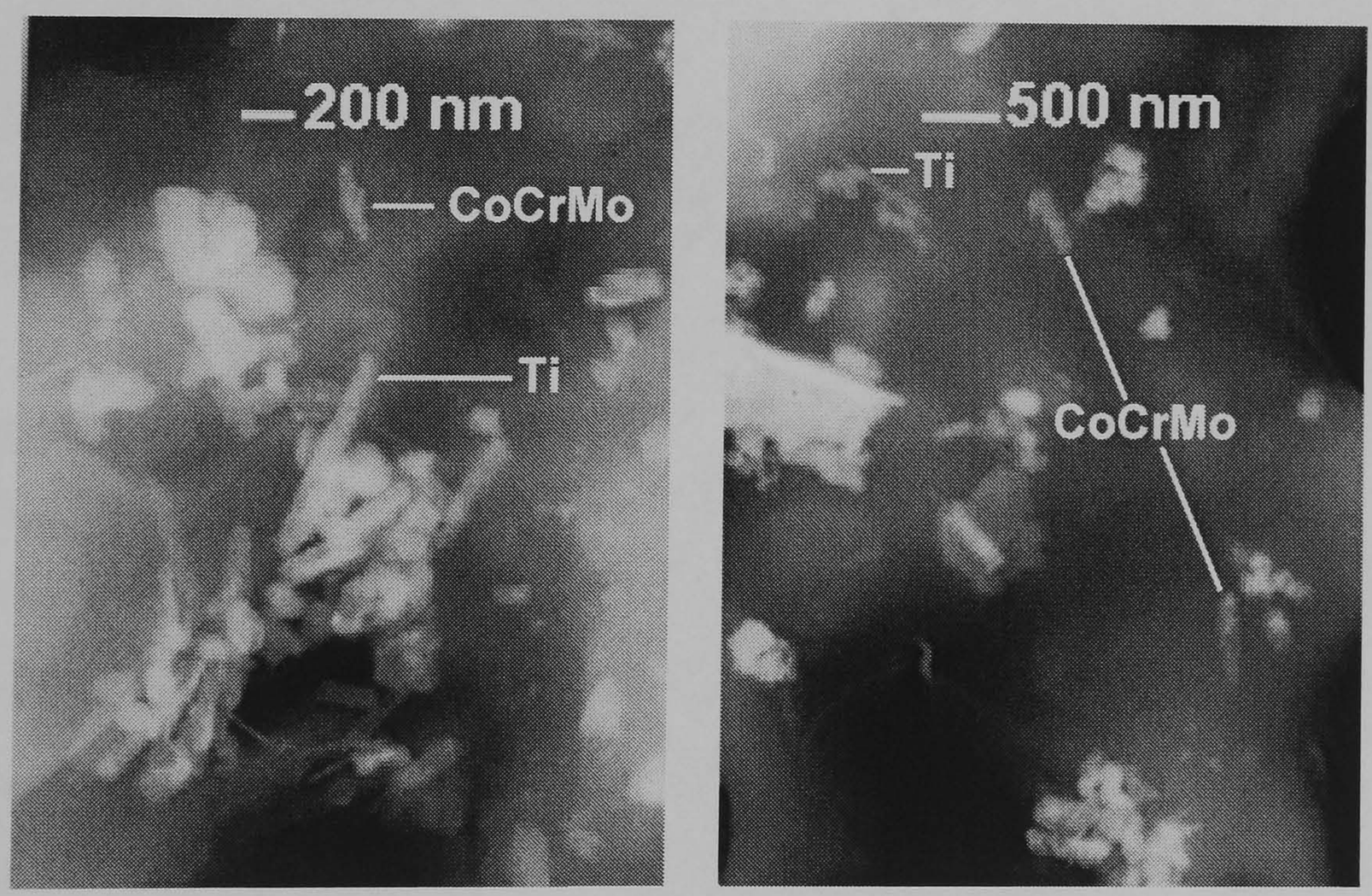


Figure 4.58: Example of agglomeration of various types of particles, images taken at × 20, 000 and × 10,000

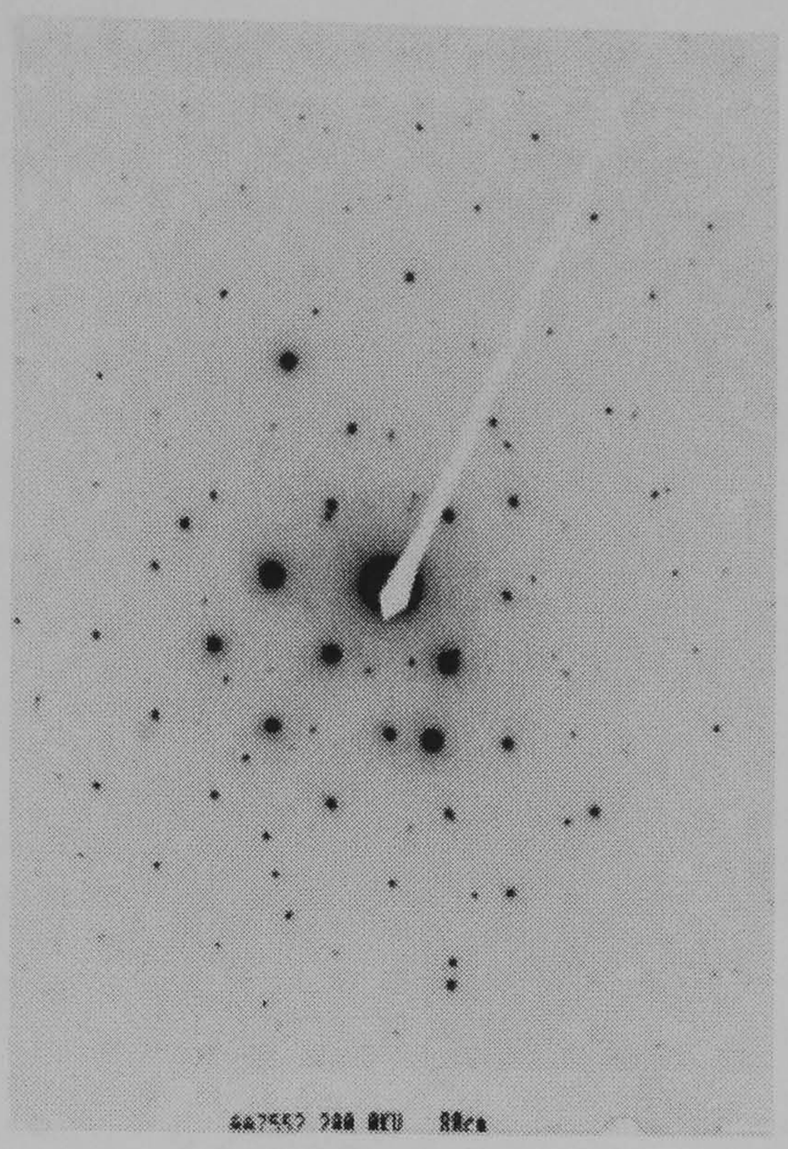

Figure 4.59: TEM image of a diffraction of a metal particle, showing the crystalline structure, this combined EDX analysis provides further evidence of the presence of metal particles

Table 4.6 (a): Summary of raw data collected from TEM image analysis, with the diameter presented in median values, mean values shown in brackets

| | **Walking with a 28 mm bearing** | **Walking with a 40 mm bearing** | **Walking with a 56 mm bearing** |
|---|---|---|---|
| | **Sample 1** | **Sample 2** | **Sample 3** |
| **Diameter (nm)** | 202 (234) | 81 (99) | 108 (133) |
| **Aspect Ratio** | 1.787 | 1.724 | 1.433 |
| **Perimeter** | 0.918 | 0.392 | 0.674 |
| **Roundness** | 2.013 | 1.678 | 2.912 |
| **Size (Length, nm)** | 313 | 135 | 201 |
| **Size (Width, nm)** | 208 | 89 | 134 |
| **Area ($\mu m^2$)** | 0.064 | 0.011 | 0.034 |
| **Number of particles analysed** | 185 | 314 | 138 |

Table 4.6 (b): Summary of raw data collected from TEM image analysis, with the diameter presented in median values, mean values shown in brackets

| | Jogging with a 28 mm bearing | Jogging with a 40 mm bearing | Jogging with a 56 mm bearing |
|---|---|---|---|
| | Sample 4 | Sample 5 | Sample 6 |
| **Diameter (nm)** | 98 (86) | 93 (132) | 85 (83) |
| **Aspect Ratio** | 2.35 | 1.416 | 2.27 |
| **Perimeter** | 0.477 | 0.491 | 0.431 |
| **Roundness** | 2.45 | 1.635 | 2.93 |
| **Size (Length, nm)** | 165 | 169 | 140 |
| **Size (Width, nm)** | 74 | 92 | 70 |
| **Area ($\mu m^2$)** | 0.010 | 0.029 | 0.074 |
| **Number of particles analysed** | 245 | 378 | 145 |

An initial examination of the data presented in Table 4.6 (b), shows that the 40 mm bearing following jogging produced the greatest number of particles for analysis. Despite the differences in particles size, the distribution of the wear particles were very similar, in that particles were found across the size groups. Figure 4.60 shows the distribution of particles generated by all bearings.

During jogging, the majority of particles were generated by the 28 mm bearing in the size group 10-250 nm, with the 56 mm bearing producing a similar distribution pattern, with no particles present in the larger particle size groups. Figure 4.60 to Figure 4.64 show the comparison of particles distribution for each bearing diameter between walking and jogging. All bearings under the two test conditions produced particles in the two smallest size groups

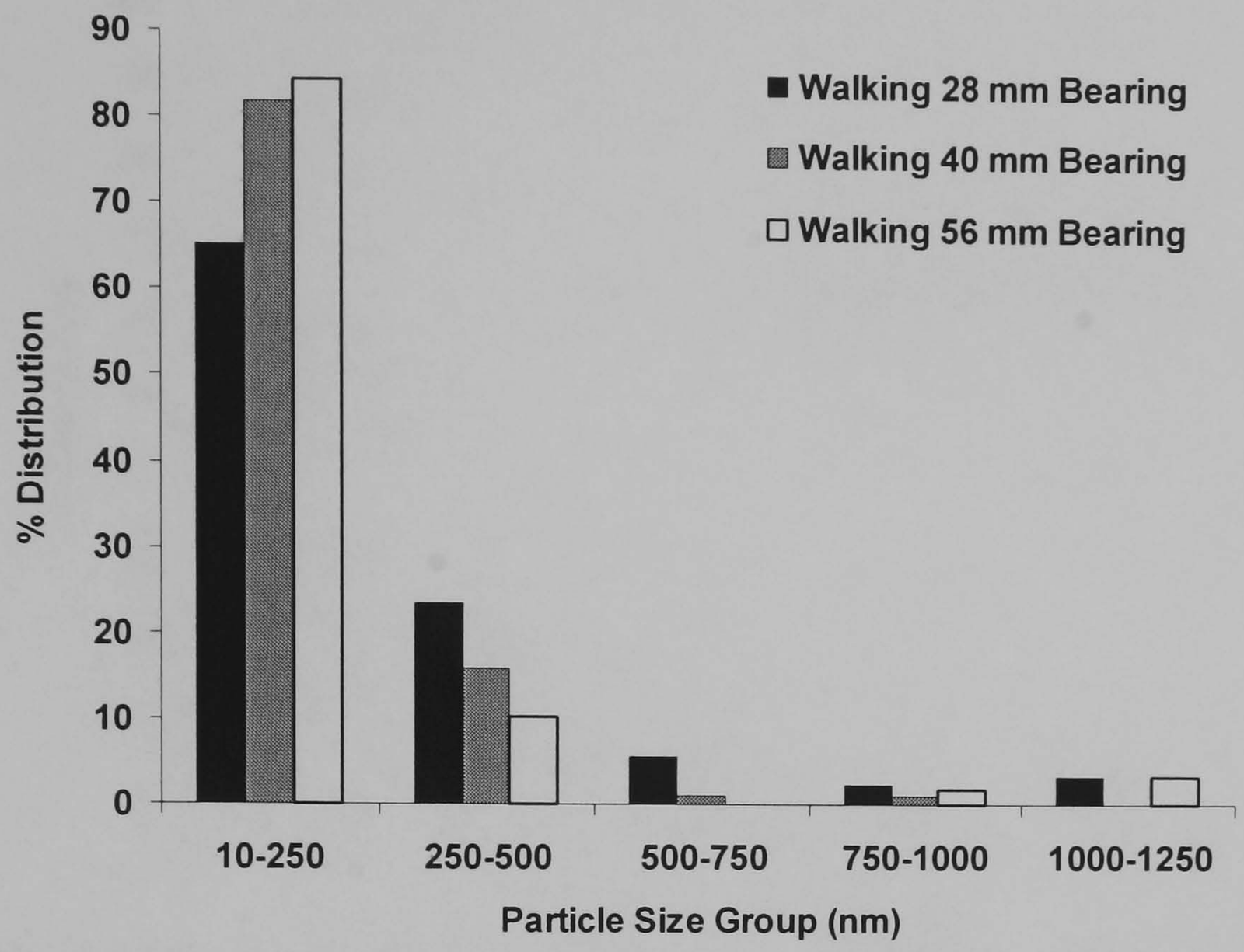


Figure 4.60: Wear particle distribution from all bearing diameters during steady state wear, showing that the majority of the wear particles were between 10 to 250 nm in size.

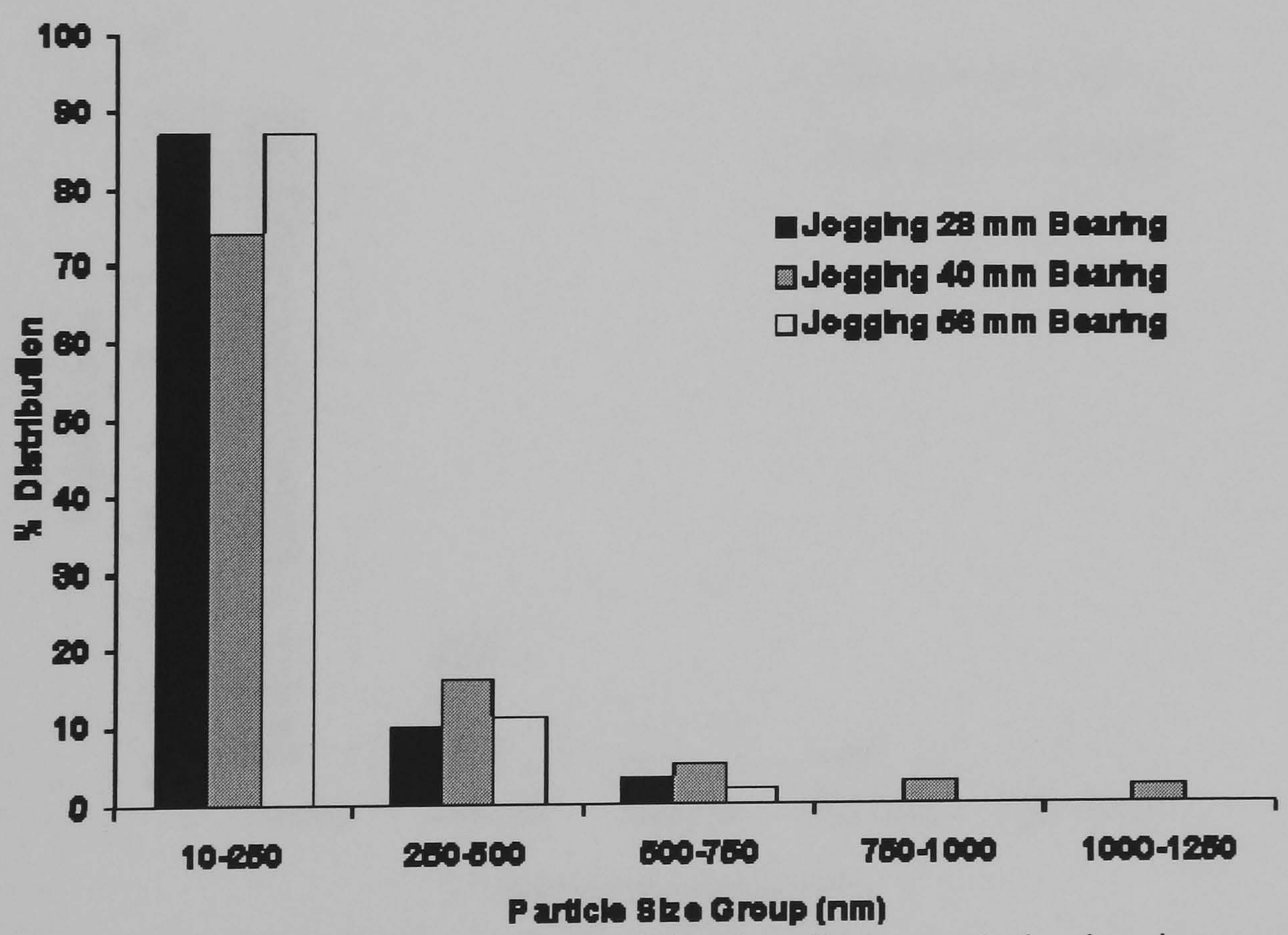


Figure 4.61: Wear particle distribution from all bearing diameters during jogging

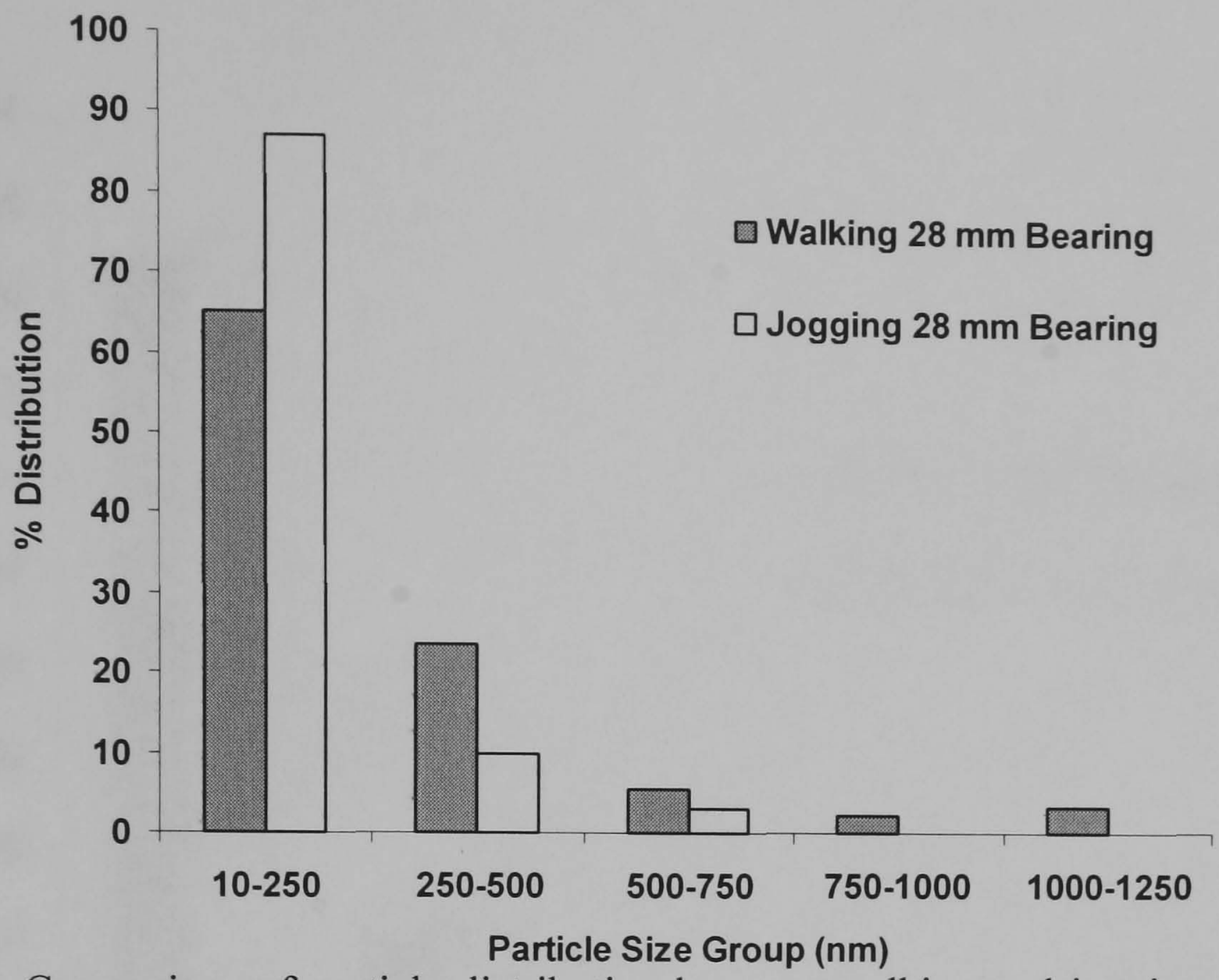


Figure 4.62: Comparison of particle distribution between walking and jogging for the 28 mm bearing

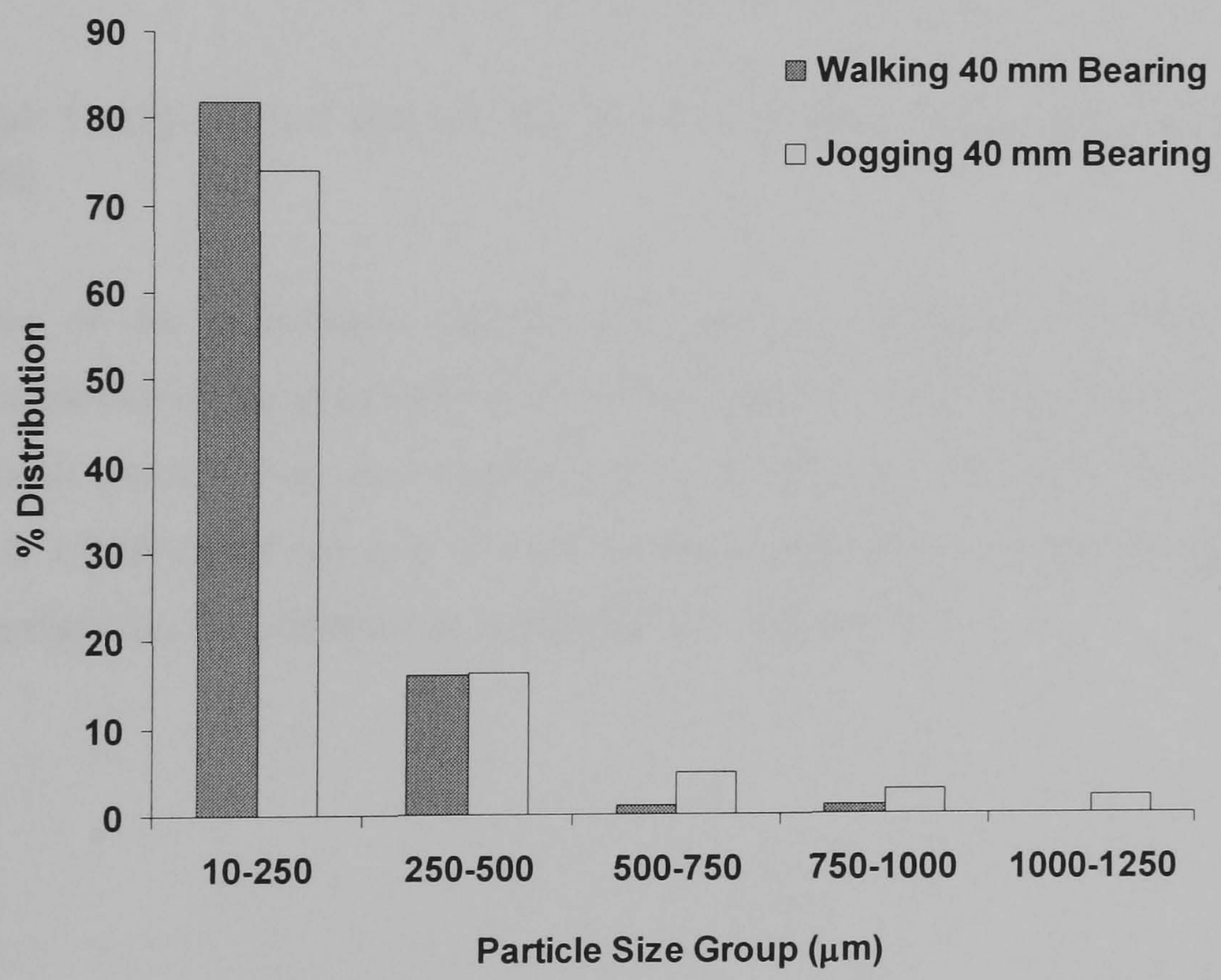


Figure 4.63: Comparison of particle distribution between walking and jogging for the 40 mm bearing

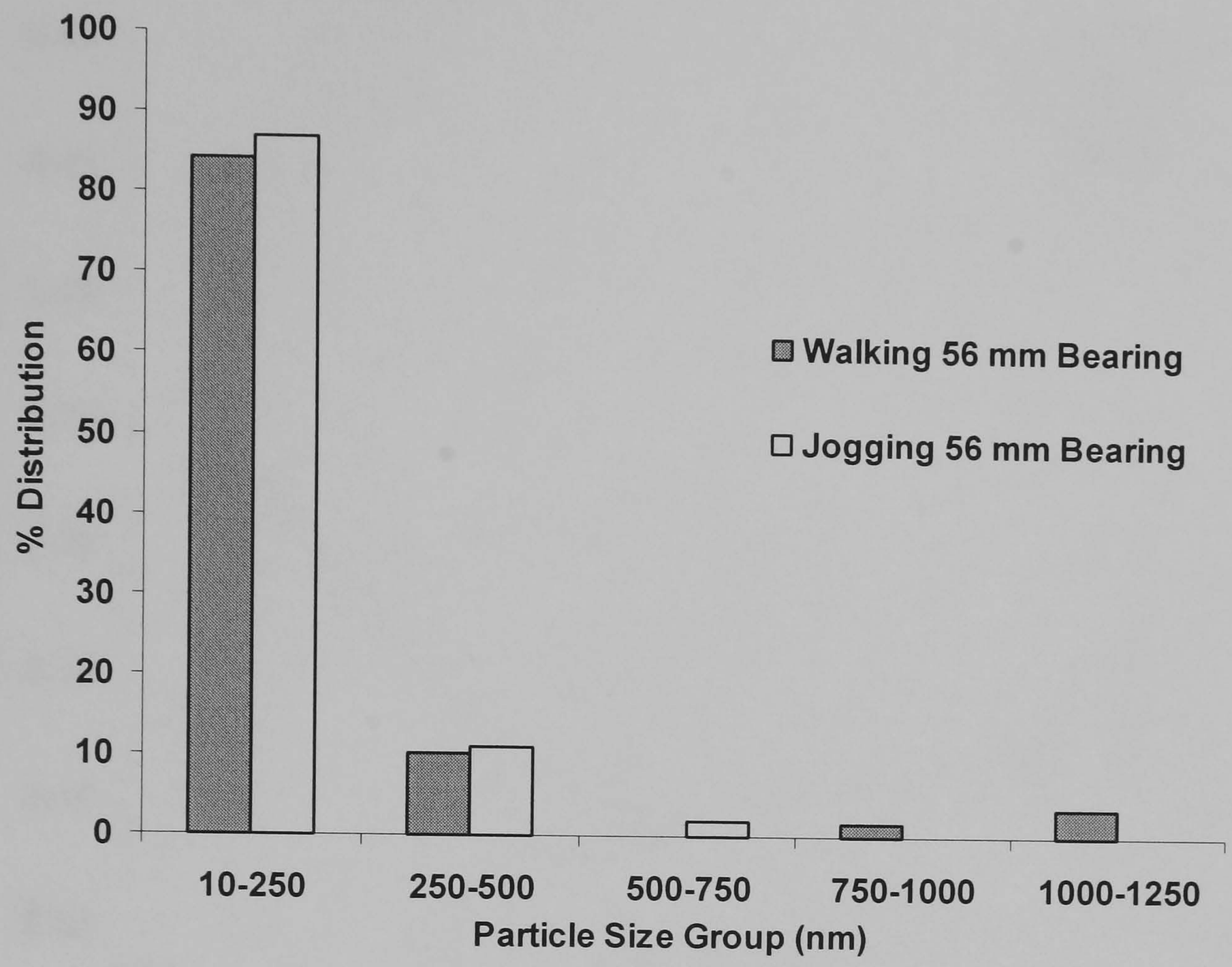


Figure 4.64: Comparison of particle distribution between walking and jogging for the 56 mm bearing

Comparison of the measured parameters of particles, obtained following steady state walking, in particular the parameter of diameter, shows that there are small but significant differences in particle size for samples analysed following walking tests for all three bearings. A visual comparison of the parameters in the form of a graph will provide an effective insight into the differences in particle size, Figure 4.65.

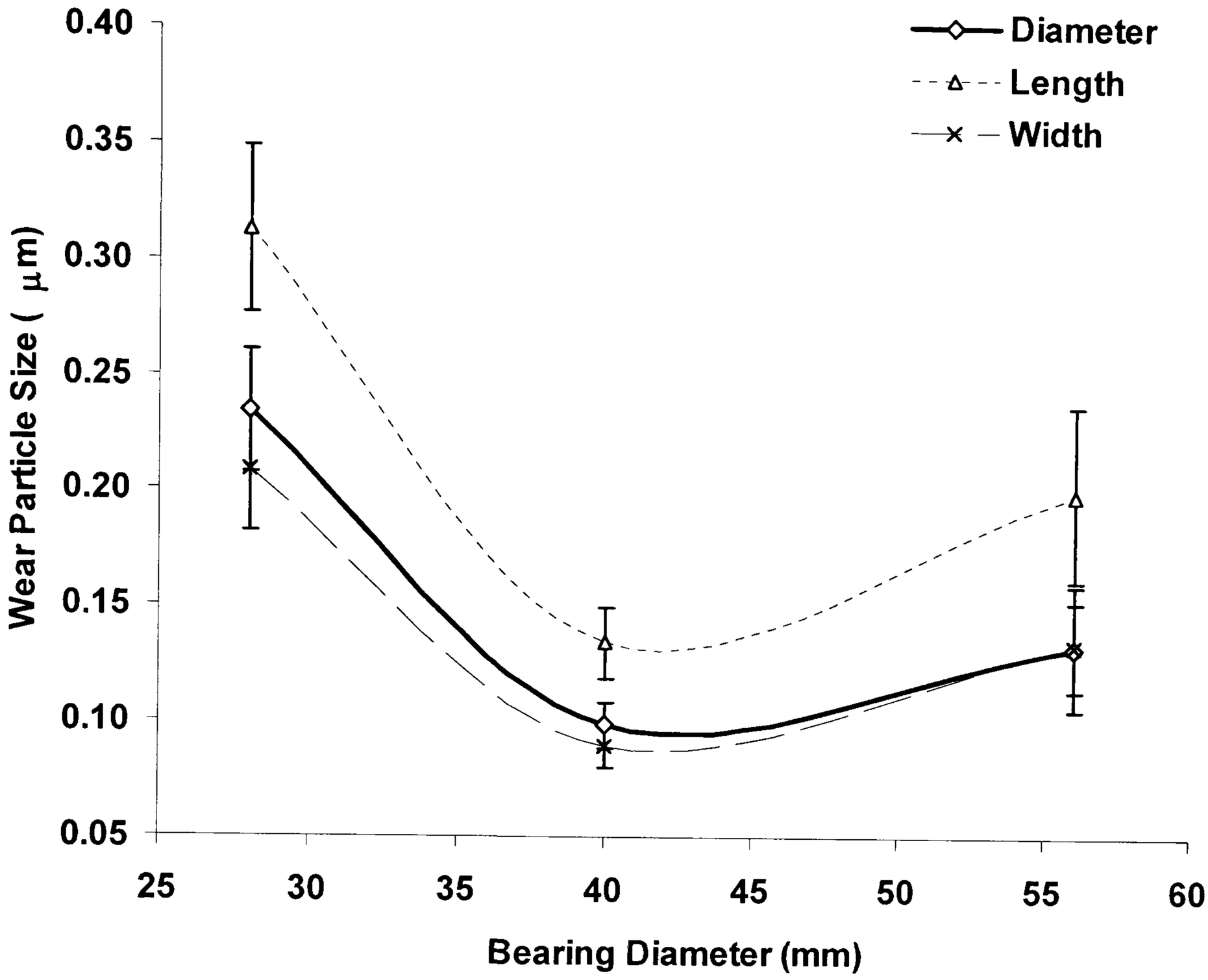


Figure 4.65: Change in CoCrMo wear particles during steady-state standard normal walking tests, showing the variation of mean wear particle size plotted against bearing diameter, length and width, showing smallest particle size produced by the 40 mm bearing. All dimensions presented in µm, error bars represent 95 % Confidence Limits

The largest wear particles were produced during walking with a 28 mm bearing, generating a mean particle size of 234 ± 13 nm (range 51-1178 nm), a statistically significant difference ($p<0.01$) in particle size when compared to particles produced by the 40 and 56 mm bearing. There was also a small but statistically significant difference between the mean particle size for the 40 mm bearing versus the 56 mm bearing at $p<0.01$, the 40 mm bearing produced particles with a mean size of 99 ± 5 nm (range 10-914 nm) whereas with the 56 mm diameter femoral head a mean particle size of 133 ± 14 nm (range 13-1145 nm) was observed.

However there are differences in the larger particle size groupings, for example no particles from the 56 mm bearing were observed between 500 to 750 nm, whilst no particles between 1000 to 1250 nm from the 40 mm bearing were seen. The distribution would suggest that the intermediate size (40 mm bearing) would not produce particles greater than 1 μm, however this does not apply to the 28 and 56 mm bearings, which have produced particles in all particle size groups.

During simulated jogging, the largest wear particles were produced by the 28 mm bearing, reflected in the results observed during walking, followed by the 40 mm bearing, the 56 mm bearing produced the smallest wear particles, this was true for all dimensions, the changes in mean particle dimension are presented in Figure 4.66.

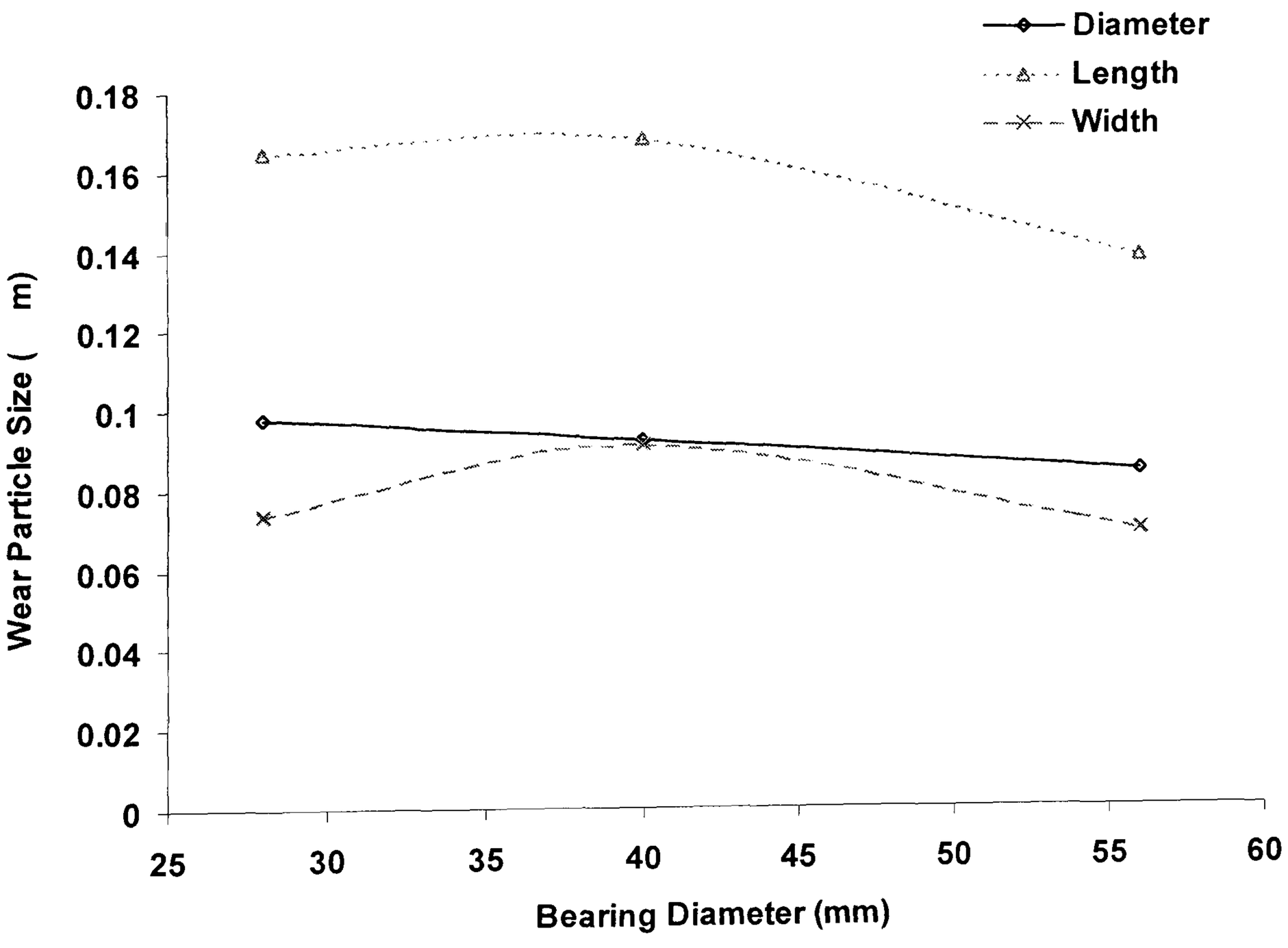


Figure 4.66: Change in CoCrMo wear particles during simulated jogging tests, showing the change in mean wear particle sizes due to simulated fast jogging.

An indicator of why the changes in particle size are occurring would be to see if any changes are occurring in the Aspect Ratio (AR) of the particles, as this ratio is dependent upon the length and width, which in turn would affect the morphology of the particles. Furthermore when there is an increase or decrease in length or width, there will be a subsequent change in Roundness, in that particles would become more oval or round in shape. Figure 4.67 shows the changes occurring in both the Roundness and AR of the particles. For the 40 mm bearing, Roundness and AR show a close relationship, however the 28 mm bearing shows a difference, with the 56 mm bearing showing a significant difference in the relationship between the roundness and AR.

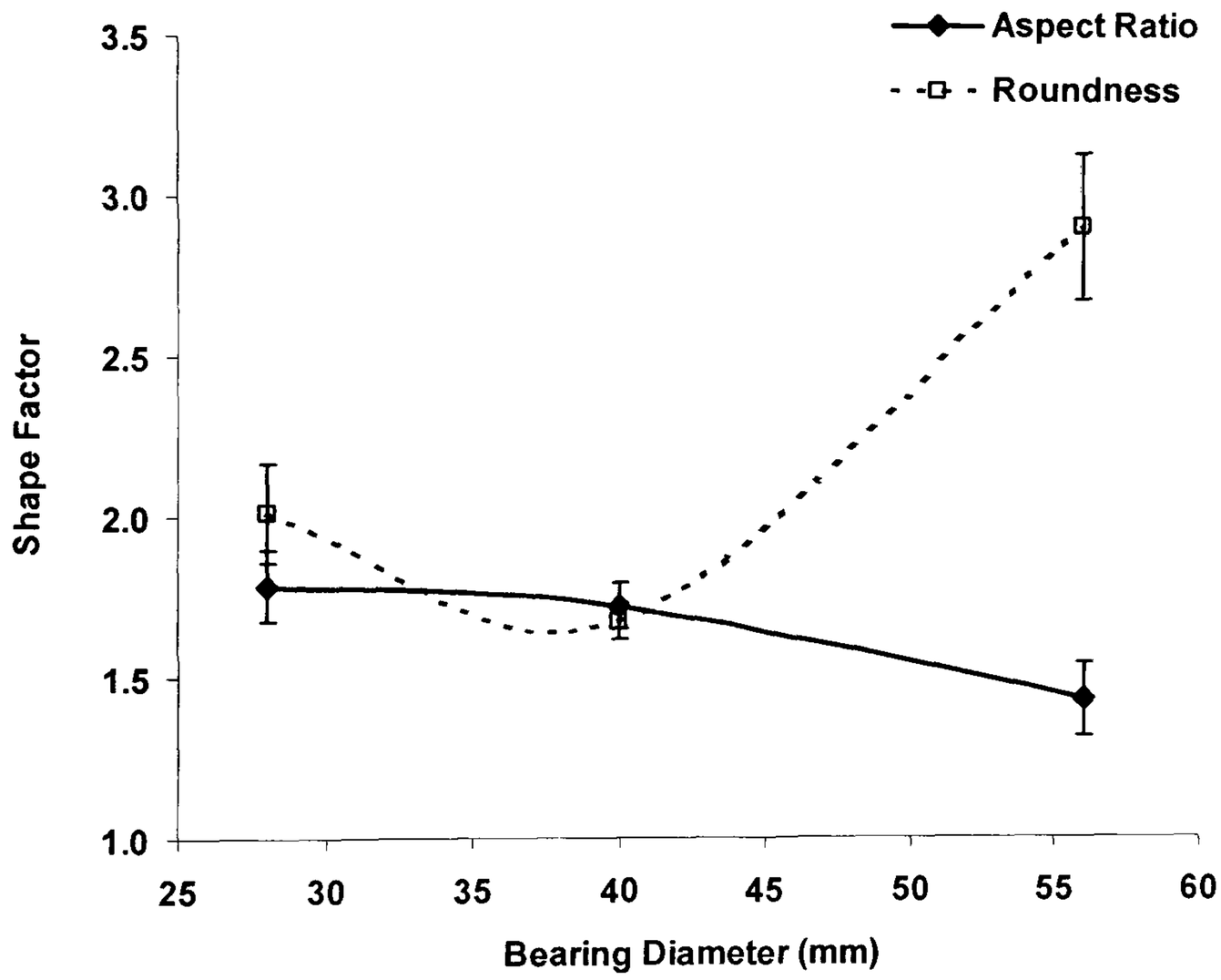


Figure 4.67: Changes in particle shape represented by the Aspect Ratio (AR) and Roundness (R) plotted against bearing diameter. Showing a decrease in AR with increasing bearing diameter, however R, shows a decrease from the 28 mm bearing to the 40 mm bearing, although R subsequently shows an increase with a 56 mm bearing. Error bars represent 95 % Confidence Limits

AR and R parameters also indicate whether a particle would be classified as round or oval particles, from the data present in Figure 4.67, the vast majority of the particles would be classified as oval in shape rather than spherical.

With regards to the roundness, all bearings show significant statistical differences, whilst the AR shows small but significant differences. This ties in with the wear particle distributions shown in Figure 4.60, where the 28 and 56 mm bearings generated particles in the 1 μm particle grouping. This would imply that the particles generated by the 40 mm bearing would tend to be more rounded in shape than the 28 or 56 mm bearing which would produce more oval shaped particles. Changes in morphology and size would ultimately be the determining factors in terms of the total accumulated surface areas that can be generated. Size as well as the number of particle are crucial parameters when determining the potential ion release that may occur following activity. If the particles generated are small in size, then ion release will be small, however if the number of particles increase, with no change in particle size then the accumulated surface area will subsequently show an increase in turn increasing the levels of ion release. A plot of length versus elongation shows the majority of particles produced by the three different bearing sizes lay within the 500 nm range with a modal elongation between 1 to 2, indicating that the majority of particles are spherical in shape, shown in Figure 4.68.

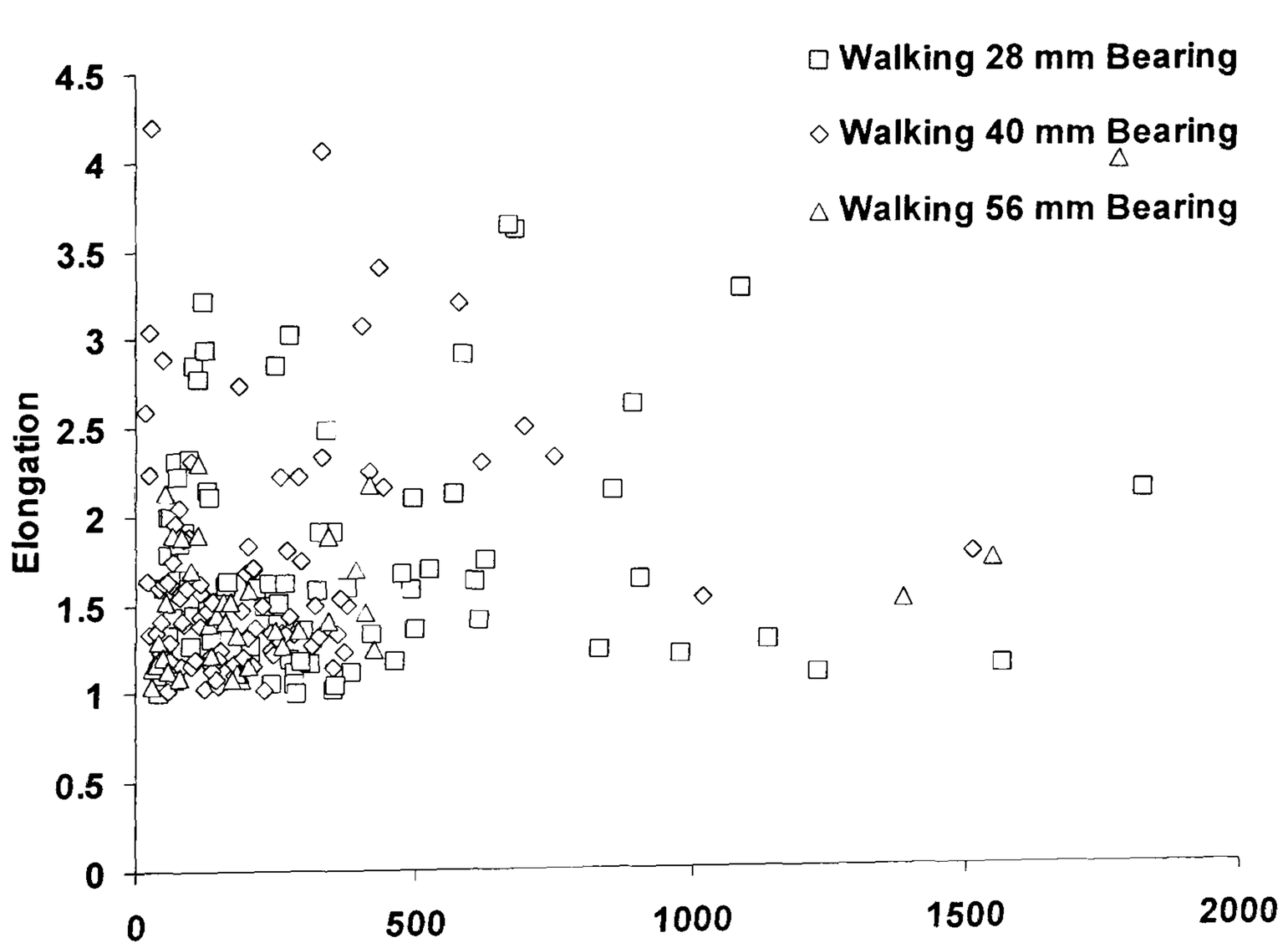


Figure 4.68: A scatter plot of Elongation versus Length for all bearing diameters, showing that the majority of particles are within a 500 nm range.

Figure 4.69 shows that jogging with a 28 mm bearing would produce only particles in the 500 nm range, whereas walking shows wide range of particle size, indicating that jogging with a 28 mm bearing would have the potential to release more ions than jogging. This result suggests that for an active patient the 28 mm bearing may not be the most suitable size.

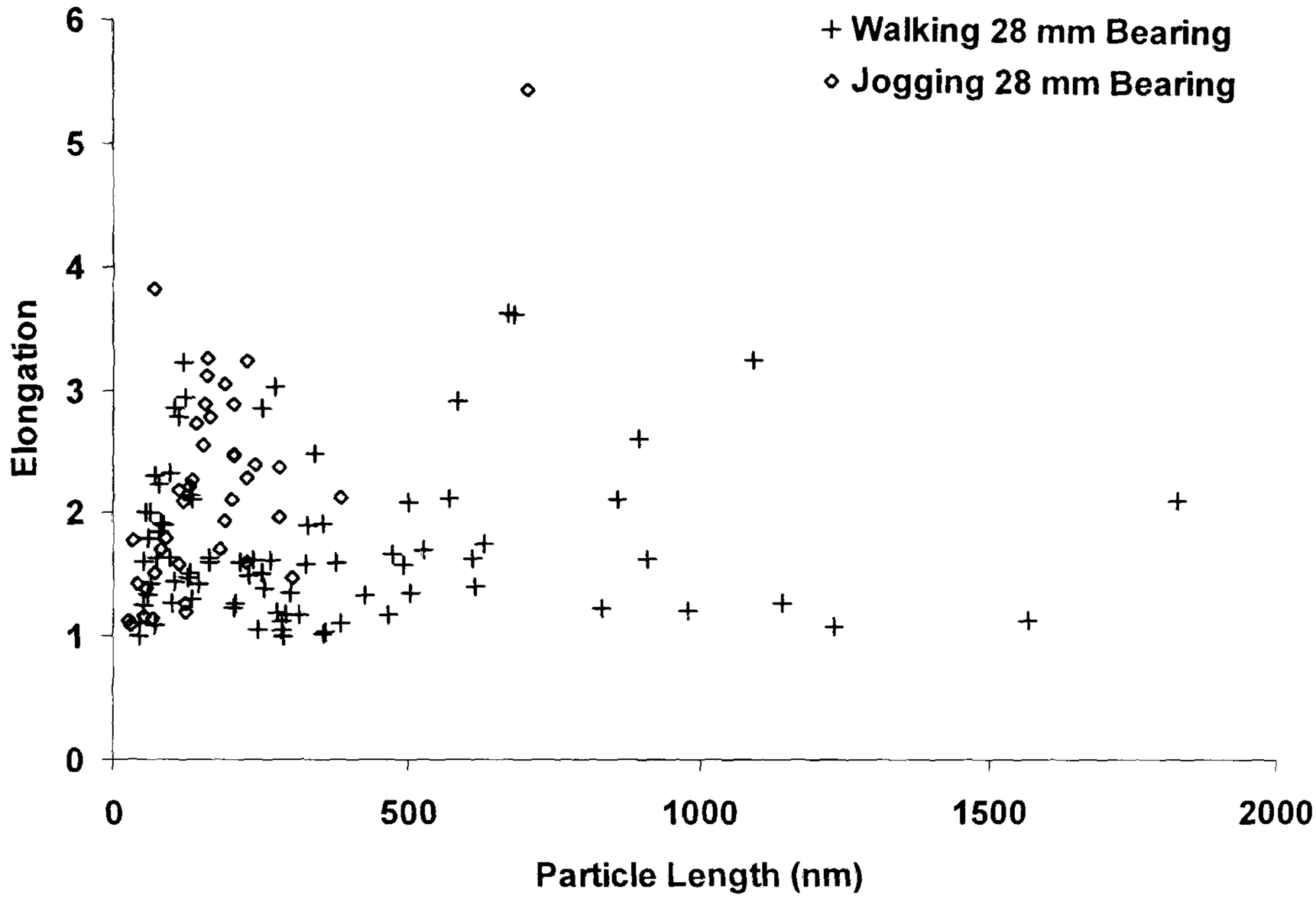


Figure 4.69: A scatter plot of Elongation versus Length for the 28 mm bearing diameters, showing that the majority of particles within a 500 nm range, with walking showing particles of greater length

However when comparing walking with jogging for the 40 mm bearing, there is clear indication that increased activity serves to change particle morphology, i.e. with increased activity there is a subsequent increase in particle length, which in turn would increase particle surface area and therefore increase ion release, shown Figure 4.70. The 56 mm bearing however produced a similar result to that of the 28 mm bearing, showing that the majority of the particles from walking and jogging to be less than 500 nm in size, however it produced fewer particles, which would in turn produce a low accumulated surface area, thereby minimising potential ion release, Figure 4.71.

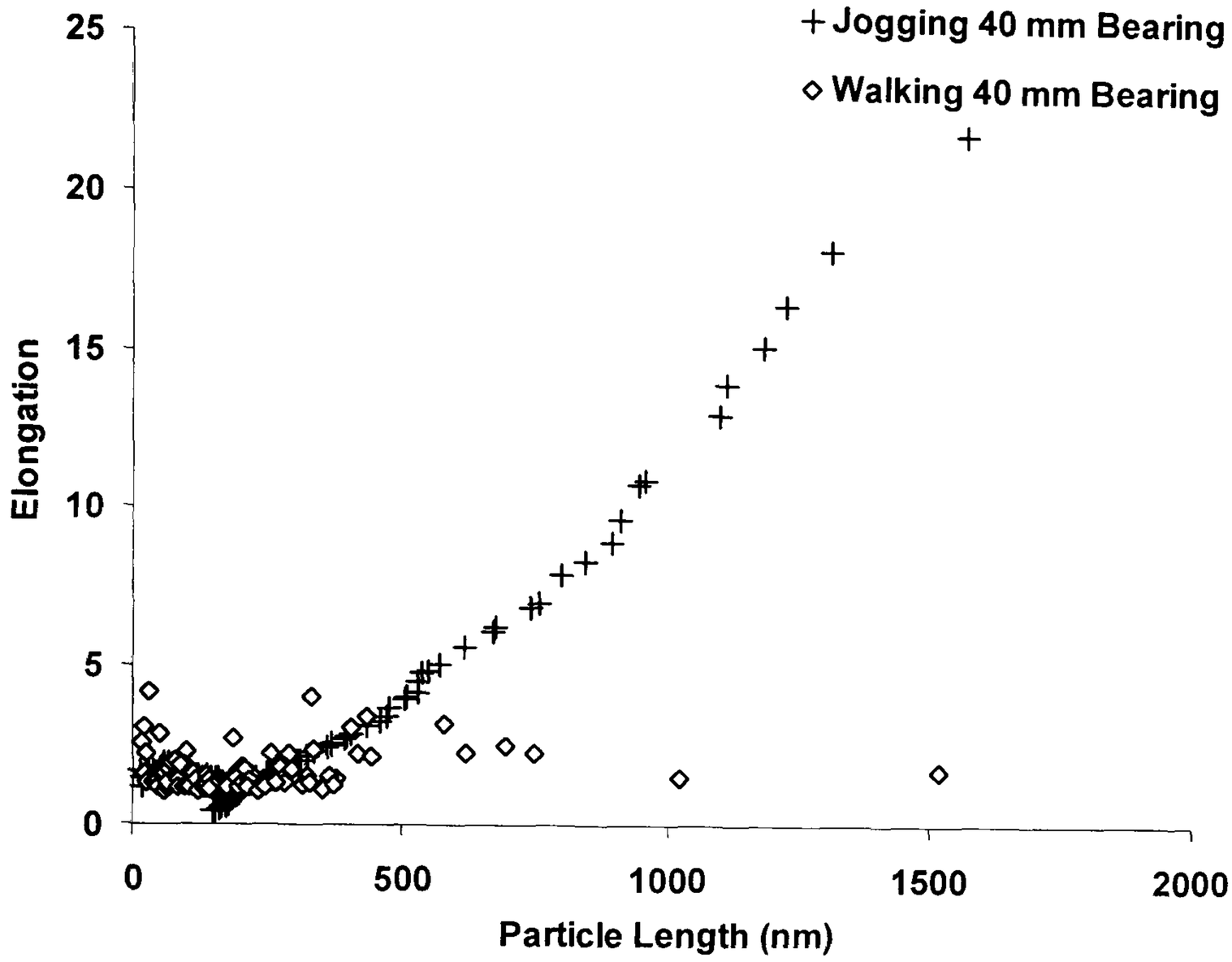


Figure 4.70: Comparison of length versus elongation for walking and jogging with a 40 mm bearing, showing an increase in length with increased activity

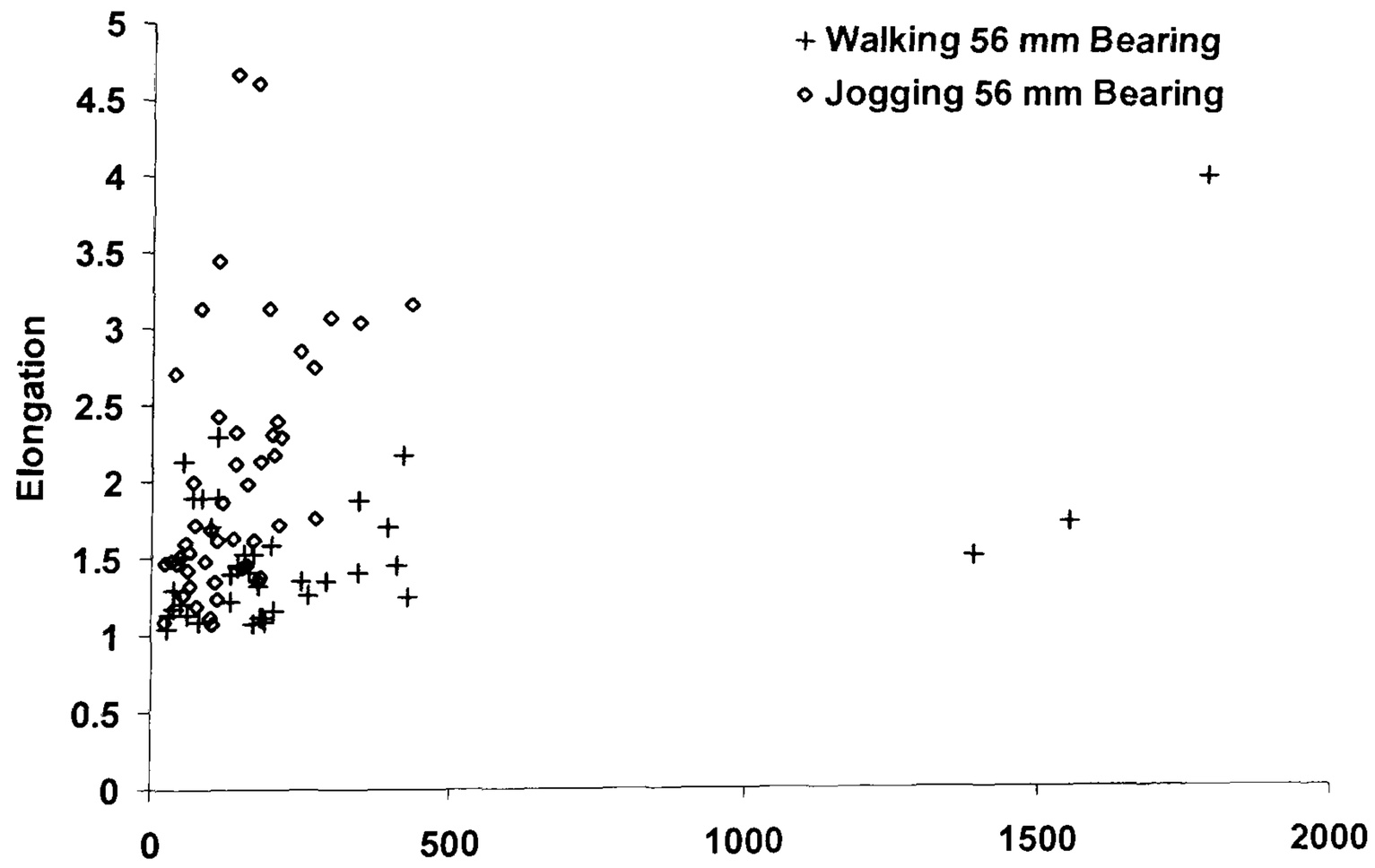


Figure 4.71: A scatter plot of Elongation versus Length for the 56 mm bearing diameters, showing that the majority of particles within a 500 nm range, with some particles from the walking test of greater length.

When considering the median size of particles, all samples indicated that the majority of the particles tended to be smaller than the mean particle size. Wear particle distribution for all bearings indicate that the majority of the particles produced during testing, whether walking or jogging are less than 250 nm in size.

# Chapter 5 Discussion

The development of an appropriate, clinically relevant test for the evaluation of total hip replacements is important as designs and materials used are improved and lifetime expectations rise compounded by the need for hip replacements that can perform under adverse conditions such as increased activity. There is currently debate as to whether wear tests can predict the clinical outcome of a total hip replacement in the long term as it recognised that *in vitro* tests in general produce lower wear rates compared to *in vivo* examinations of retrieved hip replacement components. There are a number of factors, which must be considered when evaluating the performance of THRs. These include the wear rate and wear factor, the nature of particles generated in the tests, the bearing surface parameters and the load parameters. Tests that reduce the simulation time are valuable for the rapid evaluation of novel designs, however the acceleration of tests has to be carefully evaluated in order to ensure that *in vitro* tests have clinical relevance. In the current study two bearing material combinations were evaluated, namely CoCrMo on moderately crosslinked polyethylene (5 MRads) and CoCrMo on CoCrMo. These studies were focused on the evaluation and effects of surface parameters for CoCrMo on polyethylene, and bearing diameter for CoCrMo on CoCrMo combined with increased activity and how these parameters affected the wear rate and its effect upon the particles generated during wear tests.

## 5.1 Wear of crosslinked polyethylene

In the current study, the wear of crosslinked polyethylene using a hip simulator was influenced by the area of surface roughness of the femoral head combined with increased patient activity. Under increased patient activity, such as jogging, and a virgin smooth femoral head surface, the wear rate was slightly raised. However when introducing small areas of damage combined with increased activity, the wear rate increased with increasing areas of surface damage. The present study indicated that there maybe a threshold point at which the size of the damaged area becomes a more influential factor on the wear and the generation of biologically active particles of moderately crosslinked polyethylene.

The results observed during this investigation are in good agreement with Elfick *et al* (2001) and many previous hip simulator studies (Wroblewski *et al*, 1996) who have observed similar trends, showing a biphasic wear pattern during the initial 1 to 1.5 million cycles of testing, which then decreases during steady state wear.

The CoCrMo femoral heads also produced twice the wear rate when compared to the Zirconia femoral head for walking as well as jogging, under smooth femoral head conditions. This is also in good agreement with a previous study by McKellop (1992) who reported wear rates for metal heads that were twice as high when compared to tests using ceramic heads. Hence, for active patients, using more damage resistant components, such as Zirconia femoral heads combined with UHMWPE cups, could increase implants survival time, in terms of low volumetric wear.

The wear rates generated during walking under smooth conditions are similar to previous investigations, using similar hip simulators (Wang, 1996, McKellop *et al*, 1999, Endo *et al*, 2002). Results from the present study indicate that there is a significant improvement in the resistance to wear of moderately crosslinked PE compared to non-crosslinked PE. The study by McKellop (1999) showed that crosslinked PE produced less wear compared to non-crosslinked PE, figure 5.1. Crosslinked PE produced a wear volume of 50 $mm^3$ after 10 million cycles (5 $mm^3/10^6$ cycles) as compared to non-crosslinked PE which produced a wear volume of 350 $mm^3$ (35 $mm^3/10^6$ cycles) during the same period, showing a 7 fold decrease in wear volume, a significant improvement in wear resistance. In the current study a wear volume of 260 $mm^3$ would have occurred after 10 million cycles or normal walking, however the extent crosslinking is also important parameter, in the current study the cups were only moderately crosslinked at 5 MRads.

A recent review of non-crosslinked and crosslinked PE by Schmalzried *et al* (2003) showed that patients treated with non-crosslinked PE had a mean volumetric wear rate of 88 ± 79 $mm^3$/year, whereas patients treated with crosslinked PE had a mean volumetric wear rate of 21 ± 23 $mm^3$/year, a statistically significant difference ($p = 0.0001$). Although the absolute values of wear are smaller in hip simulators compared to clinical studies, the reduction in

wear volume observed by McKellop and Schmalzried *et al*, 86 % and 79 % respectively, showing good agreement between the *in vitro* and *in vivo* studies. The relationship comparing different levels of crosslinking have shown that there is a link between increased radiation dose and reduction in wear

## 5.2 Influence of activity and surface topography

During simulated fast jogging, CoCrMo heads under smooth femoral head conditions only showed a 2-fold increase in wear when compared to walking, this despite the increase in both the load and sliding velocity.

Previous studies conducted under rough conditions using pin-on-disc machines have shown a 30-fold increase in wear (Dowson *et al*, 1985, Fisher *et al*, 2000), the wear rates observed in the current study showed significantly less wear than standard pin-on-disc machines. However results in the current study are in line with previous hip simulator studies (Wang et al, 1998, McKellop et al, 1999, Barbour et al, 2000), which show that less wear is generated during hip simulator tests than during tests with pin-on-disc machines, due to the multi-directional motion that is experienced by PE cups, compared to the uni-directional motion of pin-on-disc machines.

The current study has shown that wear shows a slight increase with increased activity, under smooth conditions. With the introduction of small areas of damage, and an increased $R_a$ of 0.39 μm, only small changes in wear were observed. Normal walking tests with an area of damage covering 20 $mm^2$ (5 mm diameter) only produced a 2-fold increase in wear, when compared to wear under smooth conditions. The results generated in the current study are in line with results published by Bowsher & Shelton (2001), who showed slight increases in wear with increased activity under smooth femoral head conditions. However, jogging under small roughened areas produced a similar result to that of jogging under smooth conditions, despite the fact that the maximum $R_p$ was triple that of the maximum $R_p$ under smooth conditions. This may be due to the surface changes that occurred during jogging, which showed evidence of self-polishing following tests under increased activity ( Figure 4.46)

Increasing the size of the damaged area to 80 $mm^2$ (10 mm diameter) did produce an increase in wear for both walking and jogging, again a 2-fold increase, at 176 $mm^2$ (15 mm diameter), wear showed a significant increase. This may be an indication that suggests there is link between increased roughness leading to increased wear, however this is only apparent once a critical area of roughness is achieved (figure 4.22). The increases in wear observed for small areas of damage are small in comparison to that of wear generated during walking and jogging with a fully roughened head, showing 13 and 20 fold increases for walking and jogging respectively. These results would therefore suggest that the size of the damaged area combined with increased activity could influence the level of wear experienced by PE cups. The wear rates generated during normal walking and simulated jogging with small areas of damage, are also lower than wear rates reported in clinical studies (Kabo et al, 1993, Bankston et al, 1995, Jasty et al, 1997).

The results therefore suggest that with increasing areas of roughness, abrasive wear mechanisms combined with fatigue failure play a significant role in the production of submicron sized particles as a result of increased activity. Increased activity would have the effect of breaking down large particles due to increased load and the frequency at which this load is applied (Bowsher & Shelton, 2001). With the area of roughness increased to cover the entire upper hemisphere of the femoral head, no particles greater than 10 μm were generated, with a volume distribution showing a average modal particle size of 1 μm for tests under simulated jogging, tests under simulated walking produced an average modal particle size of 3 μm.

The roughening of the femoral head served to change the morphology and number of particles produced during this stage of testing. Volume distributions of particles retrieved from tests under rough femoral head conditions indicated that the modal particle size was on the whole smaller than particles from tests under smooth conditions. SEM examination indicated that in general these particles tended to have a spherical shape. This is in agreement with a study by McKellop *et al* (1995), reporting that sub-micron particles are more spherical in shape.

Jogging and walking tests under a roughened area of 20 $mm^2$ produced very similar results in terms of number distributions to that of walking under the same roughened area. However the volume distributions indicate that the greatest proportion of the volume for walking tests is composed of particles with a modal size of 2 μm, ranging from 0.09 to 15 μm, whereas under jogging we see a polymodal distribution with an average modal particle size of 20 μm, with particle size ranging from 0.08 to 300 μm. With damage increased to an area of 80 $mm^2$, the number distributions again produce very similar results, both walking and jogging indicating that the greatest number of particles lying within the range of 0.1 to 1 μm. However the volume distributions show that jogging delivers that greatest concentration of bioactive particles, as the majority of particles are less than 10 μm in size.

These results suggest that abrasive wear mechanisms play a more prominent role in the production of biologically active particles rather than activity. Hence, increased activity is possible, however once the femoral head experiences damage that is greater than an area of 80 $mm^2$, implant life may be limited for younger more active patients with PE based sockets. At this stage the joint is only producing bioactive particles in large concentrations which would elicit a macrophage response resulting in osteolysis and eventual aseptic loosening. The current study has also shown that there is a threshold point at which the size of the damaged area becomes a more influential factor on the wear and the generation of biologically active particles of crosslinked PE (Figure 5.1)

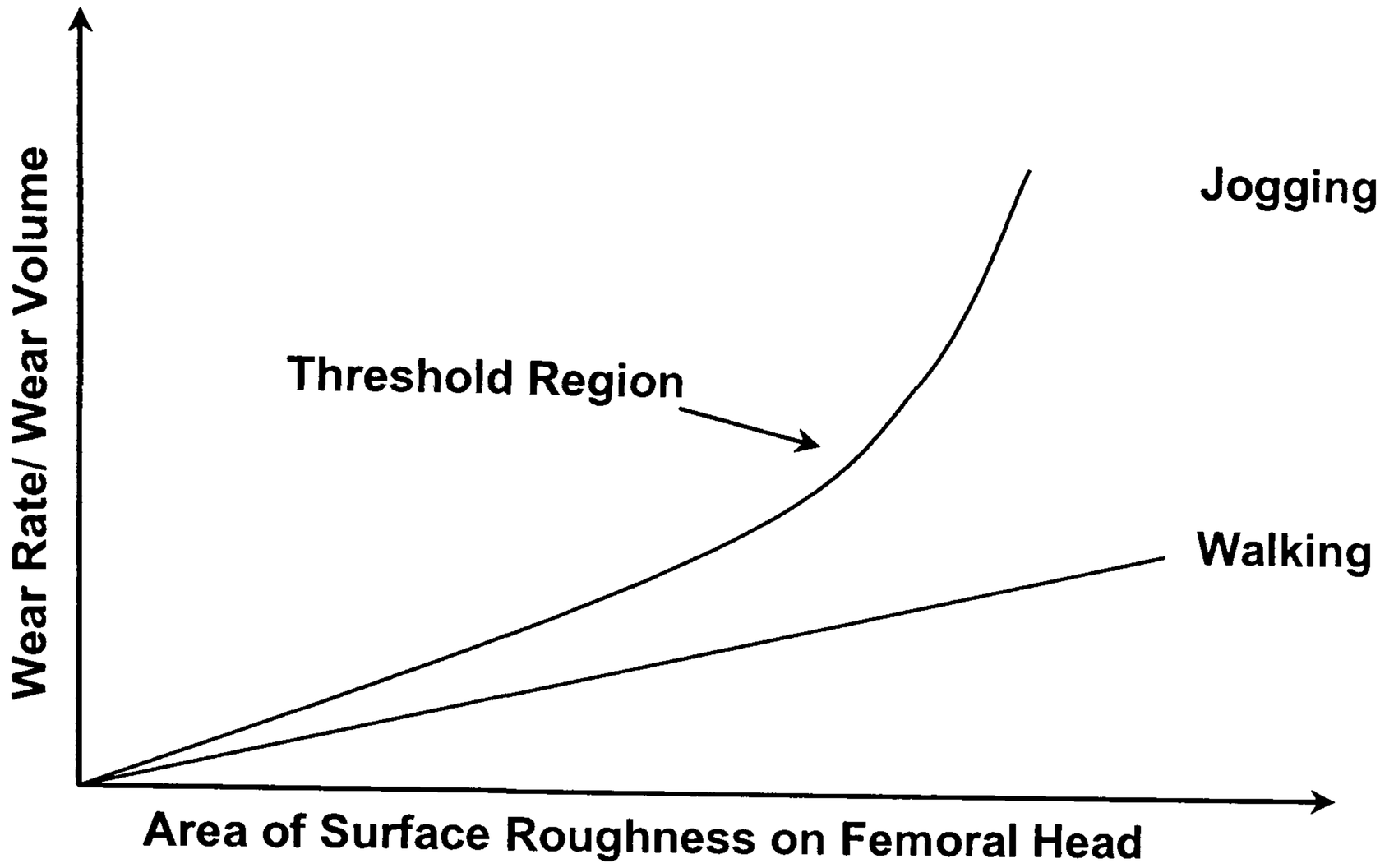


Figure 5.1 Relationship between wear and increasing area of femoral head surface damage, wear under walking continues on a linear path, however wear under jogging, produces an increase in wear with increasing area of surface roughness.

Under small areas of damage, surface roughness had little influence upon the long term wear of the PE. Small changes in surface topography were observed during jogging tests, with a reduction in surface $R_a$ from 0.4 μm to 0.28 μm and 0.34 μm, for 20 $mm^2$ and 80 $mm^2$ areas of damage respectively. The fully roughened head also showed a reduction in the $R_a$ during the course of a test, indicating that some self-polishing had occurred. The decrease in surface roughness is reflected in the reduction in wear experienced by the fully roughened head following initial jogging tests. From these results it would seem that significant changes in surface topography tend to occur over short periods of high activity.

The current study also looked at the effect of applying discrete scratches to the femoral head followed by walking and jogging tests (Barbour *et al*, 2000, Endo *et al*, 2000). Walking under a scratch of 5 mm length produced higher wear rate (32 $mm^3/10^6$ cycles) as compared to jogging, which was approximately half that of walking (15 $mm^3/10^6$ cycles). However an increase in scratch length to 10 mm and scratches covering the entire upper hemisphere served to change this view, with jogging producing the highest wear rate in

both test conditions. Walking and jogging under a 10 mm scratch produced wear rates of 22 and 39 $mm^3/10^6$ cycles respectively. Walking and jogging under scratches covering the entire hemisphere produced wear rates of 33 and 73 $mm^3/10^6$ cycles respectively. Producing a similar pattern of wear as to that of wear under small areas of roughness.

The wear rate was always higher for jogging than walking, jogging under discrete scratches showed 2-fold increases in wear compared to walking. The advantage with applying discrete scratches to the femoral head and studying the wear rate is that both factors can be quantified and a relationship between wear and damage can be more easily established.

These results would therefore imply that the test methods can produce higher rates of wear, although the rough patch is possibly more representative of *in vivo* conditions. However, whilst the application of discrete scratches may be positive in terms of quantifying wear and surface damage, it may not be the case in terms of particle size and morphology, where surface damage would play a more important role. Therefore the application of a roughened area may produce more physiologically relevant particles in size and morphology. A comparison of the wear rates observed during tests under rough patches and discrete scratches for walking and jogging show that walking with 10 mm of damage produces a significant difference in wear, this is also true for jogging with 5 mm of damage, showing almost 2-fold differences for both types of damage between the two types of activities. With damage covering the entire femoral head (discrete scratch as well rough patch) there is even greater difference, with the rough patch showing significantly greater for walking and jogging.

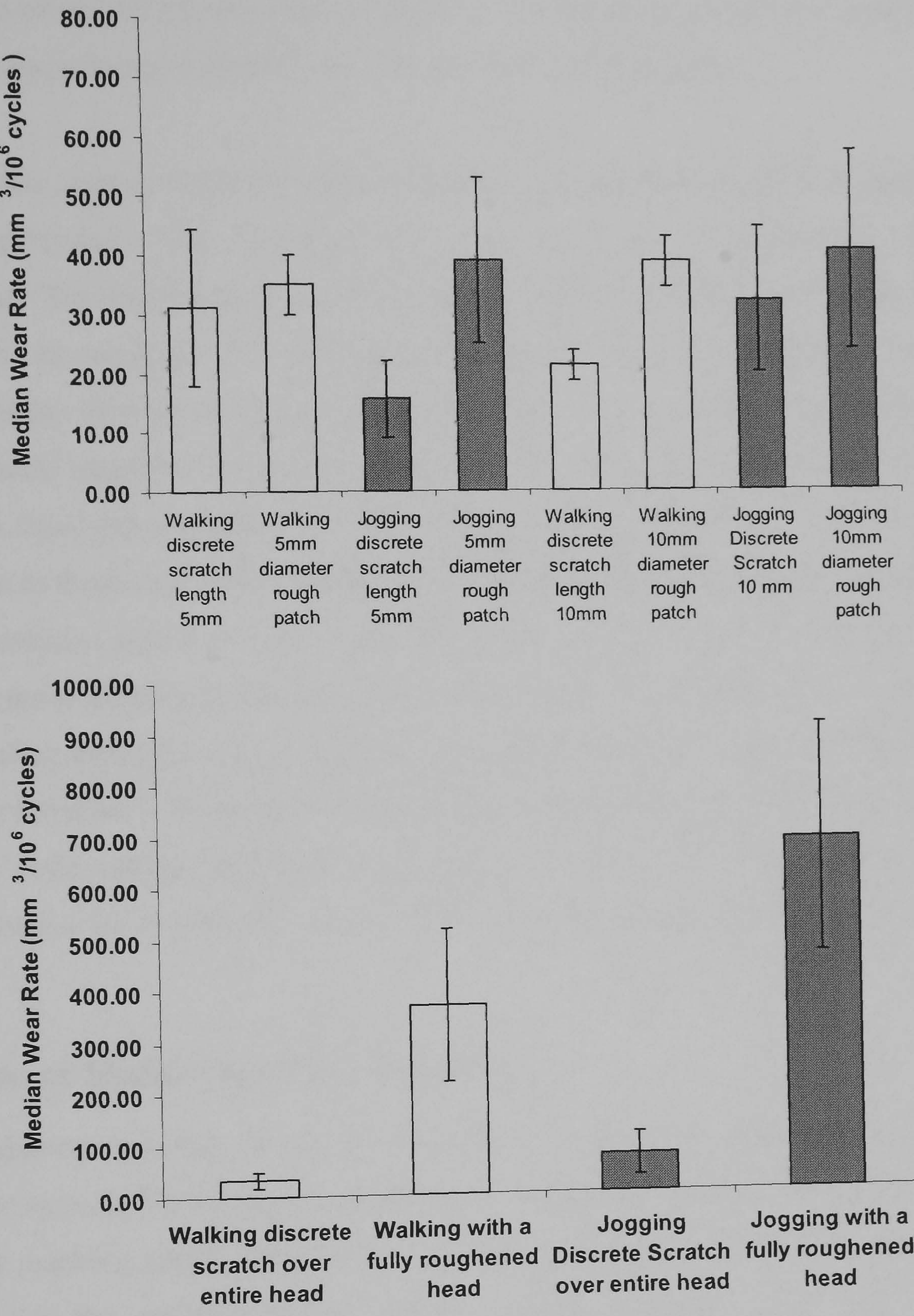


Figure 5.2: Comparison of wear rates generated under two types of damage following walking and jogging

The excessive wear generated during simulated jogging with a fully roughened suggests that femoral head damage would be an influential factor in the longevity of implants when considering more active patients. The high wear rate generated during these tests would produce greater number of particles in the bioactive range and in larger concentrations

which could stimulate the onset of osteolysis in a shorter period of time compared to the volume of wear generated during tests with small areas of damage.

This study has shown that under smooth conditions, high activity such as jogging can be still be undertaken with minimal effect on the wear of moderately cross-linked polyethylene. The introduction of small areas of surface damage had a moderately small influence on the wear rate of moderately-crosslinked UHMWPE under both high and low patient activity. However, a threshold point exists, where the area of surface damage combined with increased activity, reaches a critical value, which would lead to excessive wear and a significant increase in the number of particles produced. "The most significant risk is wear at the joint surface" (Healy *et al*, 2001), with this thought in mind high activity may be possible; however once a significant amount of damage occurs at the bearing surface, activity should be moderated to low impacts sports which would minimise the impact loading experienced by a joint replacement. However assessment of damage *in vivo* at the joint interface is very difficult. The study has shown that with the monitoring of wear over time, under certain conditions and assumptions as to patient activity, could provide some indication as to what the wear rate could be for a particular prosthesis design and patient.

## 5.3 Wear of Metal-on-metal bearings

Tests conducted on metal-on-metal bearings also produced a similar patter of results for tests under smooth femoral head conditions, showing high wear during the wear in phase, eventually reaching steady state wear at 1-2 million cycles. However the volumetric wear generated by the metal-on-metal bearings was significantly lower than metal-on-PE bearings, for all bearing diameters, although there are differences in wear between the different head diameters.

The running-in wear results for the 28 mm bearings produced similar levels of wear when compared with previous hip simulator studies (Firkins *et al*, 2001, Smith *et al*, 2001), using 28 mm diameter heads. The 40 and 56 mm diameter bearing also produced high running in

wear, with the 56 mm diameter bearing producing the highest volume of wear during the wear in phase.

All steady-state wear results in the current study showed similar quantities of wear when compared with previous studies, with the 56 mm diameter bearing showing the lowest wear rate during steady state wear. However due to the high volume of wear experienced by the 56 mm diameter bearing during the wear in phase, it appears to be the worst in the short term, i.e. 5 million cycles, or the equivalent of 3-5 years of use, in the long term however, the results show that larger diameter bearing would continue to produce lower wear rates than smaller head diameter. Results closely agreed with classical elastohydrodynamic lubrication theory, i.e. showing low rates of wear for large head diameters (56 mm). In addition to this, all steady-state wear results in the current study showed similar quantities of wear compared to previous studies.

## 5.4 Influence of activity

The wear generation was also found to be affected by the type of activity undertaken, with fast-jogging activities generating a 4–9 fold increase in wear compared to normal walking. This high increase in metal wear for simulated jogging cycles indicates a change in lubrication regime compared to normal walking, shifting from a hydrodynamic/mixed regime to a mixed/boundary regime, showing a decrease in $\lambda$ and minimum film thickness, Figure 5.3. Slow-walking also showed a sizable increase in wear compared to normal walking, indicating that it is not just high forces and sliding speeds that causes high wear. With regards to the influence of bearing diameter, the results showed that the largest head size generated the lowest wear result under all normal walking, slow walking, slow jogging and fast jogging activities simulated, demonstrating excellent wear resistance. Therefore for more active or younger patients metal on metal bearings would be another alternative to ceramic bearings due to the low levels of wear experienced by metal on metal bearings.

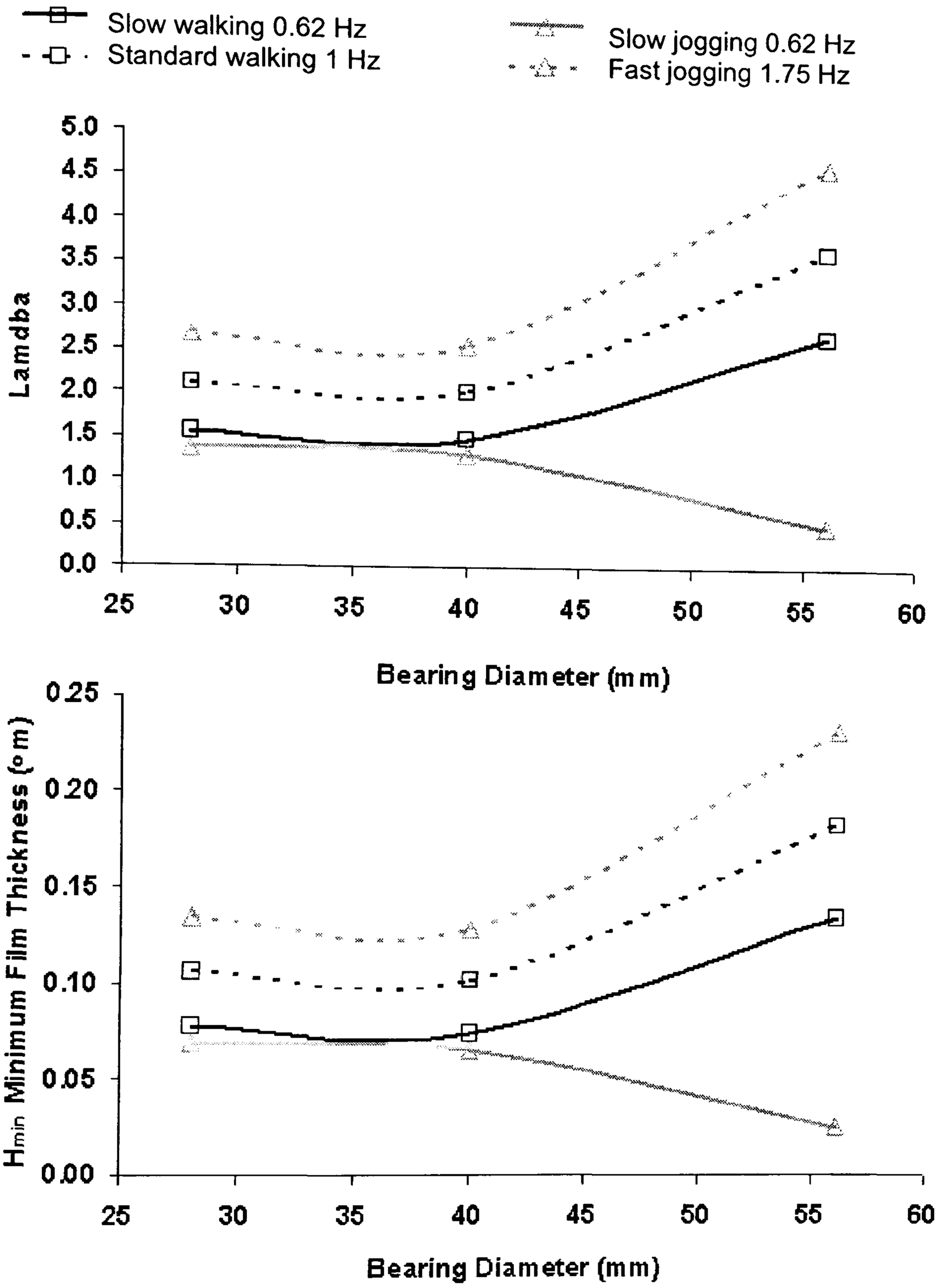


Figure 5.3: Graph showing the changes in λ and minimum film thickness ($H_{min}$, μm) with increasing bearing diameter. Calculated using equations developed by Jin *et al* (1997)

## 5.5 Particles generated during wear of polyethylene cups

Despite the low wear rate observed during steady state wear, the majority of the particles observed were in the sub-micron range, which are within the bioactive range (Fisher *et al*, 2001). Particles isolated from tests during steady state wear, ranged from 0.08 to 8 μm, with an average modal particle size of 0.35 μm and are in agreement with previously published data, which have reported a mean particle size, ranging from 0.38 to 0.7 μm (Table 2.3), with the majority of particles lying in the range of 0.2 to 10 μm. Morphological analysis of particles retrieved from tests under smooth conditions showed similarities with investigations from clinical studies. These have reported both fibril and granular type sub-micron particles, isolated from periprosthetic tissue (Campbell *et al*, 1996, Hailey *et al*, 1996, Hirakawa *et al*, 1996, Kobayashi *et al*, 1997, Schmalzried *et al*, 1997, Tipper *et al*, 2000, Elfick *et al*, 2001).

The current study confirmed the presence of smaller particles, less than 0.1 μm in size using SEM analysis. Although previous studies have not mentioned the presence of particles less than 0.1μm, this may have been as result of technique rather than the absence of small particles. A recent study by Scott *et al* (2001) showed that twice the number of particles were recovered on filter membrane with a pore size of 0.05 μm as compared to a filter with a membrane pore size of 0.2 μm, indicating that a significant number of particles were passing freely through the pores of 0.2 μm membrane filters. Therefore the use of 0.05 μm membrane filters in the current study would increase the accuracy, in number terms, of particles analysed, in turn providing a greater understanding of particle size and range of size. SEM analysis combined with the non destructive analysis of particles by the use of the PSA provided a more detailed breakdown of what is happening to particle size and morphology. The PSA was found to be a useful technique and enabled large numbers of particles to be analysed. However it was not able to resolve the smallest particles that were observed in the same samples during SEM image analysis. The smallest range of particles, 0.01 to 0.05 μm were almost universally unrecognised in the PSA particle distribution data in the current study. Indeed in previous studies using this technique (Elfick

*et al*. 2001) no small particles were observed, however this may have been compounded by agglomeration of small particles into larger clumps.

The results from the current study would imply that crosslinked PE would produce fewer particles, compared to non-crosslinked PE; although further differences were observed between non-crosslinked and crosslinked PE. Crosslinked PE produces significantly more particles in the sub-micrometer range, oval to round in shape as compared to non-crosslinked PE which tends to produce more elongated and fibril like particles (Figure 2.9). This would therefore mean that in terms of numbers, more particles may be produced by crosslinked PE, which in turn may induce a cellular response. However *in vitro* studies into the biological activity of particles has shown that elongated particles are more likely to produce a more serious inflammatory response than rounded particles (Yang *et al*, 2002). Nonetheless particles produced by crosslinked PE; which fall within the bioactive range would also induce a cellular response. A recent study by Illgen *et al* (2003) showed that crosslinked PE particles produced lower biological activity as compared to non-crosslinked PE particles. The biological response of a patient to particulates is a multifactorial process and differs from patient to patient and from material to material.

Wear is a multifactorial process, dependent upon activity, mechanisms of wear, stresses experienced by the bearing surface, motion and PE structure (Schmalzried *et al* 2003), all of which affect particle size and morphology. Current understanding of crosslinked PE shows it to be a more favourable material than non-crosslinked PE due to the extremely low wear rate.

## 5.6 Particles generated during wear of metal bearings

An alternative bearing system was also investigated in the current work, namely metal-on-metal bearings. An enzymatic protocol was developed that worked well for the isolation of metal wear particles; all protein matter was digested, no organic matter was seen during TEM analysis, and EDX confirmed the presence of metal particles, shown in Figure 4.55. The isolation protocol was shown to be a reliable technique in metal particle isolation. The current study into the effects of bearing diameter and activity and its effect upon particle

generation showed significant differences in the size and the number of particles produced for the three different diameters of femoral head sizes. All particles generated during wear tests produced particles in the nanometer range for all three types of metal femoral heads, during both high (jogging) and low activity (walking).

The results from the current study showed that all bearing sizes generated larger mean wear particle sizes compared to previous hip simulator studies. Recent studies by Fisher *et al* (2000) and Firkins *et al* (2001), using similar CoCrMo bearings, 28 mm in diameter, have reported mean wear particle sizes of 25-36 nm, whereas particles in the current study were 7 times greater at 200 nm. Although the particle size reported is large, the current study did adopt a much less corrosive extraction protocol (Catelas *et al*, 2001), which may have led to larger particles. Catelas *et al*, also studied the effects of digestion protocols on metal particles. Catelas et al found that enzymatic protocols had the least effect upon the chemical composition of metal particles. Ion concentration, following alkaline treatments were higher when compared to enzymatic techniques. Following alkaline treatments, chromium oxide particles disappeared over time and with increasing concentrations, in turn affecting particle size and composition. Enzymatic protocols appeared to be the least damaging, examination of particles following enzymatic digestion showed the presence of chromium oxide and CoCrMo particles with varying levels of Co and Cr, which would indicate that particles on the whole retained their overall chemical composition whilst also having a minimal effect upon particle size and morphology.

Although the particles are larger, they are still within the clinical range of particles reported for *in vivo* samples of retrieved tissue studies. A previous study by Doorn *et al*, (1998) isolated particles from retrieved tissue, using an enzymatic digestion protocol, and reported mean particle sizes of 81 nm, ranging from 20-834 nm, which were mainly round in shape. Particle sizes reported in the current study were within this size range, albeit with a mean size that was larger, however the particles appeared to be very uniform in morphology, round to oval shaped particles.

Data from the current study also showed that larger diameter bearings produced smaller wear particle sizes (median 90 nm) compared to 28 mm bearings. This result also agrees with clinical data reported by Doorn *et al* (1998), who showed a mean particle size of 60 nm for large diameter bearings (45 mm) and are representative of those observed in retrieved tissue studies. This may suggest that the hip simulator used in this study generates physiologically relevant wear particles, especially with the introduction of jogging. Currently there are no studies which have reported particle size and morphology of metal particles during high activity, making comparisons difficult.

With the introduction of jogging, on a 40 mm bearing the particle size showed an increase of 25 %, compared to particles generated during walking with a 40 mm bearing. This would increase the metal particle surface area and thereby potentially increase the levels of ions that are released into the body. Although the particle size was similar to that of the 56 mm bearing under normal walking, particles from the 28 mm bearing were shown to be significantly different, approximately twice the size of particles when compared to either the 40 or 56 mm bearing. The 40 mm bearing showed that with increased activity there was an increase in particle size, if this trend is then applied to both the 28 and 56 mm bearing, it would suggest that increased activity would in turn increase both mean or median particle size and therefore the number of particles generated during wear. The surface area of metal particles and implication towards ion release may be the determining factor in deciding which MOM replacement would be the most suitable for any given patient with regards to the level of activity that is likely to be undertaken by the patient.

Based on the wear particle results, the total surface area and total number of particles produced after $10^6$, was predicted, Table 5.1. The volume and surface area for each particle was calculated using the Equations 3.1 to 3.3 and then used as a ratio to determine all values. A prolate ellipsoid was used to minimise any errors in predictions, as the majority of the particles were rugby ball shaped not spherical. Theses show that under steady-state conditions the 56 mm bearing would produce lowest level of surface area, thereby minimising ion release, however jogging would substantially increase the accumulated particle surface area for all bearings.

Table 5.1: Wear rates and calculated particle surface area based on measured particle size for all bearing diameters

| | Head Diameter of MoM | | |
|---|---|---|---|
| | 28 mm | 40 mm | 56 mm |
| Mean Steady-State Wear Rates ($mm^3/10^6$ Cycles) | 0.92 | 0.39 | 0.32 |
| Total Wear Particle Surface Area Per Mc ($m^2/10^6$ Cycles) | 0.153 | 0.116 | 0.066 |

The total number of particles generated per year of use for all 28, 40 and 56 mm bearing were $3.8 \times 10^{12}$, $1.9 \times 10^{13}$ and $1.9 \times 10^{12}$ respectively and similar to previous data (Doorn *et al*, 1998, Fisher & Ingham, 2000), showing particles numbers ranging from $6.7 \times 10^{12}$ to $2.5 \times 10^{14}$. This again supports the supposition that the hip simulator used in the current study generated clinically relevant particles in terms of size and morphology and therefore the number of particles observed during analysis.

The effect of the accumulated surface area generated by these particles may have some local and systemic effects, and has been recognized as one the parameters which may affect macrophage response (Shanbhag *et al.*, 1994). However there is a question mark on how this may affect cellular response, therefore this may not be a good indicator as to how hystiocytes respond to metal particles. Studying the ion levels in erythrocytes, serum and urine of patients with metal-on-metal implants may provide a more accurate description of what is occurring *in vivo* in terms of wear and performance of a metal THR.

As the exact number of metal particles, which trigger cell toxicity, systemic problems and osteolysis are currently not known, the ultimate question of joint longevity cannot be answered. However, this data can be used for cell-culture studies to generate better results for various patient types. A recent study by Catelas *et al* (2003) showed the effects of both $Co^{2+}$ and $Cr^{3+}$ upon macrophage response and TNF-$\alpha$, with $Co^{2+}$ showing to be more toxic than $Cr^{3+}$, with indications that necrosis can be present 48 hours after particle release.

Therefore patients who are more active may be more at risk compared to normally active patients, as they would be producing increased levels $Co^{2+}$ and $Cr^{3+}$, very early on, which may induce local systemic problems. These conditions may also differ between the type of metal implants used (Lhotka *et al*,2003). Although patients that do have metal implants have shown increased levels of Cr and Co, the toxicological significance of elevated levels of Co and Cr have not been fully established (Jacobs et al, 1996, Schmalzried *et al*, 2003)

## 5.7 Particle size and Image analysis

The current study employed two techniques that have helped in the analysis of both PE and metal particles. As well as analysing particles using SEM and TEM, PE particles were also analysed using a Particle Size Analyser (PSA).; This allowed large quantities of particles to be analysed in a very short space of time, without the loss of any particles, the protocol used in this study is similar to the protocol employed by Elfick *et al* (2000). Although the PSA analyser is able to quantify large number of particles, it is however a qualitative process, it can provide information on the number and the volume of particles, but not on morphology. For detailed analysis in terms of morphology, SEM analysis is still required. The current study has found minor discrepancies when comparing results obtained via the PSA to that of results analysed using the SEM. For accurate measurements of morphology and size, SEM analysis is still a useful technique, combining this with the PSA will provide additional information as to what is happening with the particles.

With metal bearing particles the major issue is not the wear rate rather the size of the particles and the potential release of ions into the body. Analysis of metal particles using the PSA is extremely difficult, due to the size of particles that are to be analysed. TEM is an accepted technique in the analysis of particles. However previous studies have only reported the mean size of particles that have been observed, and therefore estimation of the number of particles generated and the surface area that may result from this may either be underestimated or overestimated, leading to the further errors in the prediction of implant lifetime. The current has sought to address this issue by using a more accurate method of sizing the particles (Equations 3.1-3.3). This technique can more accurately predict the

potential surface area that may generated by the particles, therefore providing a more accurate means of assessing potential ion release.

## 5.8 Influence of environment upon data collection

An additional factor to be considered was the method by which the wear rates are calculated. To obtain reliable and consistent data for analysis, initial weight measurements must be repeatable. However it was found that UHMWPE can generate static electricity, which can affect the balance and therefore the measurements obtained. This problem can be eliminated, by maintaining the balance in a controlled environment, as atmospheric humidity and temperature can cause the generation of static electricity. The problem can also be eliminated by grounding the user of the balance, this will discharge any static electricity present, and the balance will remain stable. Static electricity can affect the balance generating erroneous results, which will ultimately affect wear rate and wear volume measurement, providing a false result. However many studies that have used PE cups in tests have failed to mention this.

## 5.9 Summary

The current study has shown that in the long term when taking into account the total surface area that may be generated for an active patient, the 56 mm bearing would perform well in terms of low volumetric wear and lower levels of surface area, due to a reduced number of particles, despite the initial high wear rate during the wear in phase.

If activity is the determining factor of wear as stated by Schmalzried (1998) where ”activity determines the rate of wear and not time”, then more accurate and a standardised procedure should be adopted for the analysis and prediction of wear and particle analysis for both metal-on-polyethylene and metal-on-metal prosthesis. The techniques described in this study allow for the long term prediction of particle generation and also allows for the prediction of wear and potential surface area of particles from MoM implants, that may be generated as a result of increased activity in the long term for young and more active patients

# Conclusions

The current study has extended conventional wear testing by evaluating prostheses under more extreme testing conditions, namely extending the load parameters from those experienced typically in walking to those experienced in jogging and also to change the bearing surface parameters from those which are supplied at the point of implantation to those commonly observed at the point of a revision operation. The study has examined to bearing couples, namely metal on polyethylene and metal on metal.

The following conclusions were found for the metal on polyethylene bearing couples:

- Jogging under smooth femoral head conditions showed slight increases in wear compared to walking under smooth femoral head conditions, with no statistical difference between the two test conditions.

- Jogging under smooth conditions produced a 5-fold increase in the number of submicron sized particles as compared to walking.

- The size distribution of particles can also be influenced by the degree of patient activity undertaken.

- Wear rates under small areas of roughness ($R_a$ 1.5 μm) showed slight increases in wear for both walking and jogging.

- Wear rates observed under increasing areas of surface roughness indicate that there is a threshold point at which wear rates show a significant increase.

- Femoral heads with small areas of roughness showed some evidence of self-polishing following increased activity, which was also reflected in the decrease in wear rates observed and surface measurements obtained following tests.

- Under small areas of roughness both walking and jogging produced significantly more bioactive particles compared to walking and jogging under smooth femoral head conditions.

- Roughening of the femoral heads affects particle morphology, producing more submicron particles that are round/oval in shape.

- Roughening of the entire femoral head produced 1700 fold increase in the number of bioactive particles observed under jogging as compared to walking.

- Single scratches on femoral heads produce higher wear rates that are higher than for smooth heads, although less than for roughened areas. There is not a linear relationship between the total scratch length and the wear rate observed.

The following conclusions were found for the metal on metal bearing couples:

- Larger head diameters for metal-on-metal implants produce significantly less wear compared to small diameter implants, under steady state conditions.

- Larger head diameters produce significantly higher running in wear.

- Small head diameters (28 mm) produced a significant increase in wear particle surface area per million cycles compared to large head diameters (56 mm).

- Increased patient activity can substantially increase wear particle surface area.

- Increased patient activity can substantially increase the levels of ion release.

# Future Work

- Analysis of particles following tests under discrete scratches.

- Development of model relating wear developed under discrete scratches with that developed under roughened areas. Extend work to develop computational model for the prediction of volumetric wear.

- Perform cell culture studies of particles obtained following increased activity.

- Study effects of femoral head surface morphology following tests under rough conditions for both walking and jogging.

- Establish effects of activity on work hardening of femoral heads.

- Develop relationship between *in vitro* tests under increased patient activity with data collected from patients with total hip replacement implants.

- Quantify levels of activity and its relation to wear volume, wear rates, wear particle morphology and size.

- Develop predictive model for patient wear, give determined input parameters e.g. gait style, activity level, age, weight, expectations and develop prosthesis selection protocol for surgeon.

# References

**Affatato, S., Bersaglia, G., Emiliani, D., Foltran, I., Taddei, P., Reggiani, M., Ferrieri, P., Toni, A.** The performance of gamma- and EtO-sterilised UHMWPE acetabular cups tested under severe simulator conditions. Part 2: wear particle characteristics with isolation protocols. *Biomaterials*, Vol. 24, 2003, pp 4045-4055

**Affatato, S., Fernandes, B., Tucci, A., Esposito, L., Toni, A.** Isolation and morphological characterisation of UHMWPE wear debris generated *in vitro*. *Biomaterials*, Vol. 22, 2001, pp 2325-2331

**Archibeck, M. J., Jacobs, J. J., Black, J.** Alternate bearing surfaces in total joint arthroplasty. *Clin. Orthop. Related Res.*, 2000, Vol. 379, pp 12-21

**Athanasou, N. A.** The pathology of joint replacement. *Current Diagnostic Pathology*, 2002, 8, pp26-32

**Ayers, D. C., Taffet, S., Wang, A., Murray, D. G.** Cytokines and endosteal bone resorption in failed cemented total hip replacement. *In proceedings of the 39$^{th}$ annual meeting of the Orthopaedic Research Society*, 1993, pp 290

**Barret, D.** (eds). Essential Basic Sciences for Orthopaedics. Butterworth-Heinemann, 1994.

**Bauer, T. W., Saltarelli, M., McMahon, J. T., Wilde, A. H.** Regional dissemination of wear debris from a total knee prosthesis. *J. Bone Jt. Surgery*, 1993, Vol. 75A, pp 106-111

**Beaule, P. E., Campbell, P., Mirra, J., Hooper, J. C., Schmalzried, T. P.** Osteolysis in a cementless, second generation metal-on-metal hip replacement. *Clin. Orthop. Related Res.*, 2001, Vol. 386, pp 159-165

**Bendall, S. P., Radfar, A. J., Frondoza, C., Jinnah, R. H., Hungerford, D. S.** Metallic wear debris from perioprosthetic tissue of failed arthroplasty induces TNF-α and IL-1α release from synoviocytes. *In Proceedings of the Fifth World Biomaterials Congress*, 1996, pp 546

**Benz, E. B., Federman, M., Godleski, J. J., Bierbaum, B. E., Thornhill, T. S., Spector, M**; Transmission electron microscopy of intracellular particles of polyethylene from joint replacement prostheses: size distribution and cellular response. *Biomaterials*, 2001, 22, pp 2835-2842

**Bergmann, G., Graichen, F., Rohlmann, A.** Hip joint loading during walking and running, measured in two patients. *J. Biomechanics*, 1993, Vol. 26, No. 8, pp 969-990

**Black, J.** Biological Performance of Materials, Fundamentals of Biocompatibility. Marcel Dekker, Inc, 2000.

**Bowker P., Condie D. N., Bader D. L., Pratt D. J., Wallace W. A.** (Editor). Biomechanical Basis of Orthotic Management. Butterworth-Heinemann, Oxford. 1993.

**Bowsher, J. G.** Accelerated wear testing methodologies for total hip replacements. *PhD Thesis*, University of London, 2001

**Bruck, S. D., Mueller, E. P.** Radiation sterilisation of polymeric implant materials. *J. Biomed. Mater. Res.*, 1988, Vol. 22, pp 133-144

**Buckwalter, J. A., Mankin, H. J.,** Articular cartilage and transplantation. Arthritis & Rheumatism, 1998

**Buford, A., & Goswami, T**. Review of wear mechanisms in hip implants: Paper 1-General. *Materials & Design*, Vol. 25, 2004, pp 385-393

**Bullough, P. G., DiCarlo, E. F., Hansraj, K.K., Neves, M.C.** Pathological studies of total joint replacements. *Orthop. Clinics North America,* 1988, Vol. 19, pp 611-625

**Callister, W. D.** An introduction to Material Science and Engineering. John Wiley & Sons, Inc, 1997

**Campbell, P., Ma, S. Schmalzried, T. P., Amstutz, H.** Tissue digestion for wear debris particle isolation. *J. Biomed. Mater. Res.*, 1994 Vol. 28, pp 523-526

**Campbell, P., Ma, S., Yeom, B., McKellop, H., Schmalzried, T. P., Amstutz, H.** Isolation of predominantly sub-micron sized UHMWPE wear particles from perioprosthetic tissues. *J. Biomed. Mater. Res.*, 1995 Vol. 29, pp 127-131

**Campbell, P., Shen, Fu-Wen., McKellop, H.** Biological and tribological considerations of alternative bearing surfaces. *Clin. Orthop.*, 2004, Vol. 418, pp 98-111

**Catelas, I. Campbell, P., Medley J. B. Bobyn, J. D., Medley, J. B., Zukor, D. J., Petit, A.** Quantitative and compositional analysis of particles from metal-metal THRs. *In proceedings of the European Society for Biomaterials*, 2001, pp T46

**Catelas, I., Bobyn, J. D., Medley, J. B., Krygier, J. J., Zukor, D. J., Petit., A., Huk, O. L.** Effects of digestion protocols on the isolation and characterisation of metal-on-metal wear particles. I. Analysis of particle size and shape. *J of Biomedical Materials Research*, Vol. 55, 2001, pp 320-329

**Cawley, J., Metcalf, J. E. P., Jones, A. H., Band, T. J., Skupien, D. S.** A tribological study of cobalt chromium molybdenum alloys used in metal-on-metal resurfacing hip arthroplasty. *Wear*, 2003, No 255, pp 999-1006

**Charnley, J**. Fracture of femoral prosthesis in total hip replacement. A clinical study. *Clin. Orthop*, 1975, vol. 111, pp 105-120

**Charnley, J**. Low Friction Arthroplasty, Theory and Practice. Springer-Verlag, 1979.

**Choudhury, M., Hutchings, I. M.** The effects of irradiation and ageing on the abrasive wear resistance of ultra high molecular weight polyethylene. *Wear*, 1997, Vol. 203-204, pp 335-340

**Clarke, I.C., Good, V., and Williams, P;** Simulator wear study of high dose gamma irradiated UHMWPE cups. *Trans Society of Biomaterials*, 1997, 20, 71

**Costa, L., Luda, M. P., Trossarelli, L., Brach del Prever, E. M., Crova, M., Gallinaro, P.** Oxidation in orthopaedic UHMWPE sterilised by gamma-irradiation and ethylene oxide. *Biomaterials*, 1998, Vol. 19, pp 659-668

**Coughlan, J. J., Hug, D. P.** Ultrahigh molecular weight polyethylene. In: Mark, H. F., Bikales, N. M., Overberger, C. G., Menges, G., Kroschwitz, J. I., (eds). Encyclopaedia of polymer science and engineering. John Wiley & Sons, New York, 1986.

**Craik R. L., Oatis C. A.** Gait analysis: theory and application. Mosby, London 1995

**Curtis, P. E., Revell, P. A.** Focal adhesion in macrophages following exposure to retrieved particles. *In proceedings of the European Society for Biomaterials*, 2001, pp T48

**Doorn, P. F., Campbell, P. A., Amstutz, H. C.** Metal vs. polyethylene wear particles in total hip arthroplasty. *Clinical Orthopaedics & Related Research*, Philadelphia: Lippincott-Raven Publishers, 1996, pp S60-S68

**Doorn, P. F., Campbell, P. A., Worrall, J., Benya, P. D., McKellop, H. C., Amstutz, H. C.** Metal wear particle characterisation from metal on metal total hip replacements: transmission electron microscopy study of perioprosthetic tissues and isolated particles. *J. Biomed Mater Res.*, 1998, Vol. 42, pp 103-111

**Dowson, D.** New joints for the millennium: Wear control in total joint replacements. *Lecture presented at an Ordinary meeting of the Institution of Mechanical Engineers, The James Clayton Memorial Lecture 2000*, Medical Engineering Division, Weds 28 June 2000

**Dowson, D., Diab, M. M., Gillis, B. J., Atkinson, J. R.** Influence of counterface topography on the wear of UHMWPE under wet and dry conditions. *Polym. Prepr. Am. Chem. Soc. Div. Polym. Chem.*, 1985, Vol. 287, pp 171-187

**Dubs, L., Gschwan, N., Munzinger, U.** Sport after total hip arthroplasty. *Arch Orthop Trauma Surgery*, 1983, 101(3) pp 161-169

**Elfick, A. P. D., Smith, S. L., Green, S. M., Unsworth, A**. The quantitative assessment of UHMWPE wear debris produced in hip simulator testing: the influence of head material and roughness, motion and loading. *J. Wear*, 2001, Vol. 249, pp 517-527

**Elfick, A. P., Green, S. M., Krikler, S., Unsworth, A.** The nature and dissemination of UHMWPE wear debris retrieved from perioprosthetic tissue of THR. *J. Biomed. Mater. Res.*, 2003, Vol. 65A, pp 95-108

**Elfick, A. P., Hall, R. M., Pinder, I. M., Unsworth, A.** The influence of femoral head surface roughness on the wear of ultra high molecular weight polyethylene sockets in cementless total hip replacements. *J. Biomed. Mater. Res.*, 1999, Vol. 48, pp 712-718

**Endo, M. M., Barbour, P. S. M., Barton, D. C., Tipper, J. L., Ingham, E., Stone, M. H., Fisher, J.** Wear of crosslinked and non crosslinked ultra high molecular weight polyethylene in a hip joint simulator with smooth and damaged femoral heads. *In Proceedings of the Sixth World Biomaterials Congress, Society for Biomaterials*, 2000, pp 872

**Firkins, P. J., Tipper, J. L., Ingham, E., Stone, M. H., Farrar, R., Fisher, J**: Influence of simulator kinematics on the wear of metal-on-metal hip prostheses. *Proc Instn Mech Engrs*, Vol. 215H, 2001, pp 119-121

**Fisher, J., Bell, J., Barbour, P. S. M., Tipper, J. L., Matthews, J. B., Besong, A. A., Stone, M. H., Ingham, I.** A novel method for the prediction of functional biological activity of polyethylene wear debris. *Proc Instn Mech Engrs*, 2001, 215H, pp 127-132.

**Fisher, J., Besong, A. A., Firkins, P. J., Barbour, P. S. M**: Wear debris generation in UHMWPE on ceramic, metal on metal and ceramic on ceramic hip prostheses. *Trans World Sixth Biomaterials*, 871, 2000

**Fisher, J., Firkins, P., Reeves, E. A., Hailey, J. L., Isaac, G.H.** The influence of scratches to metallic counterfaces on the wear of ultra-high molecular weight polyethylene. *Proc Instn Mech Engrs*, 1995, 209H, pp 263-264.

**Germain, M. A., Hatton, A., Williams, S., Matthews, J. B., Stone, M. H., Fisher, J., Ingham, E.** Comparison of the cytotoxicity of clinically relevant cobalt-chromium and alumina ceramic wear particles in vitro. *Biomaterials*, Vol. 24, 2003, pp 469-479

**Goldman M., and Pruitt, L**; Comparison of the effects of gamma radiation and low temperature hydrogen peroxide gas plasma sterilization on the molecular structure, fatigue resistance, and wear behaviour of UHMWPE. *J. Biomed Mater Res*, 1998, 40(3), pp 378-384

**Goodman, S. B., Knoblich, G., O'Connor, M., Song, Y., Huie, P., Sibley, R.** Heterogeneity in cellular and cytokine profiles from multiple samples of tissue surrounding revised hip prostheses. *J. Biomed Mater. Res*, 1996, Vol. 96, pp 421-428

**Gowen, M., Wood, D. D., Ihrie, E. J., McGuire, M. K. B., Russell, R. G. G.** An interleukin-1 like factor stimulates bone resorption *in vitro*. *Nature*, 1983, Vol. 306, pp 378

**H., Healy, W., Lorio, R., Lemos, M.** Athletic activity after joint replacement. *The American Journal of Sports Medicine* 29:377-388 (2001)

**Hailey, J. L., Ingham, E., Fisher, J., Dowson, D., Wroblewski, B. M., Stone, M. H.** Ultra High Molecular Weight Polyethylene wear debris generated *in vivo* and in laboratory tests: the influence of counterface roughness. *Proc Instn Mech Engrs J. Eng. Medicine, Part H,* 210, pp 3-10

**Hall, R. M., Siney, P., Unsworth, A., Wroblewski, B. M.** The effect of surface topography of retrieved femoral heads on the wear of UHMWPE sockets. *Med. Eng. Phys.*, 1997, Vol. 19, pp 711-719

**Haynes, D. R., Boyle, S. J., Rogers, S. D.** Variation in cytokines induced by particles from different prosthetic materials. *Clin. Orthop.*, 1998. Vol. 352, pp 223-230

**Heisel H. et al.:** J Bone Joint Surg-Am 2003; 85-A: 1366- 79 Swedish National Hip Registry, 2000 report

**Heisel, C., Silva, M., Schmalzried, T. P.** Bearing surface options for total hip replacement in young patients. *J. Bone Jt. Surgery*, 2003, Vol. 85A, pp 1366-1379

**Hilton, K. R., Dorr, L. D., Wan, Z., McPherson, E. J.** Contemporary total hip replacement with metal on metal articulation. *Clin. Orthop. Related Res.*, 1996, Vol. 329S, pp S99-S105

**Huo, M.** H., Martin, R. P., Zatorski, I. E., Keggi, K. J. Ceramic total hip replacement done without cement. Long-term follow-up study. Orthop. Trans., 1995, Vol. 19, pp 400-401

**Illgen, R. L., Laurent, M. P., Watanuki, M., Hagenauer, M. E., Bhambri, S. K., Pike, J. W., Blanchard, C. R., Forsythe, T. M.** Highly crosslinked vs. conventional polyethylene particles – an *in vitro* comparison of biological activities. *Trans Orthop Res Soc*, 28, 1438, 2003

**Ingham, E., Fisher, J.** Biological reactions to wear debris in total joint replacements. *Proc Instn Mech Engrs*, 2000, 214H, pp 21-37

**Ingram, J. H., Fisher, J., Stone, M., Ingham, E.** Effect of crosslinking on biological activity of UHMWPE wear debris. *Trans Orthop Res Soc*, 28, 1439, 2003

**Isaac, G. H., Wroblewski, B. M., Atkinson, J. R., Dowson, D.** A tribological study of retrieved hip prostheses. *J. Clin. Orthop. Res.*, 1992, Vol. 256, pp 115-125

**Jacobs, J. J., Skipor, A. K., Doorn, P. F., Campbell, P., Schmalzried, T. P., Black, J., Amstutz, H. C.** Cobalt and chromium concentrations in patients with metal on metal total hip replacements. *Clin. Orthop. Related Res.*, 1996, Vol. 329, pp S256-S263

**Jin Z.M., Dowson D., Fisher J. (1997)**, Analysis of fluid film lubrication in artificial hip joint replacements with surfaces of high elastic modulus, *Proc. Instn. Mech. Engrs. Part H*, 211, 247-256.

**Katti, K., S**. Biomaterials in total joint replacement. Colloids & Surfaces B: *Biointerfaces*. 39(3), pp 133-142, 2004

**Kilgus, D. J., Dorey, F. J. Fineman, G. A. Astutz, H. C.** Patient activity, sport participation and impact loading on the durability of cemented total hip replacement. *Clin. Orthop.*, 1991, Vol. 269, pp 25-31

**Kloen, P., Marti, R.** Chronic recurrent posterior dislocation of the hip after Pipkin Fracture treated with intertrochanteric osteotomy and acetabuloplasty. *J. Bone Jt. Surgery*, 2000, Vol. 82A, pp 867

**Kobayashi, A., Freeman, M. A. R., Bonfield, W., Kadoya, Y., Yamac, T., Al-Saffar, N., Scott, G., Revell, P. A.** Number of polyethylene particles and osteolysis in total joint replacements. *J. Bone Jt. Surgery*, 1997, Vol. 79B, pp 844-848

**Kurtz, S. M., Muratoglu, O. K., Evans, M., Edidin, A. A.** Advances in the processing, sterilisation, and crosslinking of ultra-high molecular weight polyethylene for total joint arthroplasty. *Biomaterials*, 1999, Vol. 20, pp 1659-1688

**Lancaster, J.G., Dowson, D., Isaac, G.H., Fisher, J**. The wear of ultra-high molecular weight polyethylene sliding on metallic and ceramic counterfaces representative of current femoral surfaces in joint replacement. *Proc Instn Mech Engrs*, 1997, 211H, pp 17-24.

**Lerouge, S., Huk, O., Yahia, L., Witvoet, J., Sedel, L.** Ceramic-ceramic and metal-polyethylene total hip replacements. *J. Bone Jt. Surgery*, 1996, Vol.79B, pp 135-139

**Lewis, G.** Properties of crosslinked ultra-high-molecular-weight polyethylene. *Biomaterials*, 2001, Vol. 22, pp 371-401

**Lhotka, C., Szekeres, T., Steffan, I., Zhuber, K., Zweymüller.** Four-year study of cobalt and chromium blood levels in patients with two different metal-on-metal total hip replacements. *J. Orthop Res*. Vol. 21, 2003, pp 189-195

**Li, S., Burstein, A.** Ultra-high molecular weight polyethylene, current concepts review. *J. Bone Jt. Surgery*, 1994, Vol. 76A No. 7, pp 1080-1090

**Lombardi, A.V., Mallory, T.H., Vaughn, B. K., Drouillard,** P. Aseptic loosening in total hip arthroplasty secondary to osteolysis induced by wear debris from titanium-alloy modular femoral heads. *J. Bone Jt Surgery*, 1989, vol. 71A, pp 1337-1342

**Lu, Z., McKellop, H**. Frictional heating of bearing materials tested in a hip joint wear simulator. *Proc Instn Mech Engrs*, 1997, 211H, pp 101-108

**Mabrey, J. D., Afsar-Keshmiri, A., McClung II, G. A., Pember II, M. A., Wooldridge, T. M., Agrawal, C. M.** Comparison of UHMWPE particles in synovial fluid and tissues from failed THA. *J. Biomed Mater Res (Appl Biomater),* 2001, Vol. 58, pp 196-202

**Maloney, W. J., Smith, R. L., Hvene, D., Schmalzried, T. P., Rubash, H.** Isolation and characterisation of wear debris generated in patients who have had failure of a hip arthroplasty without cement. *J. Bone Jt Surgery*, 1994, vol. 77A, pp 1301-1310

**Manley, M. T., Serekian, P.** Wear Debris: An environmental issue in total joint replacements. *Clin. Orthop. Related Res*., 1994, Vol. 298, pp 137-146

**Mathews, J. B., Besong, A. A., Stone, M. H., Wroblewski, B. M., Fisher, J., Ingham, E. B.** In vitro generation of clinically relevant sterile UHMWPE wear debris suitable for use in cell culture studies. *In proceedings of the 43rd annual meeting of the Orthopaedic Research Society,* 1997, pp 768

**McKellop, H. A., Campbell, P., Park, S. H., Schmalzried, T. P., Grigoris, P., Amstutz, H., Sarmiento, A.** The origin of sub-micron polyethylene wear debris in total hip arthroplasty. *Clin. Orthop. Related Res.*, 1995, Vol. 311, pp 3-20

**McKellop, H., Clarke, I. C., Markolf, K.L., Amstutz, H.C.** *J of Biomedical Materials Research*, 1978, vol. 12, pp 895

**McKellop, H., Shen, F., DiMaio, W., Lancaster, J. G.** Wear of Gamma-Crosslinked Polyethylene Acetabular Cups Against Roughened Femoral Balls. *Clin Othorp*, 1999, 369, pp 73-82.

**McKellop, H., Shen, F., Lu, B., Campbell, P., and Salovey, R;** Development of an extremely wear-resistant ultra-high molecular weight polyethylene for total hip replacements. *J. Orthop. Res.*, 1999, 17(2), pp 157-167

**Meyer, R. W., Pruitt, L. A.** The effect of cyclic true strain on the morphology, structure and relaxation behaviour of ultra high molecular weight polyethylene. *Polymer*, 2001, 42, pp 5293-5306.

**Muller, M. E.** The benefits of metal on metal total hip replacements. *Clin. Orthop. Related Res.*, 1995, Vol. 311, pp 54-59

**Muratoglu, O. K., Bragdon, C. R., O'Connor, D. O., Jasty, M., Harris, W. H.** A novel method of crosslinking Ultra-High-Molecular-Weight Polyethylene to improve wear, reduce oxidation, and retain mechanical properties. *J. Arthroplasty*, Vol. 16, No. 2, 2001, pp 149-160

**Muratoglu, O.K., Bragdon, C. R., O'Connor, D.O., Jasty, M., Harris, W.H., Gul, R., and McGarry, F;** Unified wear model for highly crosslinked ultra-high molecular weight polyethylenes (UHMWPE). *Biomaterials*, 1999, 20, 1463-1470

**Muratoglu, O.K., Bragdon, C. R., O'Connor, D.O., Jasty, M., Harris, W.H., Gul, R., and McGarry, F;** Unified wear model for highly crosslinked ultra-high molecular weight polyethylenes (UHMWPE). *Biomaterials,* 1999, 20, 1463-1470

**Muratoglu, O.K., Bragdon, C.R., O'Connor, D.O., Skehan, H., Delaney, J., Jasty, M., and Harris, W.H;** The comparison of the wear behavior of four different types of crosslinked acetabular components. *Sixth World Biomaterials Congress Transactions, Hawaii, Society for biomaterials*, 2000, 2, 865

**Murray, D. W., Rushton, N.** Macrophages stimulate bone resorption when they phagocytose particles. *J. Bone Jt Surgery*, 1990, Vol. 72B, pp 988-992

**Naidu, S.H, Bixler, B.L, and M. Moulton;** Radiation-induced physical changes in UHMWPE implant components. *Orthopedics*, 1997, 20(2), pp 137-142

**Oonishi, H., Kuno, M., Tsuji, E., and Fujisawa, A;** The optimum dose of gamma radiation-heavy doses to low wear polyethylene in total hip prostheses. *J. Mater. Sci: Mater in Med.*, 1997, 8, 11-18

**Oonishi, H., Takayama, Y., Tsuji, E.** Improvement of polyethylene by irradiation in artificial joints. *Radiat. Phys. Chem.*, 1992, Vol. 39 No. 6, pp 495-504

**Paul, J.** Forces transmitted by joints in the human body. *Proc. Instn. Mech. Engrs. Part H*, 1966, Vol. 181-3F, pp 8-15

**Petty, W.** Total Joint Replacement. W. B. Saunders Company, 1991.

**Podsiadlo, P., Stachowiak, G. W.** 3-D imaging of surface topography of wear particles found in synovial joints. *Wear*, Vol. 230, 1999, pp 184-193

**Revell, P. A., Al-Saffar, N., Kobayashi, A**. A biological reaction to debris in relation to joint prostheses. *Proc Instn Mech Engrs J. Eng. Medicine*, 1997, 211 H2, pp 187-192

**Rieker, C., Konrad, R., Schön.** *In Vitro* comparison of the two hard-hard articulations for total hip replacements. *Proc Instn Mech Engrs*, Vol. 215H, 2001, pp 153-160

**Rose J., Gamble J. G.** (Eds.). Human Walking (2nd Edition). Williams & Wilkins. 1994.

**Saikko, V., Ahlroos, T., Calonius, O., Keränen, J.** Wear simulation of total hip prosthesis with polyethylene against CoCr, alumina and diamond-like carbon. *Biomaterials*, Vol. 22, 2001, pp 1507-1514

**Savio III, J. A., Overcamp, L. M., Black, J.** Size and shape of biomaterial wear debris. *Clinical Materials*, 1994, Vol. 15, pp 101-147

**Schmalzried, T. P., Callaghan, J. J.** Current concepts review. Wear in total hip and knee replacements. *J. Bone Jt Surgery*, 1999, Vol. 81A, pp115-136

**Schmalzried, T. P., Jasty, M., Harris, W. M.** Perioprosthetic bone loss in total hip arthroplasty: polyethylene wear debris and the concept of effective joint space. *J. Bone Jt Surgery*, 1992, vol. 74A, pp 849-863

**Schmidt, M., Weber, H., Schon, R.** Cobalt chromium molybdenum metal combination for modular hip prostheses. *Clin. Orthop. Related Res.*, 1996, Vol. 329S, pp S35-S47

**Schwartz, E., Bukata, S. V., Benz, E., Rosier, R. N., Puzas, J. E., O'Keefe, R. J.** NFKB and TNF-α are stimulated by titanium particles and are essential for bone resorption. *In proceedings of the 45th annual meeting of the Orthopaedic Research Society*, 1999, pp 305

**Scott, M., Widding, K., Jani, S.** Do current wear particle isolation procedures underestimate the number of particles generated by prosthetic bearing components. *J. Wear*, 2001, Vol. 251, pp 1213-1217

**Seiber, H. P., Rieker, C. B., Kottig, P.** Analysis of 118 second generation metal on metal retrieved hip implants. *J. Bone Jt. Surgery*, 1998, Vol. 80B, pp 46-50

**Semlitsch, M., Willert, H. G.** Clinical wear behaviour of ultra-high molecular weight polyethylene cups paired with metal and ceramic ball heads in comparison to metal-on-metal pairings of hip joint replacements. *Proceedings of the Institution of Mechanical Engineers*, 1997, Vol. 211, H1, pp 73-88

**Shahgaldi, B. F., Hearley, F. W., Dewar, A., Corrin, B.** In vivo corrosion of cobalt-chrome and titanium wear particles. *J Bone Jt Surgery*, 1995, Vol. 77B, pp 926-966

**Shanbhag, A. S., Jacobs, J. J., Black, J., Galante, J. O., Glant, T. T.** Human monocyte response to particulate biomaterials generated in vivo and in vitro. *J. Orthop. Res.*, 1995, Vol. 13, pp 792-801

**Smith, S. L., Unsworth, A.** A comparison between gravimetric and volumetric techniques of wear measurement of UHMWPE acetabular cups against Zirconia and cobalt-chromium-molybdenum femoral heads in a hip simulator. *Proc Instn Mech Engrs*, 1999, 213H, pp 475-483

**Soh, E. W., Blumm, G. W., Wait, M. E., Walker, P. S.** Size and shape of metal particles from metal on metal total hip replacements. *Trans Orthop Res Soc*, 42, 462, 1996

**Stewart, T., Tipper, J., Nevelos, J., Insley, G., Streicher, R., Ingham, E., Fisher, J.** Long term simulator studies of alumina ceramic/ceramic hip implants with swing phase micro-separation; Analysis of wear and wear debris generation. *In Proceedings of the European Society for Biomaterials*, 2001, pp T50

**Tennent, T. D., Goddard, N. J.** Current attitudes to total hip replacement in the younger patients: results of a national survey. *Annals of the Royal College of Surgeons of England*, 2000, Vol. 82 No. 1, pp 33-38

**Tipper, J. L., Ingham, E., Hailey, J. L., Besong, A. A., Stone, M. H., Wroblewski, B. M., Fisher, J.** Quantitative comparison of polyethylene wear debris, wear rate and head damage in retrieved hip prostheses. *In proceedings of the 43rd annual meeting of the Orthopaedic Research Society*, 1997, pp 355

**Tortora, G. J., Grabowski, S. R.** Principles of Anatomy and Physiology (9th Edition), John Wiley & Sons, Inc, 2000

**Wagner, M., Wagner, H.** Medium term results of a modern metal-on-metal system in total hip replacement. *Clin. Orthop. Related Res.*, 2000, Vol. 379, pp 123-133

**Wang, A. & Essner, A.** Three-body wear of UHMWPE by PMMA particles against CoCr, alumina and zirconia heads in a hip joint simulator. *Wear*, 2001, No 250, pp 212-216

**Wang, A., Polineni, V. K., Stark, C., Dumbleton, J. H.** Effect of femoral head surface roughness on the wear of ultra high molecular weight polyethylene acetabular cups. *J. Arthroplasty*, Vol. 13, No. 6, 1998, pp 615-620

**Wang, A., Stark, C., Dumbleton, J. H.** Mechanistic and morphological origins of ultra-high molecular weight polyethylene wear debris in total joint replacement prostheses. *Proc Instn Mech Engrs*, 1996, 210H, pp 141-155

**Wang, A., Sun, D. C., Stark, C., Dumbleton, J. H**. Wear mechanisms of UHMWPE in total joint replacements. *Wear*, 1995, No 181-183, pp 241-249

**Wang, A., Sun, D. C., Yau, S-S., Edwards, B., Sokol, M., Essner, A., Polineni, V. K., Stark, C., Dumbleton, J. H.** Orientation softening in the deformation and wear of ultra-high molecular weight polyethylene. *Wear*, 1997, Vol. 203-204, pp 230-241

**Wang, A., Sun, D., Stark, C., and Dumbleton, J.H;** Wear testing based on unidirectional motion: fact or artefact? *Fifth World Biomaterials Congress*, 1996, May 29-June 2, Toronto, pp 583

**White, S. E., Paxson, R. D., Tanner, M. G., Whiteside, L. A.** Effects of sterilisation on wear in total knee arthroplasty. *Clin. Orthop.*, 1996, Vol. 331, pp 164-171

**Whittle M. W.** Gait Analysis an Introduction. Butterworth-Heinemann, Oxford. 1996

**Willert, H-G., Buchhorn, G. H., Eyerer, P.** Ultra-high molecular weight polyethylene

**Willert, H-G., Semlitsch, M. F.** Reactions to articular capsule to wear products of artificial joint prostheses. *J. Biomed. Mater. Res.*, 1977, Vol. 11, pp 157-164

**Wright, V., Radin, E. L.** Mechanics of Human Joints: Physiology, Pathophysiology, and Treatment. Marcel Dekker, Inc. 1993

**Wroblewski, B.M., Siney P.D., Dowson, D., and Collins, S.N;** Prospective clinical and joint simulator studies of a new total arthroplasty using alumina ceramic heads and cross-linked polyethylene cups. *Journal of Bone and Joint Surgery*, 1996, 78-2, pp 280-285

**Yamac, T.** The extraction and characterisation of wear particles from tissues around failed orthopaedic implants of different designs. *PhD Thesis*, University of London, 1999

**Yamamoto, K., Clarke, I. C., Masaoka, T., Oonishi, H., Williams, P. A., Good, V. D., Imakiire, A.** Microwear phenomena of ultra high molecular weight polyethylene cups and debris morphology related to γ radiation dose in simulator study. *J. Biomed. Mater. Res.*, 2001, Vol. 56, pp 65-73

**Yang, S. Y., Ren, W., Park, Y., Sieving, A., Hsu, S., Nasser, S., Wooley, P. H.** Diverse and cellular apoptotic responses to variant shapes of UHMWPE in a murine model of inflammation. *Biomaterials*, Vol. 23, 2002, pp 3535-3543

**Yoon, T. R., Rowe, S. M., Jung, S. T., Seon, K. J., Maloney, W. J.** Osteolysis in association with a total hip arthroplasty with ceramic bearing surfaces. *J. Bone Jt. Surgery*, 1996, Vol. 80A, pp 1459-1468

**Zahiri, C.A., Schmalzried, T. P., Ebramzadeh, E., Szuszczewicz, E. S., Salib, D., Kim, C., Amstutz, H. C.** Lessons learned from loosening of the McKee-Farrar metal-on-metal total hip replacement. *J. Arthroplasty*, Vol. 14, No. 3, 1999, pp 326-332

# Appendix 1

## Appendix 1.1: Standard Cleaning Protocol

The following protocol was used for cleaning both specimens and relevant fixturing.

1. Scrub and rinse component in Decon-90 and deionised water, removing any foreign particles.
2. Place component within a full beaker of Decon-90 (5 %) and deionised water, and vibrate for 5 minutes in an ultrasonic cleaner.
3. Rinse in deionised water.
4. Vibrate for 10 minutes in a beaker of filtered deionised water.
5. Rinse in filtered deionised water.
6. Vibrate for 3 minutes in a beaker of filtered deionised water.
7. Rinse in deionised water.
8. Submerge component in propan-2-ol for 2 minutes ±20 seconds, if not possible, then thoroughly wipe the component in propan-2-ol.
9. Dry the component with a jet of nitrogen gas for 10 to 15 seconds, with a forcing pressure of 2.5 Bar, and the hose valve fully open.
10. Cover the components in cellophane, and store within a controlled environment (*positive air cabinet*).

## Appendix 1.2: Socket Measurement Protocol

The following protocol was used to determine the weight of all test sockets before and after wear testing.

1. Switch on the microbalance, and leave for a minimum of 2 hours to warm up.
2. Ensure all sockets are clean using the standard cleaning protocol, outlined in Appendix Four.

3. Place all sockets on a lint-free cloth next to the measuring balance, and leave for a minimum of 30 minutes to stabilise.
4. Before taking measurements, switch off air conditioning, as draughts may cause inaccurate measurements.
5. Record room temperature.
6. Calibrate microbalance (pressing Tare). Before weighing actual specimen, exercise the balance by weighing a socket, and waiting for it to reach a stable reading.
7. Take 4 weight readings of each socket, in rotation, keeping the same specimen sequence each time. While waiting for the balance to stabilise on each reading, record the appearance of each socket, i.e. number of scratches and scuff marks, plus grade the overall mirror finish.
8. The median of the four measurements weights is to be used foe wear calculations.

## Appendix 1.3: Femoral Scratching Protocol

The following protocol was used to scratch all CoCrMo femoral heads.

1. Remove all femoral heads from their protective packaging, and locate each head on a stainless steel head fixture. Once located, tap each head with a plastic hammer and a protective cloth to ensure a good fit.
2. Place one head assembly into a bench vice, positioning the head upwards, and proceed to scratch the upper hemisphere of the head with 400 grit SiC paper. Scratches should not pass lower than the horizontal equator of the head. Apply the SiC paper in a circular motion to ensure multi-directional scratching over the entire upper hemisphere. Ensure that all scratches are of a similar size to the naked eye.
3. Place the head and fixture into the contact profilometer, and take five measurements in the roughest areas to the naked eye. If the maximum $R_p$ is greater than 3 μm ± 0.5 μm for each measurement, then use 300 grit SiC paper to reduce the extent of scratching, and re-measure with five reading. If the maximum $R_p$ is less than 3 μm ±

0.5 μm for all readings, then use a 400 grit SiC paper again to increase the scratching, and re-measure with five reading.

4. Once all five readings produce a $R_p$ of 3 μm ± 0.5 μm, then take between 20 to 40 readings of the entire scratched surface of the femoral head, and calculate a median $R_a$ and $R_p$. If the median $R_a$ is higher or lower than 0.38 μm ± 0.5 μm for all readings, then again apply the grit SiC paper to reduce or increase the scratching, and re-measure to achieve a median $R_a$ 0.38 μm ± 0.5 μm for 20 to 40 readings.
5. Once the head is scratched to the correct roughness, remove from the contact profilometer, and clean thoroughly with lint-free cloths, Decon-90 and Propan-2-ol, to remove all fine metal particles.
6. Locate the next femoral head fixture and head into the bench vice, and complete steps 2 to 5 until all heads are completed.

## Appendix 1.4: Surface Topography Definitions (Taken from www.predev.com)

The surface roughness parameters used in this thesis were $R_a$, $R_p$, $R_t$, $R_v$, and are defined as:

$R_a$, Roughness Average (also known as AA or CLA) is the area between the roughness profile and its mean line, or the integral of the absolute value of the roughness profile height over the evaluation length:

$$R_a = \frac{1}{L}\int_0^L |r(x)|\,dx$$

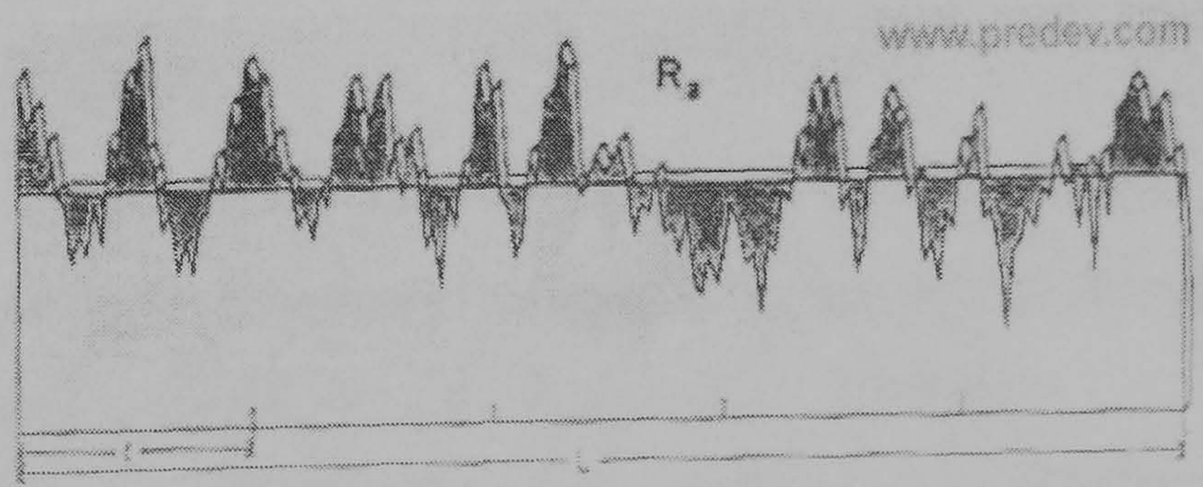

$R_p$, Peak Profile Height, is the height of the highest peak in the roughness profile over the evaluation length. Similarly, $R_v$, is the depth of the deepest valley in the roughness profile over the evaluation length.

$$R_p = |\max[r(x)]| \quad 0 < x < L$$

## Appendix 1.5: UHMWPE Wear Particle Retrieval Protocol

(Adapted from Campbell et al (1994), and Yamac (1999).

The following protocol was used to extract polyethylene wear particles from bovine serum.

1. Defrost sera.
2. Place defrosted sera into ultracentrifuge tubes to within 10 mg of each other. The tubes should be filled to a maximum of 5 mm space at the top. This is important as otherwise the tubes may collapse during ultracentrifugation.
3. Place tubes into bucket, making sure that tubes are completely dry.
4. Place the bucket in the ultracentrifuge swing-out rotor.
5. Ultracentrifuge specimens for 3 hours at 25,000 rpm at 20 °C.
6. After the initial spin, collect the top layer from each serum sample (approximately 20 ml for each sample), and place in clean a tube.

Following the collection of the PE particles from the bovine serum, the serum is digested using 5 M NaOH to aid particle separation.

7. Add an appropriate amount of NaOH pellets to the separated sera sample in order to make up 5 M NaOH solution, i.e. add 4 g of NaOH per 20 ml of sample.
8. Shake tubes gently until all the NaOH pellets have dissolved and leave at room temperature overnight.

This stage separates the PE particles from the digested sera suspension in order to finally obtain a 'clean' sample of PE on a filter to observe under SEM.

9. Place digested sera into ultracentrifuge tubes, and dilute with dW to fill tubes, balance tubes to within 10 mg of each other.
10. Ultracentrifuge samples for 3 hours at 25,000 rpm at 5-15 °C.
11. After this spin, remove the top layer and place into isopropanol/dW layers with densities of 0.96 and 0.90 $gcm^{-3}$. A small sample of PE placed in the solution can act as a marker.
12. Ultracentrifuge, as before for 2 hours at 20 °C.
13. After the spin, remove tubes and collect the interface of the two isopropanol/dW layers, this should be easy to identify, as the PE marker should indicate where the interface is.
14. Place particle suspension into clean tubes and ultrasonicate for 10-15 minutes.
15. Filter the removed suspension onto 0.1 and 0.05 μm pore size polycarbonate filters.
16. Coat with gold/carbon and view with SEM for image analysis.

## Appendix 1.6: Metal Wear Particle Retrieval Protocol

1. Centrifuge sample for 10 minutes at 16,000g
    a. Discard supernatant, pellet should remain at the bottom the tube
2. Suspend particles in 1 ml of 2.5 % Sodium Dodecyl Sulphate (SDS) in filtered dW. SDS was used as a surfactant, binding hydrophilic and hydrophobic elements within the solution, thereby removing them from the surface of metal debris.
3. Boil this solution for 10 minutes the centrifuge sample to form pellet, and discard remaining supernatant of SDS
4. Wash sample with 1 ml of 80 % Acetone and three times with 1 ml 50 mM Tris-HCl at pH 7.6 using a Phosphate Buffer (PB). This acts to modulate the pH and osmotic balance, centrifuge sample between each wash and discard supernatant.
5. Sonicate sample for a few seconds, to break up any agglomeration that may occur during centrifugation

6. Add 1.5 U of papain in 1.5 ml of PB,
7. Incubate sample for 24 hrs at 65° C
8. After incubation, centrifuge sample 10 minutes and discard supernatant
9. Resuspend pellet in 1 ml of 2.5% SDS and boil for 10 minutes, and centrifuge for 10 minutes and discard supernatant
10. Wash sample twice in 1ml of 50mM Tris-HCl (pH 7.6) and sonicate for a few seconds
    a. Centrifuge for 10 minutes and discard supernatant between each wash
11. Incubate sample with 400 µg of Protenaise K in 1 ml of Tris-HCl pH 7.6, for further 24 hrs at 55° C. Protenaise K acts to inactivate enzymatic activity within the solution and breakdown any peptide bonds.
12. Recentrifuge sample for 10 minutes and discard supernatant
13. Resuspend in 1 ml of 2.5 % SDS and boil for 10 minutes
    a. Centrifuge for 10 minutes and discard supernatant
14. Wash sample in 1 ml of 50mM Tris-HCl (pH 7.6) and centrifuge for 10 minutes and discard supernatant
    a. Once in 500 µl of 80 % acetone, this will help to dissolve and remove any remaining substances within the serum sample following enzymatic digestion
        i. Centrifuge for 10 minutes and discard supernatant
    b. And once with 1 ml of dW
        i. Centrifuge for 10 minutes and discard supernatant

Store sample in 100 % ethanol at 4°C

## Appendix 1.7: Protocol for Image Analysis using Image-Pro Plus V4

1. Load image from stored file.
2. Before any analysis is carried out the image must be calibrated for the correct units of measurements.
3. Once the image is loaded, Zoom in on the size indicator on the SEM image.

4. Go to *Measure→Calibration→Spatial*
5. The Spatial icon should now appear on the screen.
6. If this is a new calibration step, click on the *New* icon.
7. Select your units of measurements (for most SEM images this is usually in μm)
8. After this click *Image*
9. A line should now appear on screen. Drag the endpoints of the line across the size indicator on your image making sure that the line is completely straight and then click *OK* and *OK* again. Once this is done the analysis process can begin.
10. Isolation is best done in a binarised image. To do this go *to Edit→Convert to→Greyscale 8*. Greyscale 8 is enough to binaries the image for particle isolation.
11. Once converted go to *Process→Threshold.*
12. Adjust the scale of the threshold level (0-255) to the desired scale by comparing with the original image to obtain the optimum particle size.
13. Once the borders of the particle have been resolved, click Apply Mask and then Close.
14. Go to *Measure→Count/Size*
15. Select *Edit→Draw/Merge objects*
16. The *Trace* bar icon should now appear on the screen.
17. Click on the *Wand* icon. This will enable you to draw a border round the particle simply by clicking the left then the right mouse when the mouse arrow is over the particle that is to be highlighted. When this is done a green border should appear around the perimeter of the particle.
18. Once all the particles have been selected click *OK* on the *Draw/Merge* bar.
19. Particles which are combined with dark areas of the image may sometimes merge when the image is binarised. In this case a trace outline perimeter can be drawn in by clicking on the *Wand* icon once.
20. If two particles are combined together or too close, a *Split Object* option is available. For this go to *Count/Size→Edit→Split Object*. Then draw a line where the split should be by comparing with the original image, once the line is drawn click on the right mouse button.
21. After particle selection is complete click on *Measure→Select Measurements*.

22. A window will now appear containing a list of measurement parameters, click on the required parameters for your purposes.
23. For particle extraction select: Area
    Length
    Width
    Roundness
    Perimeter
    Aspect Ratio
    Diameter
24. Once selected, click *Measure* then *OK*
25. To view data, go to *View→Measurement Data.*
26. All the required should now be displayed in a table format. This data can be saved in 3 formats, Excel, ASCII or Lotus.
27. To save the data go to *File→Data to File*, give the file a name and click ok.

Parameters defined:
(http://support.mediacy.com/answers/showquestion.asp?faq=36&fldAuto=346)

Area: Reports the area of each object

Perimeter: Measurement to report the length of the outline of the highlighted object

Roundness: Reports the roundness of each object, as determined by the following formula:

$$Roundness = \frac{Perimeter^2}{4 \times \pi \times Area}$$

Circular objects will have a roundness = 1; other shapes will have a roundness > 1.

Diameter: Reports the average length of the diameters measured at two degree intervals joining two outline points and passing through the centroid.

Aspect Ratio: Reports the ratio between the major axis and the minor axis of the ellipse equivalent to the object (i.e., an ellipse with the same area, first and second degree moments), as determined by Major Axis/Minor Axis.

# Appendix 2 Papers & Abstracts

**Bowsher, J. G., Hussain, A., Williams, P., Nevelos, J., Shelton, J. C.** Effect of ion implansttion on the tribology of metal-on-metal prostheses. *J. Arthroplasty*, Vol. 19, No. 8, 2004

**Bowsher, J. G., Hussain, A., Nevelos, J., Grootveld, M, Shelton, J. C.** The importance of head diameter in minimising metal-on-metal hip wear. *Paper pending*

**Bowsher, J. G., Hussain, A., Elfick, P. D., Green, S. M., Shelton, J. C.** 'Severe' patient activity simulation substantially increased the number of submicron-sized wear particles in XLPE-on-metal hip bearing study. *Abstract in Press*

**Bowsher, J. G., Hussain, A., Williams, P. A., Nevelos, J., Shelton, J. C.** 'Severe' patient activity simulation substantially increased wear particle surface area in metal-on-metal hip bearing study the number of submicron-sized wear particles in XLPE-on-metal hip bearing study. *Abstract in Press*

**Bowsher, J. G., Hussain, A., Williams, P. A., Nevelos, J., Shelton, J. C.** $N_2$-ion implantation showed no reduction in running-in wear for metal-on-metal hip bearings. *Abstract in Press*

**Bowsher, J. G., Hussain, A., Williams, P. A., Nevelos, J., Shelton, J. C.** Larger head diameter have the potential to reduce ion release in metal-on-metal hip wear simulations. *Abstract in Press*

The Journal of Arthroplasty Vol. 19 No. 8 Suppl. 3 2004

# Effect of Ion Implantation on the Tribology of Metal-on-Metal Hip Prostheses

John G. Bowsher, PhD,*† Azad Hussain, MSc,* Paul Williams, MSc,†
Jim Nevelos, PhD,‡ and Julia C. Shelton, PhD*

**Abstract:** Nitrogen ion implantation (which considerably hardens the surface of the bearing) may represent one possible method of reducing the wear of metal-on-metal (MOM) hip bearings. Currently there are no ion-implanted MOM bearings used clinically. Therefore a physiological hip simulator test was undertaken using standard test conditions, and the results compared to previous studies using the same methods. $N_2$−ion implantation of high carbon cast Co-Cr-Mo-on-Co-Cr-Mo hip prostheses increased wear by 2-fold during the aggressive running-in phase compared to untreated bearing surfaces, plus showing no wear reductions during steady-state conditions. Although 2 specimens were considered in the current study, it would appear that ion implantation has no clinical benefit for MOM. **Key words:** metal-on-metal bearing, tribology, ion implantation, wear, cobalt chrome, hip simulator.


The use of ion-implanted Co-Cr femoral heads is believed to reduce clinical wear rates of polyethylene cups by 20% [1], increase resistance of metallic surfaces against particulate polymethylmethacrylate (PMMA) bone cement abrasion [2], and reduce corrosion [3]. This process involves implanting ions (typically nitrogen) on the surface to a depth of approximately 0.2 $\mu$m. This generates a highly doped and compressively stressed layer. This also increases hardness by 30–50% in chromium alloys by precipitation strengthening [4], plus reducing friction and increasing wettability. However, to date, no ion-implanted MOM wear studies have been reported.

At present, one of the disadvantages of modern, large-diameter MOM bearings may be their high running-in wear phase [5–7], which creates an extremely high number of wear particles. While the depth of ion implantation may be thought to be small (0.2 $\mu$m) in comparison to the wear penetration of conventional MOM (20 $\mu$m) [8], it is possible that ion implantation could confer an advantage during the running-in phase. Improved wear resistance during this critical phase would be beneficial. Currently there are no ion-implanted MOM bearings used clinically.

Therefore, the aim of this wear study was to test the hypothesis that ion implantation may minimize the severity of the running-in phase for modern 40 mm MOM prostheses.

## Materials and Methods

The 2 customized MOM bearing couples were received with nitrogen ion implantation (ion energy: 92 keV, ion dose $1x10^{17}$ ions/cm$^2$) (Corin

*From the *IRC in Biomedical Materials and Department of Engineering, Queen Mary, University of London, London United Kingdom, the †Loma Linda University Medical Center Department of Orthopaedics, Loma Linda, California USA, and ‡Corin Medical, Cirencester, United Kingdom*

Benefits or funds were received in partial or total support of the research material described in this article. These benefits or support were received from Corin Ltd., Cirencester, U.K.

Reprint requests: Dr. J Nevelos, Corin Medical, The Corinium Centre, Cirencester, UK GL 7 1YJ.



0883-5403/04/1908-3021$30.00/0
doi:10.1016/j.arth.2004.09.021

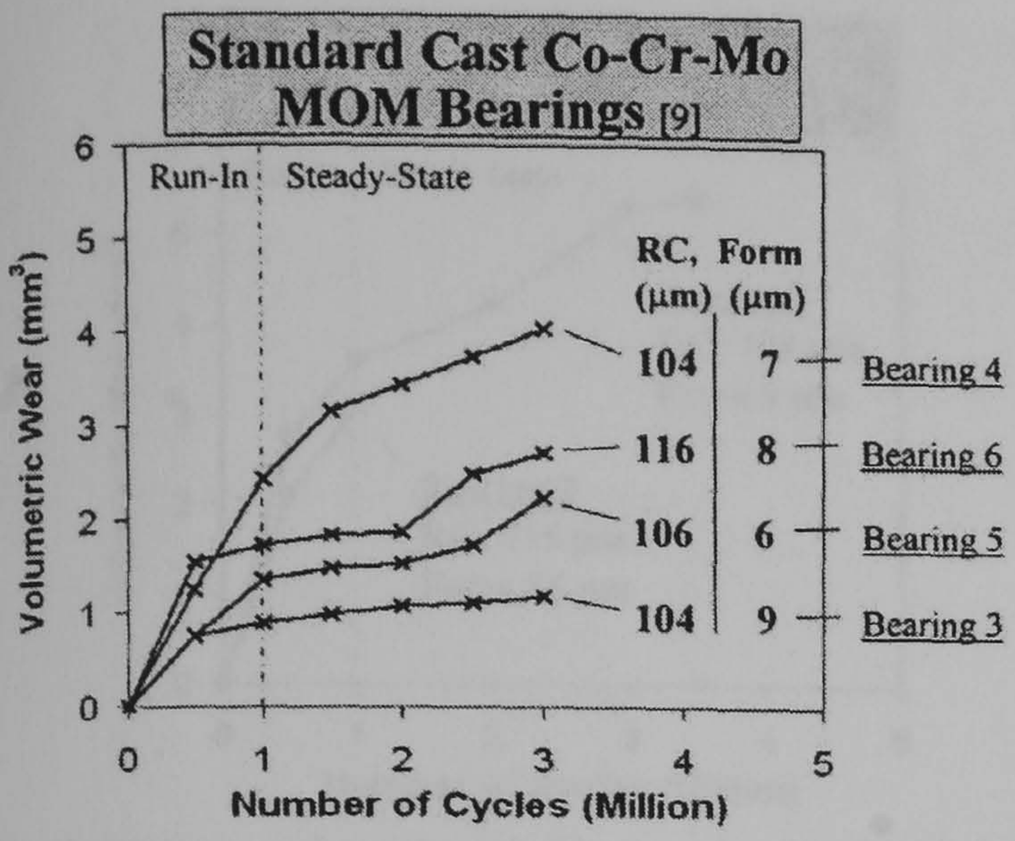


**Fig. 1.** Variation of combined (head and cup) volumetric wear versus number of cycles for running-in and steady-state wear conditions (normal walking) for the 4 "standard" cast Co-Cr-Mo (HIPed/SA) 40 mm MOM bearings [9]. RC = radial clearance, and Form = maximum deviation of sphericity.

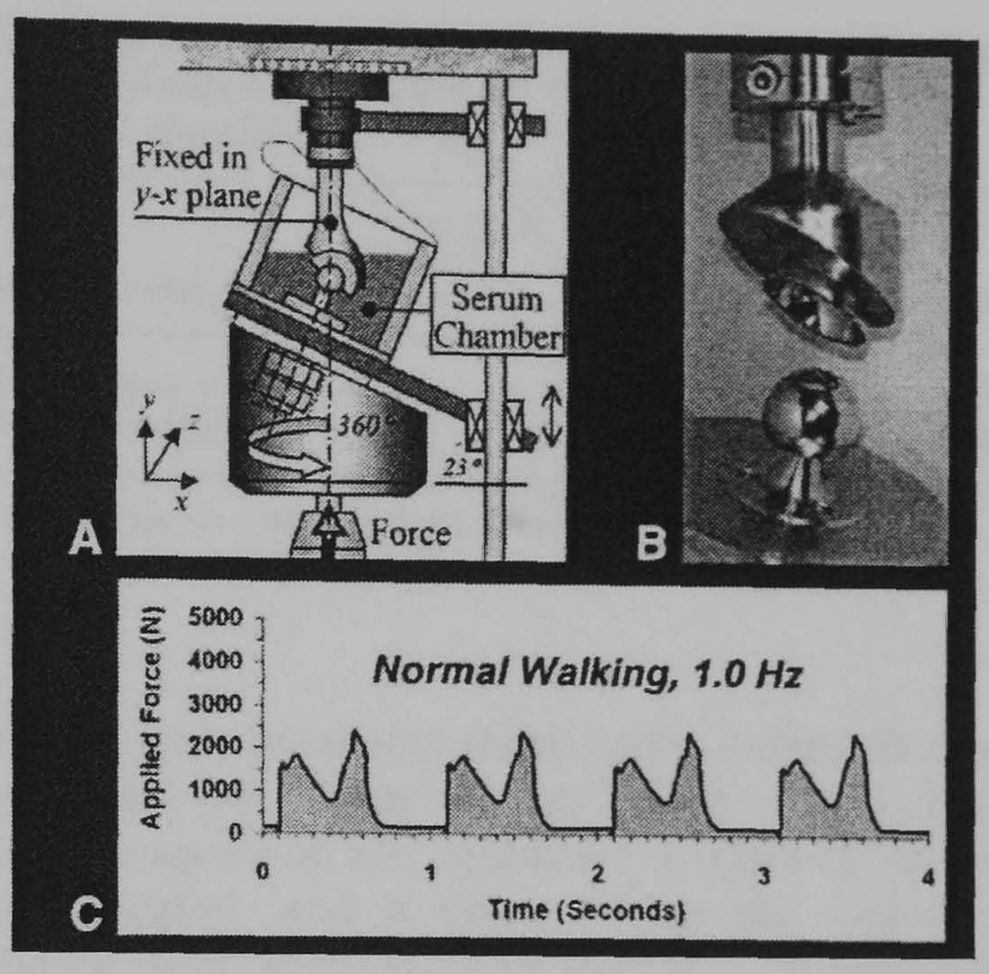


**Fig. 2.** Images showing (A) schematic of 1 test station of the MTS 8-station hip joint simulator, (B) head and cup physiological positioning (serum chamber removed), and (C) normal walking profiles timed over 4 seconds (2450 N max, 1.0 Hz).

Medical, Cirencester, UK). The depth of ion implantation was 0.2 μm. The maximum dosage of ion implantation occurred in the initial 0.1–0.15 μm (not confirmed by the authors). The wear control data was taken from our previous studies of 4 "standard" metal bearings run under matching test protocols [9] (Fig. 1). All bearings were 40 mm in diameter with similar bearing geometries (Table 1) and were manufactured from high carbon (0.3% wt) cast Co-Cr-Mo in the standard double heat-treated condition, in other words, hot isostatically pressed (HIPed) and solution annealed (HIPed/SA) (BS7252-4). The previous study demonstrated that double heat-treated bearings (with a fine carbide structure) had equivalent wear performance to "as cast" bearings under standard and severe test conditions [9]. The radial clearances in this study were just over 100 μm and were selected in an attempt to exaggerate potential differences in wear rates between the 2 groups.

An 8-station orbital hip simulator was used with all cups inclined physiologically at 35° to the horizontal (MTS Systems, Eden Prarie, MN; Fig. 2). The lubricant was 25% newborn calf serum (Sigma UK, C-6278), with a protein content of approximately 17 mg/ml. The serum test volume was 500 ml, and the chambers were maintained to 37°C, and the serum was changed every .5 million cycles. Sodium azide was added as an antibiotic (1 g/litre of sera) [10].

**Table 1.** Identity Numbers and Bearing Geometries for All Test Specimens (Ranked from Lowest to Highest Radial Clearance in Each Group)

| Bearing Identity Number | MOM Bearing Type | Radial Clearance (μm) | Maximum Deviation of Sphericity (μm) |
|---|---|---|---|
| 1 | Ion implanted | 108 | 9 |
| 2 | Ion implanted | 115 | 14 |
| | | Maximum = 115 | Maximum = 14 |
| 3 | Standard | 104 | 9 |
| 4 | Standard | 104 | 7 |
| 5 | Standard | 106 | 6 |
| 6 | Standard | 116 | 8 |
| | | Maximum = 116 | Maximum = 9 |

Abbreviation: MOM, metal-on-metal.

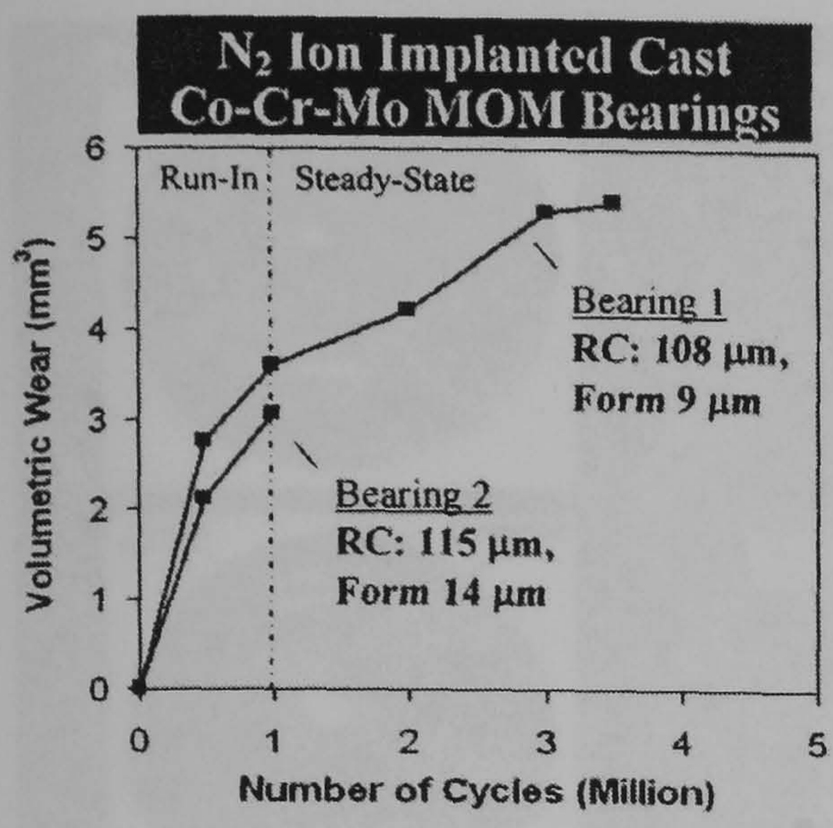


**Fig. 3.** Variation of combined (head and cup) volumetric wear versus number of cycles for running-in and steady-state wear conditions (normal walking) for the 2 ion-implanted (HIPed/SA) cast Co-Cr-Mo 40-mm MOM bearings.

Wear was calculated gravimetrically every 0.5 million cycles using an analytical balance (Precisa UK, 925M-202A/0.01 mg), and was adjusted using 7 control Co-Cr balls. All surfaces were cleaned using lint-free cloths and propan-2-ol prior to weighing. Volumetric wear rates were determined assuming a density of 8300 kg/m$^3$ for the Co-Cr-Mo alloy.

The ion implanted bearings were subjected to 1.0 million cycles of normal physiological walking (2450 N max, 1 Hz) to quantify running-in wear. Ion-implanted bearing 1 (IIB-1) was subjected to a further 2.5 million cycles of normal walking to measure steady-state wear conditions. All control MOM bearings were run to 3 million cycles of normal walking (Fig. 2C) [11]. Regression analysis was used to calculate average wear rates, and analysis of covariance (ANCOVA) was used to compare groups and calculate the level of significance.

Following all wear tests, the surface roughness of the heads and cups of IIB-1 and 1 control MOM bearing were measured (Surftest SV-400 profilometer, Mitutoyo, Japan; cut-off length of 0.4 mm). Each component was measured 4 times in an unworn region, and 6 times within the region of highest wear. Wear surfaces were also examined by scanning electron microscope (SEM).

**Table 3.** Summary of Statistical Comparisons for Ion-Implanted and Standard (Control) Co-Cr-Mo Specimens for Each Wear Condition

| | Total N | | | |
|---|---|---|---|---|
| Wear Condition | Ion Implant | Std | P value | Power |
| [A] Running-In | 6 | 12 | .003 | N/A |
| [B] Steady-State | 4 | 20 | .51 | 0.10 |

Abbreviation: Std, standard deviation.

## Results

All bearing couples generated a biphasic wear pattern, in other words, showing a high running-in phase followed by a reduced steady-state condition (Figs. 1, 3). The ratio of running-in versus steady-state was approximately 4:1 for both bearing groups (Table 2). Under running-in conditions, the 2 ion-implanted bearings showed a 2-fold increase in wear compared with the "standard" (control) bearings ($P$=.003; Tables 2 and 3). Under steady-state conditions, the ion-implanted bearings showed a 70% increase in wear rate compared with the untreated (control) bearings, but this difference was not statistically significant ($P$=.5; Tables 2 and 3).

A visual examination of the ion-implanted specimens after the initial 500,000 cycles of testing showed that a large proportion of the "black" ion-implanted surfaces wore off both head and cups, leaving a "silver" surface (Fig. 4A, B). A visual difference was also observed in the formation of transfer films, with the ion-implanted bearings producing less film formation.

**Table 2.** Linear Regression Results for All Ion-Implanted and Standard (Control) Co-Cr-Mo MOM Wear Data

| | Number of Data Points | | Slope (mm$^3$/10$^6$ Cycles) | | 95% Confid. Interval (% of Slope) | | $r$ value | |
|---|---|---|---|---|---|---|---|---|
| Wear Condition | Ion Implant | Std | Ion Implant | Std | Ion Implant | Std | Ion Implant | Std |
| [A] Running-In | 6 | 12 | 3.30 | 1.61 | 44.8 | 43.2 | 0.95 | 0.85 |
| [B] Steady-State | 4 | 20 | 0.78 | 0.46 | 49.9 | 134.1 | 0.99 | 0.35 |
| Running-In/Steady-State Ratio | | | 4.2 | 3.5 | | | | |

Abbreviation: Std, standard deviation.

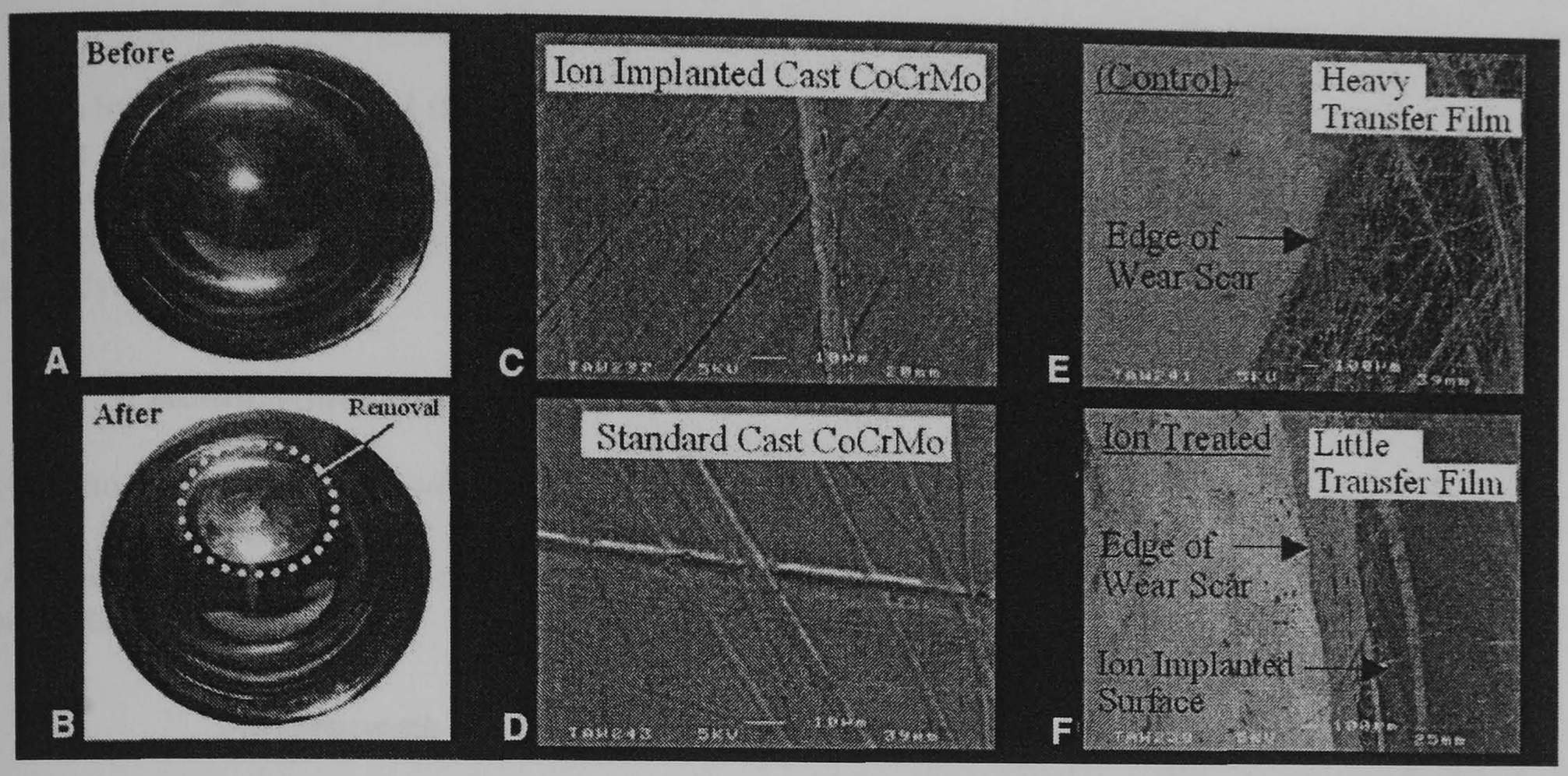


**Fig. 4.** Images of wear surfaces showing (A) ion-implanted test cup before testing, (B) ion-implanted test cup after the initial half-million cycles of walking, showing removal of the ion-implanted surface (center) following wear, (C) typical ion-implanted cast Co-Cr-Mo wear surface under SEM, showing polishing and abrasion, (D) typical "standard" (control) cast Co-Cr-Mo wear surface under SEM, showing large-scale polishing wear and abrasion, (E) transfer film buildup for (control) standard MOM bearings, and (F) little or no transfer film buildup for ion implanted bearings.

SEM examinations of all ion-implanted and control Co-Cr-Mo wear surfaces showed large polished zones interspersed with scratches (2–10 $\mu$m in width; Fig. 4C, D) . SEM images also confirmed a reduced film formation at the edge of the wear scar for the ion-implanted bearings compared with the control specimens (Fig. 4E, F) . The composition and properties of these transfer films were not investigated.

Following 3 million cycles of wear testing, the ion-implanted bearings showed a reduced surface roughness range (roughness range [$R_A$] and peak profile height [$R_p$]) compared with the control bearings (Table 4).

## Discussion

Although only 2 specimens were considered in the current study, the results suggest that the introduction of nitrogen ion-implanted modified surfaces offered no reduction in volumetric wear compared with "standard" untreated Co-Cr-Mo bearing surfaces during the running-in phase, or during steady-state conditions. Our results suggest that surface modification of MOM bearings by ion implantation may offer no clinical benefit. A large proportion of the modified surface coating appeared to have worn off in the initial half-million cycles. The depth of ion implantation (typically 0.2 $\mu$m) may have been too small in comparison to the potential running-in wear penetration of MOM prostheses (25 $\mu$m) [8]. While ion implantation may be favorable for Co-Cr-Mo surfaces articulating against ultra-high-molecular-weight polyethylene [1], the benefits for all-metal contact systems was not established.

Because both the ion-implanted bearings possessed similar geometrical tolerances to the control bearings, the cause of their higher running-in wear condition is unknown. The greater wear apparent with ion implantation could be due to less transfer film formation, thereby causing a worse boundary condition.

Following hip simulator testing, all wear surfaces created in the current study showed similar patterns and processes to those observed clinically [12] and in previous laboratory investigations of Co-Cr-Mo bearings [5,13].

**Table 4.** Surface Roughness Range (Head & Cup) of Ion-Implanted and "Standard" (Control) MOM Bearings After 3 Million Cycles of Wear Testing, Describing Both Unworn and High-Wear Regions

| | Unworn Regions | | High-Wear Regions | |
|---|---|---|---|---|
| Roughness | Ra (nm) | Rp (nm) | Ra (nm) | Rp (nm) |
| Ion-Implanted | 5–30 | 10–30 | 7–25 | 10–90 |
| Standard (Control) | 17–37 | 10–40 | 13–286 | 10–360 |

## Conclusion

Nitrogen ion implantation of the surfaces of high carbon cast Co-Cr-Mo on Co-Cr-Mo alloy hip prostheses showed no reduction in wear compared with untreated bearing surfaces under any test condition in this study.

## Acknowledgments

The authors gratefully acknowledge the Wishbone Trust for financial support and Corin Medical Ltd (Cirencester, UK) for the supply of the test components.

## References

1. Maruyama M, Capello WN, D'Antonio JA, et al: Effect of low-friction ion-treated femoral heads on polyethylene wear rates. Clin Orthop 370:183, 2000
2. McKellop HA, Rostlund TV: The wear behaviour of ion-implanted Ti-6A1-4V against UHMW polyethylene. J Biomed Mater Res 24:1413, 1990
3. Rieu J, Pichat A, Rabbe LM, et al: Ion implantation effects on friction and wear of joint prosthesis materials. Biomaterials 12:139, 1991
4. Onate JI, Alonso F, Garcia A: Improvement of tribological properties by ion implantation. Thin Solid Films 317:471, 1998
5. Chan FW, Bobyn JD, Medley JB, et al: Engineering issues and wear performance of metal on metal hip implants. Clin Orthop 333:96, 1996
6. Bowsher JG, Hussain A, Nevelos J, Shelton JC: The importance of head diameter in minimising metal-on-metal hip wear. Trans 50th Orthop Res Soc 29: 1453, 2004
7. Clarke IC, Good V, Williams P, et al: Ultra-low wear rates for rigid-on-rigid bearings in total hip replacement. Proc Inst Mech Engrs 214:331, 2000
8. Sieber HP, Rieker CB, Kottig P: Analysis of 118 second-generation metal-on-metal retrieved hip implants. J Bone Joint Surg Br 81:46, 1999
9. Bowsher JG, Nevelos J, Pickard J, Shelton JC: Do heat treatments influence the wear of large diameter metal-on-metal hip joints? An i*n vitro* study under normal and adverse gait conditions. Trans 49th Orthop Res Soc 28:1398, 2003
10. McKellop HA, Clarke IC: Degradation and wear of ultra-high-molecular-weight polyethylene. Corrosion and degradation of implant materials. In Fraker AC, Griffin CD, (eds): Second Symposium, ASTM STP 859, ASTM, West Conshohocken, PA, 1985
11. Paul JP: Forces transmitted by joints in the human body. Proc I Mech Engrs [H] 181:8, 1966
12. McKellop H, Park SH, Chiesa R, et al: *In vivo* wear of 3 types of metal on metal hip prostheses during 2 decades of use. Clin Orthop 329(Suppl):S128, 1996
13. Scholes SC, Green SM, Unsworth A: The wear of metal-metal total hip prostheses measured in a hip simulator. Proc I Mech Engrs [H] 215:523, 2001

*Clinical Orthopaedics and Related Research*

Title of manuscript (80 spaces)

# The Importance of Head Diameter in Minimising Metal-on-Metal Hip Wear

Running title (40 spaces)

**Importance of Diameter in Metal Hip Wear**

John G. Bowsher, PhD [1]
Azad Hussain, MSc [2]
Jim Nevelos, PhD [3]
Martin Grootveld, PhD [4]
Julia C. Shelton, PhD [2]

1. Department of Orthopaedics, Orthopaedic Research Center
Loma Linda University, 11406 Loma Linda Drive
California 92354, USA

2. The IRC in Biomedical Materials and Department of Engineering
Queen Mary, University of London
London, E1 4NS, UK

3. Corin Medical, Cirencester, UK

4. Barts and The London School of Medicine and Dentistry
Whitechapel, London, UK

Please address all correspondence to:

Dr. Julia C. Shelton
The IRC in Biomedical Materials and Department of Engineering
Queen Mary, University of London
Mile End Road, London, E1 4NS
United Kingdom

Phone: (44) 020-7882-5272
FAX: (44) 020-8983-1799
Email: j.shelton@qmul.ac.uk

## Abstract (200 WORDS)

The clinical benefits of further minimising wear debris and ion release in metal hip arthroplasty are exceptional. As well as low radial clearances, low surface roughness and high carbon content, bearing wear can also be minimised using larger head diameters. However, the full practical advantages of larger head sizes has yet to be demonstrated, especially under more aggressive gait activities where lubrication films breakdown. As such conditions can be a part of everyday life in young and active patients, more research is needed to improve clinical predictions. Therefore, a hip simulator study was commissioned to investigate: using twenty 28, 40 and 56 mm Co-Cr-Mo bearings, under standard and severe gait simulations, including fast-jogging. The results agreed with previous studies showing considerable reductions in volumetric wear with increasing head diameter or equivalent radius. In addition, our results showed that the greater the gait activity simulated, the more reductions in wear could be achieved by using a 56 mm bearing instead of a smaller size. Therefore, 56 mm bearings with low radial clearances offer the highest possible wear resistance for all patient types. Conversely, our study showed that large bearings with radial clearances greater than 80 μm can lead to excessive wear during both running-in and severe gait events.

## 1. Introduction

Modern metal-on-metal (MOM) hip replacements potentially offer less periprosthetic bone resorption and lower rates of revision surgery compared to traditional polyethylene-based implants[1,2,3], and as a result, are seeing rapid growth worldwide. The use of all metal surfaces facilitates larger head sizes (>32 mm), which importantly reduces volumetric wear release[4,5,6,7,8], dislocation[9,10] and stress shielding[1], plus increasing the range of joint movement without impingement. In addition, larger head sizes are also ideal for bone preservation techniques like resurfacing, which is showing excellent clinical success without the use of ultra-high molecular weight polyethylene (UHMWPE)[1,11,12,13]. Currently, modern large diameter metal-on-metal hip bearings are considered to be an attractive solution for young and demanding arthroplasty patients[1,11,13,14,15], especially those wishing to rerturn to more aggressive levels of activity or sports.

Although it is clear that larger diameter Co-Cr-Mo bearings offer many potential benefits, there still remain many unanswered questions concerning their ultimate long-term clinical success (>30 years) and design optimisation. Firstly, modern MOM bearings can still release $10^{12}$ to $10^{14}$ nanometer sized metal wear particles into the body each year[16,17,18], giving rise to sizable increases of cobalt and chromium levels in the body[19,20,21]. So far the number of reactions to such particles is minimal compared to the number of joints implanted[3,14,15,16]. However, recent studies are reporting positive correlations of biological responses to Co-Cr-Mo particles, which potentially include cytokine generation[23,24,25], systemic cell toxicity[17,26], and hypersensitivity[27]. Therefore, if MOM bearings are to be more widely implanted, especially in young and demanding patients, then efforts should be made by both engineers and surgeons to further reduce wear debris release. Secondly, the topic of head diameter has only seen few laboratory wear studies[28,29,3,6,7], typically with low numbers of test specimens. A recent simulator study by Smith et al[7] reported lower wear for 36 mm bearings compared to 28 mm's, however, low numbers of components were used, plus a simplified continuous steady-state walking model was adopted, which may itself induce sizable inaccuracies in terms of predicting joint failure for a wide range of patients[30,31]. Although there is a consensus that larger bearing sizes provide lower steady-state wear rates, (also predicted by lubrication theory)[5,8], there still remains little practical knownledge of its wider influence. Importantly, there is a lack of knowledge of the effect of head diameter on 1) running-in wear, 2) wear particle sizes, and 3) wear under more aggressive gait conditions where lubrication films breakdown:

1) Most modern artificial hip joints typically undergo a running-in phase, i.e. showing higher initial wear, and is caused by the early removal of surface asperities (polishing) and corrections in sphericity[4,29,31]. As well as obvious factors like surface roughness, bearing sphericity and hardness, running-in wear will also be influenced the resulting mode of lubrication (lambda value). However, the influence of head diameter or equivalent radius on this process has yet to be fully explored. For example, in the case of 28 mm MOM bearings (Metasul etc), the ratio of running-in (RI) wear to steady-state wear (SS) is typically 3:1[18,31,32], however, early studies by Chan et al[29], albeit using a high protein serum, reported a RI/SS ratio of 13:1 for 45 mm bearings, and suggests greater running-in wear for larger diameter bearings. As the size of the wear scar is proportional to head diameter, it is therefore possible that larger head sizes may generate higher running-in wear due to larger polishing areas. Conversely, a recent study by Goldsmith et al[6] reported a much lower RI/SS ratio of 3:1 for 36 mm bearings (matching 28 mm sizes), and therefore casts doubt on the above hypothesis. To date, it is not clear whether its just larger head diameters >36 mm that generate higher running-in wear, or just other factors like having large radial clearances etc.

2) With regards to MOM wear debris, there still remains poor knowledge of the parameters that influence wear particle sizes, especially factors like head diameter and radial clearance. Since artificial joints fail due to wear particles sizes and not volumetric wear rates[17], knowledge of wear particle sizes and their changes in concentration is inherently critical in predicting ultimate biocompatibility[17,18], and requires more research. Recent hip simulator wear studies by Firkins et al[32], Fisher et al[18], Catelas et al[33] and have all reported mean or modal Co-Cr-Mo wear particle sizes of 25, 30 and 65 nm respectivly for modern MOM bearings, thereby demonstrating that Co-Cr-Mo particles are significantly smaller than traditional UHMWPE particles, and importantly out of the bioactive range of 0.1 to 10 μm for stimulating macrophages[34]. Clinical studies by Doorn et al[16] of retrieved

periprosthetic tissue in metal-metal patients also reported smaller sized Co-Cr-Mo wear particles (mean 81 nm), however, their study also showed that mean Co-Cr-Mo particle sizes can also be as high as 192 nm. Soh et al[35] and Shahgaldi et al[36] have also reported larger Co-Cr-Mo particles up to 4000 nm in size in retrieved tissue, however, such large particles are rarely reported in hip simulator tests. In addition, most metal particles once released in the body are subjected to corrosion, and therefore reduce in size[36,16]. Therefore the large Co-Cr-Mo particles reported by Doorn et al[16] may very well have been previously bigger, thus casting further doubt on early laboratory results (mean 25 nm)[32]. A closer look at Doorn et al's data[16] also suggested that smaller 28 mm bearings (Metasuls) generally produced larger wear particle sizes (mean 120 nm) compared to those from larger 45 mm McMinn prostheses (mean 60 nm). This result has yet to be confirmed in laboratory testing, however, it is likely that an improved lubrication regime would lead to a finer polishing action, and thus smaller particles. Again, more research of the factors influencing the size, surface area and concentration of metal particles is needed. Once understood, bioactivity may be further reduced by simply chosing appropriate bearing gemotery.

3) A study by Chan et al[37] reported a 2-fold increase in metal-metal wear for 45 mm bearings under intermitant loading, and immediately suggested that larger diameter MOM bearings are sensitive to changes in kinematics and mechanics. More recent studies by the authors[38] using more aggressive gait activity simulations have shown that in fact the wear of 40 mm HC MOM bearings can increase by as much as 10-fold under activites like fast-jogging (1.75 Hz, 4500 N max), indicating a sizable breakdown in mixed lubrication. Importantly, such high increases in wear may explain why clinical wear rates of modern MOM (1.2–6 $mm^3$/year)[39] are typically 2–3 times greater than simplistic simulator data[32]. Although others factors like scratched surfaces[40], greater eccentric wear paths[32], and micro-separation[41] also contribute to higher clinical wear, it is still believed however that gait activiy is the overriding factor. Even though the volumetric wear generated under fast-jogging for the 40 mm MOM bearings was much smaller in comparison to the wear of moderately UHMWPE under similar conditions[30], such large increases in Co-Cr-Mo wear can however lead to massive increases in the total surface area for all wear partticles, causing elevated ion release. As classical elastohydrodynamic lubrication theory predicts that even larger diameter bearings (>40 mm) may offer superior wear, there is therefore, great potential for much larger diameter MOM bearings to generate minimal wear for active patients. On the other hand, as boundary wear is proportional to sliding distance, larger bearings (>40mm) could give rise to increased wear rates under excessive gait conditions simply due to increased asperity contact. Increased surface contact may also influence wear particle sizes, again increasing ion release. However, such tests have yet to be undertaken. If metal resurfacing joints are to be widely used for demanding patients, then it is therefore necessary that laboratory tests account for such conditions, as it is very possible that alternative materials and novel coatings may offer further reductions in wear particle release under these higher adverse environments.

Therefore to date, the full practical advantages and suitability of larger MOM head sizes (>32 mm) for all patient types and activity levels have not been demonstrated. Therefore, the aim of this investigation was to investigate the wear of 28, 40 and 56 mm bearings under both normal and severe gait conditions, using a realistic hip joint simulator and a relevant biological lubricant. Detailed analysis of wear particles and wear patterns were also considered and compared to clinical data. Wear predictions at 40 years were determined for a range of patients types to aid in improving prosthesis selection.

## 2. Materials and methods

### *2.1. Metal-on-Metal Hip Bearings*

A total of 18 bearing couples were supplied from a UK orthopaedic company (Corin Medical, Cirencester, UK), which included four 28 mm, ten 40 mm, and four 56 mm diameter MOM hip joints [Figure 1(a)]. All bearings were manufactured from high carbon (HC) (0.2–0.35 % wt) cobalt chrome molybdenum alloy (cast $CoCr_{30}Mo_6$ alloy to BS7252-4 (ASTM F75-92)) in the standard double heat-treated condition, i.e. hot isostatic pressed (HIPed) and solution annealed (SA). Metallurgical analysis showed that the grain size on the articular surfaces ranged from 30 to 1,500 μm, [Figure 1(b)]. Surface carbides in the form of $M_{23}C_6$ (1 to 10 μm in size) were evident on all articular surfaces, typically in chain formations, which were either precipitated within grains or at grain boundaries [Figure 1(b)]. The mean radial clearances for all 28, 40 and 56 mm bearings were: 42 μm (range 35–53 μm), 119 μm (range 104–144 μm), and 142 μm (range 131–149 μm) respectively. The mean equivalent radius $R$ (m), $[R = (R_1R_2)/(R_2-R_1)]^8$ for the 28, 40 and 56 mm bearings was: 9.6, 6.7 and 11.0 m respectively. For all components, the initial articular surface finish $S_a$ was 0.05 μm, and the maximum deviation of sphericity ranged from 3 to 13 μm. The acetabular cups were custom machined with a location spigot on their back periphery to enable adequate fixation during severe-impact wear testing [Figure 1(a)].

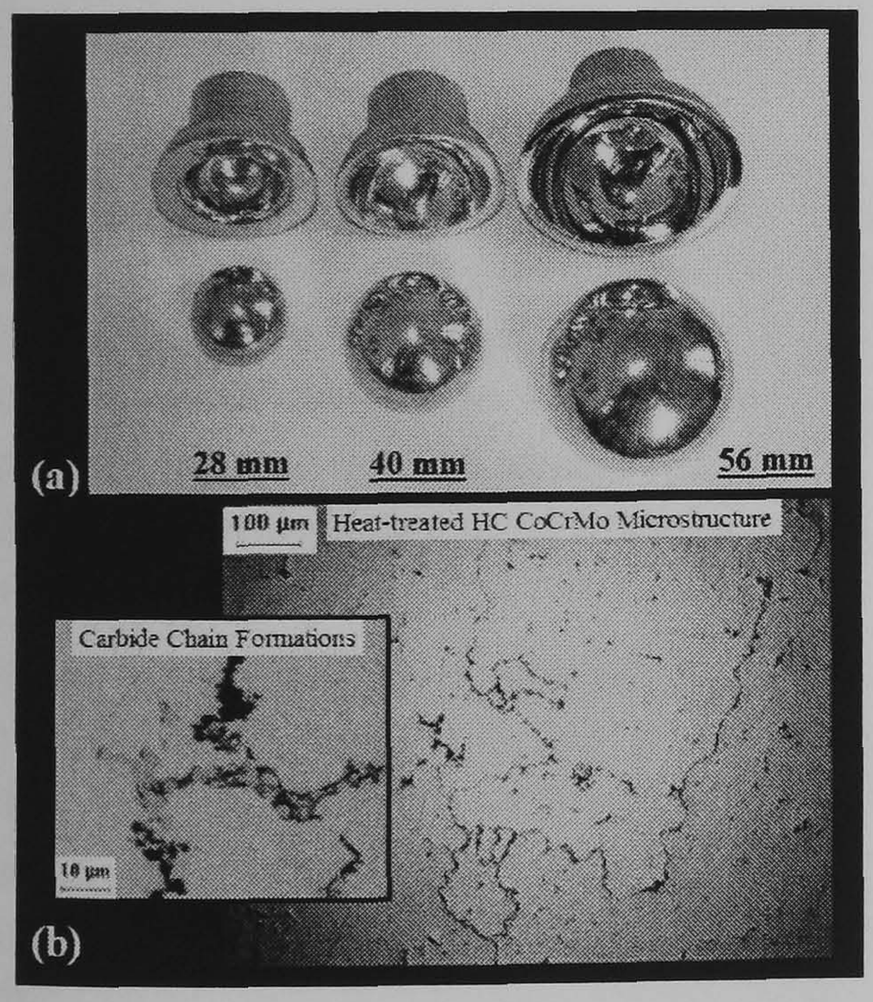


Fig. 1. Images showing (a) 28mm, 40mm and 56mm diameter HC Co-Cr-Mo test components, and (b) light-microscopy images of micro-etched HC HIPed/SA Co-Cr-Mo articular surfaces – showing grain structure and chain carbide formations. Etching involved lactic acid, HCL and $HNO_3$.

*2.2. Experimental Methods*

All wear tests were performed using an electro-hydraulic 8-station hip joint simulator (MTS Systems, USA) [Figure 2(a)]. The simulator applies a ±23° biaxial-rocking motion to represent the flexion/extension and adduction/abduction movements of the femur during ambulation [Figure 2(b)], which importantly creates a similar cross-shear and wear condition to that of the natural hip joint[42,43]. This type of simulator has been previously described in detail[30,38], and successfully used in many MOM hip wear studies[29,37,42,31,44]. The average sliding distance travelled per cycle for this type of hip simulator is 1.045D (or 29 mm for a 28 mm femoral head)[42], which is approximately 1.5 times larger than that travelled by the natural hip joint, i.e. 0.67D (or 19 mm for a 28 mm femoral head)[42,43]. However, all wear data presented in the current study has not been corrected for having a longer sliding distance (see Section 4).

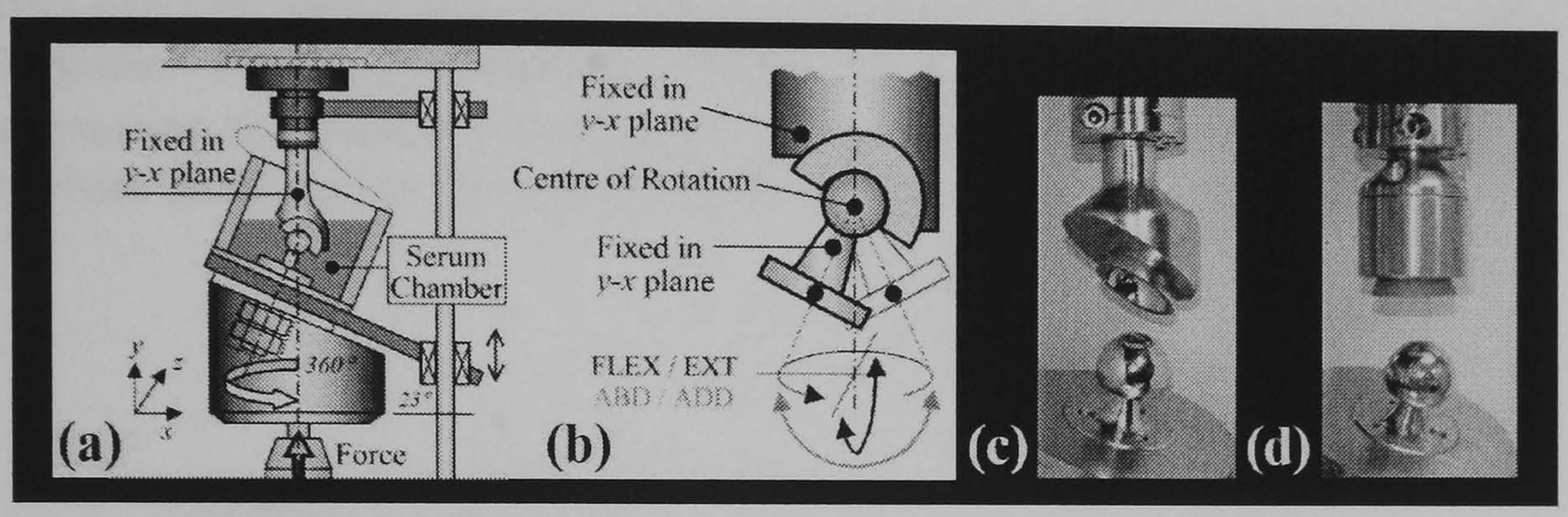


Fig. 2. Pictures of MTS 8-station hip joint simulator showing (a) machine layout, (b) definition of biaxial-rocking motion, (c) physiological positioning with superiorly inclinded cup (4x 40mm bearings only), and (d) physiological positioning with horizontal cup.

A bovine-serum lubricant system (Sigma UK, C-6278) was used for all wear tests following dilution to 25 % with 0.2 μm filtered deionised water to create a 20 mg/ml protein content sera (pH 8.0), similar to that of regenerated human synovial fluid[45,46]. No EDTA was added in view of the low calcium content; however, sodium azide was added (1 g/litre of sera) to retard bacterial degradation[47]. The lubricant was heated to approximately 37 °C during all tests, and was changed every 0.5 million cycles to help maintain properties. Lubricant volumes were maintained at 500 ml by adding 25% diluted serum.

Wear was calculated gravimetrically using an analytical balance (Precisa UK, 925M-202A/0.01 mg), and was corrected using seven controls. Test components were measured every 0.5 million cycles, or at the end of each jogging session, which involved dismantling fixtures, cleaning (including removal of all protein films), drying and weighing. Volumetric changes were determined assuming a density of 8.3 mg/mm$^3$ for the Co-Cr-Mo alloy, and all wear results were extrapolated to mm$^3$/10$^6$ cycles.

The test specimens were divided into two groups. Group one consisted of four 28 mm and four 56 mm bearings, and group two consisted of ten 40 mm bearings. Initially, all components in groups 1 and 2 were subjected to 6 and 3 million cycles of standard walking respectively, to generate steady-state wear conditions. The loading profile used for simulating normal walking (1 Hz) was based on the Paul curve[48], and was adjusted to a maximum and minimum compressive force of 2450 N and 50 N respectively to match similar studies [Figure 3(a)]. During testing, all bearing couples were positioned physiologically, i.e. cup above a moving femoral head, thereby creating similar *in vivo* wear conditions. Five 40 mm cups were superiorly inclinded at 35° to the horizontal [Figure 2(c)], with all other 40, 28 and 56 mm cups being mounted horizontally [Figure 2(d)]. Silicone seallant was used to seal mating fixturing surfaces to prevent contamination.

Following all walking tests, both groups were then subjected to one million cycles of simulated fast jogging at 1.75 Hz. The loading profile used for simulating fast jogging was based upon previous data by Bergmann et.al[49], and consisted of a one-peak cycle with a maximum joint force of 4,500 N [Figure 3(d)]. A one-hour stationary rest period every 8,000 cycles was incorporated into all jogging tests to prevent unphysiological joint temperatures. Since all jogging tests were undertaken at an increased speed of 1.75 Hz, all jogging cycles were adjusted to synchronise the load/loci pattern per cycle, thereby ensuring that the same point on the cup received the same load vector each cycle. Following random normal walking and fast jogging tests, samples of used bovine serum were collected and immediately frozen to –23 °C for storage prior to wear particle extraction.

After all fast jogging tests, both groups were then further subjected to one million cycles of normal walking to establish if the wear rates would then return to steady-state values. A further three million cycles of additional severe patient activities, including slow walking tests (0.62 Hz) and slow jogging tests (1 Hz) were then performed using two 28 mm, two 40 mm, and three 56 mm bearings. The loading profiles used for simulating slow walking and slow jogging were again based on the standard Paul[48] and Bergman[49] curves, but were adjusted to occur over a longer time period (Figures 3b and c), thereby synchronising the load/loci pattern per cycle. The resultant integrals $\int L\,dx$ for the four types of patient activities simulated in the current study are also listed in Figures 3a to d.

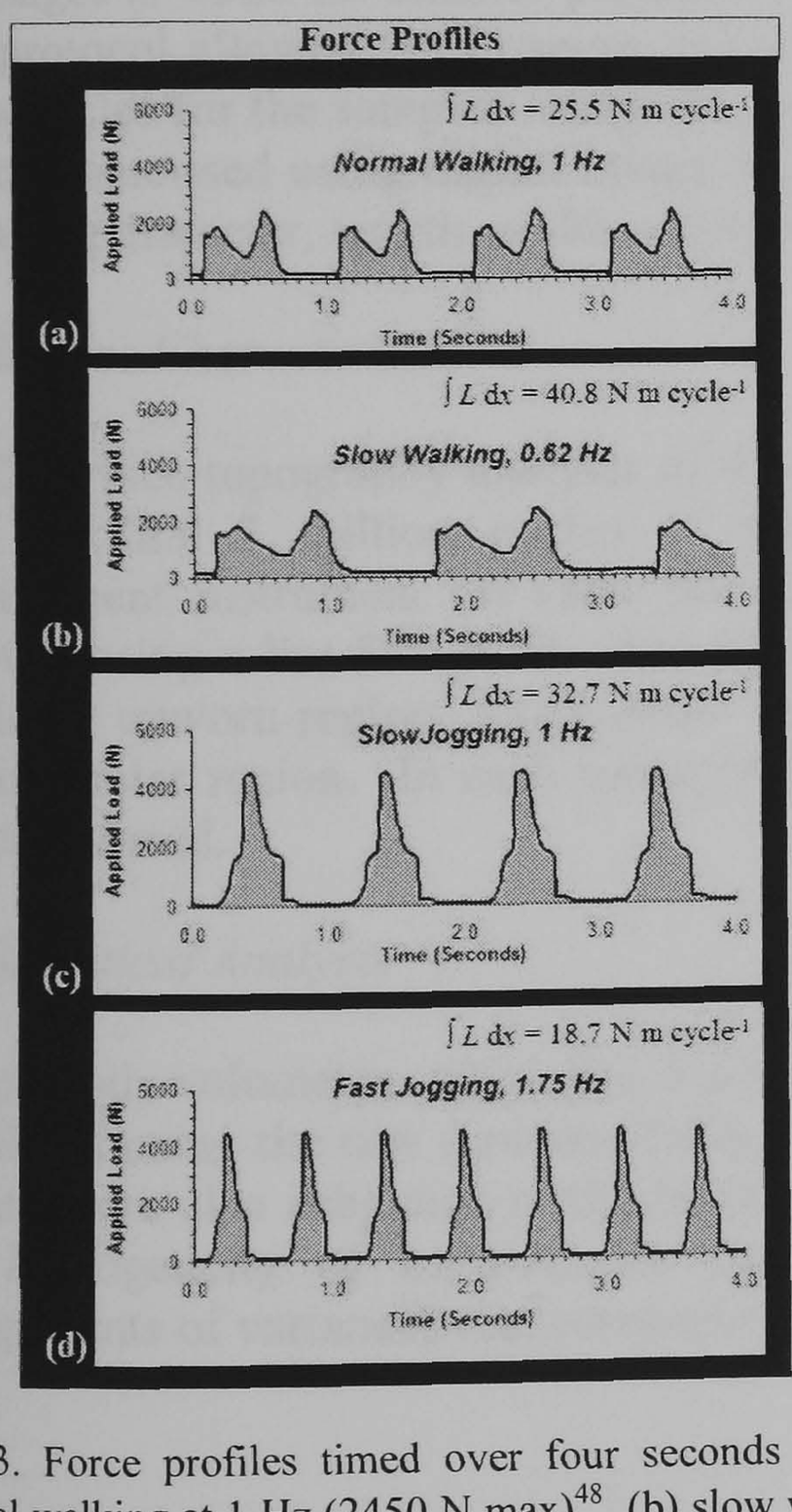


Fig. 3. Force profiles timed over four seconds for (a) normal walking at 1 Hz (2450 N max)[48], (b) slow walking at 0.62 Hz (2450 N max), (c) slow jogging at 1 Hz (4500 N max)[49], and (d) fast jogging at 1.75 Hz (4500 N max).

### *2.3. Wear Particle Extraction and Analysis*

Co-Cr-Mo wear particles were extracted and isolated from used bovine serum (BS) using a similar protocol reported by Doorn et al[16] and Catelas et al[50,33]. This enzymatic protocol has been previously shown to cause less damage to metal particles compared to the use of alkalis, such as KOH or NaOH[50]. A total of 8 BS samples were considered for analysis, and included two samples taken from separate test stations of the 28 mm, 40 mm, and 56 mm diameter prostheses following steady-state normal walking tests, and two samples from the 40 mm diameter specimens following simulated fast jogging tests, i.e. the most severe gait activity.

In brief, all samples (40 ml) were subjected to a four-loop isolation protocol, which involved centrifugation (16,000 × g), re-suspension in sodium dodecyl sulphate solution (SDS), heating, washing in acetone and a Tris-HCl solution, and incubation in 1) papain and 2) protenaise K (Sigma-Aldrich, Dorset, UK) for 24 hrs at 60°C. Prior to drying on 3 mm carbon coated copper grids for microscopy (Agar Scientific, Essex, UK), all samples were ultrasonicated to help prevent particle agglomeration. Co-Cr-Mo wear particles were then characterised using a high-resolution transmission electron microscopy (TEM, JEOL JEM 2010, Japan), operated at 200 KeV. Energy dispersive X-ray analysis (EDXA) was also used to confirm the presence of Co, Cr, and Mo particles before any photographs were taken.

The size and morphology of particles were established from digital micrographs obtained at 2 levels of magnification. For each sample, five images were obtained at ×10k for larger particles, and ten images at ×50k for smaller particles, in order to provide an overall size range of 10 to 3,000 nm. This protocol allowed the imaging of 130 or more particles per sample, with an average number of 254 particles for the samples analysed (ranging from 138 to 378 particles). Co-Cr-Mo particles were then characterised using digital image analysis software (Image Pro Plus, Media Cybernetics, USA), measuring diameter, length, width, perimeter, roundness and aspect ratio.

### *2.4. Surface Characterisation*

3D surface topography analysis of three 40 mm bearing couplings (head and cup) were measured after the first 3 million cycles of standard walking using an optical interferometric surface measurement instrument (WYKO NT 2000). Before measuring, all surface transfer films were removed using a lint-free cloth. Ten measurements per component were recorded; 3 within the mid equatorial unworn region, 3 within the upper equatorial low-wearing region, and 4 within the heavy-wearing polar region. In each measurement position, an area of approximately 0.5 mm by 0.5 mm was considered.

### *2.5. Statistical Analysis*

For both volumetric wear and wear particle data, the mean, median and standard errors were calculated using the raw (untransformed) data. However, for advanced statistical analysis, both sets of data were also subjected to the transformation of $y = \log_e(x)$ to satisfy assumptions of normality and homogeneity of intra-sample variances, and a one-way analysis of variance (ANOVA) (components of variance) was conducted, with $p<0.05$ as the level of significance.

## 3. Results

### *3.1. Running-In Wear - Standard Walking Tests*

Figure 4(a) presents the combined (head + cup) volumetric wear results as a function of number of cycles for all 28, 40 and 56 mm MOM bearings, and shows that all bearing couples generated a biphasic wear pattern, i.e. producing higher initial wear followed by a reduced steady-state condition ($p<0.05$, ANOVA). Figure 5(a) also presents the mean combined volumetric wear rates ($mm^3/10^6$ cycles or year of use) for all bearing sizes during running-in, and highlights that the 56 mm bearings generated by far the greatest running-in wear of all (7.0 $mm^3/10^6$ cycles). The lowest mean running-in wear rate was generated by the 40 mm bearings (2.2 $mm^3/10^6$ cycles), showing a clear 2–3.5 fold reduction in running-in wear compared to the 28 and 56 mm bearings respectively ($p<0.05$, ANOVA). The ratio of running-in (RI) wear to steady-state (SS) wear for all 28, 40 and 56 mm bearings were 4.5:1, 5.4:1 and 22.2:1 respectively. In addition, all bearing sizes showed greater wear loss from the acetabular cups compared to the femoral heads, typically by a factor of 2. Plus, the seven 40 mm bearings which were mounted superiorly at 35° [Figure 2(c)] showed no difference in running-in wear compared to the three bearings mounted horizontally ($p>0.05$, Student t-test), and suggests a small influence of low socket angles on initial bearing wear.

Figures 6(a) to (c) present the combined (head + cup) total volumetric wear at 1.0 million cycles (running-in wear) verses radial clearance, equivalent radius and maximum deviation of sphericity for all 28, 40 and 56 mm bearings tested (excluding two 40 mm bearings). With regards to radial clearance, all bearing sizes showed a reduction in total running-in wear with a decrease in radial clearance, [Figures 6(a)]. Overall, the larger 56 mm bearings showed the greatest influence of radial clearance, i.e. showing the greatest slope, and suggests that with smaller radial clearances (40–65 μm), the 56 mm bearings could achieve very low running-in wear (~1.0 $mm^3$). The 40 mm bearings showed a much reduced influence of radial clearance on running-in wear, however the results still suggested that with smaller radial clearances (40–65 μm), running-in wear could be reduced to only 1 $mm^3$ in the first year or million cycles. As for the 28 mm bearings, they also showed a small influence with radial clearance, producing a similar slope to the 40 mm bearings. Importantly, the 28 mm results suggest that even with lower radial clearances (15–20 μm), the 28 mm bearings will still generate ~1.5–4 $mm^3$ of Co-Cr-Mo wear in the first million cycles. With regards to equivalent radius, all bearing sizes showed a reduction in total running-in wear with an increase of equivalent radius, however, this was less evident for the 28 mm bearings ($R^2=0.03$), [Figures 6(a)]. Out of the 40 and 56 mm bearings, the 56 mm bearings showed the greatest influence of increasing the equivalent radius, suggesting a reduction in total running-in wear from 7 $mm^3$ to 4 $mm^3$ with just a small increase of equivalent radius from 11 to 13 m. As for maximum deviation of sphericity or form, all bearing sizes showed little influence if any of maximum sphericity on running-in wear, [Figure 6(c)], and indicates a weak effect of isolated areas of high roughness. The 28 mm bearings produced a positive correlation with running-in wear and max deviation ($R^2=0.7$), however, this relationship is likely to be false, and simply a result of other factors.

*3.2. Steady-State Wear - Standard Walking Tests*

Figures 4(b) and 5(b) present the mean combined (head + cup) steady-state volumetric wear rates for all 28, 40 and 56 mm couples. The results showed that the larger 40 and 56 mm bearings typically generated a clear 2–3 fold reduction in mean steady-state wear rate compared to the smaller 28 mm bearing sizes ($p<0.05$, Student t-test). In addition, the 56 mm bearings generated a further 20 % reduction in steady-state mean wear rate compared to the 40 mm bearings ($p<0.05$), suggesting superior wear resistance following running-in. In general, the wear results for all groups produced low scatter, showing no runaway wear for any bearing tested, [Figure 4(a)]. Plus, the seven 40 mm bearings which were mounted superiorly at 35° [Figure 2(c)] showed no difference in steady-state wear compared to the three bearings mounted horizontally ($p>0.05$, Student t-test).

Figures 7(a) and (b) present the combined (head + cup) steady-state wear results verses radial clearance and equivalent radius for all 28, 40 and 56 mm bearings tested (excluding two 40 mm bearings). With regards to radial clearance, all bearing sizes showed a reduction in steady-state wear with a decrease in radial clearance. Overall, the smaller 28 mm bearings showed the greatest influence of radial clearance on steady-state wear, i.e. showing the greatest slope, and suggests that with smaller radial clearances (15–20μm), 28 mm bearings may produce lower steady-state wear (~0.5 $mm^3/10^6$ cycles) compared to those in the current study (0.92 $mm^3/10^6$ cycles). Importantly, the results indicated that the lowest wearing bearings (the 56 mm's) could achieve even lower steady-state wear (<0.1 $mm^3/10^6$ cycles) with lower radial clearances (50–65 μm), showing a possible 5-fold reduction in steady-state wear compared to 28 mm bearings with low radial clearances (20μm). With regards to equivalent radius, the results again showed sizeable reductions in steady-state wear with an increase in equivalent radius, with the 56 mm bearings showing the greatest advantage.

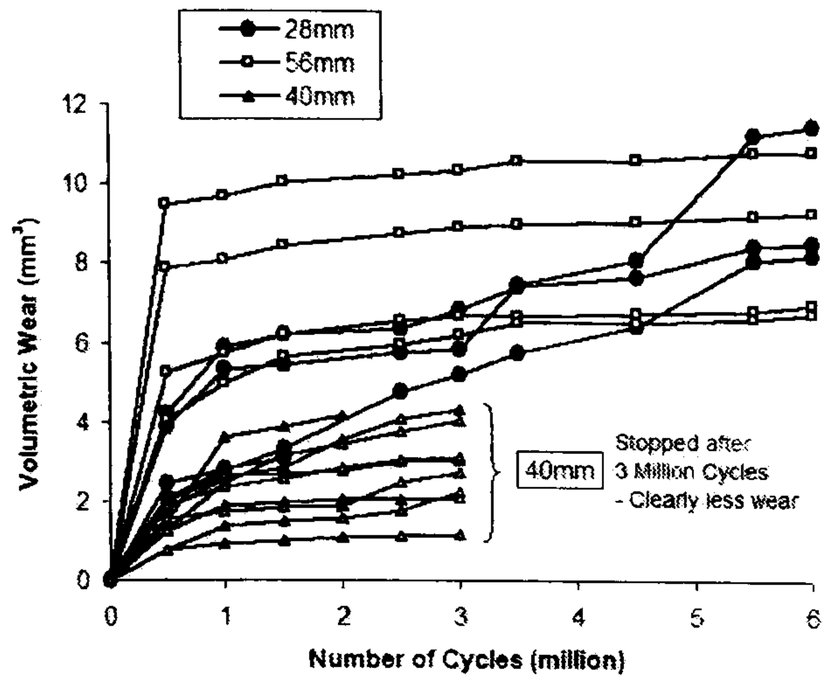


(a)

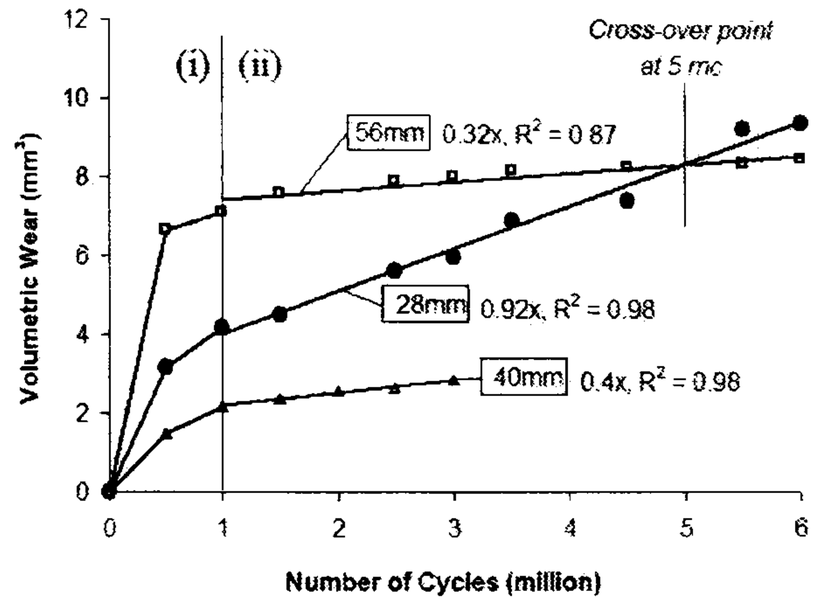


(b)

Fig. 4. Variation of combined (head+cup) volumetric wear verses number of cycles under normal physiological walking, for (a) all 18 bearing couples tested, and (b) the accumulative mean for the three bearing sizes – showing (i) running-in conditions-walking (first $1x10^6$ cycles), and (ii) steady-state (SS) conditions–walking (after $1x10^6$ cycles).

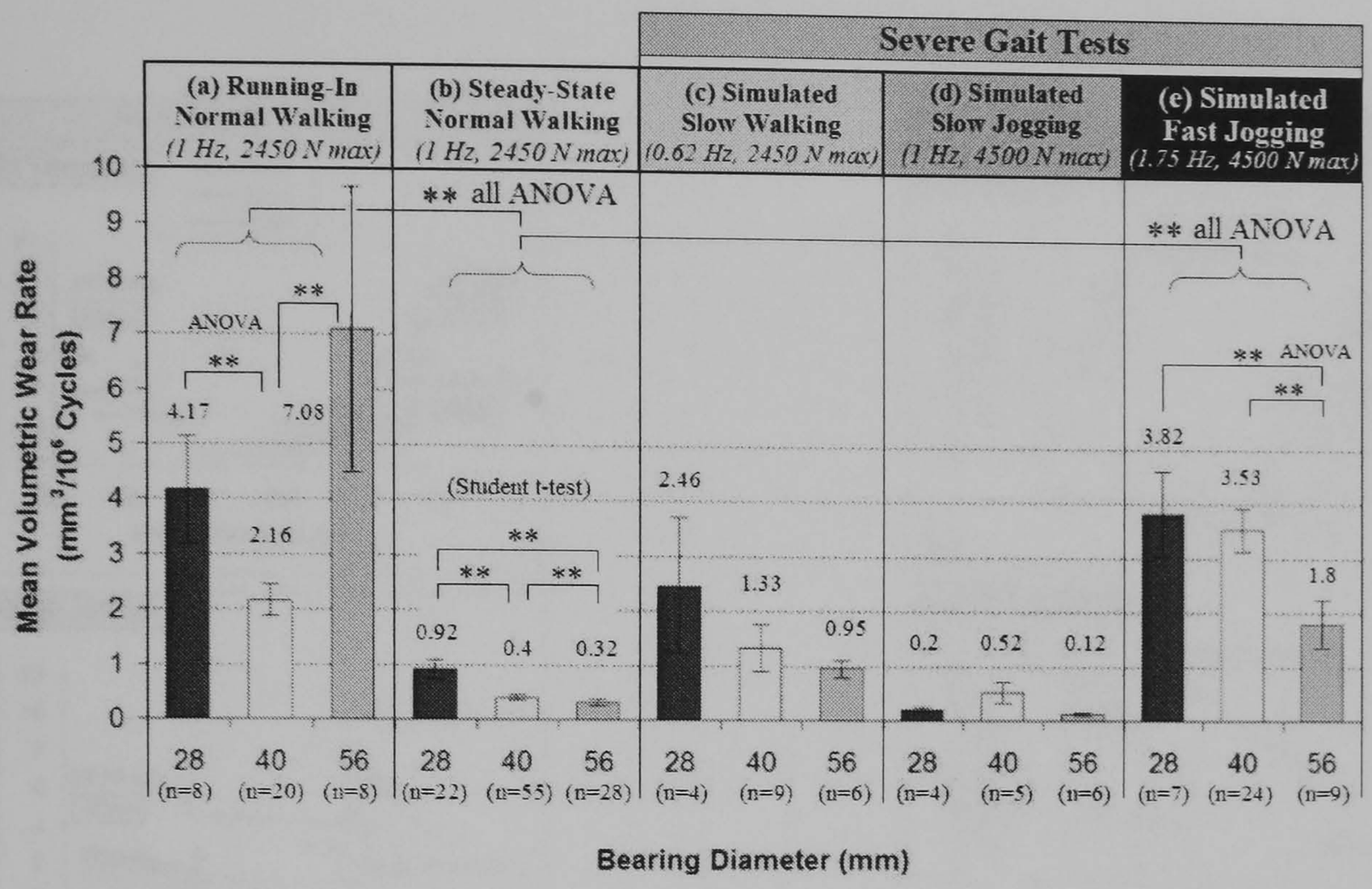


Fig. 5. Summary of mean combined volumetric wear rates (head+cup) under smooth conditions for (a) running-in wear – normal walking, (b) steady-state wear – normal walking 2450 N max 1 Hz, (c) simulated slow walking 2450 N max 0.62 Hz, (d) simulated slow jogging 4500 N max 1 Hz, and (e) simulated fast jogging 4500 N max 1.75 Hz. [The error bars represent ± SE, n = number of wear test results, ** = $p<0.05$ (Grouped ANOVA or Student t-test) i.e. statistical difference where applicable].

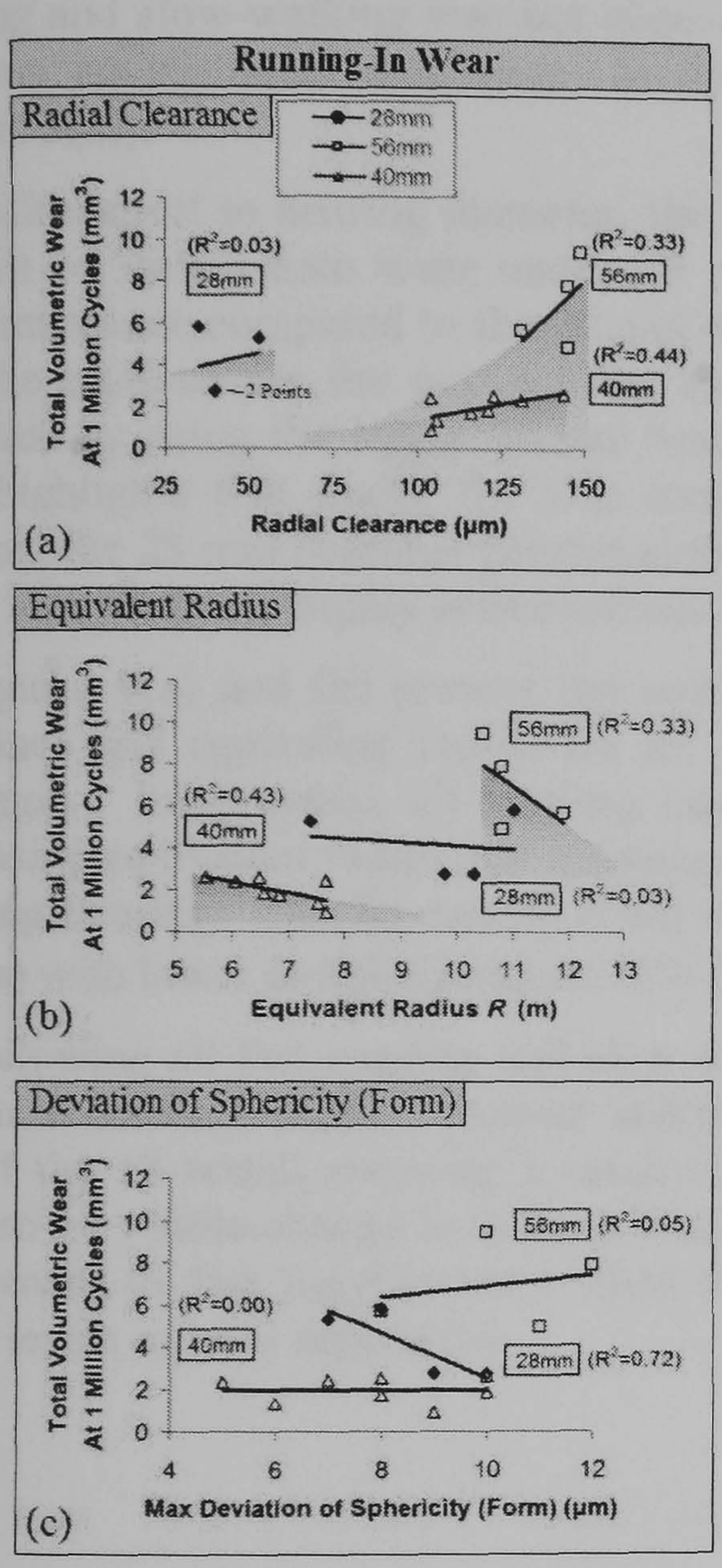


Fig. 6. The influence of bearing geometry on running-in wear for all 28, 40 and 56 mm Co-Cr-Mo bearings. Graphs shows the total volumetric wear after the first 1 million cycles verses (a) radial clearance, (b) equivalent radius, and (c) maximum deviation of sphericity or form.

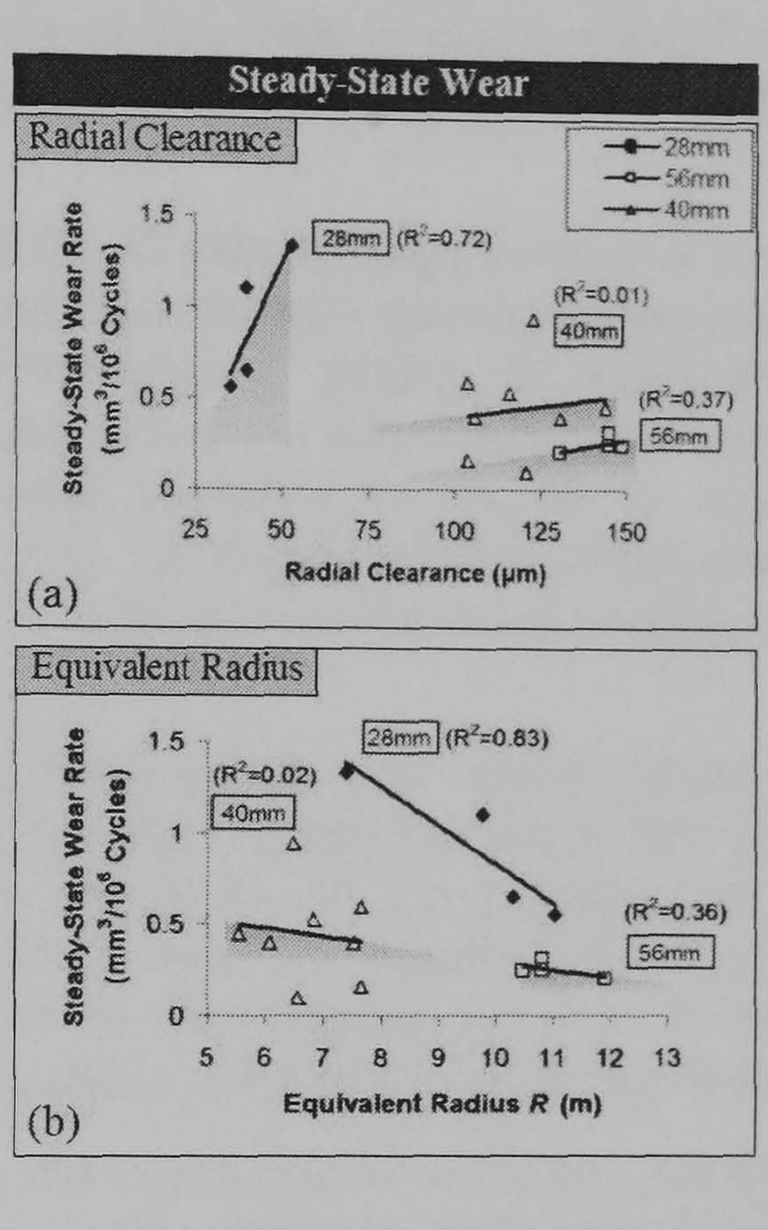


Fig. 7. The influence of bearing geometry on mean steady-state wear for all 28, 40 and 56 mm Co-Cr-Mo bearings. Graphs shows the mean steady-state wear rates verses (a) radial clearance, and (b) equivalent radius.

*3.3. Severe Patient Activity Tests*

Out of the three severe gait activities simulated, fast-jogging (1.75Hz, 4500 N max) generating the worst wear condition for all bearing sizes, typically showing a 4–9 fold increase in volumetric wear release compared to standard walking (1 Hz, 2450 N max) ($p<0.05$, ANOVA) [Figure 5(e)]. Slow-walking (0.62 Hz, 2450 N max) was the next highest ranked severe activity, typically showing a 3–fold increase in volumetric wear release compared to standard walking for all bearings ($p<0.05$, Student t-test) [Figure 5(c)]. This increased boundary contact and high wearing condition for fast-jogging and slow-walking was not observed with slow-jogging (1 Hz, 4500 N max), with all results showing no statistical differences to those generated under standard walking ($p>0.05$, ANOVA) [Figure 5(d)].

With respect to bearing diameter, the results showed that the 56 mm bearings generated the least amount of steady-state wear under all severe activities simulated, thereby demonstrating superior wear resistance compared to the 28 and 40 mm bearings after running-in. In fact, the results showed that the more-severe the gait activity simulated, the more reductions in volumetric wear could be achieved by using the larger 56 mm bearings compared to other smaller sizes (Figure 8). Figure 8 also highlights that under the two most demanding activities simulated, slow walking and fast jogging, the 28 mm bearings generated the highest wear of all, making them the worst bearing option of all for young and highly active patients.

Figures 9(a) and (b) present the combined (head + cup) fast-jogging wear results verses radial clearance and equivalent radius for all 28, 40 and 56 mm bearings tested (excluding two 40 mm bearings). Importantly, all bearing sizes showed massive reductions in fast-jogging wear with increasing equivalent radius and reducing radial clearances. The results also suggested that the lowest wearing bearings (the 56 mm's) could easily achieve even lower fast-jogging wear ($<0.4$ $mm^3/10^6$ cycles) with lower radial clearances (50–65 μm), showing a similar result to that for normal walking.

Following all fast jogging and slow walking simulations, additional normal walking tests showed that most bearing couples returned immediately to steady-state wear conditions, with only 2 bearings out of the 18 tested showing a small running-in period of 0.5 million cycles. All wear surfaces showed no visible change in surface roughness as a result of severe gait. The results also showed no differences in fast jogging wear when introducing 1 hour resting periods every 8,000 cycles, and small levels of joint separation.

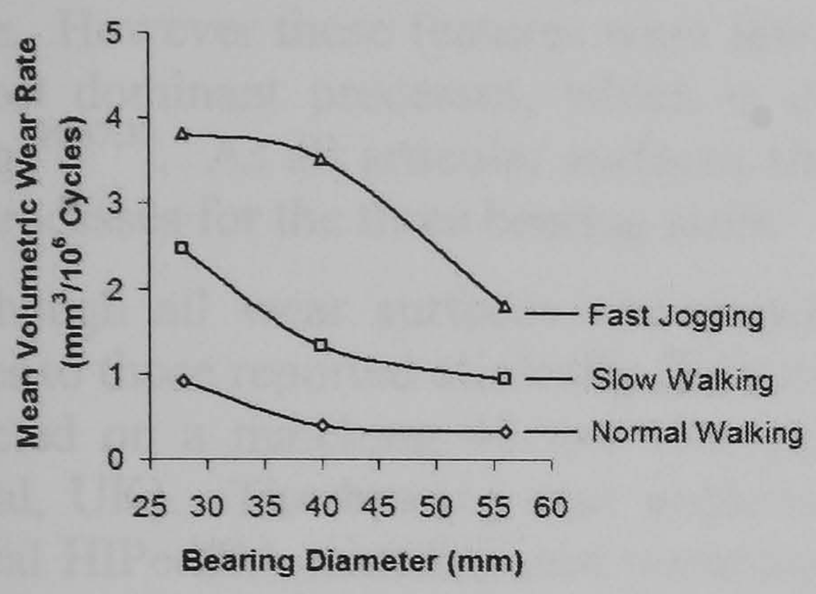


Fig. 8. The variation in mean combined MOM volumetric wear rate (head and cup) verses bearing diameter for all main patient activities simulated.

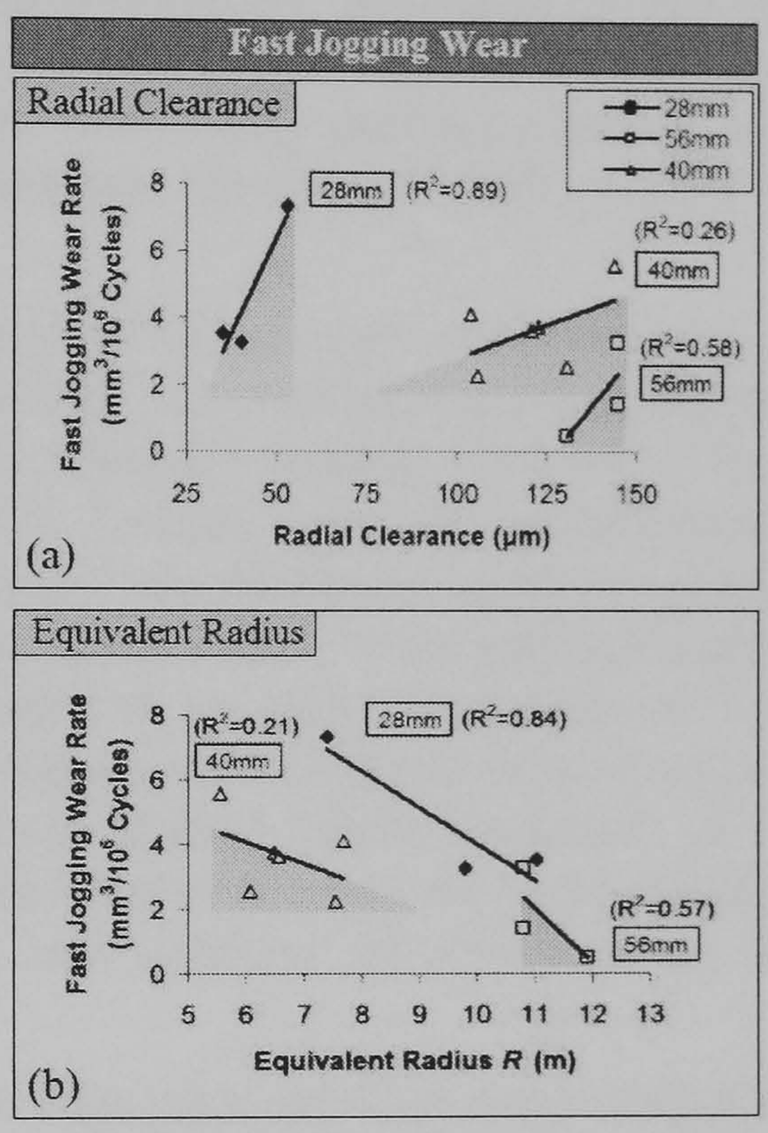


Fig. 9. The influence of bearing geometry on mean fast jogging wear for all 28, 40 and 56 mm Co-Cr-Mo bearings. Graphs shows the mean steady-state wear rates verses (a) radial clearance, and (b) equivalent radius.

### *3.4. Articular Wear Patterns & Surface Topography*

The results from a detailed SEM examination of all worn articular surfaces (at $3x10^6$ cycles or 3-years) showed no visible differences in all observed wear patterns for the 28, 40 and 56 mm diameter bearings tested (Figures 10a to g). All polar regions of the head and cups showed equal amounts of large scale polishing and moderate abrasion, the later caused by released matrix carbides (2–10 μm), therefore giving rise to large smooth zones interspersed by deep scratches (Figures 10a to c). Protein transfer films were also similar in structure for all three bearing sizes, typically showing thin patchy films within the high wear zone, as well as more highly structured film formations at the edge of the wear scar (Figures 10d and e). Evidence of carbide pullout and micro-delamination wear were also observed in isolated areas within the high wear zones, typically leading to pitting/scratching in the direction of sliding and a two-layered wear scar (1–3 μm in height) respectively (Figures 10f and g). Micro-delamination of the primary wear surface suggests a strong adhesive process occurring under boundary-contact events, causing immediate micro welding and rupture or tearing of the articular surface. However these features were few in number, with polishing and abrasive wear being by far the most dominant processes, which is in good agreement with many previous studies of MOM bearings[29,37,39]. As all articular surfaces showed common features, the overall results suggest similar wear processes for the three bearing sizes.

Although all wear surfaces and transfer films generated in the current study showed similar features to those reported clinically for retrieved MOM bearings[39], a direct SEM comparison was also conducted on a matching 42 mm diameter HC Co-Cr-Mo retrieved bearing (CORMET ®, Corin Medical, UK). The bearing was implanted in a patient for 2 years, and was manufactured from identical HIPed/SA material, and possessed similar geometrical specifications to those tested in the current study, with the exception of slightly lower radial clearances. The 2-year explanted prosthesis showed to possess lower quantities of visable wear compared to our test components at 3 million cycles. However, closer examinations of all heavily worn regions showed equal proportions of large scale polishing wear, multi-directional abrasion and carbide pullout when compared to the hip simulator generated surfaces [Figure 11(a)]. Interestly, small isolated areas of micro-delamination wear were also observed on the retrieval [Figure 11(b)], and matched the delamination features obsevered on our test components [Figures 10(g)].

As for changes in surfaces roughness following wear, the white light interferometer results showed that the polar-contacting regions of all the measured 40 mm heads and cups improved in surface roughness, showing a mean reduction from $S_a$ 0.055 μm to 0.024 μm after 3 million cycles of testing or 3-years of use ($p<0.05$), (Figure 12). This decrease in articular roughness strongly indicates a sizeable reduction in asperity heights following running-in wear and additional polishing. The change in surface roughness for the 28 mm and 56 mm diameters bearing was not recored, and such influences is out of the scope of this study.

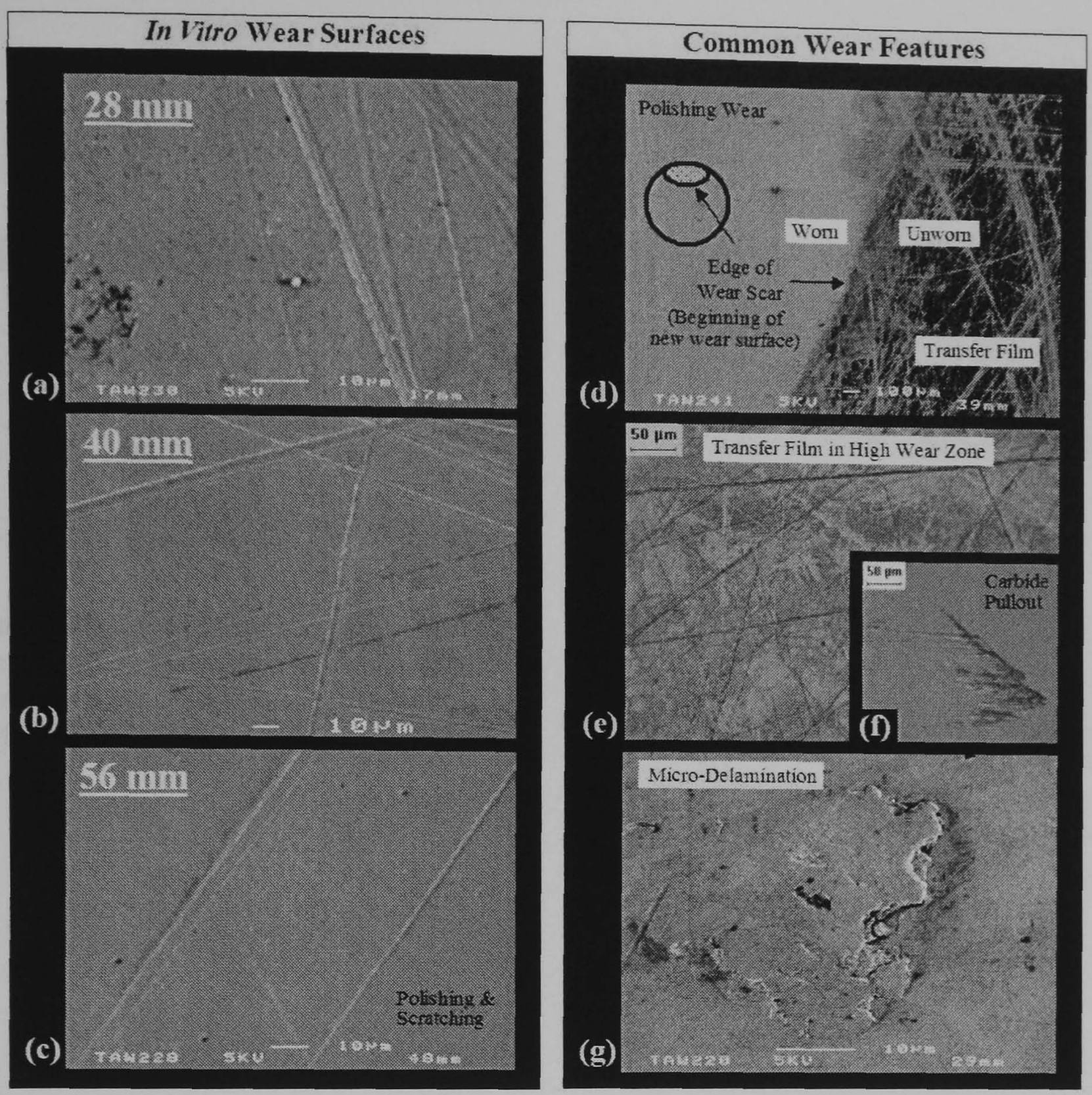


Fig. 10. Scanning electron micrographs of heavily worn surfaces from the HC HIPed/SA Co-Cr-Mo test components after 3 million cycles of hip joint simulation, showing (a) typical 28 mm cup wear surface – showing polishing scratching and micro-pitting, (b) 40 mm cup wear surface, (c) 56 mm cup wear surface, (d) typical edge of wear scar and transfer film build-up for all diameter bearings, (e) typical small area of patchy transfer film build-up within the high wear zone, (f) carbide pullout, scratching and micro-pitting, and (g) micro-delamination wear – showing surface rupture, tearing and

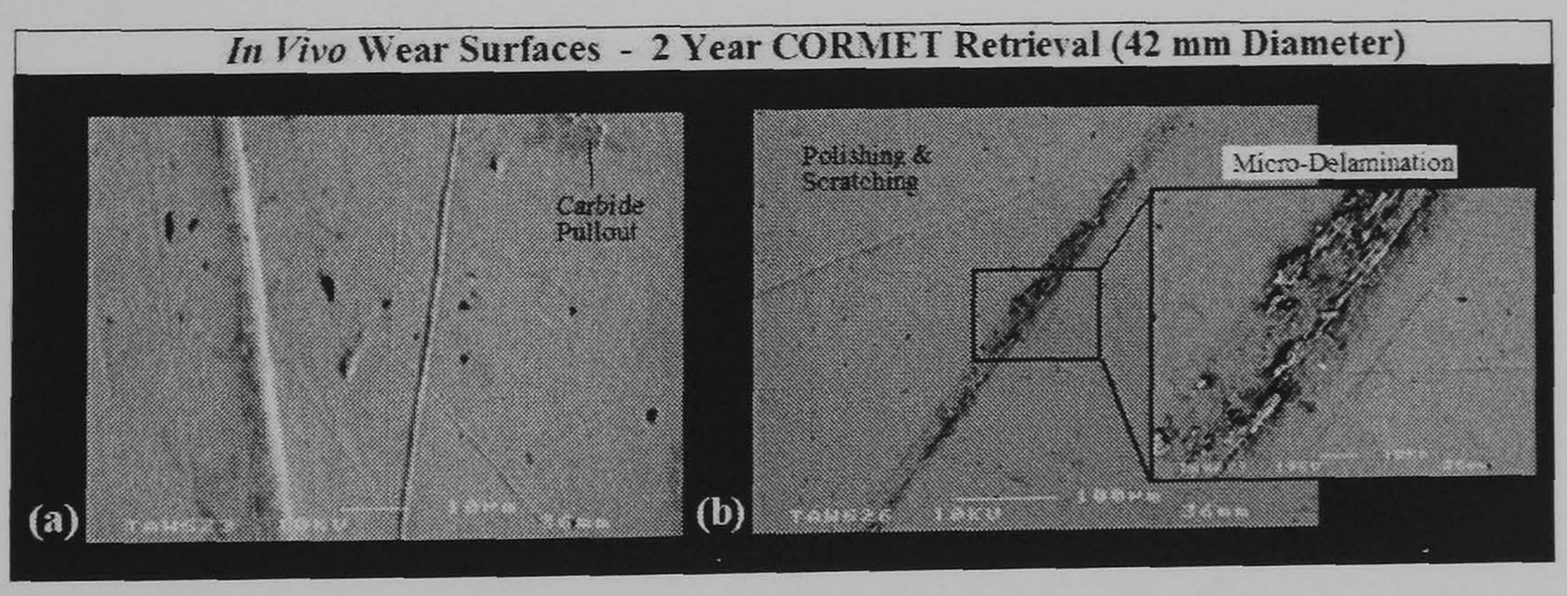


Fig. 11. Scanning electron micrographs of heavily worn surfaces from a 2-year retrieved HC HIPed/SA Co-Cr-Mo 42mm cup (CORMET, Corin Medical, UK), showing (a) polishing, scratching and carbide pullout, and (b) scuffing within high wear zone - showing micro-delamination wear.

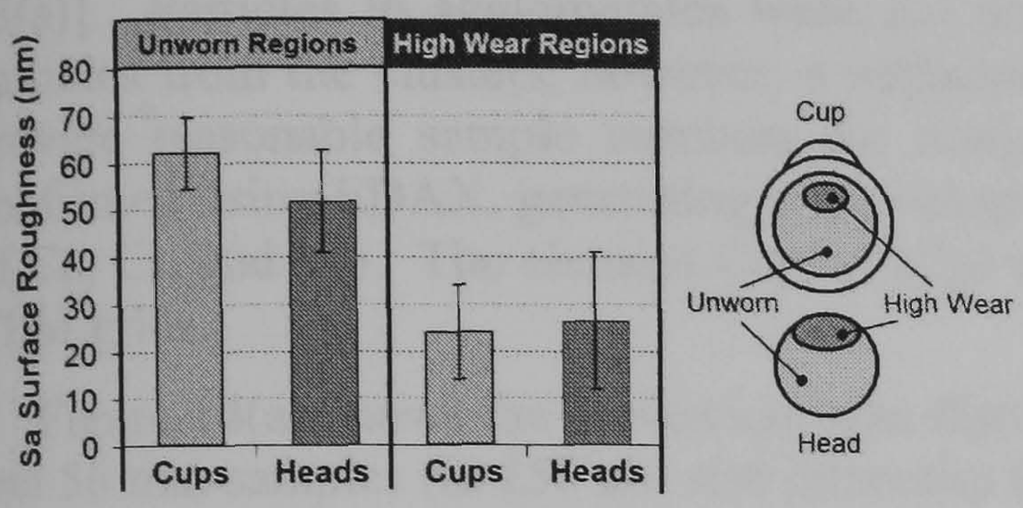


Fig. 12. Comparison of 3D surface roughness (Sa) measured from unworn (virgin) and heavily worn Co-Cr-Mo surfaces for a 40 mm diameter bearing. The error bars represent ±95% confidence limits.

*3.5. Wear Particle Analysis*

The majority of Co-Cr-Mo wear particles generated in the current study were in the nanometer range, however, particles greater than 1.1 μm were also observed, but were few in numbers (Figures 13a and b). The Co-Cr-Mo particles were uniform in morphology, with the majority being either oval or round in shape. Particles were observed in two states, either singly or in agglomerates, [Figures 13(a)]. Particles in agglomerates were not analysed due to the difficulty in separating individual particles from the clusters, however, a sufficient number of singular particles were photographed to provide reasonable sample numbers for analysis. The compositions of all wear particles were confirmed using EDAX, generating a typical spectrum shown in Figure 13(c), indicating the presence of Co, Cr, and Mo. The element Copper (Cu) was also detected due to the inevitable presence of the TEM grids.

Figure 14(a) shows the percentage size distribution of all Co-Cr-Mo wear particles for the 28, 40 and 56 mm samples (in 250 nm size intervals) for steady-state walking, and Figure 14(b) presents the influence of bearing diameter on the median wear particle sizes. The results showed that the median particle length, width, diameter and overall percentage size distribution of wear particles all varied with bearing diameter. Overall, the greatest difference in wear particle sizes was generated by the 28 mm bearings, which showed a 2-fold increase in median particle diameter (200 nm) compared to the 40 and 56 mm bearings (~90 nm) ($p<0.05$, ANOVA) [Figure 14(b)]. The 56 mm wear particles were typically 33 % larger compared to the 40 mm particles, however, this was not always statistically significant, [Figure 14(b)]. In terms of wear particle shape, the results also showed no influence of bearing diameter on wear particle aspect ratio ($p>0.05$, ANOVA), with all joints producing a similar value of 1.4.

When comparing the percentage size distribution, median length, width and diameter of wear particles generated under standard walking to those from simulated fast jogging, the results showed no statistical differences ($p>0.05$, ANOVA), thereby suggesting a small influence of increased joint velocity and load on debris generation, [Figures 15(a) and (b)]. Although strong statistical differences could not be found, fast jogging activities did show a typical 10 % increase in median wear particle size parameters, as well as generating a greater number of larger (bioactive)[34] micron-sized particles compared to standard walking [Figures 15(a)].

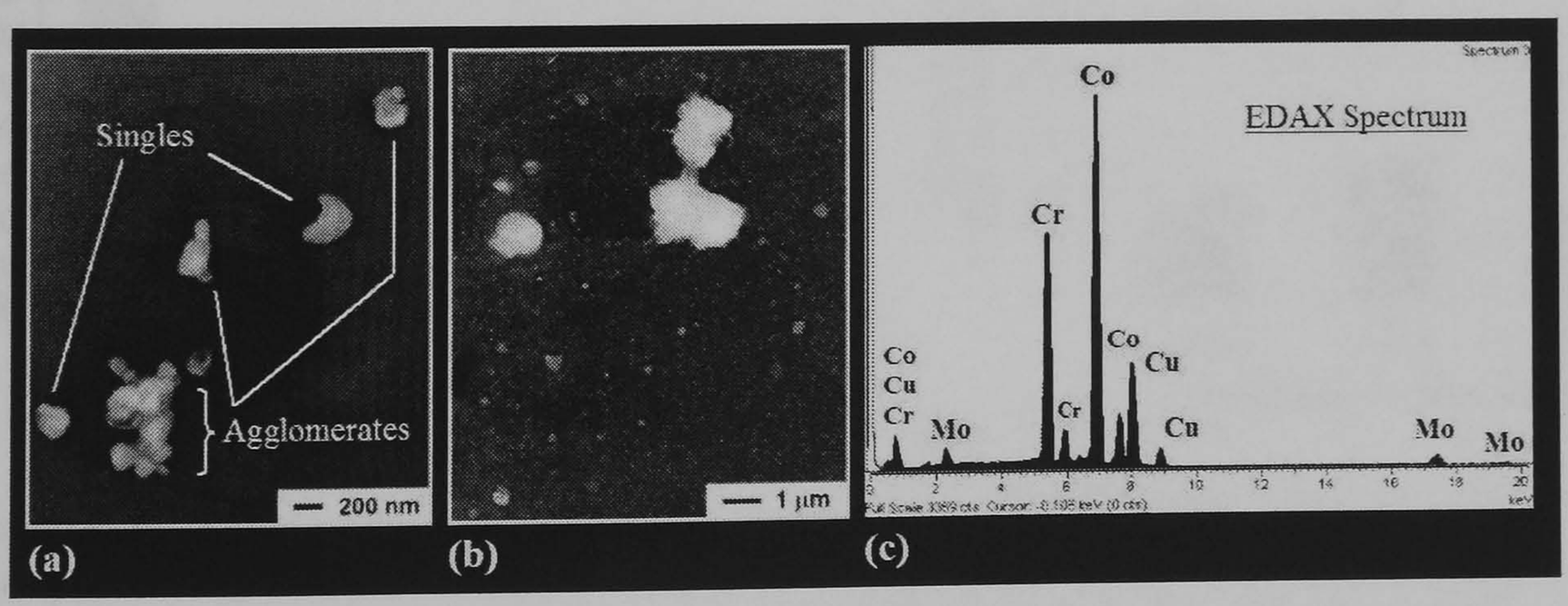


Fig. 13. Images showing: (a) a typical TEM photograph of nanometer sized Co-Cr-Mo wear particles produced in the current study, either individuals or agglomerates, (b) typical TEM photograph of larger 1 μm sized Co-Cr-Mo wear particles, and (c) typical EDAX spectrum of wear particles on the copper grid during TEM.

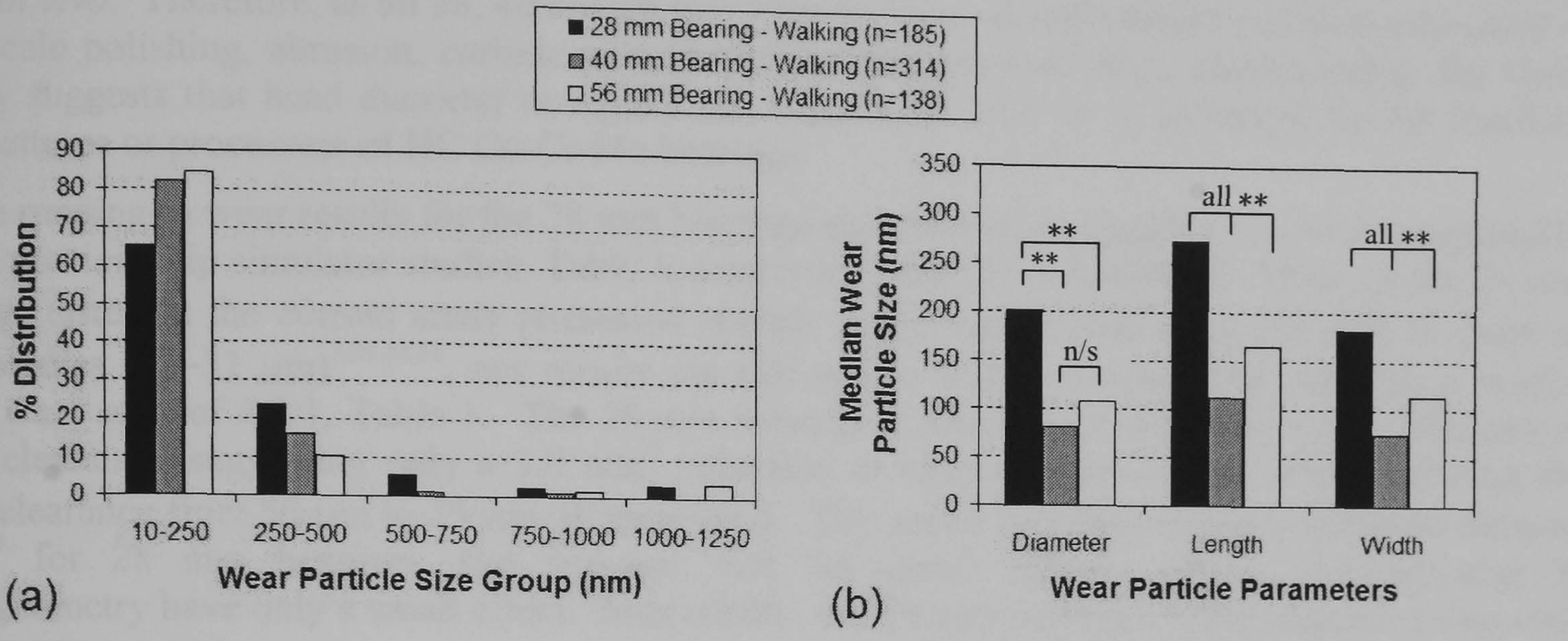


Fig. 14. The influence of bearing diameter on Co-Cr-Mo wear particle sizes under steady-state standard walking conditions, showing (a), the percentage size distribution of particles for the 28, 40 and 56 mm bearings – showing that the majority of wear particles for all diameter bearings were 10 to 250 nm in size, and (b) the variations of median particle diameter (calculated), length and width for the three diameter bearings under standard walking conditions. [n = number of wear particles examined, ** = $p<0.05$ (ANOVA), and n/s = not statistically different ($p>0.05$)].

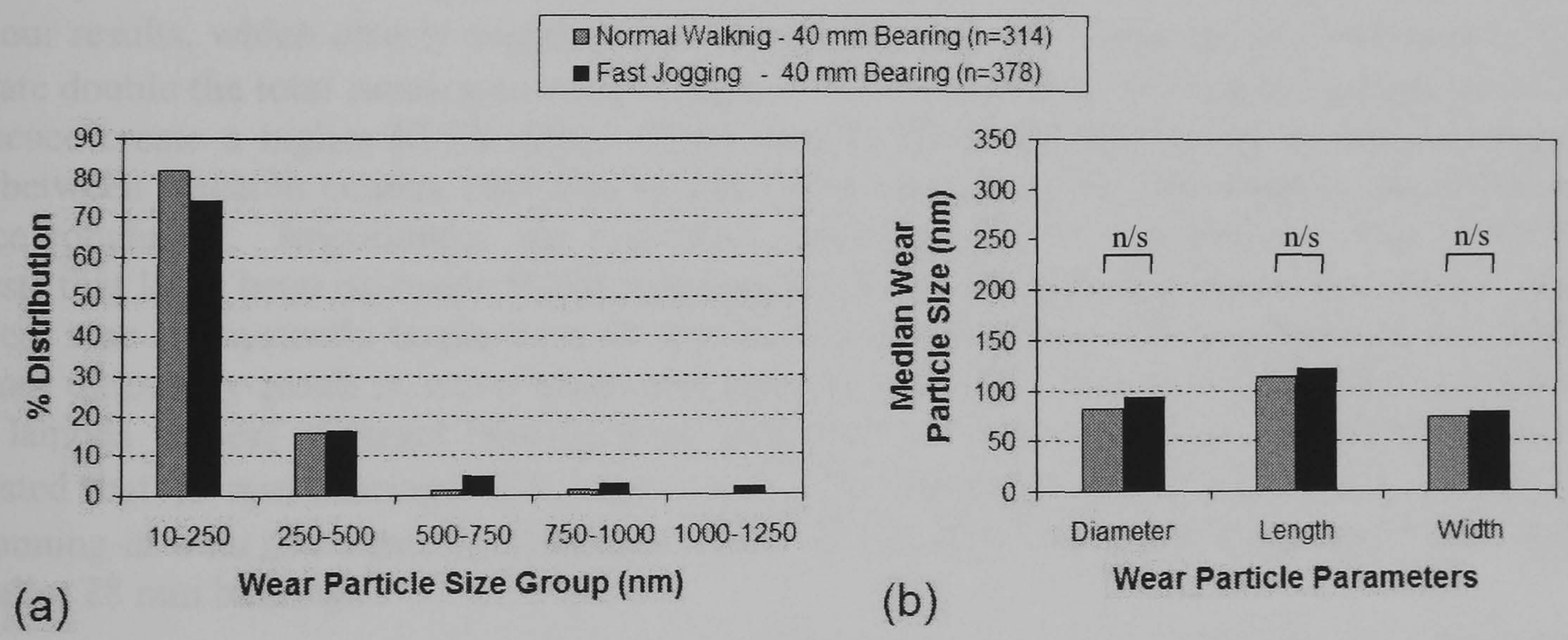


Fig. 15. A comparison of Co-Cr-Mo wear particle sizes generated under normal walking and fast jogging activities [for 40 mm bearing only], showing (a) the percentage size distribution of particles for the two activities, and (b) the variations of median particle diameter (calculated), length and width under both walking and jogging. [n = number of wear particles examined, ** = $p<0.05$ (ANOVA), and n/s = not statistically different, ($p>0.05$)].

## 4. Discussion

All wear surfaces and transfer films created in the current study showed identical patterns and processess to those previously reported for MOM bearings[29,31,37,39,51]. Importantly, all wear surfaces closely agreed with a matching 2-year retrieved MOM prosthesis (CORMET ®), which was identical in size, material, and heat-treatments. These simularities in wear features strongly suggest that the testing methods used in the current study were successful in recreating similar tribological conditions found *in vivo*. Therefore, as all 28, 40 and 56 mm wear surfaces showed almost identical quantities of large-scale polishing, abrasion, carbide pullout and isolated areas of micro-delamination, the study thereby suggests that head diameter or equivalent radius have little or no influence on the resulting wear patterns or processess of HC Co-Cr-Mo bearings.

The running-in wear results for the 28 mm bearings showed similar quantities of wear compared to eleven previous hip simulator studies, Table 1, suggesting good reproducibility. Although the 28 mm bearings tested in the current study possessed slightly higher radial clearances (42 μm) to those of other studies (22–31 μm)[7,29,32,51], our results are still in line with published data, showing a similar RI/SS wear ratio of 4.5:1, Table 1. The 28 mm running-in results also showed a weak influence of radial clearance, suggesting only a 1.0 $mm^3$ reduction in total running-in wear when reducing the radial clearance from 50 μm to 25 μm, [Figure 6(a)]. This result is similar to the findings by Scholes et al[51] for 28 mm bearings, and suggests that for lower lambda values, improvements in macrogeometry have only a small effect. Importantly, our 28 mm running-in data suggested that even with very low radial clearances (15 μm), 28 mm bearings will still generate ~1.5–2 $mm^3$ of Co-Cr-Mo wear within the first million cycles or year of use [Figure 6(a)]. Again, this result is in line with previous data, Table 1, and demonstrates that standard 28 mm un-coated Co-Cr-Mo surfaces will always generate high initial bearing wear.

The running-in wear rates for the larger 40 mm bearings (2.16 $mm^3/10^6$ cycles) were slightly high compared to a previous study by Goldsmith et al[6] for 36 mm bearings (1.20 $mm^3/10^6$ cycles), and resulted in a higher RI/SS wear ratio of 5.4:1, (Table 1). However, the radial clearances of the 40 mm bearings were again larger (119 μm) compared to those reported by Goldsmith et al[6] (71 μm), and was most likely the cause of our higher wear. Evidence to support this increase is presented in Figure 6(a) from our results, which clearly suggests that 40 mm bearings with large radial clearances of 125 μm generate double the total running-in wear compared to those bearings with radial clearances of 75 μm, and hence create a higher RI/SS ratio. Other reasons for slight differences in reported running-in wear between research centres may also be caused by disimilar wear path lengths and differences in surface roughness. Importantly, the running-in wear for the 40 mm bearings was minimal, and suggests that large head diameter MOM bearings do not suffer from high running-in wear. Although the wear scar is physically larger on a 40 mm bearing compared to a 28 mm bearing, this difference does not ultimately result in more wear, and suggests a strong influence of the superior lubrication (high lambda values) of larger bearing sizes compared to 28 mm bearings. In addition, our results suggested that 40 mm bearings with even lower radial clearances of 40–65 μm are capable of very low running-in wear (<1.0 $mm^3$), showing a clear 2–3 fold reduction in initial debris release compared to smaller 28 mm bearings.

As for very large heads, our running-in results also suggested that 56 mm bearings with low radial clearances of 40–65 μm (Equivalent radius, $R$ = 26 m) are capable of creating very low running-in wear (<1.0 $mm^3$), [Figure 6(a)], again showing an improvement over 28 mm bearings. Having said this, the 56 mm bearings in the current study produced the highest mean running-in wear rate of all head sizes (7 $mm^3/10^6$ cycles), and a RI/SS ratio of 22:1, Table 1. However, this again was most likely a result of the higher radial clearances (142 μm) for the 56 mm joints tested. Evidence to support this increase is again presented in Figure 6(a), which shows that the running-in wear of 56 mm bearings was highly influenced by radial clearance, with higher clearances leading to high wear. In summary, our running-in results strongly suggest that large diameter Co-Cr-Mo bearings (>32 mm) with small radial clearances (40–65 μm) offer minimal running-in wear and initial ion release compared to smaller sizes. On the other hand, large diameter Co-Cr-Mo bearings with radial clearances greater than 80 μm suffer from elevated running-in wear.

Table 1. Recently reported volumetric wear rates for 28 and larger CoCrMo-on-CoCrMo hip bearings (ranked from lowest to highest radial clearance) under standard walking conditions in hip joint simulators (with borad wear paths).

| Study | Head Diameter (mm) | Mean Radial Clearance (μm) | Initial $R_a$ (μm) | Carbon Content | Serum (mg/ml) | Volumetric Wear Rate ($mm^3/10^6$ Cycles) Running-In (RI) | Steady-State (SS) | Ratio RI / SS |
|---|---|---|---|---|---|---|---|---|
| Scholes *et al.* 2001 [51] | 28 | 22 | 0.008-0.030 | Low | 52 | 0.90 | 0.10 | 9.0 |
| Chan *et al.* 1999 [29] | 28 | 28 | 0.008 | High | ~70 | 0.21 | 0.06 | 3.5 |
| Firkins *et al.* 2001 [32] | 28 | 30 | 0.010-0.020 | High | 20 | 3.09 | 1.23 | 2.5 |
| Smith *et al.* 2001 [7] | 28 | 31 | 0.003-0.005 | High | 20 | 1.60 | 0.54 | 3.0 |
| Chan *et al.* 1999 [37] | 28 | 31 | 0.007 | High | ~70 | 0.40 | 0.10 | 5.0 |
| Scholes *et al.* 2001 [51] | 28 | 40 | 0.008-0.030 | Low | 52 | 0.90 | 0.75 | 1.2 |
| Rieker *et al.* 2001 [52] | 28 | 50 | 0.023 | High | 20 | 3.00–4.00 | 1.00 | 3.5 |
| Anissian *et al.* 2001 [44] | 28 | 50 | – | High | 20 | 2.22 | 1.00 | 2.2 |
| Clarke *et al.* 2000 [31] | 28 | 55 | – | High | 35 | 2.68 | 0.97 | 2.8 |
| Goldsmith *et al.* 2000 [6] | 28 | 56 | 0.008-0.025 | High | 20 | 1.00 | 0.45 | 2.2 |
| Fisher *et al.* 2000 [18] | 28 | – | – | – | 20 | 3.10 | 1.60 | 1.9 |
| | | | | | | Mean 1.80 | Mean 0.71 | Mean 3.35 |
| *Current Study* | 28 | 42 | – | High | 20 | 4.17 | 0.92 | 4.5 |
| Goldsmith *et al.* 2000 [6] | 36 | 71 | 0.006-0.035 | High | 20 | 1.20 | 0.36 | 3.3 |
| Bowsher *et al.* 2001 [38] | 40 | 119 | ~0.015 | High | 20 | 2.16 | 0.40 | 5.4 |
| *Current Study* | 56 | 142 | ~0.015 | High | 20 | 7.10 | 0.32 | Max 22.2 |
| Chan *et al.* 1996 [29] | 45 | 10–300 | 0.025-0.051 | High | ~70 | 2.00–8.00 | 0.60 | 13.3 |

As for steady-state wear, our results closely agreed with classical elastohydrodynamic lubrication theory[5,8], i.e. showing the lowest wear rate for the largest head diameter (56 mm). This result is also similar to previous simulator studies by Chan et al[29] and Goldsmith et al[6], demonstrating superior wear resistance for larger head sizes. Importantly, all steady-state wear results in the current study showed similar quantities of wear compared to previous studies.

Again, Table 1 presents the steady-state wear for eleven recent hip simulator studies of modern 28 mm MOM bearings, and shows a similar overall average steady-state wear rate of 0.71 $mm^3/10^6$ cycles compared to our results (0.92 $mm^3/10^6$ cycles) for 28 mm's. As for the larger heads, our 40 mm steady-state results (0.40 $mm^3/10^6$ cycles) also showed similar quantities of wear to those reported by Goldsmith et al[6] for 36 mm bearings (0.36 $mm^3/10^6$ cycles), Table 1. Interesting, the radial clearances for the 40 and 56 mm bearings tested in the current study were again much higher (119–142 μm) compared to the work of Goldsmith (71 μm), however, our steady-state results still showed equal quantities of volumetric wear. Although it is often difficult to compare wear rates between research centres, the low steady-state wear experienced in the current study under relatively high radial clearances still suggests a weak influence of radial clearance on steady-state wear for larger diameter MOM bearings. Further evidence to support this weak influence of radial clearance for larger head sizes is presented in Figure 7(a) from our results, which suggests a reduction in radial clearance of 50 μm will only reduce steady-state wear by 0.1 $mm^3/10^6$ cycles for 56 mm bearings, compared to 2.0 $mm^3/10^6$ cycles reduction for smaller 28 mm bearings. Nevertheless, our results still suggest that large 56 mm bearings with even lower radial clearances of 40–65 μm will offer the maximum possible wear resistance for un-coated HC Co-Cr-Mo bearings under standard walking conditions, generating a possible steady-state wear of only ~0.1 $mm^3$ per year of use or million cycles. Based on the running-in and steady-state data for all bearings, Figure 16(a) shows the predicted total volumetric wear release at 40 years of use, and further demonstrates the sizable reductions in wear release with larger bearings.

The enzymatic protocol[16,50] used to extract all Co-Cr-Mo wear particles from bovine serum was highly successful, showing minimal corrosion and organic matter. Our results showed that all bearing sizes generated larger mean wear particle sizes compared to previous hip simulator studies. For example, recent studies by Fisher et al[18] and Firkins et al[32], using similar modern HC Co-Cr-Mo bearings (28 mm) and a 20 mg/ml bovine serum, have both reported mean wear particle sizes of 25–36 nm with subsequent steady-state wear rates of 1.23 and 1.6 $mm^3/10^6$ cycles respectively. The steady-state wear for our 28 mm bearings were equal to the above studies (0.93 $mm^3/10^6$ cycles), however, our median wear particle size was 7 times higher (mean diameter 200 nm). The exact cause

of this large difference in wear particle size is out of the range of this study, however, our study did adopt a much less corrosive extraction protocol[50], which may have lead to bigger particles. Importantly, our 28 mm Co-Cr-Mo wear particles sizes were similar to clinical data reported by Doorn et al[16] for HC Metasul's, showing a mean particle size of 120 nm (range 50–192 nm). Interestingly, our data also showed that larger diameter bearings produced smaller wear particle sizes (median 90 nm) compared to the 28 mm's. This result again agrees with the clinical data reported by Doorn et al[16], showing a mean particle size of 60 nm for large diameter HC McMinn's (45 mm) (range 19–105 nm). This result suggests a strong influence of the increased joint pressures for smaller bearings, leading to increased adhesion, and larger particles. Although our study showed a clear 2-fold increase in wear particle size for the smaller bearings, many more studies are required to make more concrete conclusions, however, it is logical that an improved lubrication regime would lead to a finer polishing action, and smaller particles. Producing smaller particles out of the bioactive range of 100 to 10,000 nm for macrophage stimulation[34] has obvious benefits, and larger bearings may not just only offer reduce wear and ion release, but less osteolysis. As the exact number of metal particles which trigger cell toxicity, systemic problems and osteolysis is currently not known, the ultimate question of joint longevity cannot be answered. However, data of this type will advance the accuracy of cell-culture studies in predicting bioactivity.

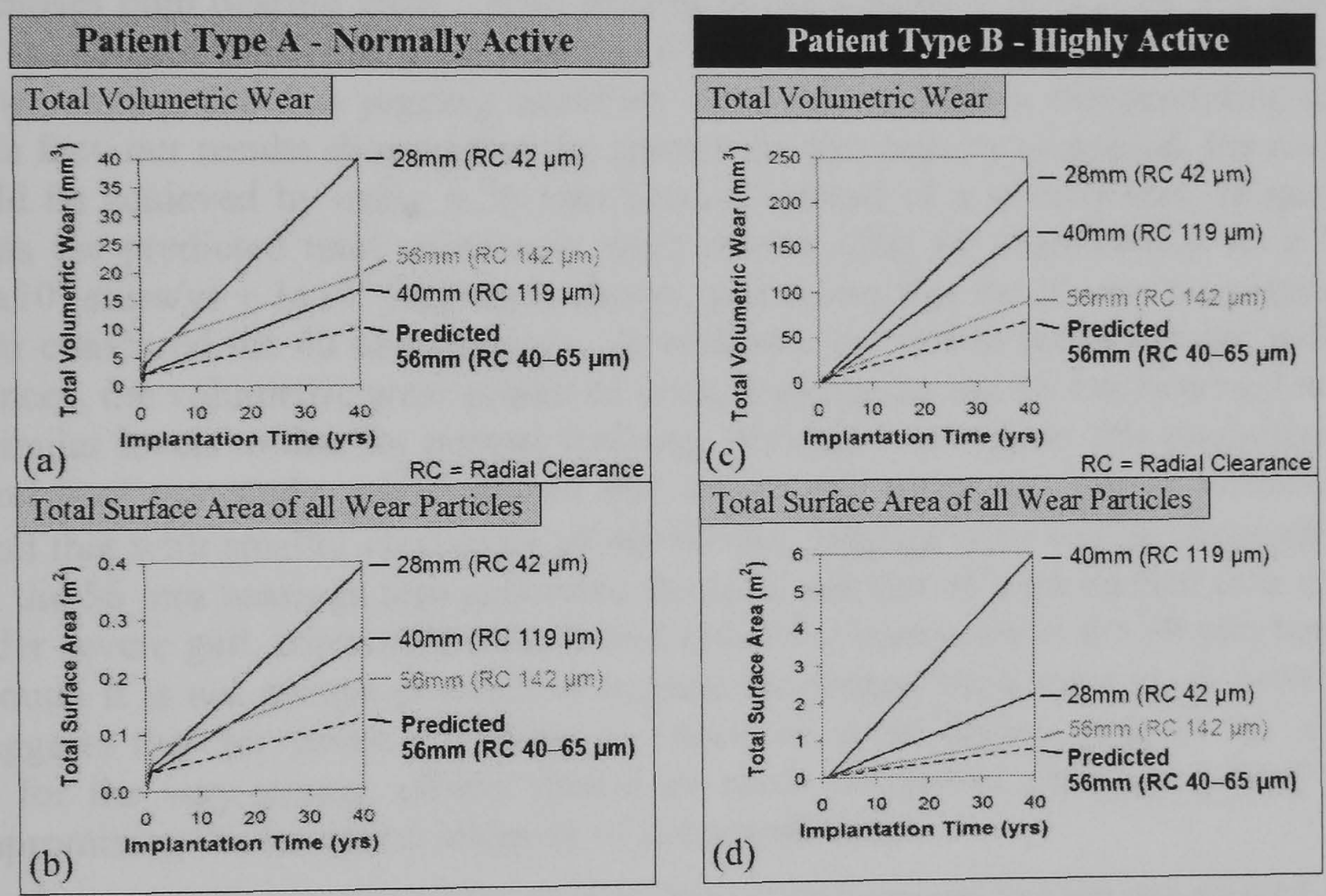


Fig. 16. Predictions of total volumetric wear and total wear particle surface area after 40 years of use for all 28, 40 and 56 mm modern Co-Cr-Mo bearings, for (a) patient type A – a low or normally active patient (undertaking ~$1x10^6$ steps/year), and (b) patient type B – a highly active patient (undertaking $2x10^6$ steps/year + $1x10^6$ jogging cycles/year).

Based on the volumetric wear and wear particle results, the total surface area and total number of wear particles produced after 40 years of implantation was predicted. The volume and surface area for every single wear particle examined in the current study was calculated using the following prolate ellipsoid equations:

$$\text{Surface Area of prolate ellipsoid} = S_{PE} = 2\pi a^2 + \frac{2\pi ab \sin^{-1}\varepsilon}{\varepsilon} \quad [1]$$

$$\text{Volume of prolate ellipsoid} = V_{PE} = \frac{4}{3}\pi a b^2 \quad [2]$$

$$\text{Eccentricity of prolate ellipsoid} = \varepsilon_{PE} = \sqrt{1 - \frac{b^2}{a^2}} \quad [3]$$

and then used as a ratio to calculate all totals. A prolate ellipsoid equation was used to minimise any errors in predictions, as the majority of wear particles were rugby-ball shaped not round (median aspect ratio 1.4). From the stead-state volumetric wear results, the total number of particles generated per year of use for all 28, 40 and 56 mm bearings were 3.8 $x10^{12}$, 1.9 $x10^{13}$, and 1.9 $x10^{12}$ respectively, and agrees with previous data[16,17,18]. Importantly, Figure 16(b) shows the predicted total surface area of all wear particles released after 40 years of use, and shows that for a normally active patient ($1x10^6$ steps/year) the 56 mm bearings generated the least total surface area compared all smaller sizes, therefore minimising subsequent ion release. The predictions also highlighted that 56 mm bearing with even lower radial clearances (40–65 μm) show much larger reductions in ion release, showing a clear 2-fold reduction compared to 40 mm bearing after 40 years.

The wear generation of all bearing diameters was found to be sensitive to the type of patient activity applied, with fast-jogging activities (4500 N max, 1.75 Hz) generating a typical 4–9 fold increase in metal wear generation compared to normal walking (2450 N max, 1 Hz). This high increase in metal wear for simulated jogging cycles indicates a significant change in lubrication action compared to normal walking, moving from a hydrodynamic/mixed regime to a mixed/boundary regime. Slow-walking (0.62 Hz) also showed a sizable increase in MOM wear release compared to normal walking (1 Hz) and was surprizing, and demonstates that it is not just high forces and sliding speeds that causes high bearing wear. With regards to the influence of bearing diameter, the results showed that the largest head size generated the lowest wear result under all normal walking, slow walking, slow jogging and fast jogging activities simulated, therefore demonstrating superior wear resistance. In fact, our results showed that the greater the gait activity simulated, the more reductions in wear could be achieved by using a 56 mm bearing instead of a smaller size, (Figure 8). Figure 16(c) presents the predicted total volumetric wear release after 40 years of use for a highly active patient, ie $2x10^6$ steps/yr + $1x10^6$ jogging cycles/yr, and shows that the 56 mm bearings generate half the total wear compared the 40 mm bearings. In addition, our results predicted that with even lower radial clearances, the volumetric wear produced under jogging for the 56 mm bearings may be further reduced to similar levels to that for normal walking. Evidence to support this prediction is shown in Figure 9a and b of our study, which shows that severe gait wear was highly influenced by radial clearance, and that with smaller clearances of 40–60 μm, jogging wear can be absolutely minimised. Importantly, the 56 mm bearings also generated the least amount of total surface area of the all wear particles under severe gait, showing a clear 2-fold reduction compared to the 40 mm bearings, Figure 16(d). Although it is not always possible to implant the largest head sizes in all patients, the study therefore suggests that for patients wishing to return to some degree of sport (or a physical job activity), or for the very young, efforts should be made to implant the largest head size possible without compromising the structural integrity of the acetabulum.

One criticism of hip simulator testing is that clinical failures are not always picked up during the testing phase due to the lack of severe conditions testing. Therefore the current study also aimed to specifically address this issue by implementing a series of severe gait conditions which would be able to detect a possible difference in *in vivo* wear performance. This aim would appear to have been achieved as all MOM bearing sizes generated using the fast-jogging cycle given the large increase in wear rate observed using this condition. As our jogging tests possessed similar forces to those created under stair ascending, tennis or dancing, i.e. common activities, more research is needed in this area to make more concrete predictions.

Although the wear generated by the larger MOM bearings under severe gait activities was much smaller compared to the use of moderately crosslinked UHMWPE, and would appear more favorable, there are still concerns however of high frictional torques with large diameter MOM bearings. It has been suggested that 28 mm bearings are more suitable for active patients in terms of minimising friction [lookup], however, more research in this area is needed as our results clearly shows that 28 mm bearings produce by far the worst wear and ion release. Although frictional torque levels were not measured for all tests in the current study, previous work by the authors have shown similar torque levels for MOM bearings and UHMWPE-on-metal (0.2–2 Nm max for walking), suggesting no elevated torque levels at all for large diameter MOM bearings. This result is also in agreement with the findings by Scholes et al, however, more research is needed.

In this study we investigated the influence of head diameter upon the wear generation of modern high carbon Co-Cr-Mo-on-Co-Cr-Mo bearing couples using both standard and severe gait simulations. Our results strongly agreed with classical lubrication theory, showing that considerable reductions in volumetric wear release can be simply achieved by increasing the femoral head diameter. In addition, our results showed that the greater the gait activity simulated, the more reductions in wear could be achieved by using a 56 mm bearing instead of a smaller size. Therefore, in order to minimise debris related biological problems in modern MOM hip arthroplasty, efforts should be made at surgeon level to implant the largest head diameter (56 mm) possible without comprimising the structural integrity of the acetabulum. Conversely, our study showed that large bearings with radial clearances greater than 80 μm can lead to excessive wear during both running-in and severe gait events. Although all MOM bearing sizes showed sizeable increases in wear under fast-jogging and slow-walking activities (3 $mm^3/10^6$ cycles), the quantities of wear however were still small compared to the use of moderately crosslinked UHMWPE under similar joint conditions (26 $mm^3/10^6$ cycles)[30]. This result demonstrates that large diameter Co-Cr-Mo resurfacing prostheses can withstand extreme joint conditions for long periods of time without leading to run away wear, and is good news for those patients wishing to return to some degree of sport or for the very young. Moreover, the 3–9 fold increases in volumetric wear for slow walking and fast jogging activities, coupled with larger wear particles for simulated jogging, all demonstrate that the simulation of just a simplistic walking model in hip joint simulation can lead to incorrect performance predictions for a wide range of patients.

## Acknowledgements

The authors gratefully acknowledge the Wishbone Trust for financial support. We are also very grateful to Corin Medical Ltd, Cirencester, UK, for the supply of all test components, and to Dr Liam Blunt of the University of Huddersfield, UK, for performing the interferometric surface analysis.

## References

1. McMinn D, Daniel J, Pynsent P: Hip resurfacing resurrected. Presented at European Hip Society, 224-225, 2002.
2. Muller ME: The benefits of metal-on-metal total hip replacements. Clin Orthop Rel Res 311: 54-59, 1995.
3. Weber BG: Experience with the Metasul total hip bearing system. Clin Orthop Rel Res 329(Suppl): 69-77, 1996.
4. Streicher RM, Semlitsch M, Schon R, Weber H, Rieker C: Metal-on-metal articulation for artificial hip joints: laboratory study and clinical results. Eng Med Part (H) 210(H): 223-232, 1996.
5. Jin ZM, Dowson D, Fisher J: Analysis of fluid film lubrication in artificial hip joint replacements with surfaces of high elastic modulus. Proc Inst Mech Eng Part (H) 211: 247-256, 1997.
6. Goldsmith AAJ, Dowson D, Isaac GH, Lancaster JG: A comparative joint simulator study of the wear of metal-on-metal and alternative material combinations in hip replacements. Proc Instn Mech Engrs, 214 (H): 39-47, 2000.
7. Smith SL, Dowson D, Goldsmith AAJ: The effect of femoral head diameter upon lubrication and wear of metal-on-metal total hip replacements. Eng Med Part (H) 215(2): 161-170, 2001.
8. Dowson D: New joints for the Millennium: wear control in total replacement hip joints. Proc Inst Mech Eng Part (H) 215(4): 335-58, 2001.
9. Amstutz HC, Grigoris P, Dorey FJ: Evolution and future of surface replacement of the hip. J Orthop Sci 3(3): 169-186, 1998.
10. Beaule PE, Schmalzried TP, Udomkiat P, Amstutz HC: Jumbo femoral head for the treatment of recurrent dislocation following total hip replacement. J Bone Joint Surg 84-A(2): 256-263, 2002.
11. McMinn D, Treacy R, Lin K, Pynsent P: Metal on metal surface replacement of the hip. Experience of the McMinn prothesis. Clin Orthop Rel Res 329(Suppl): 89-98, 1996.
12. Wagner M, Wagner H: Preliminary results of uncemented metal on metal stemmed and resurfacing hip replacement arthroplasty. Clin Orthop Rel Res 329(Suppl): 78-88, 1996.

13. Schmalzried TP, Fowble VA, Ure KJ, Amstutz HC: Metal on metal surface replacement of the hip. Clin Orthop Rel Res 329(Suppl): 106-114, 1996.
14. Amstutz HC, Grigoris P: Metal on metal bearings in hip arthroplasty. Clin Orthop Rel Res 329(Suppl): 11-34, 1996.
15. Jacobsson SA, Djerf K, Wahlstrom O: Twenty-year results of McKee-Farrar versus charnley prosthesis. Clin Orthop Rel Res 329(Suppl): 60-68, 1996.
16. Doorn PF, Campbell PA, Worrall J, Benya PD, McKellop HA, Amstutz HC: Metal wear particle characterization from metal on metal total hip replacement: transmission electron microscopy study of periprosthetic tissue and isolated particles. J Biomed Mater Res 42: 103-111, 1998.
17. Ingham E, Fisher J: Biological reactions to wear debris in total joint replacement. Proc Instn Mech Engrs, 214 (H): 21-37, 2000.
18. Fisher J, Besong AA, Firkins PJ, Barbour PSM et al: Wear debris generation in UHMWPE on ceramic, metal on metal and ceramic on ceramic hip prostheses. Trans Sixth World Biomaterials, 871, 2000.
19. Brodner W, Bitzan P, Meisinger V, Kaider A et al: Elevated serum cobalt with metal-on-metal articulating surfaces. J Bone Joint Surg Br. 79-B(2): 316-321, 1997.
20. Savarino L, Granchi D, Ciapetti G, Cenni E, Nardi Pantoli A, Rotini R, Veronesi CA, Baldini N, Giunti A: Ion release in patients with metal-on-metal hip bearings in total joint replacement: a comparison with metal-on-polyethylene bearings. J Biomed Mater Res 63(5): 467-474, 2002.
21. MacDonald SJ, McCalden RW, Chess DG, Bourne RB, Rorabeck CH, Cleland A, Leung F: Metal-on-metal verses polyethylene in hip arthroplasty: a randomised clinical trial. Clin Orthop Rel Res 406: 282-296, 2003.
22. Schmalzried T, Peters Z, Maurer B, Bragdon C, Harris W: Long duration metal-on-metal total hip replacement with low wear of the articulating surfaces. J Arthroplasty 11: 322-331, 1996.
23. Campbell PA, Wang M, Amstutz HC, Goodman SB: Positive cytokine production in failed metal-on-metal total hip replacements. Acta Orthop Scand 73(5): 506-512, 2002.
24. Catelas I, Petit A, Zukor DJ, Antoniou J, Huk OL: TNF-α secretion and macrophage mortality induced by cobalt and chromium ions in vitro-qualitative analysis of apoptosis. Biomaterials 24: 383-391, 2003.
25. Goodman SB, Lind M, Song Y, Smith RL: In vitro, in vivo and tissue retrieval studies on particulate debris. Clin Orthop Rel Res 352: 25-34, 1998.
26. Wang SW, Shi XL: Molecular mechanisms of metal toxicity and carcinogenesis. Molecular & Cellular Biochemistry 222(1-2): 3-9, 2001.
27. Yang J, Merritt K: Production of monoclonal antibodies to study corrosion products of CO-CR biomaterials. J Biomed Mater Res 31(1): 71-80, 1996.
28. Medley, JB, Chan FW, Krygier JJ, Bobyn JD: Comparison of alloys and designs in a hip simulator study of metal on metal implants. Clin Orthop Rel Res 329(Suppl): 148-159, 1996.
29. Chan FW, Bobyn JD, Medley JB, Krygier JJ, Yue S, Tanzer M: Engineering issues and wear performance of metal on metal hip implants. Clin Orthop Rel Res 333: 96-107, 1996.
30. Bowsher JG, Shelton JC: A hip simulator study of the influence of patient activity level on the wear of crosslinked polyethylene under smooth and roughened femoral conditions. Wear 250: 167-179, 2001.
31. Clarke IC, Good V, Williams P, et al: Ultra-low wear rates for rigid-on-rigid bearings in total hip replacement. Eng Med Part H 214(4): 331-347, 2000.
32. Firkins PJ, Tipper JL, Ingham E, Stone MH, Farrar R, Fisher J: Influence of simulator kinematics on the wear of metal-on-metal hip prostheses. Proc Instn Mech Engrs, 215 (H): 119-121, 2001.
33. Catelas I, Bobyn D, Vali H, Medley JB et al: Characterization of metal-metal wear particles isolated from a hip joint simulator. Trans Sixth World Biomaterials, 482, 2000.
34. Green TR, Fisher J, Stone M, Wroblewski BM, Ingham E: Polyethylene particles of a 'critical size' are necessary for the induction of cytokines by macrophages in vitro. Biomaterials 19(24): 2297-2302, 1998.
35. Soh EW, Blunn GW, Wait ME, Walker PS: Size and shape of metal particles from metal-on-metal total hip replacements. Trans 42th Orthop Res Soc, Georgia: 462, 1996.
36. Shahgaldi BF, Heatley FW, Dewar A, Corrin B: In vivo corrosion of cobalt-chromium and titanium wear particles. J Bone Joint Surg Br 77(6): 962-966, 1995.

37. Chan FW, Bobyn JD, Medley JB, Krygier JJ: Simulator wear of metal-metal hip implants under adverse load conditions. Trans 45th Orthop Res Soc, California, USA, Vol. 24, 310, 1999.
38. Bowsher JG, Nevelos J, Pickard J, Shelton JC: Do heat treatments influence the wear of large diameter metal-on-metal hip joints? – An in vitro study under normal and adverse gait conditions. Trans 49th Orthop Res Soc, New Orleans, Louisiana, USA, Vol.28, 1398, 2003.
39. McKellop H, Park SH, Chiesa R, et al: In vivo wear of 3 types of metal on metal hip prostheses during 2 decades of use. Clin Orthop Rel Res 329(S), 128-140, 1996.
40. Lu B, Marti A, McKellop H: Wear of a second-generation metal-on-metal hip relacement effect of third-body abrasive particles. Sixth World Biomaterials Congress, California, USA: 183, 2000.
41. Butterfield M, Stewart T, Williams S, Ingham E, Stone M, Fisher J: Wear of metal-metal and ceramic-ceramic hip prostheses with swing phase microseparation. Trans 48th Orthop Res Soc, USA, Vol. 27, 128, 2002.
42. Wang A, Sun DC, Yau S, et al: Orientation softening in the deformation and wear of ultra-high molecular weight polyethylene. Wear 203/204: 230-241, 1997.
43. Ramamurti BS, Estok DM, Jasty M, Harris WH: Analysis of the kinematics of different hip simulators used to study wear of candidate materials for the articulation of total hip arthroplasties. J Orthop Res 16(3): 365-369, 1998.
44. Anissian HL, Stark A, Good V, Dahlstrand H, Clarke IC: The wear patterns in metal-on-metal hip prostheses. J Biomed Mater Res 58(6): 673-678, 2001.
45. Saari H, Santavirta S, Nordstrom D, Paavolainen P, Konttinen YT: Hyaluronate in total replacement. J Rheumatol 20(1): 87-90, 1993.
46. Noordin S, Schmalzried TP, Campbell PA, et al: Synovial Fluid from Patients with Prosthetic Joint Arthroplasty: Protein Concentration and In Vivo Wear of Polyethylene. OrthopTrans 21(3), 1022-1023: 1997-98.
47. McKellop HA, Clarke IC: Degradation and wear of ultra-high-molecular-weight polyethylene. Presented at Corrosion and Degradation of Implant Materials. Second symposium, ASTM STP 859, Fraker AC, Griffin CD, Eds. American Society for Testing and Materials, Philadelphia, 351-368, 1985.
48. Paul JP: Forces transmitted by joints in the human body. Eng Med Part H 181(3-F): 8-15, 1966.
49. Bergmann G, Graichen F, Rohlmann A: Hip joint loading during walking, running, measured in two patients. J Biomechanics 26(8): 969-990, 1993.
50. Catelas I, Bobyn D, Vali H, Medley JB, Campbell et al: Changes in metal-metal wear particle characteristics with isolation protocols. Trans 46th Orthop Res Soc, Florida: 26, 2000.
51. Scholes SC, Green SM, Unsworth A: The wear of metal-metal total hip prostheses measured in a hip simulator. Proc Instn Mech Engrs, 215 (H): 523-530, 2001.
52. Rieker C, Konrad R, Schon R: In vitro comparison of the two hard-hard articulations for total hip replacements. Proc Inst Mech Eng Part (H) 215: 153-160, 2001.

# 'SEVERE' PATIENT ACTIVITY SIMULATION SUBSTANTIALLY INCREASED THE NUMBER OF SUBMICRON-SIZED WEAR PARTICLES IN A XLPE-ON-METAL HIP BEARING STUDY

+*, **Bowsher, J G; *Hussain, A; ****Elfick P D, ***Green S M; *Shelton, J C
*The IRC in Biomedical Materials and Department of Engineering, Queen Mary, University of London, London, E1 4NS, UK
+**FAX: (909) 558-6018 **Email: mail@johnbowsher.com

**Introduction** The clinical use of cross-linked polyethylene shows great potential in reducing wear generation and osteolysis in hip arthroplasty [1,2,3]. However, there are still concerns over the range of possible wear rates from cross-linked PE (XLPE) prostheses. Hip simulator studies have suggested that while XLPE generates low wear under smooth bearing surfaces, there also appears to be an increased sensitivity to scratched femoral conditions which can occur in the patient [4,5]. However, these simulator studies have not combined damaged articular surfaces with a severe gait model, i.e. to represent a worst-case situation for high-risk active patients.

Recent studies by the authors have introduced fast jogging cycles to model severe gait conditions [6]. This wear model generated a 2-fold increase in volumetric wear rates for undamaged lightly cross-linked polyethylene-on-Co-Cr-Mo bearings compared to normal walking (Table 1) [6]. When introducing scratched femoral balls, we achieved wear rates greater than 2000 $mm^3$/year. However, changes in PE wear rates are important, but changes in wear particle sizes and numbers are also critical [7]. However, to date, the factors that influence particle distributions from XLPE hip bearings are not well understood, especial under adverse gait.

Therefore, the aim of this wear study was to test the hypothesis that severe gait conditions will greatly increase the number of XLPE sub-micron-sized wear particles compared to normal walking conditions.

| Table 1 | Mean PE Wear Rate ($mm^3$/Mc) [6] *(5 Mrads γ XLPE-on-Co-Cr)* | Ratio |
|---|---|---|
| 1 Hz Normal Walking (smooth) | 20 | x10 |
| 1 Hz Normal Walking (Rough) | 200 | |
| 1.75 Hz Fast Jogging (Smooth) | 30 | x70 |
| 1.75 Hz Fast Jogging (Rough) | >2000 | |

**Materials and Methods** We received 28mm ID, 48mm OD, lightly-cross-linked (5 Mrads in gamma, GUR 1020) UHMWPE-on-Co-Cr-Mo bearings (DePuy Ltd, UK, Table 2). The cups were positioned physiologically in an orbital hip joint simulator (MTS Systems, USA). The lubricant was 25% newborn calf serum, 17 mg/ml protein content (500 ml, heated to 37 °C). All bearings were run to 2.8 million cycles of normal walking (2450 N max, 1 Hz) to achieve steady-state wear conditions [8]. One 0.6 million cycles of simulated fast jogging (4500 N max, 1.75 Hz) was then undertaken [6], with 1 hour resting periods every 8000 cycles. Then all components were roughened using SiC paper (Table 2). Additional normal walking and fast jogging tests were performed under rough conditions (Table 3).

| Table 2 | Co-Cr-Mo Surface Roughness (μm) | | |
|---|---|---|---|
| | Median Ra | Range of Ra | Rp max |
| [A] Smooth Conditions (n=4) | 0.008 | 0.005–0.015 | 0.46 |
| [B] Ø 5mm Rough Patch (n=1) | – | 0.003–0.3 | 1.35 |
| [C] Fully Rough Ball (n=3) | 0.34 | 0.188–0.539 | 1.4 |

| Table 3 | Patient Activity Type *(No. of Cycles Undertaken, $10^6$)* | |
|---|---|---|
| Femoral Head Condition | Normal Walking | Fast Jogging |
| Virgin (Smooth) | 2.8 | 0.6 |
| Ø 5mm Rough Patch (Partially Rough) | 2.0 | 0.3 |
| Fully Rough Ball | 1.0 | 0.3 |

Wear particles were extracted from 19 serum samples from 0.5 Mc of normal walking and 0.6 Mc of fast jogging [9]. PE wear particles were analysed using a Mastersizer 2000 (Malvern Instru, UK) [10]. This method calculated the size, volume and number distribution of over $>10^{12}$ particles in one sample.

**Results** All polyethylene wear particles observed were similar in size and distribution to those reported clinically using identical methods [10]. Under smooth conditions, fast jogging created a 5-fold increase in the number of sub-micron sized wear particles/Mc compared to normal walking (Table 4). Fast jogging generated far less numbers of larger wear particles (>10 μm) compared to walking (Figure 1). Under partially rough conditions, normal walking lead to a 3-fold increase in sub-micron particles/Mc. Under fully rough conditions, fast jogging lead to a 1700-fold increase in sub-micron particles/Mc (Table 4).

| Table 4 | Mean Vol. Wear Rate ($mm^3/10^6$ Cycles) | No. of Sub-micron Sized PE Particles | | Debris Ratio To Walk Smooth |
|---|---|---|---|---|
| | | Per $10^6$ Cycles | Per Step | |
| [A] Normal Walking (Smooth Balls) | 18.0 (n=41) | $4 \times 10^{12}$ | $4 \times 10^6$ | |
| [B] Normal Walking (Partially Rough Balls) | 32.4 (n=6) | $12 \times 10^{12}$ | $12 \times 10^6$ | x3 |
| [A] Fast Jogging (Smooth Balls) | 33.2 (n=46) | $19 \times 10^{12}$ | $19 \times 10^6$ | x5 |
| [C] Fast Jogging (Fully Rough Balls) | 1200 (n=4) | $7000 \times 10^{12}$ | $7000 \times 10^6$ | x1700 |

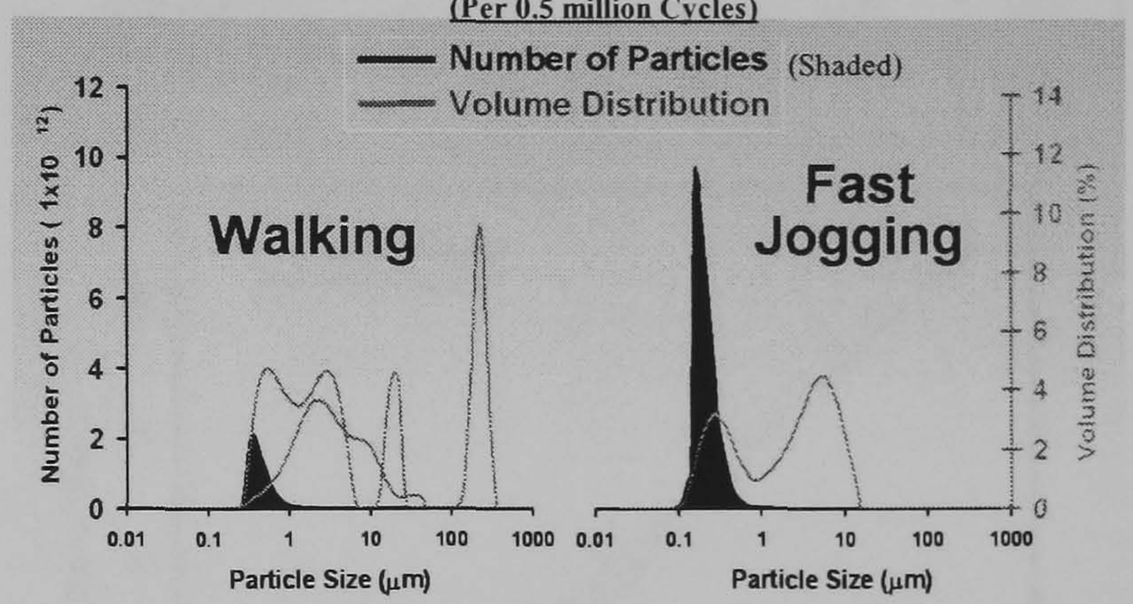


*Figure 1. Change in wear particle parameters with varying patient*

**Discussion and Conclusions** This is the first study to show that the size distribution of 5 Mrads ($N_2$) XLPE wear particles can be influenced by the degree of patient gait. Fast jogging showed a greater influence on the number of sub-micron-sized wear particles (5-fold) than on volumetric wear rate (2-fold). Fast jogging also did not generate the larger wear particles (>10 μm) produced by normal walking. Therefore our hypothesis was proved.

This result suggests that errors may be made in calculating the osteolytic potential for high-risk patients if only considering normal walking models. The clinical significance of this result suggests that highly active PE patients will generate high numbers of bioactive wear particles (0.2–10μm) [11].

Roughening of the Co-Cr-Mo femoral heads created a 1700-fold increase in the numbers of sub-micron PE particles under fast jogging. Zirconia heads would be more favourable for high-risk patients.

**References**

1. Wroblewski BM et al, J Bone Joint Surg. Br. 78(2), 280-285, 1996
2. Oonishi H et al, J Mater Sci Mater Med, 9(10), 575-581, 1998
3. Muratoglu OK et al, J Biomaterial, 20, 1463-1470, 1999
4. McKellop H et al, Clin Orthop, 369, 73-82, 1999
5. Endo MM et al, Biomed Mater Eng, 11, 23-35, 2001
6. Bowsher JG & Shelton JC, Wear, 250, 167-179, 2001
7. Ingham E, Fisher J: Proc Instn Mech Engrs, 214(H), 21-37, 2000
8. Paul JP, Proc Instn Mech Engrs (H), 181, 8-15, 1966
9. Campbell P et al, Proc Instn Mech Engrs (H), 210, 167-174, 1996
10. Elfick APD et al, J Biomed Mater Res, 65(A), 95-108, 2003
11. Green TR et al, Biomaterials, 19(24), 2297-2302, 1998

**Acknowledgements** The authors thank EPSRC, UK, for the core grant in the IRC in Biomedical Materials, and DePuy Ltd, UK.

**LLUMC, Dept of Orthop, 11406 Loma Linda Drive, Suite 606, Loma Linda, California, 92354, USA, ***Centre for Biomed Eng, University of Durham, DH1 3LE, UK, ****Stanford University, California, US

# 'SEVERE' PATIENT ACTIVITY SIMULATION SUBSTANTIALLY INCREASED WEAR PARTICLE SURFACE AREA IN A METAL-ON-METAL HIP BEARING STUDY

+*, **Bowsher, J G; *Hussain, A; **Williams, P A; ***Nevelos, J; *Shelton, J C
*IRC in Biomedical Materials and Department of Engineering, Queen Mary, University of London, London, E1 4NS, UK
+**FAX: (909) 558-6018 **Email: mail@johnbowsher.com

**Introduction** Metal-on-metal (MOM) hip arthroplasty has seen rapid growth worldwide. However, there still remains concern over their long-term biocompatibility due to systemic ion release [1]. Patients at greatest risk are the highly active males. However, there has been no *in vitro* model created to simulate these high-risk patients. In addition, there appears to be a discrepancy in MOM wear performance between clinical data and 'simplistic' hip simulator gait studies [2,3] with clinical wear being greater and more variable [4].

Laboratory MOM studies with more 'severe' gait such as intermittent loading, micro-separation etc. have generated a maximum wear rate of <1.6 $mm^3$/Mc for 28mm Co-Cr bearings (Table 1). This does not explain the large variations seen clinically. Plus, such studies do not simulate a highly active patient undertaking regular aggressive exercise, for example, jogging.

| Table 1 | MOM Wear Model Type | MOM Mean Wear Rate ($mm^3$/Mc) |
|---|---|---|
| Chan et al [2] | Intermittent Loading | 1.20 |
| Firkins et al [3] | Eccentric Wear Paths | 1.64 |
| Butterfield et al [5] | Micro-Separation | 1.54 |
| Lu et al [6] | Third-body Particles | 1.80 |
| Williams et al [7] | High Swing-Phase Load | 0.60 |
| Bowsher et al [8] | Fast Jogging Cycles | 4.00 |

The authors introduced fast jogging cycles to model 'severe' gait conditions [8,9]. This model represented the most severe published hip simulator-testing regime, creating 2–3-fold greater wear compared to other studies (Table 1). While wear rates are important, changes in wear particle sizes may also be critical [1]. To date, the factors that influence the size range of wear particles from MOM hip bearings are not well understood.

Therefore, the aim of this wear study was to test the hypothesis that 'severe' gait conditions will greatly increase the size of Co-Cr-Mo wear particles, thereby causing a sizable increase in wear particle surface area.

**Materials and Methods** We used four 40mm MOM bearings (cast high carbon (0.3 % wt) Co-Cr-Mo HIPed/solution annealed, Corin Medical, Cirencester, UK) (Table 2). The cups were inclined physiologically at 35 ° to the horizontal in an orbital hip joint simulator (MTS Systems, USA). The lubricant was 25% newborn calf serum, 17 mg/ml protein content (500 ml, heated to 37 °C). All bearings were run to 3 million cycles of normal walking (2450 N max, 1 Hz) to achieve steady-state (SS) wear conditions. Then one million cycles of simulated fast jogging (4500 N max, 1.75 Hz) was undertaken [8,9], with 1-hour resting periods every 8000 cycles.

| Table 2 | Radial Clearance | Max. Dev. Sphericity | Surface Roughness (nm) Head & Cups |
|---|---|---|---|
| 40mm Co-Cr-Mo MOM | ~119 μm | 10 μm | Ra 10-30, Rp 10-40 |

Wear particles were extracted from serum samples taken following 0.5 Mc of normal walking and fast jogging tests [10,11]. This enzymatic protocol causes less corrosion to metal particles [11]. EDAX and TEM at two magnifications, (x10k) and (x50k), were used to identify and photograph Co-Cr-Mo particles. Over 300 wear particles from each group were analysed using Image Pro Plus. Based on the volumetric wear rates and wear particle data, a total number of particles generated per million cycles was calculated for each patient activity group. Using a surface area equation for a prolate ellipsoid, the total wear particle surface area was then calculated. A needle particle is defined as having an elongation greater than 4. Both parametric and non-parametric statistics were used to calculate the level of significance. Elongation is length divided by width (aspect ratio).

**Results** The majority of Co-Cr-Mo wear particles observed were in the nanometer range, and were oval or round in shape. Large particles (>1μm) were found in both groups. Fast jogging created a 25–33% increase in mean wear particle diameter, mean length, and elongation compared to those generated under walking ($p<0.01$) (Table 3). Walking generated particles from 1 to 5 elongation, where fast jogging created particles from 1 to 20 elongation (Figure 1). For walking, 1.9% of all particles were defined as needle shaped, whereas 6.1% of all particles (a 3-fold increase) were generated in fast jogging. Fast jogging created a 20-fold increase in total wear particle surface area per million cycles compared to normal walking (Table 3).

| Table 3 | Patient Activity Type | | | |
|---|---|---|---|---|
| | Normal Walking | Fast Jogging | Ratio Walk/Jogg | p-value |
| Mean SS Wear Rates [9] ($mm^3/10^6$ Cycles) (Mc) | 0.4 | 3.53 | 8.83 | 0.001 |
| **Co-Cr-Mo Wear Particle Data** | | | | |
| **No. of Wear Particles** | **314** | **378** | | |
| Mean Diameter (nm) | 99 | 132 | 1.33 | 0.001 |
| Mean Length (nm) | 135 | 169 | 1.25 | 0.010 |
| Mean Width (nm) | 89 | 92 | 1.03 | 0.680 |
| Mean Elongation | 1.6 | 2.0 | 1.25 | 0.010 |
| Total Wear Particle Surface Area Per Mc ($m^2/10^6$ Cycles) | 0.116 | 2.42 | 21.0 | 0.001 |

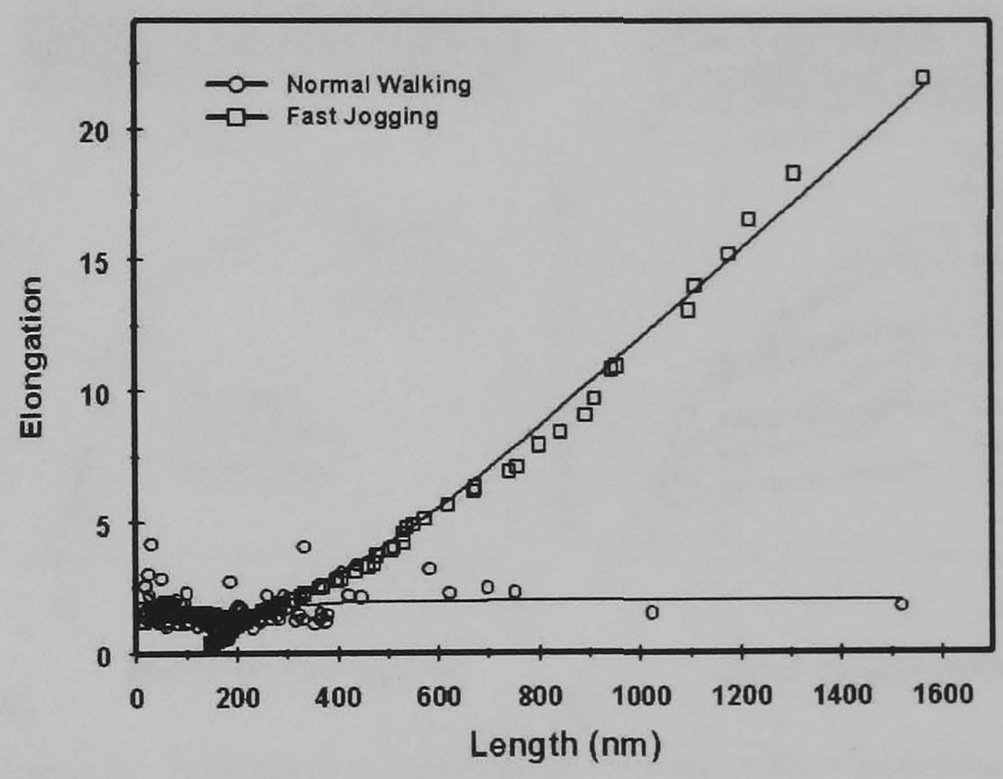


*Figure 1. Change in wear particle shape with varying patient activity.*

**Discussion and Conclusions** This is the first study to show that patient factors can affect wear particle sizes in modern MOM bearings. Simulated fast jogging created a 3-fold increase in the number of elongated (needle) wear particles compared to normal walking, and generating a 20-fold increase in total wear particle surface area per year of use compared to normal walking. Therefore our hypothesis was proved. The clinical significance of this result suggests that highly active MOM patients will exhibit greater ion release. Our Co-Cr-Mo wear particles were similar in size to those reported clinically [10].

**References**

1. Ingham E, Fisher J: Proc Instn Mech Engrs, 214(H), 21-37, 2000
2. Chan FW et al, Trans 45th ORS, Vol.24, 310, 1999
3. Firkins PJ et al, Proc Instn Mech Engrs (H), 215(1), 119-121, 2001
4. Sieber HP et al, J Bone Joint Surg Br, 81(1), 46-50, 1999
5. Butterfield M et al, Trans 48th ORS, Vol.27, 128, 2002
6. Lu B et al, Trans 6th World Biomaterials, 183, 2000
7. Williams S, Trans 7th World Biomaterials, Sydney, 2004
8. Bowsher JG et al, Trans 49th ORS, Vol.28, 1398, 2003
9. Bowsher JG & Shelton JC, Wear, 250, 167-179, 2001
10. Doorn PF et al, J Biomed Mater Res, 42, 103-111, 1998
11. Catelas I et al, Trans 6th World Biomaterials, 482, 2000

**Acknowledgements** This research was supported by Corin Medical UK

**LLUMC, Dept of Orthop, 11406 Loma Linda Drive, Suite 606, Loma Linda, CA 92354, USA, ***Corin Medical, Cirencester, GL7 1YJ, UK

# $N_2$–ION IMPLANTATION SHOWED NO REDUCTION IN RUNNING-IN WEAR FOR METAL-ON-METAL HIP BEARINGS

+**Bowsher, J G; ***Nevelos, J; *Hussain, A; **Williams, P A; *Shelton, J C
*The IRC in Biomedical Materials and Department of Engineering, Queen Mary, University of London, London, E1 4NS, UK
+**FAX: (909) 558-6018 **Email: mail@johnbowsher.com

**Introduction** The potential benefits of $N_2$–ion implantation as a surface modification to chromium bearing components in orthopaedics include a 30–50% increase in hardness, reduced friction and increased wettability [1]. Currently, the use of ion implanted Co-Cr femoral heads has been suggested to reduce clinical wear rates of polyethylene cups by 20% [2], and to increase resistance of metallic surfaces against PMMA abrasion [3]. However, to date there has been no ion implanted metal-on-metal (MOM) wear studies reported.

At present, one of the disadvantages of modern large diameter MOM bearings is their high running-in wear phase [4,5,6], which creates an extremely high number of wear particles and ions. There is a possibility that ion implantation may minimise the severity of the running-in phase for MOM bearings. Although the depth of ion implantation is small in comparison to the wear penetration of conventional MOM, small gains in wear resistance during this critical phase would be beneficial.

Therefore, the aim of this wear study was to test the hypothesis that ion implantation may minimise the severity of the running-in phase for modern 40 mm MOM prostheses.

**Materials and Methods** Two MOM bearings were manufactured by Corin Medical (Cirencester, UK), and were nitrogen ion implanted (ion energy: 92 keV, ion dose $1x10^{17}$ ions/cm$^2$) to a max. depth of ~0.2 μm. The wear performance was compared to previously reported data for eight un-treated MOM bearings studied under matching protocols [5]. All bearings were 40 mm diameter (cast high carbon (0.3 % wt) Co-Cr-Mo HIPed/solution annealed) with similar bearing geometries (Table 1).

| Table 1 | Radial Clearance | Max. Dev. Sphericity | Surface Roughness (nm) Head & Cups |
|---|---|---|---|
| Ion Implanted | ~111 μm | 14 μm | Ra 5-30, Rp 10-30 |
| (Controls) Un-Treated | ~119 μm | 10 μm | Ra 10-30, Rp 10-40 |

The cups were inclined physiologically at 35 ° to the horizontal in an orbital hip joint simulator (MTS Systems, USA). The lubricant was 25% newborn calf serum, protein content of 17 mg/ml (500 ml, heated to 37 °C), and changed every 0.5 million cycles. Wear was measured gravimetrically. Volumetric changes were determined using a density of 8300 kg/m$^3$ for Co-Cr. All studies were run to ≥3 million cycles of normal walking (2450 N max, 1 Hz) [7] to cover the transition from running-in to steady-state wear conditions (Table 2). Analysis of co-variance (ANCOVA) was used to calculate the level of significance.

| Table 2 | Running-In (RI) Phase | | Steady-State (SS) Phase | |
|---|---|---|---|---|
| | *No. Cycles ($x10^6$)(Mc)* | *No. of Data Points* | *No. Cycles ($x10^6$)* | *No. of Data Points* |
| Ion Implanted | Initial 1.0 | 6 | 2.5 | 4 |
| Un-Treated | Initial 1.0 | 21 | 2.0 | 40 |

**Results** SEM examinations of all wear surfaces showed large polished zones interspersed with scratches (2-10 μm in width), similar to those observed clinically [8]. After the initial 500,000 cycles, a large proportion of the 'black' ion implanted surfaces wore off leaving an un-treated 'silver' surface (Figure 1). Under running-in conditions, the two ion implanted bearings showed a 50% increase in mean wear compared to the un-treated (control) bearings (Figure 2, Table 3) ($p<0.05$). Under steady-state conditions, the ion implanted bearings showed an 80% increase in mean wear rate compared to the un-treated joints ($p<0.05$).

**Discussion** All MOM bearings produced a biphasic wear pattern, generating a running-in wear rate that was 5-times greater compared to steady-state. The introduction of $N_2$ ion implanted MOM modified surfaces offered no reduction in volumetric wear compared to un-treated bearings during the aggressive run-in phase, or even during steady-state. Therefore our hypothesis was negated. Our results suggest that surface modification of MOM bearings by ion implantation offers no clinical benefit. A large proportion of the modified surface coating wore off in the initial half million cycles. The depth of ion implantation (0.2μm) was undoubtedly too small in comparison to the potential run-in wear penetration of MOM prostheses (25 μm) [9].

**Conclusion** $N_2$–ion implantation did not offer any reduction in the aggressive running-in wear phase for large diameter high carbon cast Co-Cr-Mo-on-Co-Cr-Mo hip prostheses, and therefore would appear to have no clinical benefit for MOM.

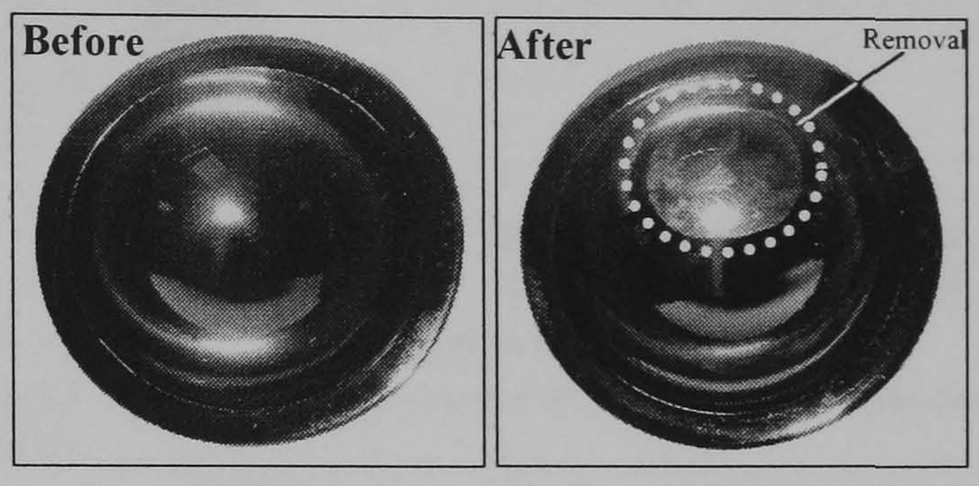


*Figure 1. Images of an ion implanted Co-Cr cup showing removal of the modified surface after the initial 500,000 cycles of hip simulation.*

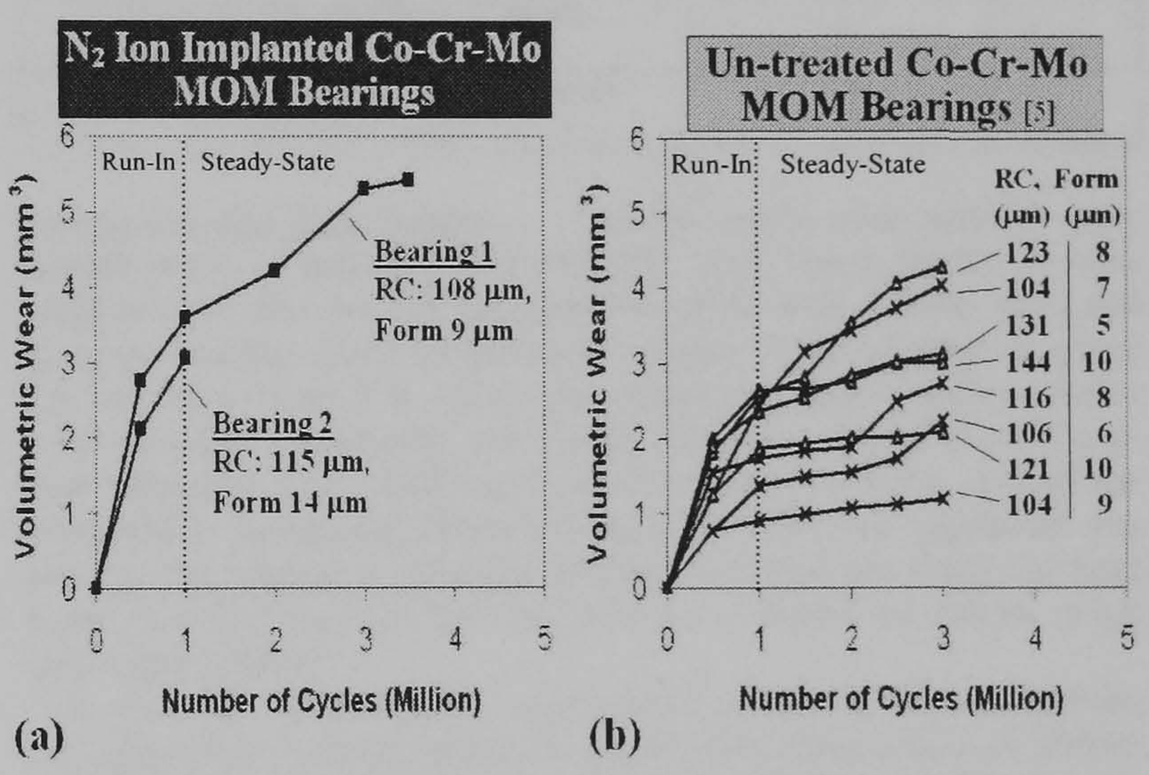


*Figure 2. Variations of combined (head+cup) MOM volumetric wear verses number of cycles under walking, (a) ion implanted,(b) un-treated.*

| Table 3 | Ion Implanted MOM | | Un-Treated MOM | | |
|---|---|---|---|---|---|
| | Mean Wear Rate (mm$^3$/Mc) | 95% CI | Mean Wear Rate (mm$^3$/Mc) | 95% CI | p-value |
| **Running-In (RI) Phase** | 3.30 | 1.49 | 2.20 | 0.48 | 0.004 |
| **Steady-State (SS) Phase** | 0.78 | 0.39 | 0.43 | 0.38 | 0.001 |
| **RI/SS Ratio** | 5.1 | | 5.5 | | |

**Acknowledgements** This research was funded by the Wishbone Trust, UK, and Corin Medical UK.

**References**

1. Onate JI et al, Thin Solid Films, 317: 471-476, 1998
2. Maruyama M et al, Clin Orthop Rel Res, 370: 183-191, 2000
3. McKellop et al, J Biomed Mater Res, 24(11), 1413-1425, 1990
4. Chan et al, Clin Orthop Rel Res, 333: 96-107, 1996
5. Bowsher JG et al, 50th ORS, San Fran, Vol.29, 1453, 2004
6. Clarke IC et al, Proc Instn Mech Engrs, 214(H-4), 331-347, 2000
7. Paul JP, Proc Instn Mech Engrs, 181(H), 8-15, 1966
8. McKellop H et al, Clin Orthop Rel Res, 329(S), 128-140, 1996
9. Sieber HP et al, J Bone Joint Surg Br, 81(1), 46-50, 1999

**LLUMC, Dept of Orthop, 11406 Loma Linda Drive, Suite 606, Loma Linda, CA 92354, USA, ***Corin Medical, Cirencester, GL7 1YJ, UK

# LARGER HEAD DIAMETERS HAVE THE POTENTIAL TO REDUCE ION RELEASE IN METAL-ON-METAL HIP WEAR SIMULATIONS

+**Bowsher, J G; *Hussain, A; ***Nevelos, J; **Williams, P A; *Shelton, J C
*The IRC in Biomedical Materials and Department of Engineering, Queen Mary, University of London, London, E1 4NS, UK
+**FAX: (909) 558-6018 **Email: mail@johnbowsher.com

**Introduction** Metal-on-metal (MOM) hip arthroplasty has seen rapid growth worldwide. However, there still remains concern over their long-term biocompatibility due to systemic ion release [1]. Therefore minimising wear particles and ion release is highly desirable.

Classical elastohydrodynamic theory suggests that fluid-film lubrication is possible in large diameter MOM bearings, and hence it is inferred that wear will be reduced [2]. Improved wear resistance for large head sizes has been demonstrated in the laboratory under both normal walking models [3,4] and a severe 'fast-jogging' model [5]. Although reductions in wear volumes are important, changes in wear particle sizes are also critical [1]. However, to date, the bearing parameters that influence the size range of Co-Cr-Mo wear particles from second-generation MOM bearings are not understood.

Therefore, the aim of this investigation was to test the hypothesis that larger diameter MOM bearings (≥40mm) will generate smaller Co-Cr-Mo wear particles compared to a 28mm size, and reduce wear particle surface area.

**Materials and Methods** 4x 28mm, 4x 40mm, and 4x 56mm diameter MOM bearings (cast high carbon (0.3 % wt) Co-Cr-Mo HIPed/solution annealed) were manufactured by Corin Medical (Cirencester, UK) (Table 1). The cups were positioned physiologically in an orbital hip joint simulator (MTS Systems, USA). The lubricant was 25% newborn calf serum, 17 mg/ml protein content (500 ml, heated to 37 °C). All bearings were run to ≥3 million cycles of normal walking (2450 N max, 1 Hz) [6] to achieve steady-state (SS) wear conditions.

| Table 1 | Mean Radial Clearance (μm) | Max. Dev. of Sphericity (μm) | Surface Roughness (nm) Head & Cups |
|---|---|---|---|
| 28 mm Dia. | 42 | 10 | – |
| 40 mm Dia. | 119 | 10 | Ra 10-30, Rp 10-40 |
| 56 mm Dia. | 142 | 12 | – |

Wear particles were extracted from 6 serum samples from 0.5 Mc of normal walking tests (for all 28, 40 and 56 mm bearing) using an established method [7,8]. This enzymatic protocol causes less corrosion to metal particles than the use of KOH or NaOH [8]. EDAX and TEM at two magnifications, (x10k) and (x50k), was used to identify and photograph both large and small Co-Cr-Mo particles respectively. 138–314 wear particles from each group were analysed using Image Pro Plus. Based on the volumetric wear rates and wear particle data, a total number of particles generated per million cycles was calculated for each patient activity group. Using a surface area equation for a prolate ellipsoid, the total wear particle surface area was then calculated. Both parametric and non-parametric statistics were used to calculate the level of significance.

**Results** The majority of Co-Cr-Mo wear particles observed were in the nanometer range, and were oval or round in shape. Large particles (>1μm) were found in all groups. The 28mm bearings generated a 2-fold increase in median wear particle diameter compared to the larger head sizes ($p<0.05$) (Figure 1). All debris generated a similar median aspect ratio ($p>0.05$). All wear particle distributions were statistically different ($p<0.05$) (Figure 1).

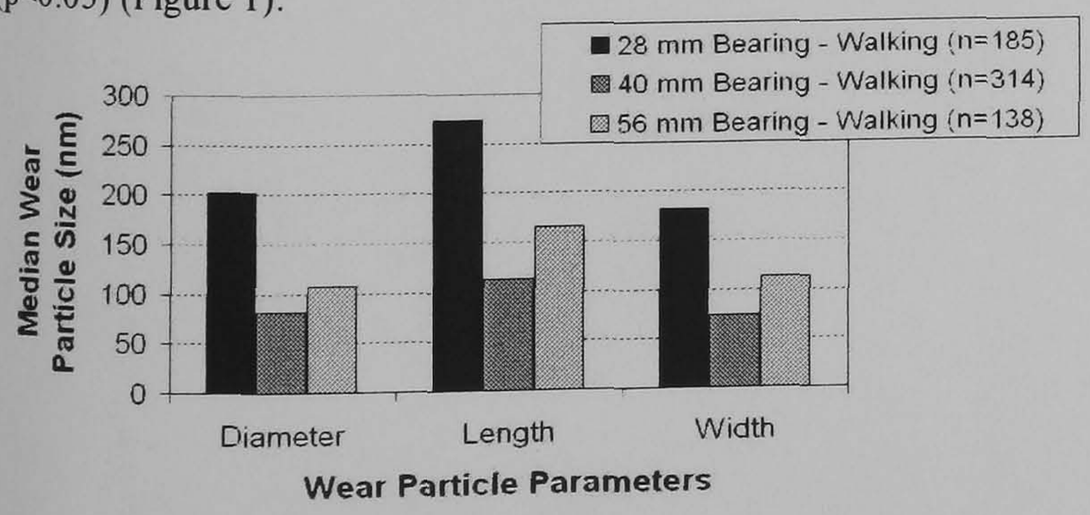


*Figure 1. Influence of head diameter on Co-Cr-Mo wear particle size.*

The smaller 28mm bearings showed a 2-fold increase in total wear particle surface area per million cycles compared to 56mm bearings ($p<0.05$) (Table 2).

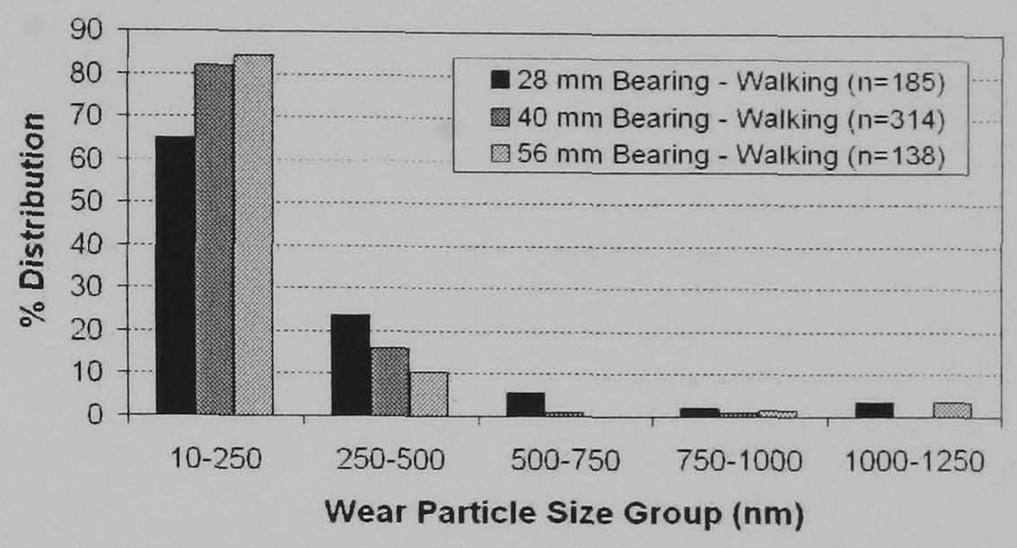


*Figure 2. Change in wear particle size distribution with varying head diameter.*

| Table 2 | Head Diameter of MOM | | |
|---|---|---|---|
| | 28 mm | 40 mm | 56 mm |
| Mean Steady-State Wear Rates [5] ($mm^3/10^6$ Cycles) | 0.92 | 0.39 | 0.32 |
| Total Wear Particle Surface Area Per Mc ($m^2/10^6$ Cycles) | 0.153 | 0.116 | 0.066 |

**Discussion and Conclusions** Our Co-Cr-Mo wear particles were similar in size to those reported clinically [7,9]. This is the first *in vitro* study to show that bearing geometry can affect wear particle sizes, and suggests that the improved lubrication regime found in larger bearings [2] may have resulted in a finer polishing action, thus creating smaller wear particles. Importantly, the 56mm diameter bearings showed a 2-fold reduction in the total wear particle surface area per year of use compared to the smaller 28mm bearings. Therefore our hypothesis was proved. The clinical significance of this result suggests that large head diameter MOM bearings have the potential to reduce ion release in hip arthroplasty patients.

It was also noted that the median sizes of our Co-Cr-Mo particles were greater compared to previous studies. Simulator studies by Firkins et al [10], Fisher et al [11], and Catelas et al [8] have all reported mean Co-Cr-Mo wear particle sizes of 25, 30 and 65 nm respectively for modern MOM bearings. This difference may be a result of these studies using a more corrosive particle extraction protocol (KOH or NaOH) [8], or varying testing parameters. Clinical studies of retrieved periprosthetic tissue in metal-metal patients by Doorn et al [7] and Shahgaldi et al [9] have both reported larger Co-Cr-Mo wear particles (mean 81–200 nm), plus showing wear particles can be as big as 4000 nm in size.

**Acknowledgements** This research was funded by the Wishbone Trust, UK, and Corin Medical UK.

**References**

1. Ingham E, Fisher J, Proc Instn Mech Engrs, 214(H), 21-37, 2000
2. Dowson D, Proc Instn Mech Engrs, 215(H), 335-3358, 2001
3. Medley et al, Clin Orthop Rel Res 329S: 148-159, 1996.
4. Smith SL et al, Proc Instn Mech Engrs, 215(H), 161-170, 2001
5. Bowsher JG et al, Trans 49th ORS, Vol.28, 1398, 2003
6. Paul JP, Proc Instn Mech Engrs, 181(H), 8-15, 1966
7. Doorn PF et al, J Biomed Mater Res, 42, 103-111, 1998
8. Catelas I et al, Trans 6th World Biomaterials, 482, 2000
9. Shahgaldi BF et al, J Bone Joint Surg Br, 77(6), 962-966, 1995
10. Firkins PJ et al, Proc Instn Mech Engrs, 215(H), 119-121, 2001
11. Fisher J et al, Trans 6th World Biomaterials, 871, 2000

**LLUMC, Dept of Orthop, 11406 Loma Linda Drive, Suite 606, Loma Linda, CA 92354, USA, ***Corin Medical, Cirencester, GL7 1YJ, UK